REGIONAL HYDRAULIC FUNCTION OF STRUCTURAL ELEMENTS AND LOW-PERMEABILITY FORMATIONS IN FLUID FLOW SYSTEMS AND HYDROCARBON ENTRAPMENT IN EASTERN-SOUTHEASTERN HUNGARY

by
Brigitta Czauner
M.Sc. Geology

Dissertation submitted to the Geology and Geophysics Ph.D. program of the Doctoral School of Earth Sciences, Eötvös Loránd University, Budapest in partial fulfillment of the requirements for the degree of Doctor of Philosophy in Earth Sciences

Chair of the Ph.D. School: Gyula Gábris, D.Sc.
Chair of the Ph.D. Program: Andrea Mindszenty, D.Sc.

Supervisor: Judit Mádl-Szőnyi, Ph.D., Associate Professor

Eötvös Loránd University
Budapest, Hungary
2012

ACKNOWLEDGEMENTS

This study was well supported personally, financially, and technically as well, thus I have very many to thank.

First of all, I wish to thank Dr. Judit Mádl-Szőnyi, my supervisor, for set me going on the fascinating way of hydrogeology, than offer me the research topic that I have been working on since my graduate studies. I am also grateful to her for generating and patronizing the R&D project with the MOL Plc., and my partial Ph.D. education at the University of Alberta (Edmonton, Canada), as well as for providing me the possibility to participate at several memorable conferences in Hungary and abroad too. Eventually, I am very thankful for her continuous personal and professional support, as well as for the acquaintance with Prof. József Tóth. I would like to very thank to Prof. Tóth for his honouring friendship, and for introducing me into the gripping world of hydraulics and petroleum hydrogeology. My study followed in his track in the hydraulic investigation of the Great Hungarian Plain, while he partly managed my work as well. I am also grateful to him for proposing and supporting my year-long (2009-2010) partial Ph.D. education at the University of Alberta (Edmonton, Canada) where I studied among others petroleum hydrogeology, and I also had the opportunity to work together with Prof. Tóth on my research project.

This study was supported by data and also financially by the MOL Hungarian Oil & Gas Company Plc., through a Research and Development (R&D) project came off between the MOL Plc. and the Eötvös Loránd University for 2009-2011 (supervisor: Dr. Judit Mádl-Szőnyi). I would like to personally thank András Király (International Exploration and Production Director, INA – Industrija nafte, MOL Group) for the recognition of the hopefulness of this research, as well as the initiation of the R&D project. I am also grateful to Viktor Sőreg (Director, Eurasian Exploration Projects, MOL Plc.) for carrying on the project, professionally supporting the study, and permitting the presentation of the results. I wish to thank Károly Kiss (Senior Exploration Expert, Project Manager; Unconventional Exploration Projects, MOL Plc.) for managing the project, providing me the data, and consulting with me from that I benefited a lot regarding the handling of data and the cognition of the Study Areas. I also would like to thank Béla Lakos (New Technologies and R&D Senior Expert, MOL Plc.) for his support and efforts around the R&D project. Eventually, I am grateful to all employees of the MOL Plc., who assisted my work by data collection or professional advices.

I am grateful to the Eötvös Loránd University (ELTE) (Budapest, Hungary) for providing me a three years-long Ph.D. fellowship (2008-2011), then a 'TÁMOP' (Social

Renewal Operational Programme) predoctoral employment (02-09/2012) in order to finish my dissertation. I wish to thank the past and present Head of the Department of Physical and Applied Geology (ELTE), Prof. Andrea Mindszenty and Prof. József Pálfy for providing me the work conditions and technical background at the Department. I am also grateful to all of my colleagues and friends at the Department. Particular thanks to Dr. Anita Erőss and Dr. Szilvia Simon who supported me professionally, personally, and patiently as well, and to Klára F. Nagyné Gulyás for the indispensable administrative assistance. Eventually, also the water well data collecting efforts of past and present students of the Department are very much appreciated.

I wish to thank the staff of the Department of Earth and Atmospheric Sciences at the University of Alberta (Edmonton, Canada) for providing me the opportunity to study there and from them. I am especially grateful to Dr. Ben J. Rostron for my admission into the hydrogeology group.

Also thanks to Dr. László Lenkey (associate professor, ELTE Department of Geophysics and Space Science) and Dr. István Almási (president, Dome GeoConsulting Inc.) for their temperature and hydrostratigraphic data, respectively.

Grateful thanks to my "in-house" rewievers, Dr. Szilvia Simon (assistant lecturer, ELTE), Dr. György Pogácsás (associate professor, ELTE), and Viktor Sőreg (MOl Plc.) for carefully reading of the first version of my manuscript; their advice and suggestions also significantly improved the quality of the final product.

Finally, I am most grateful to my parents, József Czauner and Brigitta Czaunerné Ádám, for their love, patience and trust with which they fundamentally support my life, my studies, and the completion of this dissertation. Cheers to Zsé for her sisterhood and encouragement. Thanks to my beloved Péter Zentai for his befriending and the relaxing moments. Eventually, I am very grateful to all of my relatives and friends who rooted for me and was waiting for me a lot.

ABSTRACT

The results of a regional scale hydrogeological research conducted in the Eastern-Southeastern Great Hungarian Plain (Pannonian Basin, Hungary) in order to investigate the hydraulic role of faults and low-permeability formations in subsurface fluid flow systems and hydrocarbon entrapment are presented. Study Areas (~10,400 km^2) were chosen based on their differing geological characteristics, thus a regional scale Pre-Neogene basement high (Battonya High), and two regional scale depressions (Derecske Trough, Békés Basin) were studied. During data analysis and interpretation, first the hydrostratigraphical build-up of the Study Areas was determined. Afterwards, hydraulic data of 3629 (water and hydrocarbon) wells were interpreted in order to map the groundwater flow systems, because moving groundwater as a geologic agent determine the distribution of temperature, salinity, hydrocarbon accumulations, etc. Thus the primary objectives of the subsequent temperature and hydrochemical data analysis considering their reliability as well were the support of the hydraulic interpretations and the examination of their anomalies. As a result, regional characterization of the Study Areas revealed that the overpressure dissipation from the Pre-Neogene basement strata through the Pannonian sedimentary fill of the basin towards the unconfined and approximately hydrostatic Great Plain Aquifer is controlled by the structural and sedimentological heterogeneities of the regionally extensive aquitard units. These heterogeneities usually coincide with fluid-potential, geothermal, and hydrochemical anomalies, as well as hydrocarbon occurrences. Consequently, diagnostic relationships were recognized among these phenomena, while in their relation system the way of overpressure dissipation proved to be the primary controlling factor defined by the geological build-up. Accordingly, seven regions were distinguished within the Study Areas that can be characterized by seven basic types of pressure-elevation profiles traced back to the differences in the geological build-up and consequently in the way of overpressure dissipation. Finally, based on the exploration of the diagnostic relationships among these issues and the deduced pressure-elevation type-profiles, a hydrogeology-based methodology was worked out, which can be usable directly or indirectly for initial reservoir prognosis in areas with differing data supply during groundwater, geothermal, or hydrocarbon exploration, or field data-based preparation for hydrodynamic modeling. Important segments of the method development were the improvement of pressure-elevation profile interpretation, the determination of the average groundwater density values being typical of the Study Areas, as well as the correction of hydraulic calculations in case of pressure data measured in gas columns.

HUNGARIAN ABSTRACT – ÖSSZEFOGLALÁS

Doktori disszertációm témája a vetők és alacsony permeabilitású képződmények felszínalatti folyadék áramlási rendszerekben és szénhidrogén csapdázódásban betöltött szerepének hidrogeológiai tanulmányozása regionális léptékben. A kelet és délkelet alföldi kutatási területek (~10.400 km^2) kiválasztása geológiai különbözőségeik és hasonlóságaik alapján történt, így egy pre-neogén aljzatmagaslatot (Battonyai-hát), és két regionális depressziót (Derecskei-árok, Békési-medence) vizsgáltam. Az adatelemzés és értelmezés során elsőként a vizsgálati területek hidrosztratigráfiai felépítését határoztam meg. Ezt követően 3629 (víz és szénhidrogén) kút hidraulikai adatait dolgoztam fel a felszínalatti vízáramlási rendszerek feltérképezése céljából, mivel földtani hatóényezőként ezek határozzák meg többek közt a hőmérsékletnek, a víz sótartalmának, és a szénhidrogén felhalmozódásoknak a felszínalatti eloszlását is. Következésképpen, a további hőmérsékleti és vízkémiai adatfeldolgozás elsődleges célja az értékek eloszlásában mutatkozó anomáliák vizsgálata, valamint – tekintve az adatok megbízhatóságát is – a hidraulikai értelmezés alátámasztása volt. A kutatási területek ily módon elvégzett regionális hidrogeológiai jellemzése (állapotfelmérése) eredményeként megállapítható, hogy a túlnyomás lecsengését a pre-neogén aljzat felől a megközelítőleg hidrosztatikus nyomásállapotú Nagyalföldi Vízvezető felé a vízrekesztő rétegek szerkezeti és szedimentológiai heterogenitásai határozzák meg. Mivel ezen heterogenitások egybeesése igen gyakori folyadék-potenciál, hőmérsékleti és vízkémiai anomáliákkal, valamint szénhidrogén felhalmozódásokkal, diagnosztikus összefüggést mutattam ki ezen jelenségek együttes előfordulása közt, míg kapcsolatrendszerükben a túlnyomás lecsengésének a geológiai felépítés által definiált módja bizonyult meghatározónak. Mindezek alapján végül hét régiót különítettem el a kutatási területeken belül, amelyek geológiai felépítésbeli eltéréseikre visszavezethetően hét különböző nyomás-eleváció profil alaptípussal, azaz túlnyomás lecsengési móddal jellemezhetők. Végezetül és mindeközben a diagnosztikus összefüggések és az azokból levezetett nyomás-eleváció profil alaptípusok alapján kidolgoztam egy hidrogeológiai alapú módszert, amely direkt vagy indirekt módon is alkalmazható adatokkal különböző mértékben ellátott területeken, akár felszínalatti víz, geotermikus, vagy szénhidrogén kutatás kezdeti szakaszában, vagy numerikus modellezés előkészítéseként. A módszertani fejlesztés legfőbb elemei a következők votlak: a nyomás-eleváció profilok értelmezésének továbbfejlesztése; a kutatási területekre jellemző átlag felszínalatti vízsűrűségek meghatározása; valamint a gázoszlopban mért nyomás adatokkal történő hidraulikai számítások korrekciója.

TABLE OF CONTENTS

The Figure and Table Appendix can be found in a separated volume.

The electronic version of the dissertation is attached on a CD.

The compiled and applied data base is under the MOL Plc.'s secrecy protection, and cannot be published not even in this dissertation.

LIST OF SYMBOLS

SYMBOL	S.I. UNIT	DESCRIPTION
d_{wt}	m	Depth of the water table, positive above the well head
E	N/m^2 or Pa	Bulk modulus fluid elasticity
g	m/s^2	Gravitational acceleration
EC	µS/cm	Electric conductivity
grad$h$ or $\Delta h/\Delta l$	m/m	Hydraulic gradient
grad$T$ or $\Delta T/\Delta l$	°C/km	Thermal gradient
h	m	Hydraulic head
$h_w(GWC)$	m	Water's hydraulic head on the gas-water contact GWC (calculated from $p_{(GWC)}$)
$h_w(z_2)$	m	Water's hydraulic head calculated from $p_g(z_2)$
$h_w(z_2)$*	m	Water's hydraulic head calculated from $p_w(z_2)$
i_z	W/m^2	Heat flux
K	m/s	Hydraulic conductivity
k	m^2	permeability
l	m	Length/distance
p	Pa (or MPa)	Fluid or pore pressure
$p_{(GWC)}$	MPa	Pressure on the gas-water contact (GWC)
p_{fr}	Pa	Fracture pressure
$p_g(z_2)$	MPa	Pressure measured at z_2 elevation in a gas column
p_{st}	Pa	Hydrostatic pressure
$p_w(z_2)$	MPa	Pressure would be measured at z_2 elevation in a water column
q	m/s	Volumetric flow rate or flux or specific discharge
R_0	%	Vitrinite reflectance
s	km	Horizontal distance along cross-sections
S	mg/L or g/L	Salinity
T	°C	Temperature
TDS	mg/L or g/L	Total dissolved solid content
z	m	Elevation relative to see level, positive above sea level
z_0	m	Elevation of the ground surface or well head
Δh	m	Change in hydraulic head
Δh_{wg}	m	Difference of $h_w(z_2)$ and $h_w(z_2)$*
$\Delta\Phi$	m^2/s^2	Change in fluid potential
α	m^3/m^3°C	Volumetric temperature expansion coefficient
β	m^2/N or 1/Pa	Compressibility of water
γ	MPa/km	Vertical pressure gradient
K	W/Ks	Thermal conductivity
ρ	kg/m^3	Density
σ_e	Pa	Effective stress
σ_T	Pa	External load or total vertical stress (=p+σ_e)
Φ	m^2/s^2	Fluid potential

LIST OF SUBSCRIPTS

SUBSCRIPT	DESCRIPTION
av	average
dyn	dynamic
g	gas
h	horizontal
max	maximum
min	minimum
sb	subhydrostatic
sp	superhydrostatic
v	vertical
w	water

LIST OF ABBREVIATIONS

ABBREVIATION	DESCRIPTION
AF	Aquifer
AT	Aquitard
B	Barrier
BB	Békés Basin
BBSA	Békés-Battonya Study Area
Bék	Békés High
BH	Battonya High
Bi	Biharnagybajom High
b-Pa1	Faults terminate below the top of the Algyő Aquitard
b-Pa2	Faults terminate in the Pre-Neogene basement and cross-cut also the Algyő Aquitard
BSA	Berekfürdő Study Area
C	Conduit
C(s,z)	Hydrochemical cross-section
C(x,y)	Iso-concentration map
C(z)	Concentration versus elevation (profile)
Ca^{2+}	Calcium ion
CH_4	Methane
Cl^-	Chloride ion
Co	Compaction
CO_2	Carbon-dioxide
CO_3^{2-}	Carbonate ion
CovsOp	“Compaction versus overpressure problem”
DSA	Derecske Study Area
DT	Derecske Trough
E	East

ELTE	Eötvös Loránd University
EOV	Egységes Országos Vetületi rendszer', the Uniform National Projection system in Hungary
Fáb-Nsz-Or	Fábiánsebestyén-Nagyszénás-Orosháza Area
Fig.	Figure
AFig.	Figure can be found in the Figure Appendices
Fm.	Formation
fms.	formations
Fu	Furta High
GWC	Gas-water contact
h(s,z)	Hydraulic cross-section
h(x,y)	Fluid potential map
H_2S	Hydrogen sulfide
H_2SiO_3	Silicic acid
HC	Hydrocarbon
HCO_3^-	Bicarbonate ion
K^+	Potassium ion
M.	Member
Ma	"mega annum before present" = "million years ago"; it refers to age
Mg^{2+}	Magnesium ion
MHL	Mid-Hungarian Line
MOL Plc.	Hungarian Oil and Gas Company Plc.
MS Excel	Microsoft Excel
MT	Makó Trough
N	North
N_2	Nitrogen gas
Na^+	Sodium ion
NO_3^-	Nitrate ion
Op	Overpressure
OpG	Overpressure generation
p(z)	Pressure versus elevation (profile)
Pa_1	Lower Pannonian (s.l.)
Pa2	Faults cross-cut only the Upper Pannonian (*s.l.*) strata
Pa_2	Upper Pannonian (s.l.)
Pre-Pa	Pre-Pannonian
Pre-Ng	Pre-Neogene
PWS	Bottom-hole pressure measured in the shut-in period of drill stem test
PWST	Static formation pressure estimated by extrapolating the logarithmically ascending pressure build-up curves recorded during drill stem tests
R&D	Research and Development
R_e	Reynolds' number
S	South
s.l.	"sensu lato" = "in the broad sense" /Latin/
s.s.	"sensu stricto" = "in the strict sense" /Latin/
S_2	Disulfur gas
SO_4^{2-}	Sulphate ion

Szarv	Szarvas High
Szegh	Szeghalom High
T	Temperature
T(s,z)	Geothermal cross-section
T(x,y)	Isotherm map
T(z)	Temperature versus elevation (profile)
W	West

LIST OF FIGURES

LIST OF TABLES

#	TITLE	PAGE #
4.1	Number of available wells and data, as well as the covered elevation and drilling time intervals in the Study Areas (DSA and BBSA)	43
6.1	The fundamental geological characteristics, which proved to determine the hydraulic differentiation of the regions	130

List of A-Figures and A-Tables can be found in the Figure and Table Appendix volume.

"Whither hydrogeology?
… increasing specialization can be expected with growing numbers of 'qualified' or hyphenated sub-disciplines appearing, such as: environmental, contaminant, agricultural, eco-, and ***petroleum hydrogeology****."*
/Prof. József Tóth, 2012/

1 INTRODUCTION

1.1 Premises

Structural elements generally represent key geological factors in subsurface fluid flow systems. As flow paths and/or barriers, fractures and faults have crucial effects on the formation of thermal springs (e.g., GRASBY and HUTCHEON, 2001), groundwater inflows in mines (e.g., MAYO and KOONTZ, 2000), hydrocarbon migration pathways and traps (e.g., MATTHÄI and ROBERTS, 1996), hydrothermal mineralization (e.g., GE and GARVEN, 1992; LONERGAN et al., 1999), as well as on diagenetic and fluid-induced rock deformational processes (e.g., GE and GARVEN, 1992, 1994). In addition, synsedimentary faults also control the changes in lithological facieses, i.e. the thickness of the permeable layers. Thus, this kind of faults influences also indirectly the fluid conductivity of the cross-cut formations (e.g., ZOUHRI et al., 2004). However, it is usually hard to study the hydraulic behaviour of faults in spite of its significance, since data are rarely available from the fault zones themselves.

Furthermore, fractures and faults play a more significant hydraulic role in low-permeability formations, as only potential fluid flow pathways. Survey of these flow impeding zones is fundamental in hydrocarbon exploration (e.g., BENNION et al., 1996; KASAP et al., 1996; SAMAHA et al., 1996; LEE and MICHAELS, 2000), radioactive waste disposal (e.g., ROBERTS et al., 1999; DISTINGUIN and LAVANCHY, 2007; AVIS et al., 2009), and carbon dioxide geological storage (e.g., WHITTAKER and ROSTRON, 2003; ANDERSON and NEWELL, 2004; KALDI, 2005; METZ et al., 2005; BACHU, 2008) site-characterization as well. However, the research of low-permeability environments still have a lot of theoretical and practical questions, as well as unsolved problems, such as the difficulties of reliable hydraulic testing, the parameters' scale dependence, the query of fluid flow laws' validity, and the movable fluids' quantity.

Considering the two disciplines mostly dealing with these questions, hydrogeological and petroleum geological study approaches in the examination of faults' and low-permeability formations' hydraulic behaviour are significantly differing regarding the aspects and methods as well. On one hand, hydrogeology mainly examines the effects of faults on groundwater flow patterns particularly on the basis of hydraulic, hydrochemical and thermal data analysis, as well as related surface phenomena (TÓTH, 1999). In addition, most of the related hydrogeological investigations are limited to local, i.e. smaller than basin scale issues. On the other hand, petroleum exploration focuses on fault-sealing analysis primarily based on the petrophysical properties of fault zones and juxtaposed strata (SORKHABI and TSUJI, 2005) in order to determine the role of faults in hydrocarbon migration and entrapment. Accordingly, these explorations are usually limited to local, reservoir scale problems. Although petroleum hydrogeology has already applied hydrogeological principles and techniques to petroleum exploration on the basis of the hydraulic theory of petroleum migration (TÓTH, 1980), there were only scarcely attempts (e.g., TÓTH and OTTO, 1993; VERWEIJ, 2003) to study the hydraulic role of faults in hydrocarbon entrapment by hydrogeological methods. In case of low-permeability formations, both disciplines' interpretations based on pointwise data are highly loaded by uncertainties.

1.2 Project History

Approaching from the hydrogeological side, but supported by the MOL Hungarian Oil & Gas Company Plc. within the confines of a Research and Development (R&D) project, in the Great Hungarian Plain part of the Pannonian Basin first Prof. József Tóth and Dr. István Almási referred to the possible relationship among structural elements, sedimentological heterogeneities, and subsurface fluid-potential anomalies based on their regional scale hydraulic study (TÓTH and ALMÁSI, 2001). In order to examine this hypothesis I carried out a complex structural, hydrostratigraphic, hydraulic and hydrochemical interpretation for the local scale (1800 km^2) study area of Berekfürdő (Eastern Pannonian Basin, Hungary) and its surroundings (Fig. 1.1) in my M.Sc. thesis (CZAUNER, 2008) also supported with data by the MOL Plc. This work i) confirmed that the formation of a significant (positive) fluid-potential anomaly detected by TÓTH and ALMÁSI (2001) is determined by faults, ii) demonstrated the heterogeneity of the Algyő Aquitard in the study area, which is otherwise thought to be a regionally extensive flow barrier zone in the Pannonian Basin, as well as iii) explained the juxtaposed occurrence of a thermal water reservoir and a gas field. Namely, the two identified

vertically conducting and horizontally sealing strike-slip fault zones may act as lateral seals of a gas field, and might ensure the active water pressure of its reservoir system as well. Subsequently, the junction of the fault zones near Berekfürdő represent the southern limit of the prolific hydrocarbon-bearing aquifers, while simultaneously causes intensive water upwelling, which produces the thermal water of the Berekfürdő Spa (Fig. 1.2) (CZAUNER, 2008; CZAUNER and MÁDLNÉ SZŐNYI, 2008; CZAUNER et al., 2008; CZAUNER and MÁDL-SZŐNYI, 2011).

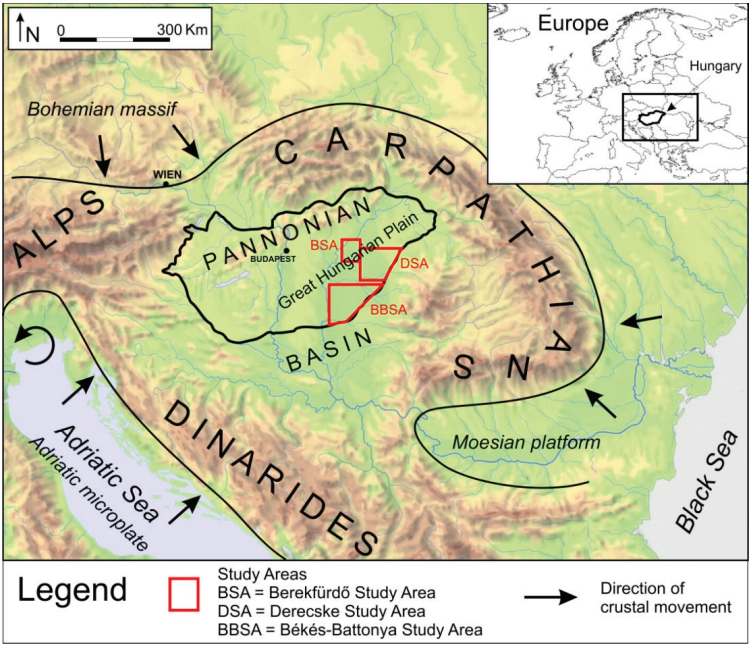

Figure 1.1 Location of the Study Areas in the Pannonian Basin, Hungary (modified after ZENTAI, 1996), as well as the crustal movement directions in the Basin and its vicinity (based on BADA et al., 2007)

My Ph.D. research plan was formulated based on these local scale results, as the exploration of further, regional scale basement highs and depressions with the same objectives. Since our conception favorably met with the research plans of the MOL Hungarian

Oil & Gas Company Plc., a Research and Development (R&D) project came off between the MOL Plc. and the Eötvös Loránd University in 2009 (supervisor: Judit Mádl-Szőnyi, Associate Professor). The 3 year-long (2009-2011) project titled "Research of petroleum entrapment connecting to fluid-potential anomalies" was supported with data and also financially by the MOL Plc., while the research results were reported annually (CZAUNER and MÁDLNÉ SZŐNYI, 2009, 2010, 2011).

Beyond the R&D project, completion of this dissertation is also due to my one year-long Ph.D. partial education at the University of Alberta (Edmonton, Canada) where I could work together with Prof. József Tóth and study among others petroleum hydrogeology.

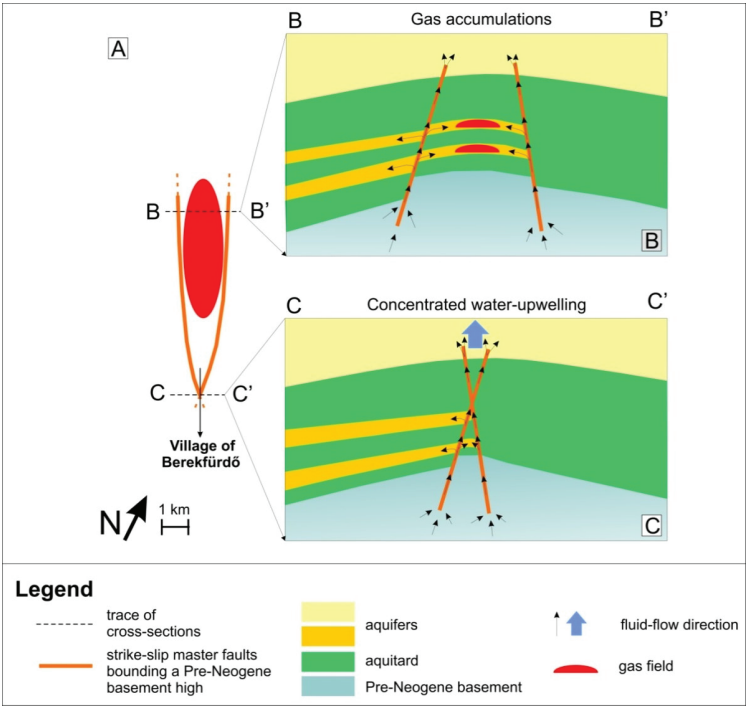

Figure 1.2 Schematic diagram of the interpreted phenomena around the Berekfürdő High representing a map (A) and two cross-sections (B and C) (modified after CZAUNER and MÁDL-SZŐNYI, 2011, Fig. 10). For details see also the text.

1.3 Objectives

Starting from the above considerations, initial purpose of the present Ph.D. research work was to i) investigate the hydraulic role of faults and low-permeability formations in subsurface fluid flows and hydrocarbon entrapment through the joint application and development of different, particularly hydrogeological research techniques; then ii) utilize the recognized diagnostic relationships for hydraulic and/or hydrodynamic (hydrocarbon/geothermal) reservoir prognosis.

Accordingly, study areas were chosen in the Great Hungarian Plain (Pannonian Basin, Hungary) based on their differing geological characteristics, such as the stratigraphy, tectonics, and tectonic activity. Consequently, after a local scale Pre-Neogene basement high (Berekfürdő High) also one of a regional scale (Battonya High), as well as two regional scale depressions (Derecske Trough, Békés Basin) (Fig. 1.1) were studied according to the following objectives:

1. Regional scale hydrogeological (i.e. hydraulic, geothermal, hydrochemical) characterization of the Study Areas, determination of the subsurface fluid-potential distribution in particular.
2. Exploration of diagnostic relationships among the fluid-potential distribution and anomalies, the temperature and hydrochemical anomalies, the hydraulic conductivity of structural elements and sedimentological build-up, as well as the occurrence of hydrocarbon accumulations.
3. Utilization of the recognized diagnostic relationships for the understanding of the formation of known hydrocarbon accumulations.
4. Method development for the implementation of the above detailed points #1-3, which can be usable in the initial research phase of groundwater/geothermal/hydrocarbon exploration, or as a field data-based preparation for numerical modeling.

2 THEORETICAL BACKGROUND

2.1 Hydraulic behaviour of faults

2.1.1 Hydraulic role of faults in fluid flows

Faults can both be barriers (seals) and conduits (leaks) for fluid flow. It depends on several factors, such as the petrophysical properties (porosity, permeability, capillarity) of the fault zone and the juxtaposed formations (undeformed host rock), which are usually in the focus of petroleum geological researches (JONES et al., eds., 1998; SORKHABI and TSUJI, eds., 2005). Furthermore, fault zones can have highly complex geometries divided into fault rock (or fault core) and fault damage zone (CAINE et al., 1996). The latter, which is affected by high fracture density, usually has higher permeability than its environment (MORETTI et al., 2000), while often only a small percentage of larger faults control the flow properties throughout the fault network (O'BRIEN et al., 2003). However, the fault rock, on one hand in deformation or shear bands (AYDIN, 2000) generally shows reduced permeability by one to three orders of magnitude compared to the associated undeformed rocks (SORKHABI and TSUJI, 2005). On the other hand, in brecciated fault zones the permeability of the fault rock can be higher even than that of the damage zone (AYDIN, 2000). Another determining factor is the relative orientation and dip-angle of the fault plane: vertical fractures (e.g. strike-slip faults) are generally more effective than dip-slip faults as conductors of fluids (GUDMUNDSSON, 2001). Besides, the present stress field is also decisive. High fault-normal stress reduces aperture, thus inhibiting fluid flow, whereas high fracture-parallel compressive stress increases the ability of faults to stay open and transport fluids (AYDIN, 2000). The significance of the role of pore pressure in tectonic processes – such as faulting – manifests in their interplay. Pore pressure buildup reduces the effective stress and frictional resistance in the rock mass, which can lead to fracturing (TERZAGHI, 1923). Consequently, high fluid pressure is capable of opening fractures at any depth and thus facilitating vertical and lateral flow (AYDIN, 2000). On the other hand, while pore pressure growth causes hydraulic fracturing, opening of fractures results in pressure dissipation. However, the presence of faults impeding fluid flows aids to maintain the overpressure.

In addition, most of the above mentioned factors can show spatial and temporal variability. Spatial changeability means space and direction dependence too, while temporal variability firstly depends on the fault's activity. During the active, opening and developmental phases of a structural element it is usually more conductive – mainly thanks to

the induced pressure drop –, than the host rock. However, in the inactive periods fractures tend to close, as well as the circumstances of cementation and other diagenetic processes are also more favourable. Consequently, in low-permeability formations inactive faults can serve as flow pathways only if during their active period coarser grained sediments intruded into the fault plane, for example from intersected sand bodies (DEWHURST et al., 1999).

Eventually, due to the spatial and temporal variability of all the known and unknown factors it is almost impossible to generalize the hydraulic role of faults as conduits or barriers for fluid flow. Furthermore, data are rarely available from the fault zone itself. However, the subsurface fluid-potential field, the formation water chemistry and some other hydrogeological phenomena can also be used as indirect indicators of the fault zone's hydraulic properties. From the point of view of hydrogeology, in a simplified case, the fault zone related "barriers" have lower permeability than that of the cross-cut aquifer, while "conduits" represent higher permeability zones (UNDERSCHULTZ et al., 2005). Consequently, faults as approximately linear heterogeneities may cause significant anomalies in the fluid-potential distribution, as well as in the joint temperature and water chemical characteristics. However, the interaction between the fault's permeability and the fluid-potential distribution affects back and force. For instance, the model of MATTHÄI and ROBERTS (1996) shows an example for the case when the distribution of fluid potential causes the spatial variability in a fault's hydraulic behaviour resulting in a high-permeability fault acting as a direction dependent barrier for fluid flows. The case study of my M.Sc. thesis represents similar results based on the interpretation of field data (see also Chapter 1.2.) (CZAUNER, 2008; CZAUNER and MÁDLNÉ SZŐNYI, 2008; CZAUNER et al., 2008; CZAUNER and MÁDL-SZŐNYI, 2011). Therefore, in the course of the investigation of hydraulic behaviour of faults it is not simply recommended, but it is essential to pay attention – beside the permeability of the cross-cut layers and the fault – to the fluid-potential field as well, which provides indirect information.

Beyond the hydraulic phenomena, corroborating evidences for fault zone barriers can be the accumulation of hydrocarbons on one side of the fault, and the discontinuities in the formation water chemistry across the fault. While on the other hand, the connection of leaking faults with the land surface can cause springs with thermal and/or chemical anomalies (e.g., MÁDL-SZŐNYI and TÓTH, 2009; SIMON et al., 2011), or can recharge deeper aquifers (e.g., UNDERSCHULTZ et al., 2005).

Finally, also the so far presented situations are much more complicated in reality, because of the previously mentioned temporal and spatial variability of the hydraulic behaviour of faults, as well as that of the fluid-potential field too.

2.1.2 Hydraulic role of faults in hydrocarbon entrapment

Determination of a fault's barrier or conduit behaviour is more complicated in case of multiphase flow, because trap forming faults have to be leaking water while retaining hydrocarbons. After all, one of the previously mentioned evidences for fault zone barriers is the accumulation of hydrocarbons on one side of the fault. Conversely, it is thought to be worth exploring possible petroleum traps in the vicinity of barrier faults. Consequently, petroleum geology specifically focuses on fault-sealing analysis, the applicability of that is primarily restricted to normal faults in clastic reservoirs (SORKHABI and TSUJI, 2005), while the assessment needs a vast amount of data, also from the fault zone itself.

However, during hydrocarbon exploration, it is not definitely necessary to search for low-permeability faults, because also a high-permeability fault can be acting as a direction dependent barrier for fluid flow, as it emerged from the model of MATTHÄI and ROBERTS (1996), and the case study of CZAUNER and MÁDL-SZŐNYI (2011). Since this hydraulic behaviour depends mainly on the distribution of the fluid-potentials, it can be analysed best by hydrogeological methods. These are particularly appropriate for regional scale reconnaissance, and can also contribute to local scale researches. Moreover, the greatest advantage of these techniques is that they can determine the spatially variable hydraulic behaviour of faults (e.g. vertically conduit, transversally barrier) without data from the fault zone itself.

In proposing the hydraulic theory of petroleum migration TÓTH (1980, 1988) (see also Chapter 4.3.3.2) has already pointed out the significance of hydrogeological principles and research techniques in petroleum exploration. However, faults have been scarcely added to this concept yet (e.g., TÓTH and OTTO, 1993).

2.2 Hydraulic behaviour of low-permeability formations

2.2.1 Hydraulic properties and hydrodynamic conditions of low-permeability formations

Low-permeability environments are most commonly associated with fine-grained sedimentary deposits such as shales and clays, but also crystalline rocks, evaporites, and highly compacted and cemented sandstones could compose these zones. However, no properly tested geologic media have proved to be entirely impermeable yet, while large regions composed of low-permeability lithologies are often significantly more permeable than small volumes of the same rock, owing to the presence of joints, fractures, and faults (e.g.,

BREDEHOEFT et al., 1983; NEUZIL, 1994). Based on laboratory and regional studies, permeabilities between 10^{-17} and 10^{-23} m^2 have been obtained at porosities between 0.1 and 0.4 (NEUZIL, 1994) (Fig. 2.1A). Consequently, permeability can vary along a wide range pending the scale or volume of interest (Fig. 2.1B), which throws significant difficulties in the way of spatial extrapolation of the pointwise measured permeability values (e.g., CLAUSER, 1992; DEMING, 1993; INGEBRITSEN et al., 2008, pp. 15-18).

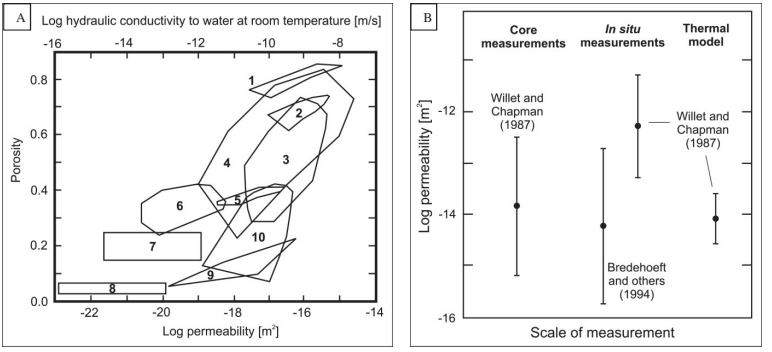

Figure 2.1 Some of the lowest known permeabilities and their scale dependence (based on NEUZIL, 1994, Fig. 1; INGEBRITSEN et al., 2008, Fig. 1.6). **A)** Plot of laboratory-derived permeability versus porosity data with the corresponding hydraulic conductivity values to water at room temperature for a variety of natural argillaceous media (based on NEUZIL, 1994, Fig. 1). Legend: 1 and 2 – bottom deposit (North Pacific); 3 – Pleistocene to Recent (Quebec, Mississippi Delta, Sweden); 4 – Gulf of Mexico; 5 – Sutherland Group (Saskatchewan); 6 – Pierre Shale (central South Dakota); 7 – Lower Cretacous (Western Canada); 8 – Eleana Formation (Nevada); 9 – Japan and Alberta, Canada; 10 – Upper Triassic, Mid-Miocene, Lower Pliocene (Italy). **B)** Upper-crustal permeabilities determined at several distinct sampling scales at well-studied localities in the Uinta Basin, Utah (based on INGEBRITSEN et al., 2008, Fig. 1.6). Permeabilities determined by direct hydraulic measurement at core and *in situ* scales are consistent with basin-scale values estimated using a numerical model constrained by geothermal data. However, this is only the case if a representative subset of *in situ* measurements is selected (BREDEHOEFT et al., 1994). The simple average of *in situ* values from WILLET and CHAPMAN (1987) is likely biased by oversampling of permeable zones.

Beyond the determination of an average permeability value, description of fluid flow rates represents a further problem in low-permeability formations. Applicability of Darcy's generally used linear flow law[1] (DARCY, 1856) (Fig. 2.2) is questionable in these zones nowadays as well (FREEZE and CHERRY, 1979, pp. 72-74; INGEBRITSEN et al., 2008, pp. 2-6). Apparent departures from a linear relation between a hydraulic gradient d*h*/d*L* and the volume

[1] $q = -Kgradh$, where q the volumetric flow rate or flux, or specific discharge [L/T], K the hydraulic conductivity [L/T], *gradh* the hydraulic gradient [-]

flux q (Fig. 2.2) were reported in the literature as early as 1899 (e.g., KING, 1899; DERYAGIN and KRYLOV, 1944; VON ENGELHARDT and TUNN, 1955; MITCHELL and YOUNGER, 1967; WANG and LIU, 2005; XIONG et al., 2009), but many of these experiments have since been shown to have been flawed or incorrectly interpreted (by e.g., OLSEN, 1965; NEUZIL, 1986). Mechanisms suggested to explain "non-Darcian" behaviour of the media are generally changes in the properties of water, such as viscosity, near solid surfaces, which result in a finite threshold value of hydraulic gradient (dh/dL) below that Darcy's law does not apply (e.g., KÉZDI, 1969; RÉTHÁTI, 1974; BYERLEE, 1990; MARTON, 2009).

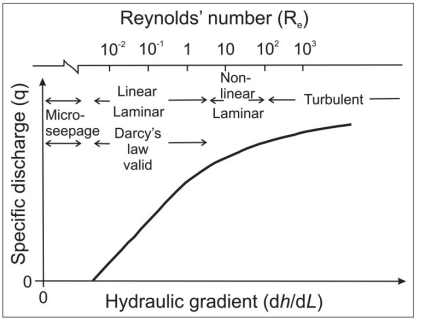

Figure 2.2 Limits of Darcy's law (based on FREEZE and CHERRY, 1979, Fig. 2.28). The upper limit for application of Darcy's law is usually estimated on the basis of the dimensionless Reynolds' number (R_e), which parameterizes the relative strengths of inertial and viscous forces (REYNOLDS, 1883).

Besides, in multiphase fluid systems also the "permeability jail" problem could appear, for instance in tight gas sandstones. According to the basic notion, in tight rocks there exists a saturation region (55-80% water saturation) in which the relative permeabilities to both gas and water are so low (<2%) that neither phase has any effective flow capacity. Because each phase blocks the other from moving, it appears the formation is completely locked up and the fluids are in "jail" (CLUFF and BYRNES, 2010).

Finally, it is worth mentioning, that in low-permeability environments fluid flow can also evolve in response to driving forces other than the hydraulic gradient (i.e. coupled flows). Geologic media in which significant coupled flow occurs are called geologic membranes (NEUZIL, 1986). For instance, fluid flow in these media is found to be driven not only by hydraulic head gradients (hydraulic flow) but also, through coupling, by chemical, electrical, and temperature gradients (MITCHELL, 1976). This non-hydraulic fluid flow as a result of coupling is called osmosis.

2.2.2 Mechanical compaction, overpressure, and turbulent flow in low-permeability formations

Mechanical compaction induced overpressure is particularly typical of low-permeability formations. However, strong negative feedback can appear between the two phenomena as follows. Mechanical compaction occurs in response to an increase in effective stress, instead of being a direct response to an externally imposed load or vertical stress, according to Terzaghi's law (TERZAGHI, 1923):

$$\sigma_T = \sigma_e + p \tag{1}$$

where σ_T [M/Lt^2] the external load or total vertical stress, σ_e [M/Lt^2] the effective stress, p [M/Lt^2] the fluid pressure in the pores (see also Fig. 2.3). At the same time, compaction results in porosity decline, which can lead to pore pressure growth if fluids cannot escape from the compacting layers in the necessary rate (i.e. that could be maintain the equilibrium between the increasing effective stress and pore pressure) usually as a result of flow impeding effect of low-permeability strata (e.g., BETHKE, 1989). Moreover, significant increase in the pore pressure above hydrostatic pressure could reduce the effective stress, and consequently reduce or stop compaction. If there is no compaction, fluid cannot release from storage, there is no movable fluid resource. Thus, although overpressure represents a significant flow driving force, fluid flows do not exist without (movable) fluids. Accordingly, in this situation volume flux (or specific discharge, q) is relatively independent of the permeability and hydraulic gradient, however controlled by the rate of compaction (BJØRLYKKE, 1999).

According to BJØRLYKKE (1999), after compaction was stopped in the above detailed way, the ratio of pore pressure and effective stress does not change, thus fracture or leakoff pressure (GAARENSTROOM et al., 1993) cannot be hit. However, pore pressure can be enhanced also by other forces, such as chemical compaction being typical of sedimentary basins below 2-3 km depth (BJØRLYKKE, 1999), or tectonic compression for example in the Pannonian Basin (TÓTH and ALMÁSI, 2001; BADA et al., 2007). The generated overpressure in these cases can reach the fracture pressure, which is usually about 80-85% of the lithostatic pressure or total vertical stress (it is approximately equal to the horizontal minimum stress (GAARENSTROOM et al., 1993; BJØRLYKKE, 1999) (Fig. 2.3). In other words, reduction in effective stress can cause weakening of the rock framework to such an extent that it can lead to the opening of hydraulic fractures and joints, as well as to the reactivation of faults.

Subsequently, hydraulic fracturing allows of pore pressure drop and fluid release, while analysis of the generated flow raises further questions. On one hand, fluid flow concentrated in the fractures cannot be described by Darcy's law, because in this case

permeability is independent of the intergranular permeability of the rock matrix. Actually, it becomes a dynamic variable pending the volume flux, since fractures are kept open by the elevated pore pressure and fluid flow. In addition, the fractures' lifetime and the episodic or continuous passing of the process depend on the rate of overpressure dissipation. It is worth mentioning, that invasion percolation theory (e.g., FRISCH and HAMMERSLEY, 1963; WILKINSON and WILLEMSEN, 1983; BERKOWITZ, 2002) seems to be the most promising solution or method for the description of fluid flows in fractured and porous rocks as well. This technique remove the scaling limitations, but the dynamic framework is still missing entirely, since it handles secondary hydrocarbon migration as controlled by the balance between the gravity and capillary forces alone (WELTE et al., 2000). On the other hand, hydrocarbon gases migrating in the fractures usually represent turbulent flow due to the higher flow rates that also cannot be described by Darcy's law, since the relationship between q and $\mathrm{d}h/\mathrm{d}L$ becomes nonlinear as significant amounts of energy are lost to turbulence. However, this kind of non-Darcy flow (i.e. at high flow rates) is thought to have greater practical importance as occurs in areas of cavernous porosity (in carbonate rocks and lava flows), as well as in the near-wellbore region of high-capacity gas and condensate reservoirs (KALAYDJIAN et al., 1996). Thus it is a well-studied flow domain where accepted flow equations are available (e.g., FORCHHEIMER, 1901; WHITAKER, 1996).

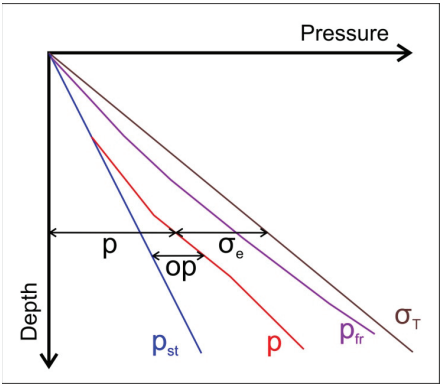

Figure 2.3 Pressure and stress nomenclature. Legend: p – pore/fluid pressure, σ_e – effective stress, σ_T – external load or total vertical stress ($=p+\sigma_e$) ($\approx$ lithostatic pressure), p_{st} – hydrostatic pressure, p – fluid pressure, op – overpressure or excess pressure above hydrostatic ($=p-p_{st}$), p_{fr} – fracture pressure /$\approx$ horizontal minimum stress (GAARENSTROOM et al., 1993) $\approx$ 0.80-0.85 σ_T (BJØRLYKKE, 1999)/

3 STUDY AREAS

The sum total ~10,400 km^2 regional research area cover the eastern-southeastern part of the Great Hungarian Plain (Hungary) containing the following regions (the Study Areas' corner points are presented by EOV[2] co-ordinates, while inside these areas the touched frontiers always constitute the Study Areas' boundaries as well) (Fig. 1.1):

1) Derecske Trough and its surroundings /Y_{EOV} 800-880, X_{EOV} 180-250/ (hereafter Derecske Study Area - DSA) (Fig 3.1)
2) Battonya High and Békés Basin /Y_{EOV} 750-840, X_{EOV} 100-170/ (hereafter Békés-Battonya Study Area - BBSA) (Fig 3.2)

Having investigated the local Pre-Neogene basement high at Berekfürdő, it was intended to study next a Pre-Neogene depression, and thus the region of Derecske Trough (1) was chosen based on the following aspects: (i) tectonically active zone with an extensive fault system; (ii) observable fluid-potential anomalies (TÓTH and ALMÁSI, 2001); (iii) known hydrocarbon accumulations; (iv) including the current exploring area of the MOL Plc. (Y_{EOV} 813-875, X_{EOV} 200-244).

Afterwards, in order to make the results generalizable and to improve the methodology, another Study Area was chosen as well around the Battonya High and Békés Basin (2) according to similar aspects as in the case of the Derecske Trough /(ii)-(iv)/, and to some further considerations such as: (v) tectonically less active areas; (vi) Battonya High is a regionally extensive basement ridge compared to the Berekfürdő High where however, the Pannonian strata are almost undisturbed; (vi) Békés Basin is a geologically lesser-known unit where the inverse application of the methodology developed in the other study areas could be evolved.

Since the above detailed objectives and the MOL Plc. were interested in these two Study Areas in particular, and considering the project's duration as well, an about 10 km wide zone between the DSA and BBSA was eliminated from the research.

In the following chapters, first the Pannonian Basin as a framework, and then the study areas' distinctive characteristics will be presented. In the latter case, in the geological introductions beside the literature review also my research experiences (seismic

[2] EOV: 'Egységes Országos Vetületi rendszer', the Uniform National Projection system in Hungary using the horizontal (easting) Y_{EOV} and vertical (northing) X_{EOV} plane-co-ordinate axes. The co-ordinate axes are orthogonal along which distances are expressed in metres /by six-digits/ (or kilometres by triple-digits).

interpretations, discussions with MOL experts) will be summarized focusing on the information that will be necessary later in the dissertation (during the interpretation of the hydrogeological results). Furthermore, since the regional hydrogeological characterization of the Study Areas was completed in the presented Ph.D. work, and will be discussed in details among the research results (see Chapter 6), in this chapter, only the most important and relevant geological information will be summarized. Finally, since this dissertation primarily deals with the issues of secondary hydrocarbon migration and accumulation, the other elements of petroleum systems will be only shortly reviewed, and the known accumulations will be listed for each Study Areas focusing on the reservoir horizons' position (above/below the top of the Algyő Aquitard – its significance see later).

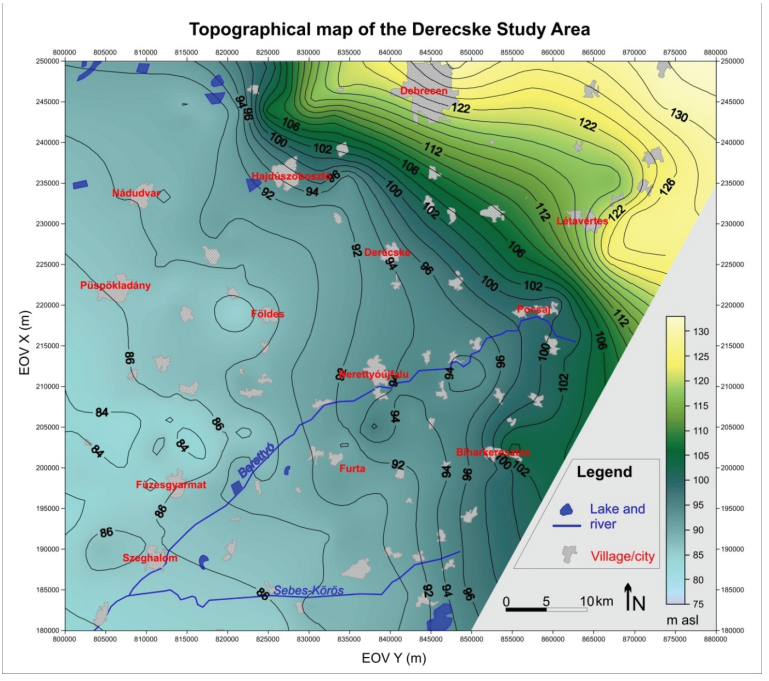

Figure 3.1 Topographical map of the Derecske Study Area (E-Hungary, Fig. 1.1) constructed from surface elevation data of wells

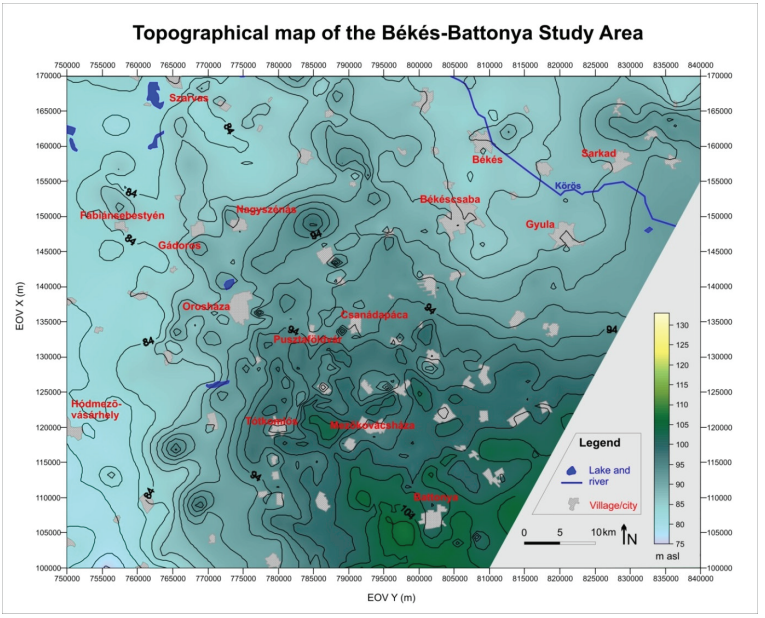

Figure 3.2 Topographical map of the Békés-Battonya Study Area (SE-Hungary, Fig. 1.1) constructed from surface elevation data of wells

3.1 Pannonian Basin

3.1.1 Physiographic setting

The Pannonian Basin is located in the eastern part of Central Europe (Fig. 1.1). The near-circular intermontane depression of about 500 km in diameter is almost completely surrounded by the Carpathian Mountains to the north and east, by the Dinarides to the south, and by the Alps to the west. While the average elevation of the surrounding mountains is above 1000 m, that of the Pannonian Basin is only about 150 m. However, a few isolated mountains emerge from the plains with maximum elevations up to 1015 m, which divide the Pannonian Basin into smaller basins. Among these basins, the Great Hungarian Plain occupies the largest area (~100,000 km^2) in the central part of the Pannonian Basin, which in fact extends beyond the actual state border of Hungary to the east and to the south. Hereafter, the Hungarian part of the Great Hungarian Plain (~52,000 km^2) will be discussed.

In the studied parts of the Great Hungarian Plain, relative topographic highs can be found at the northeastern part of the DSA (maximum z ≈ 130 m asl) and above the Battonya High (maximum z ≈ 105 m asl), while a particularly low surface elevation area coincides with the Békés Basin (maximum z ≈ 80 m asl) (Fig. 3.1 and 3.2).

3.1.2 Regional tectonic history

The Pre-Neogene basement of the Pannonian Basin is divided by the ENE-WSW trending Mid-Hungarian (or Zagreb-Zemplin) Lineament (CSONTOS et al., 1992) into two large units (mega-units or composite terranes), namely the Tisza (South Pannonian) or Tisza-Dacia Mega-unit (Tisia Terrane) and the ALCAPA (North Pannonian) Mega-unit (Fig. 3.3). These were juxtaposed only during the last stage of the Pre-Neogene restructuring of the Pannonian realm in the Late Oligocene – Early Miocene. The Tisza Mega-unit where the Study Areas are located is built-up by three Middle Cretaceous – Early Neogene structural units, which form NE-SW trending belts divided by regionally extensive fault zones.

The Pannonian Basin is a Neogene intermontane sedimentary depression, which underwent a polyphase history of back-arc extension followed by late-stage compressional reactivation, as an integral part of the Alpine–Carpathian–Dinaric orogenic system (Fig. 1.1). Extensional formation of the basin started in the Early Miocene, whereas its structural reactivation (i.e. inversion) has been taking place since Late Miocene to recent times as a consequence of the counterclockwise rotation and NNE directed indentation of the Adriatic microplate, as well as the blocking of the Carpathian subduction zone (Fig. 1.1) (BADA et al., 2007).

Among the results of extension two phenomena have to be emphasized according to the objectives of this dissertation. On one hand, the present Pannonian Basin is characterized by moderate crust (~25 km), and drastic mantle lithosphere (~60 km) thinning (HORVÁTH, 1993), and anomalously high basal heat flow (80-100 mW/m^2) (DÖVÉNYI and HORVÁTH, 1988). On the other hand, since the style and amount of extensional deformation throughout the basin was not uniform, it resulted in the formation of several sub-basins separated by basement highs (Fig. 3.3) (RUMPLER and HORVÁTH, 1988; TARI et al., 1992). For instance, in the basement of the Great Hungarian Plain NW-SE trending rift-type basins (Békés Basin, Makó Trough,) were opened (HORVÁTH, 1993), while in the conjugate shear zones NE-SW directed pull-apart basins (e.g., Derecske Trough) were developed (TARI, 1994). Thus, the

network of the dominantly NE-SW trending fault zones, which characterizes the basement of the basin system, was evolving in this period (CSONTOS et al., 1992).

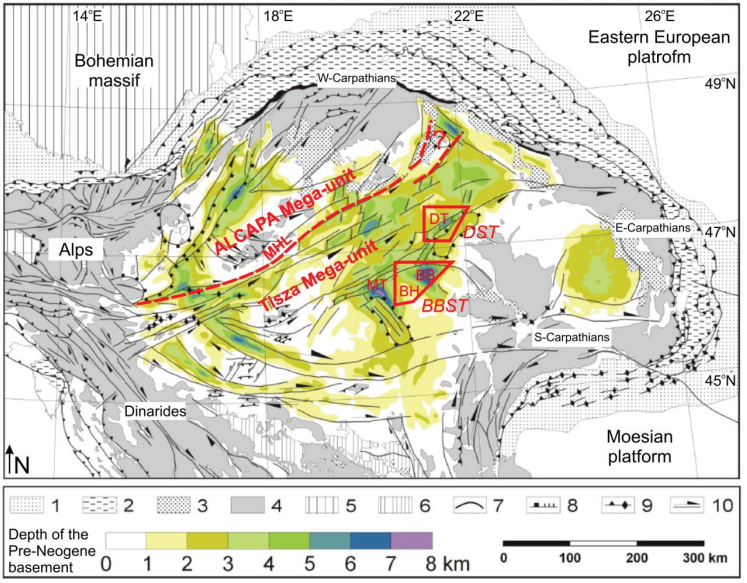

Figure 3.3 Structure map of the Pannonian Basin and its vicinity showing the major Neogene structural elements and the depth of the Pre-Neogene basement (modified after HORVÁTH, 2007, Fig. 52). Legend: 1 – molasse foredeep; 2 – flysch belt; 3 – Neogene calc-alcaline volcanic rocks; 4 – inner Alpine, Carpathian, and Dinaric mountains; 5 – Bohemian massif; 6 – ophiolites; 7 – Carpathian Klippen belt; 8 – normal fault; 9 – reverse fault and anticline axis; 10 – strike-slip fault. Abbreviations: MHL – Mid-Hungarian Line; DT – Derecske Trough; BB – Békés Basin; BH – Battonya High; MT – Makó Trough. Study Areas of the present work (DSA, BBSA) are signed by the red polygons.

During the subsequent Late Miocene 'post-rift' phase, the basin was in a tectonically relaxed state, and the subsidence continued as a result of thermal cooling. Besides, after repeated isolations, by the end of the Middle Miocene, the entire Intra-Carpathian region was completely and finally isolated from the world's seas, forming the Lake Pannon. During the post-rift phase, this lake was gradually filled up by prograding delta systems originating in the elevated Carpathians.

The last period of the basin evolution began when the basin became completely landlocked and constrained on all sides, whilst the N-NE directed indentation of Adria continued, and easily built up significant intra-plate stresses within the weakened Pannonian

lithosphere (BADA et al., 2007). Consequently, the stress field has been changing from extension to compression during Pliocene to Quaternary times. According to the latest compilation of data on the present-day stress pattern in the Pannonian Basin, an overall rate of about 1.5-4 mm/year (GRENERCZY et al., 2005) shortening is detectable, while stresses directly propagate from Adria through the Dinarides into the Pannonian Basin. Thus the inversion first started in the southwestern part of the basin at the end of the Miocene, and then gradually migrated towards more internal parts of the system, i.e. to the east (BADA et al., 2007). Finally, as a result of the lithosphere shortening, the further uplift of the elevated areas, and at the same time, the further subsidence of the depressions can be observed in the Pannonian Basin today.

3.1.3 Sedimentary fill of the basin

The heavily deformed Pre-Neogene basement of the Great Hungarian Plain consists of Mesozoic carbonate rocks, volcano-sediments, and Palaeozoic metamorphic rocks (HAAS et al., 2010). Generally, these are fractured and weathered, and the carbonate rocks are intensively karstified.

During the syn- and post-rift stages, the Pre-Neogene basement was overlaid by a Neogene-Quaternary sedimentary sequence reaching a thickness of up to 7 km (Fig. 3.4 and 3.5). The sediments of the syn-rift cycle (Early-Middle Miocene) were deposited in a rapidly subsiding basin and in a sedimentary environment, which gradually changed from terrestrial to marine. Typically, in the Great Hungarian Plain these sediments are thin (up to 300 m) or missing (BÉRCZI et al., 1988). It is partly due to the erosion following the inversion at the end of the Middle Miocene (12-9 Ma), and on the other hand, the sub-basins in the central part of the Great Hungarian Plain were far away from the sources of clastic material and acted as 'sediment starved basins' (MATTICK et al., 1988) in this period. The preserved rocks generally consist of coarse clastics, organo-detritic limestone, and locally (in the northern part of the basin) rhyolite tuff.

The cessation of rifting and the commencement of the Late Miocene post-rift phase are marked by a regional unconformity. During the post-rift stage, clastic sediments were deposited in a lacustrine environment by delta systems prograding from the Carpathian arc toward the basin center. One major delta system moved in from the NW and another from the NE (BÉRCZI and PHILLIPS, 1985), but also smaller delta systems may have developed from other directions.

Figure 3.4 The Great Hungarian Plain's Neogene generalized stratigraphy and hydrostratigraphy, hydrocarbon system elements (seal/reservoir/source rocks), and the main tectonic events (also based on TÓTH and ALMÁSI, 2001; HORVÁTH, 2007)

The stratigraphic subdivision of the upward-shoaling sedimentary succession deposited by these delta systems was based on the various depositional facies of the system (GAJDOS et al., 1983; BÉRCZI et al., 1988; JUHÁSZ, 1992). However, since in a prograding delta system the facies boundaries, and thus the defined lithostratigraphic units are also time-transgressive, the succession of these units represents a general spatial relationship rather than a definite temporal relationship between the individual units.

The lithostratigraphic units of the upward-shoaling Pannonian succession, which can be fairly well separated in seismic sections and well-logs as well, are the following (Fig. 3.4 and 3.5). The basement highs are locally covered by a maximum 100 m thick coastal conglomerate and sand unit commonly referred to as the "Békés Basal Conglomerate Formation" (GAJDOS et al., 1983). The upwards subsequent Endrőd Formation consists of basal calcareous marls and clay marls. The carbonate content of the calcareous marl can reach 95-100% locally (e.g., at the Battonya High) (MAGYAR et al., 2001), and consequently the formation shows brittle deformation in these places. The average thickness of the formation is 20-300 m, which in isolated locations may reach up to 800 m. Above the basement highs, it is usually directly overlain by the Algyő Formation (delta slope facies) and it is hard to separate them (JUHÁSZ, 1992). The superjacent Szolnok Formation represents the prodelta facies generally characterized by turbidites. It occurs in the deep sub-basins reaching a thickness of up to 1000 m, but it usually pinches out along the flanks of the basement highs. The formation consists of a cyclic alternation of consolidated sandstone beds, siltstone, and clay marls (JUHÁSZ, 1992). The next Algyő Formation indicates the delta slope facies, which covers the entire Great Hungarian Plain, and its thickness ranges from 100 to 1400 m. Its matrix predominantly consists of poorly-to-well consolidated siltstone and clay marl encasing relatively more permeable sand lenses, which were deposited at the base as reworked turbidite, or in the upper part as mouth-bar rhythm and submarine channel fill (POGÁCSÁS et al., 1988). Additionally, also above basement highs the lithology of the formation can be sand dominated. Commonly, the strata dip between 5-7º, and often reach 18-20º. The top of this formation, which is actually a time-transgressive (delta slope) facies, represents the boundary between the Lower and Upper Pannonian[3]. The delta plain and delta front units of the subsequent Újfalu Formation dominated by unconsolidated coarse clastic sediments are rich

[3] The conventional Hungarian "Upper/Lower Pannonian" subdivision of the Pannonian chronostratigraphic stage (i.e. Pannonian *s.l.* = Late Miocene – Pliocene) may be confusing, because the boundary between the Lower and Upper Pannonian (s.l.) units is a time-transgressive facies boundary (i.e. the top of the Algyő Formation), and not a chronostratigraphic boundary (SZALAY and SZENTGYÖRGYI, 1988). Nevertheless, the use of this nomenclature is common and facilitates the description.

in sand bodies, which were deposited as distributary mouth bars and channel fill rhythms (POGÁCSÁS et al., 1988). Their thickness commonly reaches 20-50 m, and they often merge laterally with one another (JUHÁSZ, 1992). The alluvial plain deposits of the following Zagyva Formation contain thin bedded sequences of sand, silt, and clay, and are dominated by silt (Juhász, 1992). By the end of the Pliocene, the depositional environment became predominantly terrestrial and over 1000 m of clastic sediments (Nagyalföld Formation) were accumulated consisting of thin-bedded silts, clay, and sand.

During the Quaternary, fluvial and eolian deposits were formed (RÓNAI, 1985). As a result, loess, sand, and gravel dominate the surficial geology of the Great Hungarian Plain.

3.1.4 Hydrogeology

3.1.4.1 Hydrostratigraphy

Hydrostratigraphically, the shallower Pre-Neogene formations make up one unit, the hydraulic properties of which cannot be established reliably due to insufficient data according to TÓTH and ALMÁSI (2001), and MÁDL-SZŐNYI and TÓTH (2009). However, ALMÁSI (2001) defined this unit as an aquifer characterized by the same porosity and permeability values as that of the overlying Pre-Pannonian Aquifer. Additionally, also in most of this thesis' Study Areas (i.e. DSA and BBSA) the Pre-Neogene basement proved to be acting as an aquifer according to the pressure-elevation profiles (see also Chapters 5-6).

The Neogene basin fill has been divided into five regional units based on the chronostratigraphic divisions, lithologic facies types, and reported values of permeability (Fig. 3.4) (TÓTH and ALMÁSI, 2001; MÁDL-SZŐNYI and TÓTH, 2009). Consequently, the lithostratigraphic and hydrostratigraphic nomenclature mostly overlap each other. The lowermost unit of the basin fill is the Pre-Pannonian Aquifer including the Pre-Pannonian Neogene formations and the Békés Formation with an estimated hydraulic conductivity of $K \approx 10^{-6}$ m/s, which is primarily due to tectonic fracturing and faulting. The superjacent Endrőd Aquitard ($K \approx 10^{-9}$-10^{-8} m/s), Szolnok Aquifer ($K \approx 10^{-7}$-10^{-6} m/s), and Algyő Aquitard ($K \approx 10^{-8}$-10^{-7} m/s) can be correlated to the Endrőd, Szolnok, and Algyő Formations respectively. The uppermost Great Plain Aquifer ($K \approx 10^{-5}$ m/s) includes the Újfalu and Zagyva lithostratigraphic formations, as well as the surficial Quaternary sediments characterized by the good spatial connectivity of highly permeable bodies of silts, coarse sands, and gravels. Large amounts of

groundwater are produced from the upper part of this aquifer, while the lower part of it provides thermal water.

The dense network of structural elements, such as the most common normal faults and strike-slip fault zones, created or rejuvenated by intensive Neogene tectonics, has destroyed the regional integrity of the basement and the basin fill, both in lateral and vertical directions (HORVÁTH and CLOETINGH, 1996). These faults sometimes dissect the entire rock framework from the Pre-Neogene basement to the Quaternary (RUMPLER and HORVÁTH, 1988), and compose lithologic discontinuities, which can become highly conductive avenues to pore pressure propagation and fluid flow. Consequently, the Neogene sedimentary fill of the basin can be considered as a hydraulic continuum over the geologic time scale (TÓTH and ALMÁSI, 2001).

3.1.4.2 Fluid-potential field

Based on the interpretation of the observed subsurface fluid potential patterns, TÓTH and ALMÁSI (2001) have separated two superimposed and laterally extensive groundwater flow-domains characterized by different driving forces and water types in the Great Hungarian Plain. The lower domain of slightly saline water /total dissolved solids (TDS) content: 10,000-38,000 mg/L (MÁDL-SZŐNYI and TÓTH, 2009)/ is strongly overpressured (0.5-35 MPa in excess of hydrostatic pressure) supposedly due to the vertical compaction of the basin fill and the lateral tectonic compression of the basement (e.g., VAN BALEN and CLOETINGH, 1994; TÓTH and ALMÁSI, 2001; ALMÁSI, 2003). The dominant fluid flow direction in this system is upward. On the other hand, the upper regime of fresh water /TDS: 420-2500 mg/L (MÁDL-SZŐNYI and TÓTH, 2009)/ is driven by gravity due to the elevational differences in the topography. Namely, groundwater recharge can be observed on the topographic highs, while discharge occurs in the topographic depressions. In addition, regarding the generally small topographic relief of the Great Hungarian Plain, great parts of the plain can be characterized by low-gradient through flow conditions. The depth of the transitional zone between the overpressured and the gravity-driven flow domain is widely variable from 200 to 1700 m, and does not coincide with boundaries of litho- or hydrostratigraphic units according to TÓTH and ALMÁSI (2001). However, communication between the upper and lower domains occurs by diffusion across geological strata and/or through discrete high-permeability structural and sedimentological discontinuities. Hydraulic distinction between the two domains is possible just in those places where the two systems

represent opposite flow directions (e.g., gravitational down-flow /recharge/ coincides with overpressured up-flow). Otherwise, upward flow conditions can be observed in the entire depth interval, and only water chemical characteristics could help to define the origin of waters (i.e. Pre-Neogene basement or ground-surface), as well as the transition zone of the two flow domains (MÁDL-SZŐNYI and TÓTH, 2009).

3.1.4.3 Groundwater chemistry

In regional flow systems, typically in the direction of flow and with increasing depth the content of total dissolved solids (TDS) content increases, while the anions change from bicarbonate through sulfate to chloride, and the cations from calcium-magnesium through calcium-sodium, sodium-calcium to sodium, among other changes (CHEBOTAREV, 1955; BACK, 1966). Partly due to these systematic changes in the groundwater's chemical composition, the hydrogeochemical facies of the waters originated in the Pre-Neogene basement is of NaCl-type (ERDÉLYI, 1976; MÁDL-SZŐNYI and TÓTH, 2009) with 10,000 to 38,000 mg/L TDS. This formation fluid of the basement during upwelling comes into contact with the non-meteoric originated groundwater (VARSÁNYI and Ó. KOVÁCS, 2009) of the Neogene sedimentary basin fill, which generally belongs to the $NaHCO_3$-type, or in shallower depths with the infiltrated meteoric water of $(Ca,Mg)\text{-}(HCO_3)_2$-type (MÁDL-SZŐNYI and TÓTH, 2009).

Consequently, the elevated sodium and chloride content of groundwater usually correlate with the discharge areas and with the flow systems of the higher order. Additionally, the H_2SiO_3 content is a generally used parameter during the determination of the origin and subsurface residence time of groundwater. It can be derived from the pH and temperature dependent, time-consuming weathering of silicates. As a result, the H_2SiO_3 content of groundwater primarily depends on the time-span of rock-water interaction, and shows its average value around 17-20 mg/L (HEM, 1989; DRISCOLL, 2003). In the Great Hungarian Plain, most of the thermal waters produced from Upper Pannonian aquifers represent elevated H_2SiO_3 content (> 50 mg/L) (GÁL, 1981) compared to the previously mentioned averages.

3.1.5 Geothermics

The value of surface heat flow in the Pannonian Basin is generally between 80-100 mW/m^2, whereas in the surrounding areas it is 40-60 mW/m^2 (DÖVÉNYI and HORVÁTH, 1988;

LENKEY, 1999). The geothermal gradient commonly reaches 50-60 ºC/km, which almost double the value of the average continental thermal gradient (30 ºC/km) (OTTLIK et al., 1981; DÖVÉNYI and HORVÁTH, 1988). The annual average surface temperature is around 11 ºC (RADÓ, 1974a,b,c). The most significant heat source in the Pannonian Basin is related to the moderate crust (~25 km), and drastic mantle lithosphere (~60 km) thinning (STEGENA et al., 1975; HORVÁTH et al. 1979; HORVÁTH, 1993).

The effects of groundwater flow on the temperature and heat flow distribution in Hungary were discussed in several earlier studies, and they were also evaluated quantitatively at local scale (i.e., < 100 km^2) in thermal karstic aquifers, Quaternary-Neogene sandstone aquifers, and hydrocarbon reservoirs (e.g., STEGENA, 1958, 1982, 1989; VÖLGYI, 1977; ALFÖLDI et al., 1978; KORIM, 1994; HORVÁTH et al., 1979; OTTLIK et al., 1981; DÖVÉNYI et al., 1983; RÓNAI, 1985). LENKEY (1999) did the first regional scale quantitative modeling study on the effects of groundwater flow on the thermal field concluding that within the zone of abnormally high fluid pressures, heat transport is achieved by conduction, assuming that fluid flow is driven by vertical compaction (LENKEY, 1999). Also according to ALMÁSI (2001) the dominant heat transfer mechanism at the regional scale in the Great Hungarian Plain is conduction, while heat distribution is controlled by the rock framework's thermal conductivity, and by the groundwater flow systems. Generally, the average surface heat flow correlates well with the complex topography of the high thermal conductivity Pre-Neogene basement. Additionally, in the vicinity of basement highs underneath recharge areas, the surface heat flow may not always reflect possible cooling effects of descending meteoric water compared to adjacent areas, because of the overwhelming influence of the proximity of the basal heat source (ALMÁSI, 2001).

3.1.6 Petroleum system

3.1.6.1 Source, sealing, and reservoir rocks

In the Pannonian Basin, the predominant source rocks are of Middle and Late Miocene (Lower Pannonian) age (Fig. 3.4 and 3.5). These are the gas-prone terrestrial pelitic rocks deposited in delta slope (Algyő Formation) and delta plain (Újfalu Formation) environment, and the gas and oil prone marls deposited in marine and deep basin environment (Middle Miocene rocks, Endrőd Formation). Generally, the Mesozoic and Paleogene source rocks are ignored because the hydrocarbons generated from them were most likely lost during the

process of basin evolution (SOMFAI, 1994). In the Neogene source rocks, 80% of the kerogen is of Type III and 20% is of Type II (GEIGER et al., 1991) while the total organic carbon content (TOC) is ranging between 0.5-1.5% (SZALAY, 1988). Maturation of Neogene source rocks in the Pannonian Basin is an ongoing process, which commenced about 9.5-6.5 Ma (SZALAY, 1988), and significantly accelerated by the large basal heat flow (80-100 mW/m^2) (DÖVÉNYI and HORVÁTH, 1988). The source rocks found at depths shallower than 1500 m (Újfalu Formation and in some places the upper part of Algyő Formation) are generally immature, with a vitrinite reflectance of $R_0 < 0.4\%$ (SZALAY, 1988), while the organic matter is in the process of biochemical degradation (SOMFAI, 1994). Diagenetic gas is being generated from source rocks with a maturation level of $R_0 = 0.4\text{-}0.6\%$ (CLAYTON et al., 1994). Regarding the catagenetic hydrocarbons generated by thermal metamorphosis of organic matter, the Middle Miocene source rocks along the axis of the deep troughs are within the zone of dry gas generation ($R_0 > 2\%$, ~4100-5600 m depth), while source rocks of the lower part of the Lower Pannonian (Endrőd Formation) are within the zone of wet gas generation ($R_0 = 1.3\text{-}2\%$, ~3400-4500 m depth), and source rocks of the upper part of the Lower Pannonian (Szolnok Formation, and the lower part of the Algyő Formation) are within the zone of oil generation ($R_0 = 0.6\text{-}1.3\%$, ~2000-4000 m depth) (Fig. 3.5) (SZALAY, 1988). Additionally, many reservoirs have high temperatures, ranging between 100-180 ºC and suggesting that "in-reservoir maturation" may also be a possible process (SZALAY and KONCZ, 1993). In conclusion, the hydrocarbons generated from the mature source rocks are ~67% gas (90% CH_4, 10% CO_2 and N_2), and ~33% oil (mostly paraffinic, with little S_2, and density in the range of 700-900 kg/m^3) (GEIGER et al., 1991).

Generally, the potential source rocks are also excellent sealing rocks for petroleum reservoirs. By and large, there are two regionally traceable sealing zones in the Neogene basin fill (Fig. 3.4 and 3.5), namely the Endrőd and Algyő Formations, which in fact show significant heterogeneities.

Ages of reservoir rocks vary from Palaeozoic to Pliocene (Fig. 3.4 and 3.5). The upper (~1000 m) fractured and fissured portion of the Pre-Neogene basement rocks, as well as the conglomerates at the Pannonian base (Békés Formation) have quite good reservoir characteristics. The Endrőd Formation, as well as the Algyő Formation also store hydrocarbons in the basal marls (e.g., on the Battonya High at about 2000 m depth), and in sandstone lenses, respectively. However, the most significant Pannonian reservoir zones can be found in the Szolnok and Újfalu Formations, although the thickness of the individual

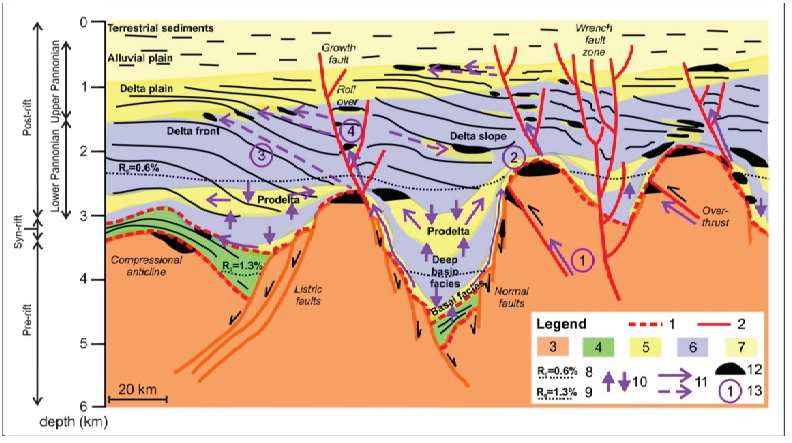

Figure 3.5 Generalized diagram of the Great Hungarian Plain's petroleum system (based on POGÁCSÁS et al., 1988, Fig. 23; SZALAY, 1988; JUHÁSZ, 1992; SZALAY and KONCZ, 1993). Legend: 1 – unconformity; 2 – fault; 3 – Pre-Neogene (pre-rift) basement rocks; 4 – Middle Miocene (syn-rift) formations; 5 – carrier beds and reservoirs; 6 – source and sealing rocks; 7 – high-permeability formations with low hydrocarbon potential; 8 – line of constant vitrinite reflectance (R_0=0.6%), oil generation line; 9 – line of constant vitrinite reflectance (R_0=1.3%), wet gas birth line; 10 – primary hydrocarbon migration; 11 – secondary hydrocarbon migration; 12 – hydrocarbon accumulation; 13 – basic types of secondary hydrocarbon migration systems by SZALAY and KONCZ (1993) (for details see the text). Depositional environments are represented by the following stratigraphic units: basal facies – Békés (Basal Conglomerate) Formation (part of the Pre-Pannonian Aquifer); deep basin facies – Endrőd Formation (Aquitard); prodelta – Szolnok Formation (Aquifer); delta slope – Algyő Formation (Aquitard); delta front and delta plain – Újfalu Formation (part of the Great Plain Aquifer); alluvial plain – Zagyva Formation (part of the Great Plain Aquifer); terrestrial facies – Quaternary formations (part of the Great Plain Aquifer).

sandstone layers rarely exceeds 70 m also in these zones. Finally, the thin bedded sequences of sand in the Zagyva Formation contain only small hydrocarbon fields (e.g., Battonya) (GEIGER et al., 1991).

3.1.6.2 Accumulations

The pattern of hydrocarbon field distribution in the Great Hungarian Plain correlates remarkably well with the location of basement highs and the associated anticline structures in the Neogene sediments (Fig. 3.5) (POGÁCSÁS, 1990; SZALAY and KONCZ, 1993). Most of the wildcat wells were drilled to a depth interval of 600 to 3200 m, and predominantly on basement highs, anticline structures, and stratigraphic traps (e.g., pinch outs) previously identified on seismic profiles. Prospecting of the more complex stratigraphic and facies anomaly traps, as well as that of the deeper, fractured basement reservoirs came to the front in the 1980's (POGÁCSÁS, 1990). Eventually, the potential reservoir quality strata in the deep basinal structures are in the forefront of the present exploration (e.g., in the Makó Trough).

The thus recognized hydrocarbon traps being typical of the Great Hungarian Plain are generally related to (POGÁCSÁS et al., 1988) paleogeomorphic domes (e.g., Pre-Neogene basement highs); deposited arches (e.g. syntectonically above basement highs); thrust faults; block faults; growth faults; 'roll-over' anticlines; wrench faults; unconformities; turbidite pinch outs; basal transgressive sands and conglomerates; prodelta – delta slope fans, slumps, canyon fills; delta front sands; and delta plain bars (Fig. 3.5).

Most of the known petroleum accumulations are located above the oil generation line (SZALAY, 1988), and consist mainly of gas (often with condensate) and secondarily of oil, but mixed oil and gas accumulations are also common. Several gas accumulations are characterized by the presence of "inert gases" like CO_2, N_2, and H_2S. CO_2 is the dominant inert gas, which may reach a concentration of 20-90 volume % (GEIGER et al., 1991). The Algyő field (Fig. 3.6) is the largest mixed hydrocarbon accumulation in Hungary. At the time of its discovery, in the early 1960's, the estimated amount of "original oil in place" was 76 million metric tons, while the estimated amount of "original gas in place" was 109 billion m^3 (SOMFAI, 1994). Other large oil fields, such as Szeged, Demjén, Szank, Szeghalom, Battonya, and Pusztaföldvár (Fig. 3.6), had each approximately 6-9 million metric tons of original oil in place. The original gas in place of other important gas fields ranges between 29-4 billion m^3 (e.g. Hajdúszoboszló, Pusztaföldvár, Szeghalom, Üllés, Szank, Nagykörű, Sarkadkeresztúr,

and Endrőd; see Fig. 3.6) (DANK, 1988). Most of the other known accumulations are about two orders of magnitude smaller than the ones mentioned above.

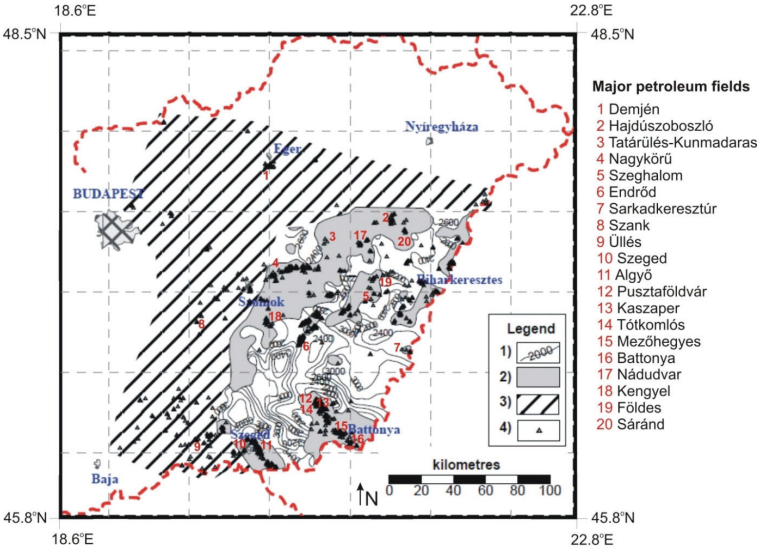

Figure 3.6 Distribution of known hydrocarbon accumulations and their spatial relation with the top of the oil generation zone in the Great-Hungarian Plain (modified after ALMÁSI, 2001, Fig. 2.27). Legend: 1 – depth of the oil generation line (m); 2 – basement highs covered by immature reservoir and source rocks; 3 – areas of un-mapped maturity conditions; 4 – petroleum accumulation

3.1.6.4 Migration

Having seen the areal distribution of source rocks and hydrocarbon accumulations, as well as the depth distribution of the oil and gas generation zones, it also has to be considered in order to understand the characteristic migration patterns that all of the potentially mature source rocks are found below a depth of about 1800 m, i.e. in the overpressured zone. Based on these observations, it could be established that hydrocarbons generated in the deep troughs ("hydrocarbon kitchens") were expelled vertically (upward and downward) from the overpressured source rocks into the adjacent carrier beds (primary migration), in which they were transported radially outward, toward the flanks and tops of basement highs (secondary migration) (Fig. 3.5) (HORVÁTH et al., 1988; SZALAY, 1988; SZALAY and KONCZ, 1993).

Thus, the superhydrostatic pressures are thought to be the principal driving force also for vertical and lateral hydrocarbon migration (SZALAY, 1988; SZALAY and KONCZ, 1993). For that reason, according to HORVÁTH et al. (1988) most of the oil and gas fields in the Great Hungarian Plain can be found above basement highs, or locally within the basement, and above the oil generation line (SZALAY, 1988).

However, according to TÓTH and ALMÁSI (2001), the lateral components of the present-day hydraulic gradients are directing fluids toward the centers of the deep sub-basins. Consequently, they suggested that the overpressure is dominantly generated by lateral tectonic compression, which can be derived from the present-day stress regime characterized by changing from extension to compression from Pliocene times (see also Chapter 3.1.2).

Considering these conflicting theories, it could be established that fluid migration pathways may be controlled by complex mechanisms, the significance of that can change in space and time as well. Accordingly, it is also worth reckoning with the remigration of pre-existent hydrocarbon accumulations simultaneously with the changing stress regime.

Finally, either way, the major avenues of secondary hydrocarbon migration are the regional unconformity between the Pre-Pannonian and Pannonian units, as well as the Pre-Neogene and Neogene fault zones (Fig. 3.5) (DANK, 1988; POGÁCSÁS et al., 1994). Further migration zones are provided by the fractured and weathered surface of the Pre-Neogene basement, the prodelta turbidites, as well as less frequently the delta slope and delta front sediments (Fig. 3.5).

3.2 Derecske Trough and its surroundings

3.2.1 Tectonics

The Derecske Trough's pre-rift basement, which exceeds the 6500 m depth in the central part of the trough (Fig. 3.7), is composed of NW verging nappe slices. After the Cretaceous thrusting of these sheets, two further main tectonic reactivations happened in transtensional stress field, namely 1) Early to Middle Miocene normal faulting, and 2) Late Miocene through Quaternary to present-day strike-slip faulting (WINDHOFFER and BADA, 2005).

The Derecske Trough opened as a pull-apart basin in a shear zone between two wrench fault zones (Fig. 3.7). The strike-slip movement started in the Middle Miocene has continued, probably with less activity, until recent times as well indicated by the faults

(mainly negative flower structures), which cut even the uppermost Pannonian strata (Fig. 3.8) (RUMPLER and HORVÁTH, 1988). According to WINDHOFFER et al. (2005), also the basement's overpressure may contribute to the reactivation of faults, and consequently any one of the neotectonic wrench fault zones could be reactivated.

The NE-SW trending left lateral strike-slip fault zone bounding the northern edge of the trough is mostly extensional and right stepping, while the total displacement along the fault system is about 4.5-6 km. Probable migration of the hydrocarbons accumulated in the tectonic zone, as well as the present conduit or barrier behaviour of the structural elements refer to that the tectonic movements did not happen continuously, but rather periodically (LEMBERKOVICS et al., 2005).

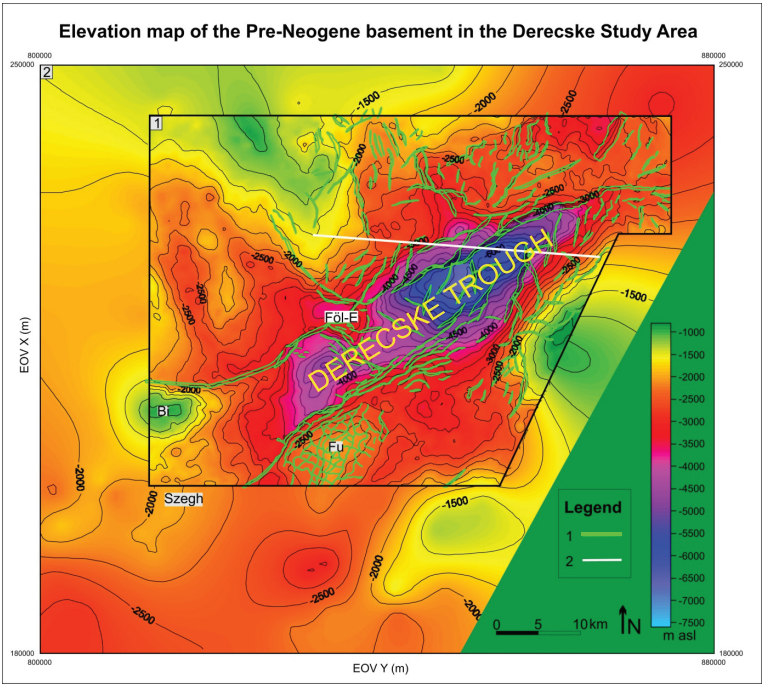

Figure 3.7 Elevation map of the Pre-Neogene basement in the Derecske Study Area combining (1) the map of the MOL Plc. regarding its current exploring area (MOL Plc., 2009*), and (2) the map constructed for the total DSA from borehole data. Legend: 1 – fault, 2 – trace line of cross-section represented in Fig 3.8. Abbreviations: Fu – Furta High, Bi – Biharnagybajom High, Szegh – Szeghalom High, Föl-E – Földes-East

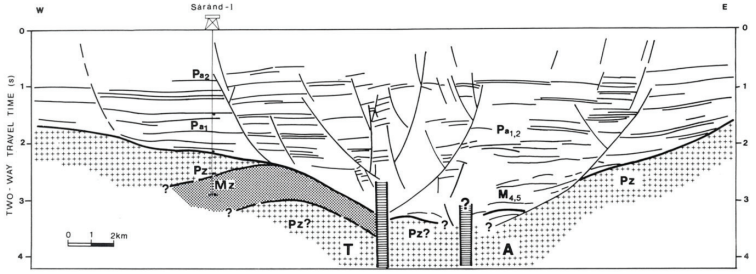

Figure 3.8 Interpreted reflection seismic profile across the Derecske Trough (RUMPLER and HORVÁTH, 1988, Fig. 9). For location see Fig. 3.7. Abbreviations: Pa_2 – Upper Pannonian (s.l.), Pa_1 – lower Pannonian (s.l.), $M_{4,5}$ – Badenian and Sarmatian, Mz – Mesozoic, Pz – Palaeozoic. T and A indicate strike-slip displacement toward and away from the viewer, respectively.

The wrench fault zone on the southern-southeastern margin of the trough is less sharp, possesses less structural elements, but southward virgation through "foiled" normal faults from the middle section of the trough. Eventually, the northern and southern main fault zones form a junction in the northern third of the trough in its axis (LEMBERKOVICS et al., 2005).

In the surroundings of the Derecske Trough, several local basement highs can be found. Among them, the Furta, Szeghalom, and Biharnagybajom highs will be in particular interest of the dissertation (Fig. 3.7). The Pre-Neogene basement approaches the land surface at these highs by about 2500 m, 2000 m, and 1000 m, respectively. The Furta high (on the southern margin of the Derecske Trough) is densely covered with a network of basement faults, while the overlying Pannonian succession is almost undeformed. The two other and really shallow highs belong to a chain of Middle Miocene extensional exhumations of the crystalline metamorphic basement (further example is the Szarvas High discussed later (see Chapter 3.3.1)) (M. TÓTH et al., 2003). In case of the Biharnagybajom high's tectonics, the northern main fault zone of the Derecske Trough dominates leaning on the northern side of the high, and continuing as a negative flower structure in the Pannonian strata above the high (POGÁCSÁS et al., 1989). On the Szeghalom high, at the western termination of the Derecske Trough, marginal growth faults are frequent (M. TÓTH et al., 2003).

3.2.2 Stratigraphy, Hydrostratigraphy

The Pre-Neogene basement consists of mainly Palaeozoic metamorphic rocks, as well as sparsely Mesozoic carbonate rocks and volcano-sediments (HAAS et al., 2010).

The Pre-Pannonian Miocene formations usually can be found in the deeper depressions, such as in the northeastern and southwestern sub-basins of the Trough (Fig. 3.7). Hydrostratigraphically these strata build-up the Pre-Pannonian Aquifer, and usually behave similar to the Pre-Neogene formations (see also Chapter 5).

The Pannonian delta system arrived at the Trough from the NE (BÉRCZI and PHILLIPS, 1985), and the Pannonian succession can reach the 6000 m in thickness showing the further distinctive characteristics (see also A-Table 5.1) comparing to the general features described in Chapters 3.1.3. Areal extension of the Endrőd Formation/Aquitard is restricted to the deepest, central part of the trough. Lithologically, low-permeability clay marls dominate the formation, which consequently shows effective aquitard characteristics. Also the Szolnok Formation/Aquifer can be found in the axial, central part of the trough where it can reach the 1000 m in thickness (Derecske-1 well: 1020m), while pinches out northward toward the trough's margins (JUHÁSZ, 1992). Contrarily, in the southern surroundings of the trough it can be observed in (maximum) 500 m thickness. Compared to the Szolnok Formation/Aquifer in the Békés Basin, this facies is coarser-grained probably due to the closer sediment supply, as well as it has higher porosity and permeability (see also A-Table 5.2). The generally 200-1000 m thick Algyő Formation/Aquitard in the NE part of the trough contains also the pelitic overbank and slope apron deposits of the deep water facies (JUHÁSZ, 1992). Consequently in these areas, and also where the Szolnok Formation is missing (usually in the marginal areas), the Algyő and Endrőd Formations could build-up one thick and effective low-permeability (i.e. aquitard) unit. However, in some places, such as above basement highs and in their forelands facing the direction of sediment transport, sand lenses and intercalations can be frequently observed. Additionally, on the northern flank of the Trough, the formation is more densely cut by fractures and faults than in the south of the Trough. In conclusion, the Algyő Aquitard, which is generally thought to be a regionally extensive and effective low-permeability unit, is actually quite heterogeneous in the region of the Derecske Trough. Additionally, it is also definitely more pelitic and thinner above the Szeghalom and Biharnagybajom Highs due to their great distance from the NE sediment supply. The Újfalu Formation's delta front sediments can reach the 1000 m thickness in a well-defined area in the Trough and in the north of that where a wide morphological shelf formed around 6.8-9.1 Ma (JUHÁSZ et al., 2007). The Zagyva Formation usually pinches out where the Újfalu Formation represents this extreme thickness. Hydrostratigraphically, the Újfalu, Zagyva, and Nagyalföld Formations build-up the Great Plain Aquifer unit, which can reach the 2000 m thickness as well.

3.2.3 Hydrogeology, Geothermics

TÓTH and ALMÁSI (2001), and ALMÁSI (2001) established in their regional (Great Hungarian Plain) scale hydraulic study that the gravitational flow system represents recharge conditions in most of the DSA, and discharge conditions in the SW part of it. Furthermore, the overpressured flow system shows regional upwelling, while fluid-potential anomalies can be observed around Biharkeresztes.

Regarding hydrochemistry, as a result of a regional scale project VARSÁNYI and Ó. KOVÁCS (2009) stated that groundwaters produced from 650-1350 m depth interval (Great Plain Aquifer) around Püspökladány, Földes, and Hajdúszoboszló (Fig. 3.1) are Cl^- type waters, which show significant enrichment in oxygen and hydrogen heavy isotopes. The authors distinguished these waters as originated from "above elevated basement blocks" from the HCO_3^- type groundwaters of the "deep sub-basins" such as the Békés Basin and Makó Trough. The differentiation was based on the hydraulic role of the Algyő Aquitard, which is usually thinner and less homogeneous above the basement highs than in the sub-basins.

The average surface heat flow value in the region is higher than 100 mW/m^2 (HORVÁTH et al., 2004), while among the studied areas the highest geothermal gradient was observed in the Derecske Trough (Derecske-1 well) as 44,3°C/km (DÖVÉNYI and HORVÁTH, 1988). Additionally, URBANCSEK (1965) has already explained the occurrence of geothermal anomalies around Szeghalom, Furta, and Berettyóújfalu (Fig. 3.1) by the presence of structural lines.

Several thermal water occurrences are known and exploited in the area, such as in Hajdúszoboszló (water temperature (WT): 73°C; water salinity (WS): 5 g/l; reservoir depth (RD): ~400-1000 m), Debrecen (WT: 68°C; WS: 4.6 g/l; RD: ~1100 m), and Berettyóújfalu (WT: 63°C; WS: 2.3 g/l; RD: ~1400 m) (Fig. 3.1) (GÁL, 1981). Interestingly, in the first two cases the thermal water resources were discovered during hydrocarbon exploration by Ferenc Pávai-Vajna in 1925 and 1929-33, respectively.

3.2.4 Hydrocarbon accumulations

The most favorable conditions for hydrocarbon generation in the Great Hungarian Plain now exist in the Derecske Trough where the Middle Miocene and part of the lowermost Pannonian source rocks are within the dry gas generation zone, whereas much of the Lower Pannonian source rocks has already reached the zone of oil generation. Furthermore, also the

pelite/psammite ratio (>0.5) and the average organic carbon content (0.86%) of the Lower Pannonian source rocks in the Derecske Trough (SZALAY, 1988) represent the highest values in the Study Areas.

On the other hand, the role of strike-slip faults in hydrocarbon entrapment first came to the front of interest in Hungary during the Derecske Trough's exploration. Hydrocarbon (mainly gas) fields can be found in the post-rift wrench fault zones bounding the trough, and most of them have pools in the Upper Pannonian strata (above the top of the Algyő Aquitard) as well. Consequently, these indicate the role of faults in hydrocarbon migration from the (Pre-Pannonian) Miocene source rocks towards the Pannonian reservoirs, as well as suggest the existence of a regional hydrocarbon accumulating belt along the Pannonian-Quaternary strike-slip fault zones (POGÁCSÁS, 1990).

Also the basement highs in the south of the Derecske Trough (e.g., Biharkeresztes, Biharnagybajom) possess significant hydrocarbon accumulations in Pre-Pannonian Miocene and Lower Pannonian reservoirs, while the oil field of Szeghalom accumulated particularly in the Pre-Neogene basement high (Fig. 3.1 and 3.7). These accumulations contain particularly gases, usually with high CO_2 content (KÁROLY KISS, MOL Plc., personal communication, 2009).

Finally, the gas field of Hajdúszoboszló (Fig. 3.1) is one of the greatest in Hungary with Paleogene-Cretaceous flysch, (Pre-Pannonian) Miocene Sarmatian carbonate, and Lower Pannonian sandstone reservoirs (DANK, 1990).

3.3 Battonya High and its surroundings

3.3.1 Tectonics

The elevated Pre-Neogene basement approaches the land surface by about 1000 m at the (Hungarian) apical part of the high, then gradually subsides northeastward below 3000 m depth, while east- and westward into the Békés Basin and Makó Trough, respectively (Fig. 3.9).

The Pre-Neogene basement of the narrow ridge is characterized by NE-SW striking, stacking up, imbricated structures (GROW et al., 1989) containing two major south dipping Cretaceous reverse faults bordering allochthonous nappes, which faults were extensionally reactivated during Miocene times (POGÁCSÁS, 1990). According to TARI et al. (1999), the Battonya unit slid down from above the Algyő High's strata (in the east of its present

position) (Fig. 3.10) during the Miocene (Karpatian-Badenian) extension, while the major detachment faults and the further joined normal faults cut through the plains of the Cretaceous thrust sheets as well sinking into the deeper crust. Furthermore, in the mostly undisturbed Pannonian strata, only the rejuvenations of these normal faults, as well as some growth faults along the ridge's margins can be observed.

Besides, on the northwestern subsiding flank of the high (around Fábiánsebestyén, Nagyszénás, and Orosháza; Pre-Neogene basement depth around 3000m (Fig. 3.9)) at least two transform faults can be found sinking into greater than 10 km depth. These NE-SW and NW-SE striking fault zones related to extensional tectonics may intersect each other near to Fábiánsebestyén. However, there has not been observed any structural element in the Pannonian or younger strata in the region yet (PAP, 1993).

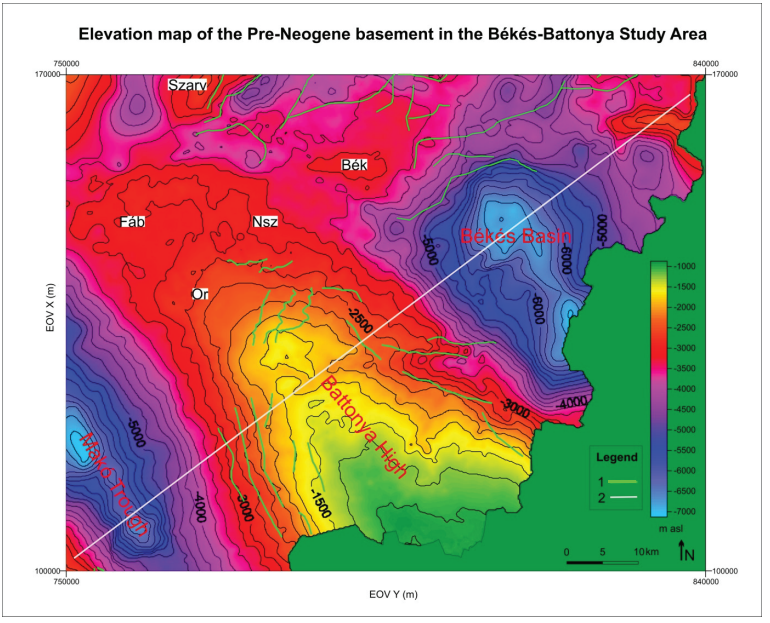

Figure 3.9 Elevation map of the Pre-Neogene basement in the Békés-Battonya Study Area (MOL Plc., 2011*). Legend: 1 – fault, 2 – trace line of cross-section represented in Fig 3.10. Abbreviations: Szarv – Szarvas High, Bék – Békés High, Fáb – Fábiánsebestyén, Nsz – Nagyszénás, Or - Orosháza

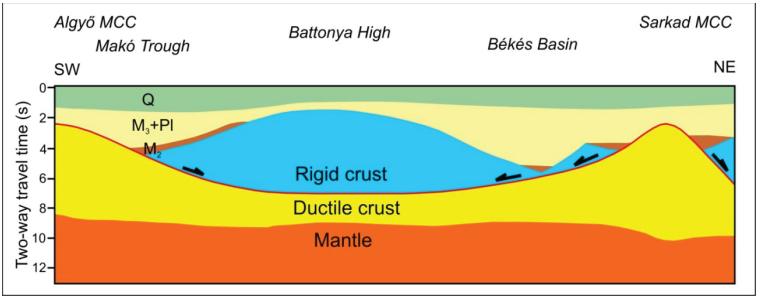

Figure 3.10 Interpreted reflection seismic profile across the Makó Trough, Battonya High, and Békés Basin (HORVÁTH, 2007, Fig. 79). For location see Fig. 3.9. Abbreviations: M_2 – Middle Miocene, M_3-Pl – Upper Miocene – Pliocene, Q – Quaternary, MCC – metamorphic core complex (~exhumation of the crystalline metamorphic basement)

Finally, the Battonya High is a currently uplifting area due to the basin inversion started at the end of the Miocene. Interestingly, the deeper northwestern part of the Pre-Neogene basement is ascending more intensively than the southeastern part, which is in a higher position at present (VIKTOR SŐREG, MOL Plc., personal communication, 2011).

In addition, in the north of the so-called Fábiánsebestyén-Nagyszénás-Orosháza Area (defined above), a Pre-Neogene basement high in the vicinity of Szarvas (Fig. 3.9) belonging to the earlier mentioned chain of Middle Miocene extensional exhumations of the crystalline metamorphic basement (see Chapter 3.2.1) (M. TÓTH et al., 2003) is worth being mentioned. Also around this basement high approaching the land surface by about 3000 m, mainly marginal and growth faults occur in the overlying Pannonian strata.

3.3.2 Stratigraphy, Hydrostratigraphy

The Pre-Neogene basement consists of mainly Mesozoic carbonate and Palaeozoic metamorphic rocks (HAAS et al., 2010). Pre-Pannonian Miocene formations usually can be found on the flanks of the Battonya High, while nearly missing on the top of the structure. Hydrostratigraphically these strata build-up the Pre-Pannonian Aquifer, which usually behaves similar to the Pre-Neogene formations (see also Chapter 5.3.1).

The Pannonian delta system arrived at the Battonya High at latest, thus this area was the last unfilled part of the Lake Pannon (inside the present borders of Hungary). Consequently, the calcareous marl ("Tótkomlós") member of the Endrőd Formation/Aquitard

deposited in a starving basin far from the siliciclastic sediment sources. This condensed formation can be found in the whole area of the Battonya High, but usually only in a very thin (see also A-Table 5.1) and areally diachronous layer, which was deposited between 11.5-8 Ma (i.e. in some places 10 m thick calcareous marl could represent 2.5 million year-long sedimentation). However, in the NE of the high's summit zone, thickening of the Tótkomlós Member can be observed, while in the summit zone also carbonate facies occur where (particularly around Battonya and Tótkomlós) the carbonate content of the calcareous marl could reach the 95-100% (MAGYAR et al., 2001). Consequently, the formation is usually strongly fissured and fractured in these areas representing rather aquifer than aquitard features. Besides, in the Fábiánsebestyén-Nagyszénás-Orosháza Area, as well as above the high around Szarvas the clayey marl content of the Endrőd Formation/Aquitard is higher. The Szolnok Formation/Aquifer is insignificant or missing in the summit zone of the high, however it is thickening toward the surrounding basins (i.e. Békés Basin in the east, Makó Trough in the west, the Fábiánsebestyén-Nagyszénás-Orosháza Area in the north, as well as the high around Szarvas in the far north) where it usually represents low-permeability conditions. The Algyő Formation/Aquitard contains more sandstone intercalations above the ridge region (K. JUHÁSZ et al., 1989), and consequently the Algyő Aquitard is more heterogeneous than usually.

3.3.3 Hydrogeology, Geothermics

TÓTH and ALMÁSI (2001), and ALMÁSI (2001) established in their regional (Great Hungarian Plain) scale hydraulic study that the gravitational flow system represents recharge conditions along the Battonya High, and midline areas in its surroundings. Furthermore, the overpressured flow system shows regional upwelling, while moderate fluid-potential anomalies can be observed along the high.

Regarding the hydrochemical features, the previously mentioned study of (see also Chapter 3.2.3), VARSÁNYI et al. (1997, 1999), and VARSÁNYI and Ó. KOVÁCS (2009) rated the water samples of the Battonya High (from 650-1350 m depth interval) into the HCO_3^- type groundwater group of the "deep sub-basins", which can be characterized also by relatively lesser enrichment in oxygen and hydrogen heavy isotopes. The contradiction between the basement high character of the Battonya High and the rating of its groundwater into the type of "deep sub-basins" (characterized by thick and homogeneous Algyő Aquitard unit) is suppressed and remained unresolved, however this theory was based on only four samples.

The average surface heat flow value in the region is higher than 110 mW/m^2 (HORVÁTH et al., 2004), while the geothermal gradient in the Tótkomlós-I well was determined as 41,6°C/km (DÖVÉNYI and HORVÁTH, 1988). Several thermal water occurrences are known and exploited in the area, such as in Orosháza-Gyopárosfürdő (water temperature (WT): 46°C; water salinity (WS): 1.6-1.7 g/l; reservoir depth (RD): 900m), Nagyszénás (WT: 94°C; WS: 5.2 g/l; RD: 3000 m), Mezőkovácsháza (WT: 63°C; WS: 3.3 g/l; RD: ~1500m), Tótkomlós (WT: 56°C; WS: 3.6 g/l; RD: ~1960 m), Szarvas (WT: 36°C; RD: 570 m) (Fig. 3.2) (GÁL, 1981). Interestingly, regarding the temperature and depth values, water salinities are relatively low.

However, URBANCSEK (1965) observed relatively high NaCl contents in the groundwater around Gádoros and Csanádapáca (Fig. 3.2), and explained the phenomena by the presence of structural lines. In the same area, in wells around Fábiánsebestyén and Nagyszénás (Fig. 3.2 and 3.9) high-temperature steam inflows were observed from Triassic brecciated dolomites about 3000-4300 m depth interval. For instance, from the a well around Fábiánsebestyén 3698-4239 m deep section 5000-8500 m^3/day water of 160°C containing 20% steam inflow passed through 1.5 month, which refers to an extensive reservoir. The water's salinity was > 25 g/l and dominated by NaCl. Also these hot steam rises could be interpreted most probably as upwellings along tectonic belts (PAP, 1993).

3.3.4 Hydrocarbon accumulations

The extensive hydrocarbon fields of Pusztaföldvár, Tótkomlós, and Battonya (Fig. 3.6) located above the basement high consists of Lower and Upper Pannonian reservoirs that can reach also the 100 m thickness. Most of the pools have active edge and bottom water pressure, while water invasion is a usual problem in the producing wells (VÁNDORFI, 1965; JÁRAI, 1982). Additionally, in the Tótkomlós and Battonya-East fields several wells perished in gas blowouts (DANK, 1990), which could be explained by hitting overpressured strata (BUDA, 1986; BUDA et al., 2004). The Triassic brecciated dolomites representing the best reservoir characteristics among the Pre-Neogene formations proved to be barren for hydrocarbons in the Fábiánsebestyén-Nagyszénás-Orosháza Area (Fig. 3.9) though significant hot steam resources were explored (see also Chapter 3.3.3).

3.4 Békés Basin

3.4.1 Tectonics

The Békés Basin (Fig. 3.9) as a structural unit in the south of the Derecske Trough and in the east of the Battonya High contains over 6500 m Neogene sedimentary rocks. The still ongoing subsidence of the basin started in the Early Badenian (SZENTGYÖRGYI, 1989).

The southern half of the basin is underlain by multiple Cretaceous allochtonous nappes, which were modified again by Miocene rifting (extension) and strike-slip movements. Consequently, the depression consists of extensional or oblique-extensional asymmetric grabens suggesting control by east and northeast trending strike-slip faults (GROW et al., 1989). However, beyond the rejuvenations of the surrounding NW and E-SE striking wrench fault zones on the northern and western margins of the basin, as well as some growth faults also located on the margins, the Pannonian succession is relatively undisturbed.

Additionally, a local basement high can be found on the northwestern margin of the Békés Basin as well (Fig. 3.9). Also around this henceforth so-called Békés High approaching the land surface by about 3000 m, mainly marginal and growth faults occur in the overlying Pannonian strata, similarly to the Szarvas High.

3.4.2 Stratigraphy, Hydrostratigraphy

Beside the previously described marginal areas (see also Chapter 3.3.2), the Pre-Neogene basement's lithological build-up is unknown in the deepest central and southeastern part of the basin (SZENTGYÖRGYI, 1989; HAAS et al., 2010). The average thickness of the Pre-Pannonian Miocene formations is about 100 m indicating that this area was a starving basin during the rifting phase far from the sediment sources (but also significant amount of later erosion could be made probable) (GROW et al., 1989). The basal marl of the Endrőd Formation/Aquitard is highly fractured in several wells (RÉVÉSZ et al., 1989). During the Pannonian at least two delta systems arrived in the basin, one from NW, and another from NE direction. Sediments of the latter system are finer grained, more pelitic that can be observed particularly in the NE parts of the basin (and around the Szeghalom High as well) where the sandstone bodies of the Szolnok Formation are intercalated with the pelitic prodelta sediments of the delta system arrived from the NE. In these areas the Algyő Formation/Aquitard includes the delta slope, prodelta, and basal marl formations as well, that cannot be distinguished from each other lithologically or by well-logs (K. JUHÁSZ et al., 1989).

Furthermore, in the central parts of the basin where the Szolnok Formation/Aquifer in a thickness of about 700-800 m (see also A-Table 5.1) consists of sandstones it represents in fact low-permeability conditions. (Similar conditions can be observed in the Fábiánsebestyén-Nagyszénás-Orosháza Area, as well as around the Szarvas and Békés Highs.) It can probably due to i) the finer grain size of the sandstones deposited from the distal part of the delta system far from the sediment sources, as well as to ii) the mechanical and chemical compaction. The thickness of the Great Plain Aquifer reaches its maximum (> 3000 m) in this basin among the Study Areas.

3.4.3 Hydrogeology, Geothermics, Hydrocarbon accumulations

TÓTH and ALMÁSI (2001), and ALMÁSI (2001) established that the gravitational flow system represents discharge conditions, and also midline areas in the south of the Basin. However, they could not draw reliable conclusions about the overpressured flow system due to the lack of data. Regarding the hydrochemical features, the already mentioned study of VARSÁNYI and Ó. KOVÁCS (2009) (see also Chapter 3.2.3) rated the water samples of the Békés Basin originated from above the top of the Algyő Aquitard into the HCO_3^- type groundwater group of the "deep sub-basins", which can be characterized also by relatively lesser enrichment in oxygen and hydrogen heavy isotopes. That can be explained by the effective flow barrier behaviour of the Algyő Aquitard, which impede the upwelling of the high salinity groundwater of the overpressured system. In addition, the occasionally high (dissolved) methane content of the water wells around Békés and Békéscsaba is a well-known phenomenon.

The average surface heat flow value in the region is 80-100 mW/m^2 (HORVÁTH et al., 2004). Several thermal water occurrences are also known and exploited in the area, such as in Békés (water temperature (WT): 51°C; water salinity (WS): 1.7-2 g/l; reservoir depth (RD): 700-800 m), Békéscsaba (WT: 76°C; WS: 2.5 g/l), Gyula (WT: 93°C; WS: 5.1 g/l; RD: ~1970 m) (Fig. 3.2) (GÁL, 1981).

Hydrocarbon accumulations in commercial quantities are only known from the basement highs framing the basin to the north and northwest (e.g., Sarkadkeresztúr (Fig. 3.6), Szarvas and Békés Highs (Fig. 3.9)).

4 APPLIED DATA AND METHODS

In order to achieve the study objectives, the following major characteristics of the research areas had to be determined:

i) (hydro)geological build-up: tectonics, stratigraphy, hydrostratigraphy
ii) hydraulic/hydrodynamic conditions: fluid flow systems, directions of fluid flow driving forces, possible migration pathways and fluid traps
iii) geothermal conditions: regional distribution of temperature values
iv) hydrochemical conditions: regional distribution of salinity

In other words, during data analysis and interpretation, first the geological (stratigraphic and tectonic), and then the hydrostratigraphic build-up of the Study Areas had to be determined as a base for the further data analysis and interpretation. Subsequently, the main objective was the mapping of groundwater flow systems by interpreting hydraulic data, because moving groundwater as a geologic agent determine the distribution of temperature, salinity, hydrocarbon accumulations, etc. (TÓTH, 1999). Thus most time and effort were devoted to hydraulic data preparation and processing. On the other hand, the primary objectives of temperature and hydrochemical data analysis considering their reliability as well was i) the support of hydraulic interpretations, and ii) the examination of relationships among hydraulic, thermal, and hydrochemical anomalies. Applied methods were chosen and developed according to these aims.

Accordingly, the first target of my Ph.D. research work was to make up a database being suited for the proposed characterization. Regarding the task's complexity, from differing sources several data types were collected, that can be sorted into two major groups, namely well data, and seismic interpretations.

Well data were available from water and hydrocarbon wells completed in the DSA between 1891 and 2008, while in the BBSA between 1885 and 2010. The base, hydraulic, water chemical, chronostratigraphic, porosity, and permeability data, as well as the lithostratigraphic subdivision of some boreholes of the hydrocarbon wells were put at our disposal by the MOL Plc. in electronic format (MS Excel spreadsheet). The base, hydraulic, water chemical, and permeability data of the water wells were collected from the original (paper-based) well records being available at the documentation departments of the Mining and Geological Institute of Hungary, as well as of the 'VITUKI' Environmental Protection

and Water Management Research Institute Non-Profit Company. Further base and hydraulic well data were available also from the Hungarian Thermal Water Well Cadaster, which is available at the VITUKI Non Profit Company as well. Temperature data were put at our disposal from the Geothermal Database of Hungary (DÖVÉNYI et al., 2002) by László Lenkey (associate professor, ELTE Department of Geophysics and Space Science) in electronic format (text files). Finally, hydrostratigraphic data were available from ALMÁSI (2001) in electronic format (MS Excel spreadsheet). The two latter databases contain also water and hydrocarbon well data.

Considering the extension of the Study Areas, as well as the differing build-up and quality of the available data sources, organization and significant culling of the well data was required following the data acquisition. During these time-consuming processes, several overlaps and typing errors had to be cleared and revised, while on the other hand, missing data could be also recovered (into one database from another). Eventually, a set of base data for each wells were produced, containing of necessity the identifying names/numbers, EOV co-ordinates, and elevations of the rotary tables or well heads. The year of drilling and bottom depth of the wells are mostly known as well. The number of wells presenting in this data set, as well as the covered depth and drilling time intervals can be seen in Table 4.1. Preparation and processing of the further well data, such as hydraulic, water chemical and temperature data will be presented in the sub-chapters below. In addition, also the records of hydrocarbon inflows documented during formation tests were used for interpretation as possible indicators of favorable hydrocarbon trap and migration zones.

Seismic interpretations, such as litho- and chronostratigraphic surfaces, as well as tectonic elements were provided by the MOL Plc. in electronic format (grid maps and polygons). Additionally, areal position of the known hydrocarbon fields was also delivered.

In this chapter the applied data, their quality and quantity, as well as the steps of data preparation and processing including my methodological developments as well are presented systematically for each characterizing work phase (i-iv) and data type.

The referred A-Figures and A-Tables can be found in the Figure and Table Appendix volume. However, the compiled **data base is under the MOL Plc.'s secrecy protection, and cannot be published not even in this dissertation.**

		number of wells	interval of bottom elevations (m asl)	time interval of drillings	number of available data before culling				
					H	T	WC	CS	HS
DSA	HC well	434	(-267)-(-5103)	1905-2006	70	241	182	65	185
	water well	1712	117-(-2136)	1903-2008	1663	138	49	-	3
BSA	HC well	594	(-255)-(-5757)	1941-2010	163	47	158	-	306
	water well	1932	84-(-2963)	1901-2008	1932	96	47	-	-

Table 4.1 Number of available wells and data, as well as the covered elevation and drilling time intervals in the Study Areas (DSA and BBSA). Abbreviations: HC – hydrocarbon, H – hydraulic, T – temperature, WC – water chemical, CS – chronostratigraphic, HS - hydrostratigraphic

4.1 Tectonics

4.1.1 Applied data

Tectonic elements of the Study Areas were provided by the MOL Plc. in electronic format as polygons being fittable to given stratigraphic surfaces. In the Derecske Study Area referring to the current exploring area of the MOL Plc. (corner point co-ordinates: Y_{EOV} 813-875, X_{EOV} 200-244), the following surface maps were equipped with the polygons of the main structural elements (i.e. faults): Pre-Neogene basement, Pannonian basement, top of the Lower Pannonian (i.e. top of the Algyő Aquitard), chronostratigraphic surface of 8.3 Ma; while in the Békés-Battonya Study Area: Pre-Neogene basement, Pannonian basement. Additionally, in the questionable and data-deficient areas I also interpreted faults on the seismic sections at a Landmark workstation provided by the MOL Plc. Furthermore, tectonic activity of the main fault zones could be deduced from the upper termination of the faults (i.e. the upward reached depth), as well as from the literature review.

4.1.2 Data preparation and processing

Fault-polygons were visualized by the Golden Software Surfer 8 primarily on the surfaces where they were identified, and for the interpreter's guidance also on further surfaces that are probably cross-cut as well. Eventually, during the hydraulic, water chemical, and temperature data processing, fault-polygons were delineated on the respective maps, while fault plains were represented by lines in the cross-sections as well based on projections from the maps and my complementary seismic interpretations.

4.2 Hydrostratigraphy

Hydrostratigraphic units can be determined based on the fluid transmitting and storing capacities of the rock framework, which can be characterized by the porosity, permeability, and hydraulic conductivity of that. These properties primarily depend on the lithology, and this correspondence usually allows of the determination of a homogeneous lithostratigraphic unit as one hydrostratigraphic unit. Following these principles, regional hydrostratigraphy of the Great Hungarian Plain was worked out by TÓTH and ALMÁSI (2001) based on the formation classification of the strata considering the regional lithologic and stratigraphic characteristics of the rock framework (see also Chapter 3.1.4.1).

Since only scarce porosity and permeability data were available from the Study Areas, the determination of their hydrostratigraphic build-up was primarily based on the identification of the lithostratigraphic units, which were then matched to the regional hydrostratigraphic units in the way defined by TÓTH and ALMÁSI (2001).

4.2.1 Applied data

In the DSA permeability data were attainable from 21 water wells and only from shallower depth than 1650 m. In addition, porosity and permeability data measured on core samples were provided by the MOL Plc. from 29 hydrocarbon wells, while in the BBSA from 25 wells.

The database of TÓTH and ALMÁSI (2001) can be found in the digital appendix of the Ph.D. dissertation of ALMÁSI (2001), where the hydrostratigraphic subdivision (i.e. top and bottom depths of the hydrostratigraphic units) of several borehole sequences is available. For the DSA 186, while for the BBSA 178 wells' hydrostratigraphic subdivision can be found in this database.

Furthermore, in case of the DSA, chronostratigraphic subdivision (i.e. depth of time horizons) of 65 borehole sequences, while in the BBSA depth data of seismically interpreted time horizons, as well as formation tops and bottoms from 242 wells were also provided by the MOL Plc.

Additionally, seismically interpreted stratigraphic surfaces were also put at our disposal by the MOL Plc. in both study areas, however in case of the DSA only referring to their current exploring area (corner point co-ordinates: Y_{EOV} 813-875, X_{EOV} 200-244). List of the delivered surfaces can be found in A-Table 4.2.

4.2.2 Data preparation

4.2.2.1 Well data

Permeability data of the water wells were referred to the middle of the screened depth interval, while porosity and permeability data of the hydrocarbon wells were referred to the middle of the core-sampled depth interval, which was also corrected for the true vertical depth in the inclined wells. Porosity data culling was only possible when the analyzing method was known, and henceforth only the data determined by the routine analyzing methods were used.

Subsequently, considering the regional scale of the study, as well as the scarce data distribution, first the lithostratigraphic, and then the hydrostratigraphic units were determined (A-Table 4.2), while the few porosity and permeability data were only used as controlling and supporting parameters. Accordingly, average values were calculated for each lithostratigraphy-based hydrostratigraphic unit where data was available.

The lithostratigraphy-based hydrostratigraphic classification happened in the following way. In case of both Study Areas, the hydrostratigraphic subdivision data (i.e. top and bottom depths of the hydrostratigraphic units) of ALMÁSI (2001) were first adapted into the database of the present Ph.D. dissertation. This process included nomenclatural synthesis, and elevation conversion from the Adriatic to the Baltic reference sea level (i.e. 1 m above the Adriatic sea level – 0.6747 m = 1 m above the Baltic sea level).

Subsequently, the formation classification data provided by the MOL Plc. were matched to the hydrostratigraphic units, while the chronostratigraphic data were first matched to formation boundaries, and then to the corresponding hydrostratigraphic units (A-Table 4.2). (Correlation among the litho- and hydrostratigraphic units has already been presented in Chapter 3.1.4.1.) Afterwards, in case of the DSA, these data were basically used for controlling the hydrostratigraphic subdivision data adapted from ALMÁSI (2001). While in the BBSA these data could not only verify but also complement the data adapted from ALMÁSI (2001), and consequently by-passing the overlaps altogether 305 boreholes' hydrostratigraphic subdivision are available in this region. It is worth mentioning that when the depth data of a formation top/bottom was differing in the ALMÁSI (2001) and MOL database, always the latter was chosen because the former has pointwise data from wells, while the latter has data derived from horizons being correlated among wells.

The areal and bottom depth distribution of the finally prepared and further on used hydrostratigraphic data can be seen in A-Fig. 4.2.1-2 and 4.2.3, respectively.

4.2.2.2 Mapped data

The seismically interpreted stratigraphic surfaces were provided by the MOL Plc. in electronic format as grid maps. These were visualized by the Golden Software Surfer 8 program. Afterwards, the depth maps of the DSA were converted into elevation maps by using the surface topography map and the depth contour maps (the latters were extracted from the former) using the Grid/Math function of the Golden Software Surfer 8. Finally, the identified formations were matched to the corresponding hydrostratigraphic units (A-Table 4.2). Additionally, in the DSA outside of the current exploring area of the MOL Plc. where seismic interpretations were not available bounding surfaces of the hydrostratigraphic units were interpolated from the well data using kriging method by the Golden Software Surfer 8.

4.2.3 Data processing

The produced hydrostratigraphic database including pointwise well data and maps were used (i.e. applied and visualized) hereafter only according to our objectives, and also taking notice of the hydraulic, temperature and water chemical data distribution. Namely, during the hydraulic, water chemical, and temperature data processing, hydrostratigraphy along the constructed profiles, maps, and cross-sections was interpreted.

4.3 Hydraulics

4.3.1 Principles of calculations and corrections

Two kind of hydraulic data were available pending the data source.

On one hand, in the water well records stabilized water level data measured after well completion and being referable to the middle of the screened depth interval are given. With the knowledge of the well head's elevation where the standing water level is measured from, and the water density, also the hydraulic head (h) and the aquifer's pore pressure (p) can be calculated respectively.

On the other hand, from hydrocarbon wells static formation/pore pressure data (p) are mostly available. These are usually determined by extrapolating the logarithmically ascending pressure build-up curves recorded during drill stem tests (DSTs). From the static pressure value referred to the middle of the tested depth interval with the knowledge of the appropriate density value hydraulic head (h) can be calculated as well.

Conversion of pore pressure (p) and hydraulic head (h) data into one another is based on the following principles.

Hydraulic head (h) is equal to the height of a vertical fluid column relative to an arbitrary datum plane (z=0) commonly chosen at sea level. It is directly proportional to, thus a measure of, the fluid potential (Φ) in a given point of rock framework, which represents the amount of mechanical energy contained by a unit mass of incompressible fluid, in the following way (HUBBERT, 1940):

$$\Phi = g \cdot z + p / \rho = g \cdot h \qquad (2)$$

and

$$h = z + p /(\rho \cdot g) \qquad (3)$$

where Φ the fluid potential [L^2/T^2], g the gravitational acceleration [L/T^2], z the elevation above datum plane [L], p the gauge pressure (= absolute pressure - atmospheric pressure) [M/LT^2], h the hydraulic head [L], ρ the density of water [M/L^3]. Additionally, the $\rho \cdot g$ term in Eq. (3) expresses the specific weight of the fluid, which numerically equals the vertical pressure gradient (γ) in a water column of density ρ. In other words, since g is a constant value (9.8067 m/s^2), vertical pressure gradient of a fluid (or gas) depends on its density. For instance, in case of water density of 1000 kg/m^3, γ = 9.81 MPa/km.

Since flow between two points can be generated by the difference in their mechanical energy ($\Delta\Phi$), considering Eq. (2) and the constant value of g (9.8067 m/s^2), the hydraulic gradient ($\mathrm{grad}h = dh/dl$ [-]; where l is the length of flow path [L]) represents the fluid flow driving force, which determines the fluid flow direction as well. Statutorily, fluid flows from the places of higher potential towards that of the lower potential, i.e. from higher towards lower h values, and consequently in the opposite direction of hydraulic gradient.

Accordingly, conversion of pore pressure (p) and hydraulic head (h) data into one another is possible by using Eq. (3) where z equals to the elevation of the middle of the screened and perforated depth intervals in water and hydrocarbon wells, respectively, while h and p are measured values. Since g is constant, only the determination of a constant fluid density (ρ) requires some further considerations and calculations. Namely, although density depends on the salinity, temperature, pressure, and gas content of water, thus varying in space and time, fluid potentials of differing points can be compared only if the same density value were used in Eq. (3) (HUBBERT, 1940; LUSCZYNSKI, 1961). In other words, in this regional scale study a single, average groundwater density value had to be determined for the whole Study Area, namely 1000 kg/m^3. This is a good approximation as the effects of salinity and

temperature on groundwater density roughly equalize each other in the Study Areas (Appendix 1), while the pressure and dissolved gas content has a less significant effect (e.g., OSIF, 1988; ADAMS and BACHU, 2002), and the role of free gas content will be discussed later in this sub-chapter. However, in order to control the conformance of this value (i.e. the 1000 kg/m^3 water density), as well as to understand better the local hydraulic phenomena probably pending the actual fluid densities too, further attempt were also made for the determination of area specific density values in cases of the two main Study Areas (Appendix 1). As a result, considering i) the reliability of the applied salinity data (see also Chapter 4.5.2); ii) the lack of simultaneous availability of salinity, temperature, and pressure data regarding one measuring point; and iii) the finally used data being averages and typical for given depth intervals; the calculated densities cannot be reckoned as reliable and representative data. In other words, the error of correction may exceed the change that could be caused by the correction itself, while actually the calculated densities, namely 993 and 985 kg/m^3 in the Derecske and Békés-Battonya Study Areas, respectively, do not show significant deviations /maximum (+39) m or 2%, and (+106) m or 4% deviation in h in the DSA and BBSA, respectively/ from the results of calculations applying the 1000 kg/m^3 density value (Appendix 1). Notwithstanding, also the possible effect of the application of these area specific corrected density values was taken into account during the interpretations. However, hydraulic conditions interpreted based on the original and calculated pressure and hydraulic head data proved to be concordant (see also Chapters 5 and 6).

Eventually, it is worth mentioning that the effect of water density differences as regional fluid flow driving force is negligible considering the general salinity and temperature conditions of the Pannonian Basin's groundwater (see also Chapters 3.1.4. and 3.1.5). Thus, the above reasoning only refers to the possible error of hydraulic calculations introduced by the otherwise required application of a constant density value.

Additionally, also the effect of groundwater's free gas content was taken into account as a source of error in the hydraulic calculations. Since several pressure data were measured during gas inflow, thus presumably in a gas column, calculating hydraulic head (h) by using water's density (1000 kg/m^3) or vertical pressure gradient (9.81 MPa/km) from these gaseous pressure data could cause significant deviation compared to the real potential regarding the water leg. These errors may be observed as (apparent) positive anomalies in the fluid potential field. Because one of this Ph.D. research work's objectives was to examine the role of faults and low-permeability formations in the development of fluid potential anomalies, it was

necessary to identify among the mapped anomalies the apparent ones caused by the presence of gas accumulations (i.e. hydraulic calculation errors).

It is possible through calculating the pressure that would be measured in a water column in the same depth where the pressure was measured in the gas column, and then the corrected hydraulic head could be determined using the water's density of 1000 kg/m^3 (Appendix 2). However, since some required data (density of the gas, elevation of the gas-water contact) were not available, and every hydraulic calculation was performed by using the constant (water) density value of 1000 kg/m^3, thus an approximate method also had to be worked out to determine the difference $/\Delta h_{wg(max)}/$ between the water's hydraulic head calculated with water density i) from pressure data measured in the gas column and ii) from pressure data would be measured in a water column at the same depth. The method and calculations can be seen in Appendix 2. As a result, the maximum error $/\Delta h_{wg(max)} = 254$ m/ in both Study Areas proved to be negligible below about 2000 m depth, and thus development of potential anomalies cannot be explained only by the presence of gas accumulations. However, in shallower depths (mostly in the Great Plain Aquifer) the deviation $/\Delta h_{wg(max)} = 254$ m/ could be significant, and it cannot be excluded that the known gas accumulation induces the potential anomalies. However, it is also worth mentioning that even if these potential anomalies can lead to false deductions about the faults and low-permeability strata's hydraulic behaviour, these could be the diagnostic indications of hydrocarbon, and particularly gas accumulations, which finally could also refer to the conduit behaviour of the ambient faults at least in he past.

4.3.2 Data culling and preparation

Water well data were collected from the original (paper-based) records of 1716 wells in the DSA, and 2944 wells in the BBSA. However, not all of them possess the required data, i.e. base data, top and bottom depth of the screened interval, standing water level. Consequently, only 1697 and 1932 wells' data were used from the DSA and BBSA, respectively. In case of these wells, hydraulic head was calculated referring to the middle of the screened interval (z) by the following equation:

$$h = z_0 + d_{wt} \tag{4}$$

where h the hydraulic head [L], z_0 the elevation of the well head [L], and d_{wt} the depth of the water table (standing water level) [L], which is increasing upward by convention (i.e. it is

positive above and negative below the well head). Then based on Eq. (3), also the pore pressure (p) was calculated by using the constant density value of 1000 kg/m^3.

Hydrocarbon well data were put at our disposal by the MOL Plc. in electronic format (MS Excel spreadsheet). However, also the original (paper-based) well records were reviewed, since during data processing reliability and reality of some data became questionable, and several digital data had to be revised indeed. The thus re-examined database contains the results of formation tests of 95 and 324 wells in the DSA and BBSA, respectively, such as static pressure values estimated by extrapolating the logarithmically ascending pressure build-up curves recorded during drill stem tests (so-called 'PWST' data), bottom-hole pressures measured in shut-in periods (so-called 'PWS' data), as well as production data. Formation tests, which did not provide pressure data were deleted first. Among the remnants, those pressure data were cancelled, which were measured i) in the well head, producing or tubing string, because these data are irrelevant regarding the static formation pressure; ii) during production, because static formation pressures were required; iii) without fluid inflow, because the origin of the measured pressure (rather drilling mud) and reliability of the test is questionable in these cases. Consequently, only the shut-in bottom-hole (PWS) and static formation pressure data (PWST) remained in the database. When also PWS and PWST data were available from a formation test, always the PWST was chosen for further application, because this extrapolated value is the most representative regarding the original hydraulic conditions of the formation. After the conversion from the Adriatic to the Baltic reference sea level of the elevation of the rotary tables, the middle of the tested depth intervals and their elevations were determined as reference points where the pressure values can be referred to. Since the measured depth of the perforated sections were given, in inclined wells also the true vertical depth values had to be calculated before elevation conversion. (It was possible with the knowledge of the well bottoms' measured depth and EOV co-ordinates as well.) Furthermore, when pressure measurement was not carried out in the perforated interval, but in a usually shallower depth (deviation could be of the order of 100 m), pressure data had to be converted referring to the middle of the perforation. (Otherwise, where gauging happened in the perforated section, and deviation from the middle of that was less significant, conversion was neglected.) Calculations were performed by using the pressure gradient of water of 1000 kg/m^3 density (γ_w = 9.81 MPa/km). Eventually, from the finally applied static pressure values referred to the middle of the tested depth intervals hydraulic heads (h) were calculated by Eq. (3) as well, using again the density value of 1000 kg/m^3. The possible error caused by the application of this density value, as well as its significance in the interpretations

are discussed in Chapter 4.3.1 and Chapter 5. As a result, 209 hydraulic data of 84 hydrocarbon wells, and 353 hydraulic data of 163 hydrocarbon wells were applied during the subsequent data processing in the DSA and BBSA, respectively. Areal and depth distribution of these data can be seen in A-Fig. 4.3.1-2 and 4.3.3-4, respectively.

In addition, during data culling a further aspect was the time of well completion and measuring as well, because data measured after or during well completion were required in order to achieve the best approximation of the original hydraulic conditions of the formation. This premise was realized in both kind of wells, since records of the water wells were documented after well completion as usual, while pressure data were measured in the first exploration wells (in every field) not disturbed by production.

4.3.3 Data processing

During hydraulic data processing and interpretation three methods were used to "visualize" the subsurface fluid-potential field. These are the followings in the order of building on each other: construction of i) pressure-elevation profiles, ii) tomographic fluid potential maps, and iii) hydraulic cross-sections.

4.3.3.1 Pressure-elevation /p(z)/ profiles

Pressure vs. elevation or p(z) profile is the most frequently applied method in hydrodynamic analyses, which *sensu stricto* allows of the examination of the vertical component of fluid flow directions by comparing the vertical pressure gradient to the ideal hydrostatic condition.

By definition, if the vertical pressure gradient (γ) is hydrostatic ($\gamma_{hyd} = \rho g$ = 9.81 MPa/km beside water density of 1000 kg/m^3) there is no vertical fluid flow, since gravity and buoyancy forces affecting on water molecules are in equilibrium. However, fluid can flow horizontally even in this case, for instance in midline areas of gravitational flow systems. Thus, hydrostatic conditions in one well do not mean definitely that the system is static. On the other hand, among hydrodynamic conditions a sort of force throws off the balance and generates vertical fluid flow, whilst the vertical pressure gradient becomes dynamic (γ_{dyn}). If $\gamma_{dyn} < \gamma_{hyd}$, fluid flows downward ($\gamma_{dyn}$ is subhydrostatic), while in the inverse case upward (γ_{dyn} is superhydrostatic). In a composite basin where multiple flow systems exist, the transient zone between two systems representing opposite flow directions can also be

observed in p(z) profiles indicated by the change (inflection point) of the vertical pressure gradient from superhydrostatic to subhydrostatic, or vice versa. Incidentally, where flow systems converge from opposite directions, these transient zones as potential minimum zones provide favorable conditions for hydraulic hydrocarbon entrapment.

Furthermore, based on the relative magnitude of the vertical pressure gradient, as well as on the character of its changes, also the hydraulic behaviour of faults and low-permeability strata can be interpreted according to the conclusions of this work. (Thus although **these considerations already belong to the results of this Ph.D. research work**, it is worth displaying them in this subchapter as methodological developments.) In other words, based on the interpretation of pressure data from higher permeability zones by p(z) profiles, also hydraulic behaviour of the intercalated lower permeability zones where data are usually not available can be deduced.

In case of a deep energy source, which induces fluid upwelling such as the overpressure in the Pannonian Basin, a low-permeability zone (layer or fault) always can be observed as a "break" or "jump" in the p(z) profile (Fig. 4.3.5.b-c, respectively). Upward flowing fluid hitting this zone comes up against a barrier, and can flow across it only by a more significant energy loss and thus higher pressure gradient than the previous strata. Consequently, energy accumulated at the bottom of the low-permeability zone, which after all maintains the overpressure (that could be generated originally by vertical compaction, lateral compression, etc.). Accordingly, vertical pressure gradient could be higher in the underlying than in the overlying higher permeability strata of the low-permeability zone. This elevated pressure gradient in a higher permeability strata in turn refers to the presence of the overlying lower permeability zone, and at the same time to the though reduced but existing permeability of that. Because, if a formation (or fault) could perfectly impede fluid flow (i.e. be impermeable) and there was not hydraulic communication between the over- and underlying aquifers, although overpressure could evolve in the underlying aquifer, the vertical pressure gradient would be hydrostatic indicating the lack of vertical fluid flow (Fig. 4.3.5.e). Thus, the more effective aquitard (i.e. low-permeability zone) results in the lower vertical pressure gradient in the underlying strata and the higher vertical pressure gradient in the aquitard itself (Fig. 4.3.5.c). This latter phenomenon (i.e. high γ) is represented by the jump-like pressure drop in the p(z) profile, which also due to the usual lack of data in low-permeability zones. If the aquitard is less effective (i.e. more permeable) for instance due to cross-cutting conduit faults, the "jump" (i.e. pressure drop) is smaller, or only a "break" can be seen in the p(z) profile (Fig. 4.3.5.b). However, if γ exceeds the lithostatic vertical pressure gradient ($\approx$ 25

MPa/km), which is usually displayed by significant pressure data scatter in a narrow depth interval as well, it may be an 'apparent' γ representing the variable pressure conditions of a fractured, faulted rock framework otherwise characterized by low-permeability matrix (Fig. 4.3.5.d). Whilst also the opening of the fractures can be explained by the highly overpressured conditions themselves. This interpretation could be further supported by the variability of the proper hydrostratigraphic place of data in a narrow depth interval.

Besides, in the order of profiles d-c-b-a in Figure 4.3.5 the change in pressure conditions can be followed during the opening (or rejuvenation) of a conduit fault in a low-permeability zone when dissipation of overpressure can be materialized through the upwelling (γ_{dyn}) of fluids (and gases) along the fault. In addition, increasing fault density modulates pressure conditions in the same way. The break- or jump-like pressure drop and the high vertical pressure gradient inside the aquitard refer to pressure dissipation along scarce fractures and faults, since in the low-permeability matrix heterogeneities represented by the conduit faults increase the hydraulic conductivity only locally. However, as fault density increases pressure dissipation becomes more continuous, uniform, and diffuse ("refraction angle" of the pressure gradient line decreases) as hydraulic conductivity increases (distributes) in the whole matrix. Between the two extremities, namely the jump-like and diffuse pressure dissipation the transition is continuous of course (in the order of d-c-b-a pictures in Fig. 4.3.5).

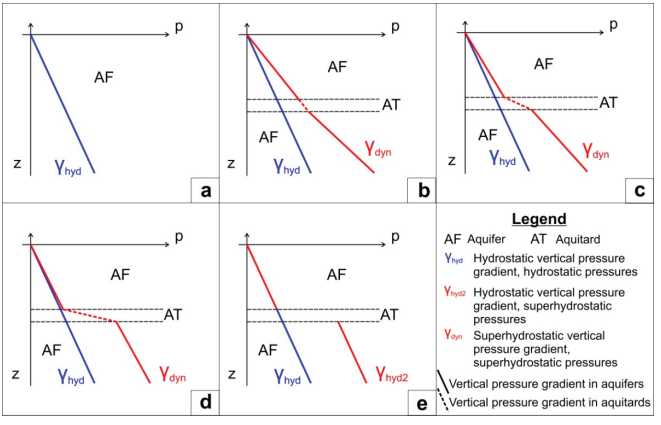

Figure 4.3.5 P(z) profiles representing pressure distribution **a)** in an aquifer (~hydrostatic conditions) **b)** in aquifers separated by a less effective aquitard (for instance by a low-permeability strata cross-cut by faults), **c)** in aquifers separated by an aquitard, **d)** in aquifers separated by a hydraulically fractured aquitard, **e)** in aquifers separated by an (ideally impermeable) aquiclude.

As it was already mentioned, p(z) profile *sensu stricto* allows of the examination of vertical fluid flow directions, thus theoretically only data derived from one well can be interpreted in a p(z) profile. However, considering that in the Study Areas of this Ph.D. work one well usually provides only one hydraulic data, application of p(z) profiles had to be extended for areas based on two criteria. Namely, wells interpreted in one p(z) profile had to have approximately the same land surface elevation, because position of the reference hydrostatic pressure gradient line depends on it as starting from the land surface's elevation[4] (z_0). On the other hand, hydrostratigraphic build-up regarding the units and their thicknesses as well also had to be approximately concordant, since otherwise phenomena caused by hydrostratigraphic changes could not be jointly interpreted. Beyond these criteria, also the areal and depth distribution of hydraulic data were taken into account, while extent of the area represented by one p(z) profile was determined by using the "trial and error" approach as well in order to achieve a reasonable balance between interpretability and reality. Accordingly, several p(z) profiles were constructed first for smaller areas, and then some were divided up, while others were fused by the time the final p(z) profiles were completed. As a result, 38 and 35 p(z) profiles were constructed in the DSA and BBSA, respectively, for areas of extent of approximately 5x5 km, and with maximum variance in topographical elevations of 10 m (otherwise the maximum difference in the Study Areas is 50 m). Location of areas represented by the profiles can be found in A-Fig. 4.3.1-2, while the p(z) profiles among the results in A-Fig. 5.3.1.2-86 and 5.3.1.148-216 for the DSA and BBSA, respectively.

Moreover, since all of the p(z) profiles were delineated in the same scale (i.e. for the same elevation interval: z = 200-(-6000) m asl) in order to get comparable diagrams, pressure data in shallow depths (calculated from hydraulic heads of water wells) are less visible and interpretable due to their relatively high number (and density). Therefore, further p(z) profiles were constructed in the necessary cases for the elevation intervals of z = 150-(-200) m asl or z = 150-(-300) m asl, and/or z = 200-(-1500) m asl in the DSA, and z = 200-(-1000) m asl in the BBSA. These profiles can also be found among A-Fig. 5.3.1.2-86 and 5.3.1.148-216 for the DSA and BBSA, respectively.

In the p(z) profiles beyond the data points also the (reference) hydrostatic vertical pressure gradient line (γ_{hyd}=9.81 MPa/km) starting from the average land surface elevation of the given area /$z_{0(av)}$/, and the hydrostratigraphic units are represented in order to support the interpretation. Finally, also dynamic vertical pressure gradients were calculated in the feasible

[4] In this regional scale study the uppermost boundary of groundwater flow systems was the land surface instead of the water table regarding the usual only a few meter difference between them.

cases (i.e. when enough data probably representing one gradient were available) using the chosen pressure values, while the gradient lines were only roughly drawn on the diagrams, since these do not represent average gradients of point clouds but only that of the chosen pressure data of sets. Fitting of the gradient lines (i.e. selection of the pressure data probably representing one gradient) happened by considering i) the hydrostratigraphic unit boundaries where change of gradient can be usually expected due to the change in hydraulic conductivity; ii) the number and areal position of wells, from which the data derived; iii) the analysis of tomographic fluid-potential maps and hydraulic cross-sections, which though were constructed after the p(z) profiles, but the combined interpretation of the three data processing methods provided the final outcome. In addition, during the judgment of a gradient value being approximately hydrostatic it was considered that 0.1 MPa deviation in pressure equals to 10 m in hydraulic head, while 0.01 MPa only to 1 m (based on Eq. 3).

4.3.3.2 Tomographic fluid-potential maps /h(x,y)/

In fluid-potential maps the horizontal distribution of hydraulic heads, thus the lateral fluid flow directions can be examined. Driving force is perpendicular to the equipotentials along which the value of fluid-potential (hydraulic head - h) is constant, while fluid flows from the equipotentials of higher h to that of the lower h values, thus in the opposite direction of the hydraulic gradient (grad$h$).

By definition, potential or potentiometric map can be constructed for one horizontal aquifer, however it is rarely realized in practice. It is more often particularly in areas characterized by low data density, as well as dipping and/or faulted strata that potential map is prepared for a given depth (elevation) interval. In this way, also the effects of heterogeneities in hydraulic conductivity can be interpreted for instance along strata boundaries and faults. Furthermore, comparing the so-called tomographic potential maps, which are constructed for successive elevation intervals, also vertical flow directions could be interpreted among them.

In addition, hydraulic behaviour of structural elements and low-permeability strata can also be interpreted by examining potential maps, since these heterogeneities could generate characteristic anomalies in the fluid-potential field (e.g., TÓTH, 2003; UNDERSCHULTZ et al., 2005). Namely, discontinuity of the equipotentials may indicate the presence of low-permeability formations (e.g., barrier faults) (Fig. 4.3.6.a), though looking at it in an adequately small scale these discontinuities represent very high hydraulic gradients indeed. In other words, there is fluid flow (hydraulic continuity) across the barrier surfaces and strata as

well, only the flow component in that direction is negligible compared to the flow component being parallel with the barrier. Additionally, if only the transversal flow is impeded along a fault due to for instance the differing hydraulic conductivity of the juxtaposed layers or to the fluid flow directing out of the fault plane, but vertical flow is possible, then a so-called potential escarpment (TÓTH, 2003) could develop, which represents again high hydraulic gradient due to the transversally hampered flow (Fig. 4.3.6.b). On the other hand, high-permeability faults and so-called sedimentary windows can generate positive and negative potential anomalies as well. The formers could develop at the downstream, while the latters at the upstream side forming potential mounds or ridges (diverging flow lines) (Fig. 4.3.6.d), and potential depressions or bays (converging flow lines) (Fig. 4.3.6.e), respectively.

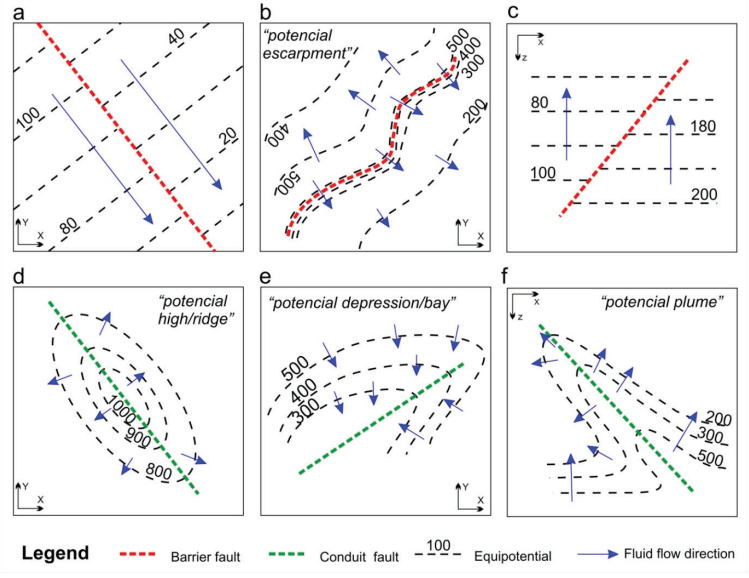

Figure 4.3.6 Barrier and conduit fault-induced fluid potential anomalies in potential maps (**a**, **b**, **d**, **e**) and hydraulic cross-sections (**c**, **f**)

For hydrocarbon entrapment practically any kind of potential anomaly could subserve by impeding fluid flow in at least one direction (TÓTH, 2003). However, flow gathering negative anomalies in the fluid-potential field of hydrocarbons provide the most favorable conditions for their entrapment. In this Ph.D. work the regional potential field of water was

mapped, which allows of the research of hydraulic hydrocarbon traps. These traps form due to regional energy minima where flow systems converge from opposite directions, then for instance turn vertically up to discharge into shallower zones, and leave their hydrocarbon cargo under some kind of a screening mechanism, such as the retaining screens of poorly permeable rocks, or salient pressure/temperature/salinity drop (TÓTH, 1980). Afterwards, in view of the regional potential field of water, further local scale studies using for instance the "UVZ method" (DAHLBERG, 1995) could appoint the possible places for hydrodynamic hydrocarbon entrapment. These traps represent local energy minima in one-way fluid flow fields conjugated characteristically with anticlinal or domal structures, and homoclinally dipping sands where hydrocarbons can separate from flowing groundwater due to their differing density resulted in different buoyancy force acting on them (HUBBERT, 1953).

In this work, two tomographic potential map series were made up in the two main Study Areas. Elevation intervals were chosen based on the depth distribution of the data, as well as on the initial interpretation of p(z) profiles. Thus an important aspect was that "breaks" and "jumps" in the profiles fall at interval boundaries. However at the same time hydrostratigraphic build-up was not taking into account, only in the course of interpretation. Accordingly, in both Study Areas 10-10 tomographic potential maps were constructed covering the whole areas and elevation intervals from the land surface to z = (-4000) m asl in the DSA, and z = (-5000) m asl in the BBSA. Elevation intervals can be found in A-Table 4.3, while the potential maps among the results in A-Fig. 5.3.2.2-11 and 5.3.2.31-40 in the DSA and BBSA, respectively. Hydrocarbon (mostly gas in the DSA) inflows and seismically interpreted faults are also indicated in the maps.

Contouring (i.e. drawing of equipotentials) was made by hand in order to avoid the errors possibly caused by computational interpolation, as well as to provide the chance for applying personal experiences, and the knowledge of the given study areas too. However, data distribution and quantity below z = (-600) m asl elevation did not allow of the contouring of h values for the whole areas, while linear interpolation was not possible since distribution of potentials (i.e. density of equipotentials) depends on several factors and is usually not uniform as also known from those parts of the Study Areas where enough data were available for contouring. Thus the completed interpretation is rather conservative, but also more reliable. In addition as a result, the areas characterized by anomalously high or low hydraulic gradients were also indicated in the maps. Finally, it is worth emphasizing that arrows in the interpreted potential maps only sign the direction of the horizontal component of fluid flow driving force, while the flow intensity also depends on the hydraulic conductivity of the flow medium.

4.3.3.3 Hydraulic cross-sections /h(s,z)/

Final step of hydraulic data processing was the construction of hydraulic cross-sections, which represent hydraulic head values along a vertical plane in the function of the measuring points' elevation (z) and horizontal distance from the end of the section (s). Consequently, also the vertical and lateral flow directions can be studied along the section. Furthermore, in case of approximately parallel sections, lateral flow directions among them could be determined as well.

Similarly to potential maps, hydraulic behaviour of structural elements and low-permeability strata can also be interpreted by examining the induced potential anomalies in the hydraulic cross-sections as well. Thus low-permeability formations (e.g., barrier faults) could cause apparent discontinuities in the equipotentials, namely anomalously high hydraulic gradients (Fig. 4.3.6.c), while high-permeability faults and lenses could generate positive and negative potential anomalies as well. Positive anomalies can develop at the downstream, while negative anomalies at the upstream side forming potential plumes or noses (diverging flow lines) (Fig. 4.3.6.f), and potential depressions or tubes (converging flow lines), respectively.

Regarding hydrocarbon entrapment the same considerations are valid as in case of the potential maps (see Chapter 4.3.3.2.).

Two solutions can be used for the construction of hydraulic cross-sections, namely i) trace line of the section is laid out by connecting wells, or ii) wells are projected perpendicularly into a straight section line from inside a given distance. In this work the latter method (ii) was applied, thus the section traces were laid out by taking into account the data distribution, as well as the location of areas, which were proved to be interesting from the point of view of this Ph.D. research during the interpretation of p(z) profiles and tomographic potential maps. Subsequently, data points were projected into the sections always perpendicularly to the trace line and from inside the distance of 3 km. Consequently, 7 and 6 cross-sections were constructed in the DSA and BBSA, respectively. Location of the sections can be found in A-Fig. 4.3.1-2, whilst the cross-sections among the results amidst A-Fig. 5.3.3.1-21 and 5.3.3.22-39 in the DSA and BBSA, respectively. Contouring (i.e. drawing of equipotentials) was made by hand for the same reasons as in case of the fluid-potential maps. Hydrocarbon (mostly gas in the DSA) inflows, as well as seismically interpreted faults and hydrostratigraphic units are also indicated in the sections. However, in the DSA, since almost no data were available from the Endrőd Aquitard and Szolnok Aquifer, only the top and

bottom of the Algyő Aquitard (i.e. the bottom of the Great Plain Aquifer, and the top of the Szolnok Aquifer if it presents, respectively), as well as the Pre-Neogene basement are delineated (in the temperature and hydrochemical cross-sections as well).

Beyond the hydraulic head values of wells, also the intersections of equipotentials contoured in the potential maps were represented in the cross-sections as points referring to the middle of the given elevation intervals. These data usually fit to the flow net build-up by the well data, thus support i) the contouring along the sections, ii) the adequate choice of elevation interval boundaries, which were used during the construction of tomographic potential maps, as well as iii) the choice of projection distance of 3 km. However, data distribution and quantity did not allow of the contouring of *h* values along the whole sections, while linear interpolation was not possible since distribution of potentials (i.e. density of equipotentials) depends on several factors and it is usually not uniform as also known from those parts of the Study Areas where enough data were available for contouring. Thus the completed interpretation is rather conservative, but also more reliable. In addition as a result, the areas characterized by anomalously high or low hydraulic gradients were also indicated in the sections. However, it is worth emphasizing that arrows in the interpreted sections only sign the direction of fluid flow driving force, while the flow intensity also depends on the hydraulic conductivity of the flow medium. Additionally, it is also worth mentioning that due to the vertical exaggeration of the cross-sections driving force directions are not necessarily perpendicular to the equipotentials. Finally, during the determination of the lateral driving force (~flow) directions also the regional hydraulic gradient's direction known from the tomographic maps have to be considered if the section's strike deviates from that.

4.4 Geothermics

4.4.1 Principles

Temperature of groundwater depends on the heat source and thermal conductivity of the rock framework, as well as on the thermal exchange coefficient of water. In the homothermal zone where solar radiation has already no effect the vertical heat-flux (i_z) arose from the Earth's internal heat can be described on the analogy of Darcy's definition for specific discharge or flux (q) in the following way:

$$i_z = \frac{\mathrm{K}\Delta T}{\Delta z} \tag{5}$$

where i_z is heat flux [ML^2/T^3L^2], K is thermal conductivity [ML^2/T^3TL], $\Delta T/\Delta z$ is vertical geothermal gradient (or grad$T$) [T/L]. K depends on the composition and intrinsic thermal conductivity of the solid and liquid components, on the porosity, on the temperature, as well as on the method of measurement and estimation or averaging. The worldwide average value of geothermal gradient is about 30°C/km.

Temperature of flowing groundwater usually deviates from the value that could be expected based on the thermal conductivity of the surrounding rocks due to convective heat transport, particularly in fissured and cavernous rocks. In basins characterized by gravitational fluid flow systems, geothermal gradients usually show positive correlation with vertical hydraulic gradients. Thus in recharge areas temperature increases to a lesser degree with depth compared to the average geothermal gradient due to the cooling effect of downward flowing waters of lower temperature. On the other hand, in discharge areas upwelling groundwater warms up its surroundings. These phenomena represent the advective heat transport of gravitational flow systems according to TÓTH (1984).

4.4.2 Applied data

Temperature data are usually less reliable than hydraulic data regarding the measuring methods and the number of possible disturbing factors (DÖVÉNYI et al., 1983; DÖVÉNYI and HORVÁTH, 1988; DÖVÉNYI et al., 2002). For instance, in water well records usually the outflowing water temperature is documented, which is not adequately representative for the formation temperature. Thus, original temperature data registered in well documentations were not applied in this work, since one by one correction of these data would point beyond the scope and objectives of this study.

However, temperature data of 382 and 148 wells in the DSA and BBSA, respectively, were available from the Geothermal Database of Hungary (DÖVÉNYI et al., 2002) in electronic format (text files). It contains the culled and qualified temperature data of water and hydrocarbon wells below 200 m depth and above temperature of 30°C. (Thus, from shallower depths temperature data were available only in the original well records, but these were not used for the above described reasons.) Data culling, correcting, and qualification were accomplished by DÖVÉNYI et al. (2002) based on the available data of wells, and on the method of measurement. To name but a few among temperature data types in the decreasing order of reliability: corrected steady-state temperature, bottom-hole temperature, maximum temperature, temperature measured during drill stem test, temperature of inflowing (from the

formation into the borehole) and outflowing (from the well head) water. These data were ranked from 1 (best quality) to 9 (worst quality), while 0 means the lack of some base well data.

Starting from this initial database, during data preparation elevation conversion of reference points from the Adriatic to the Baltic Sea level was necessary in case of the hydrocarbon wells. Then those wells were cancelled, which do not have temperature data corrected to the elevation of the reference point or have temperature data ranked by 0. Consequently, 1121 temperature data of 372 wells in the DSA, and 429 temperature data of 143 wells in the BBSA were applied during the subsequent data processing. Areal and depth distribution of these data can be seen in A-Fig. 4.4.1-2 and 4.4.3, respectively.

4.4.3 Data processing

Since the primary objective of temperature (and hydrochemical) data analysis was the support of hydraulic interpretations, also these data were processed by the same methods as hydraulic data.

First, temperature vs. elevation or T(z) profiles were constructed for the same areas as p(z) profiles where also temperature data were available. Thus 35 and 14 T(z) profiles were completed in the DSA and BBSA, respectively. For their location see A-Fig. 4.4.1-2, while the profiles can be found among the results in A-Fig. 5.3.1.87-121 and 5.3.1.217-230 in the DSA and BBSA, respectively.

Similar to the use of hydrostatic vertical pressure gradient as a base of comparison in hydrodynamic analysis, also geothermal gradient analysis require some reference value. In this work two possible grad$T$ values came up, namely the continental average of 30°C/km, and the Pannonian Basin's average of 50°C/km. In order to relieve the interpretation, both were represented in the T(z) profiles started from the annual average surface temperature of 11 °C (RADÓ, 1974a,b,c). Data based thermal gradients were calculated in the feasible cases (i.e. when at least three data probably representing one gradient were available) using the chosen temperature values, while the gradient lines were only roughly drawn on the diagrams. Finally, considering that temperature data are usually less reliable than hydraulic data, absolute temperature data were interpreted rather statistically, whilst thermal gradients were of primary importance. As a result, average of the data applied in this work equaled to the Pannonian Basin's average of 50°C/km, which already represents positive anomaly compared

to the world average, while all of the data fall above the 30°C/km thermal gradient line. Consequently, during the interpretation of data the 50°C/km geothermal gradient was called as the "average", however always keeping in mind that also negative anomalies compared to this average show positive anomaly in relation to the continental average (30°C/km). /Incidentally, lower temperature data usually received worse qualification from DÖVÉNYI et al. (2002)./

In addition, also the hydrostratigraphic units are presented in the T(z) profiles in order to support the interpretation.

Secondly, tomographic isotherm maps /T(x,y)/ were made up for the same elevation intervals as fluid-potential maps, with the exception of the uppermost slice in the DSA, and the two uppermost slices in the BBSA where temperature data were unavailable. Consequently, 9 and 8 isotherm maps were constructed in the DSA and BBSA, respectively, using kriging method by the Golden Software Surfer 8 program. (Made by hand contouring was avoided in this case considering the minor importance of these maps compared to the potential maps and cross-sections.) During interpretation it is important to take into account, that this computational interpolation may be questionable in areas where only a few or no data are available (particularly in the marginal areas). Elevation intervals can be found in A-Table 4.3, while the isotherm maps among the results in A-Fig. 5.3.2.12-20 and 5.3.2.41-48 in the DSA and BBSA, respectively. Hydrocarbon (mostly gas in the DSA) inflows and seismically interpreted faults are also indicated in the maps.

Finally, geothermal cross-sections /T(s,z)/ were compiled by using the same projection method and along the same traces as hydraulic cross-sections, while contouring was made by hand for the same reasons as in case of the hydraulic cross-sections. Location of the sections can be found in A-Fig. 4.4.1-2, while the cross-sections among the results amidst A-Fig. 5.3.3.1-21 and 5.3.3.22-39 in the DSA and BBSA, respectively. Hydrocarbon (mostly gas in the DSA) inflows, as well as seismically interpreted faults and hydrostratigraphic units are also indicated in the sections.

However, data distribution and quantity did not allow of the contouring of temperature values along the whole sections, though linear interpolation is less affected by errors than in case of the hydraulic data, since geothermal gradient proved to be more uniform in those areas where enough data were available. (It can be explained by the less variable thermal conductivity of rocks compared to their hydraulic conductivity.) Thus the completed interpretation is rather conservative, but also more reliable. In addition as a result, the areas

characterized by anomalously high or low temperature gradients were also indicated in the sections.

4.5 Hydrochemistry

4.5.1 Principles

Chemical composition of groundwater is usually studied by comparing the absolute and relative quantities of the dissolved components mostly by using Stiff- or Piper-diagrams. These methods visualize the main hydrochemical components, such as the Na^+, K^+, Mg^{2+}, Ca^{2+} ions, and Cl^-, SO_4^{2-}, HCO_3^-, CO_3^{2-} anions. However, in the Study Areas of this work, only in a few cases were available all of these parameters measured in one water sample. Consequently, and considering also the complementary character of the hydrochemical analysis, only the salinity or TDS (total dissolved solids content) data were interpreted in the present study. Finally, the use of (only) these data, as well as the comparability with the hydraulic and temperature analysis required the application and development of other methods than the usual ones (i.e. Stiff-, Piper-diagrams).

4.5.2 Data culling and preparation

Water well data were collected from the original (paper-based) records of 1716 wells in the DSA, and 2944 wells in the BBSA. During data culling, usual hydrogeological criteria, as well as the criteria of HITCHON and BRULOTTE (1994), and HITCHON (2000) were applied beside the main objective of this work (i.e. analysis of TDS contents).

First, those wells were cancelled, which did not possess the base data, as well as the top and bottom depth of the screened interval, or the depth of the water sampling. In the remnant wells, reference points of the hydrochemical analyses were determined as the middle of the screened depth interval in case of the outflowing water samples, or as the given elevation where the water sample of depth was taken. Then in order to filter out the analytical errors, those water samples were cancelled in which Na^+ content value was not recorded (it is the most basic hydrochemical parameter of groundwater, which could not equal to zero or a negative value, only if it was calculated – erroneously), and/or the ionic balance calculation showed larger error than 5%. Next culling criterion was that pH should have been between 4 and 10, otherwise acid wash contamination, wash from cement job, or by chance typing error

in decimal point could be supposed. NO_3^- and CO_3^{2-} contents rarely represented higher values than 4 and 100 mg/L respectively, and always in shallow depths (< 500 m) where it can be explained by surface contamination. /Otherwise (i.e. in greater depths) it would be a culling criterion as well./ Subsequently, in water samples where TDS was missing it could be calculated if electric conductivity (*EC*), or its reciprocal electrical resistance was measured by the following equation:

$$TDS = EC * A \tag{6}$$

where TDS the total dissolved solids content [M/L^3], *EC* the electric conductivity [T^3I^2/L^2M] (µS/cm), *A* a dimensionless conversion factor usually varies between 0.55 and 0.75 in most groundwater (FREEZE and CHERRY, 1979, pp. 140) pending the ionic composition of the solution. Based on water samples in which TDS and electrical conductivity were also recorded, the average value of *A* could be calculated as 0.98 in the DSA, and 1.02 in the BBSA. Thus in Eq. (6) these values were applied for the two main Study Areas, respectively, and consequently almost all of the water samples were provided with an originally documented or calculated TDS value. Afterwards, also those samples were cancelled in which the difference between the TDS and the sum of the ions exceeds 5%. Eventually, since water samples were not taken necessarily after the well completion, while the original, undisturbed hydrochemical conditions were aimed to analyze in this work, also those samples were deleted which were taken later than one year after well completion, or simply did not record the date of sampling. Finally, among the analyzed parameters only the TDS content values were interpreted based on the objectives of this work (see Chapters 4.5.1. and 3.1.4.3.), while in the BBSA also the HCO_3^- concentrations were taken into account during the interpretation (see also Chapter 6.1.3). As a result, 482 water samples of 482 water wells in the DSA, and 47 water samples of 47 wells in the BBSA were applied during the subsequent data processing.

Hydrocarbon well data were put at our disposal by the MOL Plc. in electronic format (MS Excel spreadsheet). However, also the original (paper-based) well records were reviewed, since during data processing reliability and reality of some data became questionable, and several digital data had to be revised. The thus re-examined database contains water sample analyses of 464 and 159 wells in the DSA and BBSA, respectively. After the conversion from the Adriatic to the Baltic reference sea level of the elevation of the rotary tables, the middle of the tested depth intervals and their elevations were determined as reference points of the hydrochemical analyses. Since the measured depth of the perforated sections were given, in inclined wells also the true vertical depth values had to be calculated before elevation conversion. Afterwards, data culling was carried out in the same way (i.e.

based on the same criteria) as in case of the water well samples, with the exception of TDS calculation, since it was recorded in every sample, while electric conductivity was not measured. As a result, 192 water samples of 106 water wells in the DSA, and 318 water samples of 158 wells in the BBSA were applied during the subsequent data processing.

Areal and depth distribution of the finally used data can be seen in A-Fig. 4.5.1-2 and 4.5.3-4.

Finally, some further theoretical considerations also have to be taken regarding the reliability of hydrochemical data. Namely, during the above described data culling process only the lack of data and the analytical errors could be taken into account, while quality of the sampling and analyzing methods remained unknown. Accordingly, it causes significant uncertainty particularly in the representativeness of hydrocarbon well samples, which are usually outflowing water samples and easily contaminated by drilling mud the composition of that remained unknown as well. Consequently, the hydrochemical data are the less reliable among the well data.

4.5.3 Data processing

Since the primary objective of hydrochemical (and temperature) data analysis was the support of hydraulic interpretations, also these data were processed by the same methods as hydraulic data.

First, deviating from the hydrogeological practice (i.e. Stiff/Piper-diagram construction) concentration vs. elevation or so-called TDS(z) profiles were prepared for the same areas as p(z) /and T(z)/ profiles where also hydrochemical data were available. Thus 25 and 23 C(z) profiles were completed in the DSA and BBSA, respectively. For their location see A-Fig. 4.5.1-2, while the profiles can be found among the results in A-Fig. 5.3.1.122-146 and 5.3.1.231-253 in the DSA and BBSA, respectively.

Though TDS usually shows increase with depth, it is not usual to determine regionally characteristic gradient values, because its value depends on several factors (e.g., lithology, initial water composition, mixing, etc.) beyond depth. Consequently, a reference gradient value as the hydrostatic pressure gradient in the p(z) profiles, or the average geothermal gradients in the world and in the Pannonian Basin, cannot be defined in case of the hydrochemical data interpretation. On the other hand, in Hungary there are no guides, such as the “Opus Handbook – Formation Waters of Western Canada” (Johnson, 1992), which contains the characteristic chemical properties of the individual formations, that could be

serve as a ground for comparison. Thus, analysis was primarily based on the comparison of the TDS(z) profiles with each other, as well as the profiles of the DSA and BBSA.

Additionally, also the hydrostratigraphic units are presented in the TDS(z) profiles in order to support the interpretation during that it is important to continuously keep in mind the above detailed (see Chapter 4.5.2.) unreliability of hydrochemical data.

Secondly, tomographic iso-concentration (contour) maps /TDS(x,y)/ were made up for the same elevation intervals as fluid-potential maps, with the exception of the lowermost slice in the DSA, and the two uppermost slices in the BBSA where water chemical data were unavailable. Consequently, 9 and 8 iso-concentration maps were constructed in the DSA and BBSA, respectively, using kriging method by the Golden Software Surfer 8. (Made by hand contouring was avoided in this case considering the minor importance of these maps compared to the potential maps and cross-sections.) During interpretation it is important to take into account, that this computational interpolation may be questionable in areas where only a few or no data were available (particularly in the marginal areas). Elevation intervals can be found in A-Table 4.3, while the maps among the results in A-Fig. 5.3.2.21-29 and 5.3.2.49-56 in the DSA and BBS, respectively. Hydrocarbon (mostly gas in the DSA) inflows and seismically interpreted faults are also indicated in the maps.

Finally, hydrochemical cross-sections /TDS(s,z)/ were compiled by using the same projection method and along the same traces as hydraulic cross-sections, while contouring was made by hand for the same reasons as in case of the hydraulic cross-sections. Location of the sections can be found in A-Fig. 4.5.1-2, while the cross-sections among the results amidst A-Fig. 5.3.3.1-21 and 5.3.3.22-39 in the DSA and BBS, respectively. Hydrocarbon (mostly gas in the DSA) inflows, as well as seismically interpreted faults and hydrostratigraphic units are also indicated in the sections. However, data distribution and quantity particularly in case of hydrochemical data did not allow of the contouring of concentration values along the whole sections. Thus the completed interpretation is rather conservative, but also more reliable.

5 RESULTS AND INTERPRETATIONS

The referred A-Figures and A-Tables can be found in the Figure and Table Appendix volume.

5.1 Tectonics

Tectonic maps reflect the structural build-up of the Study Areas that could be come to know partly from the literature review as well (see also Chapter 3.2.1).

In the highly tectonized Derecske Study Area mostly strike-slip fault zones can be observed in the Pre-Neogene basement (Fig. 3.7), as well as their joint flower structures in the Pannonian strata (A-Fig. 5.2.1-2). Only around the Furta High can be noticed the almost complete lack of Pannonian faults above the grid-like faulted Pre-Neogene basement. However, in spite of the Pannonian basement's fault map (A-Fig. 5.2.1), the Pannonian strata above the Földes-East area are densely faulted according to my seismic interpretations. In addition, outside of the current exploring area of the MOL Plc. where no data were provided (in the maps), also the Szeghalom area represents significant amount of Pannonian and earlier faults as well. Furthermore, although these tectonic maps show only the main structural elements, in the north of the Derecske Trough, i.e. in its northern bounding strike-slip fault zone, according to the MOL Plc.'s experts and the literature review (see also Chapter 3.2.1) as well fault density is higher than in the south of the Trough. Finally, both strike-slip fault zones along the Trough are also currently active tectonically (e.g., WINDHOFFER and BADA, 2005).

In the Békés-Battonya Study Area only a few structural elements can be observed, particularly along the Battonya High's margins, as well as in the northern part of the Study Area joining to the fault systems located in the south of the Derecske Trough (Fig. 3.9, A-Fig. 5.2.4). Among the structures around the Battonya High, Pannonian faults are mostly atectonic (synsedimentary or growth faults), and consequently presumably inactive today.

5.2 Hydrostratigraphy

During the hydraulic, water chemical, and temperature data processing, hydrostratigraphy along the constructed profiles, maps, and cross-sections were interpreted. The characteristic thicknesses of the hydrostratigraphic units in each Study Area can be seen in A-Table 5.1.

The scarce porosity and permeability data could not been extended or interpreted regionally, although average values were calculated for each lithostratigraphy-based hydrostratigraphic unit where data were available (A-Table 5.2). These values show more or less correspondence with the average values referring to the whole Great Hungarian Plain (TÓTH and ALMÁSI, 2001). Additionally, it is conspicuous that the Algyő Aquitard's permeability (of the order of 10^{-13} m^2) is highest in the Battonya High Area among the Study Areas and hydrostratigraphic units as well; while in the Békés Basin the Szolnok Aquifer represents by far the lowest permeability (of the order of 10^{-16} m^2) among the Study Areas beside a medium porosity value (7.4%). However, also considering the number of wells (see also Chapter 4.2.1), these averages cannot be reckoned as reliable and representative values, thus the previous conclusions are not sufficiently established, tough seem to be true based on the p(z) profiles (see also Chapter 5.3.1).

Among the elevation maps of the hydrostratigraphic units the followings are presented from both Study Areas: Pre-Neogene basement (Fig. 3.7 and 3.9), Pannonian basement (or top of the Pre-Pannonian Aquifer) (A-Fig. 5.2.1 and 5.2.4), bottom of the Algyő Aquitard (or top of the Szolnok Aquifer, or top of the Endrőd Aquitard where Szolnok Aquifer not exists) (A-Fig. 5.2.2 and 5.2.5), top of the Algyő Aquitard (or bottom of the Great Plain Aquifer) (A-Fig. 5.2.3 and 5.2.6). Among the Pannonian strata Algyő Aquitard was chosen for presentation, because it proved to have the most significant control role in the dissipation of overpressure (see also Chapter 6.1).

5.3 Hydraulics, Geothermics, and Hydrochemistry

During hydraulic, temperature, and hydrochemical data processing the same methods were applied, since the primary objective of temperature and hydrochemical data analysis was the support of the hydraulic interpretations. Consequently, and according to the main objective of this work, it was possible the search for correlation among fluid-potential, temperature, and hydrochemical anomalies that could be expected based on the role of regional groundwater flows as agents of subsurface transport and accumulation. However, it is important to notice that the deviations in configuration (or shape) of the same hydraulic, temperature, and hydrochemical anomalies in maps and cross-sections has not to be taken into account considering the given data density. All in all, it is worth presenting the results in the order of applied methods instead of the order of data types.

5.3.1 Pressure-, temperature-, and TDS-elevation profiles

In order to facilitate the interpretation of profiles, maps showing the position of profiles and cross-sections, faults and topography in the Study Areas are presented in A-Fig. 5.3.1.1. and 5.3.1.147. Numbering of the pressure- /p(z)/ (A-Fig. 5.3.1.2-86 and 5.3.1.148-216), temperature- /T(z)/ (A-Fig. 5.3.1.87-121 and 5.3.1.217-230), and TDS-elevation profiles /TDS(z)/ (A-Fig. 5.3.1.122-146 and 5.3.1.231-253) is consistent irrespectively of data type, but with reference to the studied region. Profiles are presented in the Figure and Table Appendix volume type by type, thus first the p(z), then the T(z), and thirdly the TDS(z) profiles, since profiles representing the same type of data have to be compared with each other, for instance T(z) profiles with T(z) profiles. It has particular significance in case of the p(z) profiles where usually only a few (one or two) data were available from one profile, thus adjacent profiles often had to be jointly interpreted. Furthermore, p(z) profiles are presented in the decreasing order of their elevation interval (from z = 200-(-6000) m asl to z = 150-(-200) or -(-1000) m asl in the DSA and BBSA, respectively). However, descriptions of the profiles are displayed in the order of the studied regions in order to avoid repetitions. In the descriptions "gaseous pressure data" mean pressure data measured beside gas inflow, thus presumably in a gas column (see also Chapter 4.3.1). Pressure and temperature gradient values are signed in the diagrams. Superhydrostatic vertical pressure gradient (γ_{sp}) refers to upward flow conditions, while subhydrostatic vertical pressure gradient (γ_{sb}) to downward flow conditions.

5.3.1.1 Derecske Study Area

#1

p(z) (A-Fig. 5.3.1.2-4): Above z = 0 m asl subhydrostatic pressure data and slightly subhydrostatic vertical pressure gradient (γ). Below z = 0 m asl sub- and superhydrostatic data, superhydrostatic γ.

T(z) (A-Fig. 5.3.1.87): Average gradient of the data in the Great Plain Aquifer is higher than that of the Pannonian Basin's average of 50°C/km (called as the "average" in the followings).

TDS(z) (A-Fig. 122): Two salient maximums can be found at the bottom of the Great Plain Aquifer (TDS: 17,600 and 16,800 mg/L). The two higher values (>5000 mg/L) in shallow depth (above z = 0 m asl) is due to these samples extremely high Cl^- concentration (>1800 mg/L), that could be also surface contamination.

Interpretation: Downward flow down to z = 0 m asl, than upward flow in greater depth.

#2

p(z) (A-Fig. 5.3.1.5-7): Data are available from water wells of the Great Plain Aquifer, and one from the Algyő Aquitard. z = 150-0 m asl: subhydrostatic γ, below z = 0 m asl slightly superhydrostatic γ, overpressured data from the Algyő Aquitard.

T(z) (A-Fig. 5.3.1.88): Temperature gradient (grad*T*) is higher than the average (50°C/km).

TDS(z) (A-Fig. 5.3.1.123): Data are available only from shallow depth.

Interpretation: Downward flow down to z = 0 m asl, than upward flow in greater depth.

#3

p(z) (A-Fig. 5.3.1.8-10): Above z = (-150) m asl slightly subhydrostatic γ, below it subhydrostatic, however highly superhydrostatic γ can be observed only below z = (-850) m asl.

T(z) (A-Fig. 5.3.1.89): z = (-200)-(-700) m asl: data above the average, grad*T* lower than the average. Below z = (-850) m asl: increasing values at the bottom of the Great Plain Aquifer, while grad*T* (149°C/km) is rather apparent due to data scatter.

TDS(z) (A-Fig. 5.3.1.124): Also higher values at the bottom of the Great Plain Aquifer.

Interpretation: Upward flow up to z = (-150) m asl, while below z = (-850) m asl salient increase in pressure and slight heat accumulation. Some heterogeneity could be supposed in the Great Plain Aquifer at about this depth.

#4

p(z) (A-Fig. 5.3.1.11-13): Data are available only from water wells of the Great Plain Aquifer showing subhydrostatic γ down to z = (-250) m asl, which deeper becomes slightly superhydrostatic.

T(z) (A-Fig. 5.3.1.90): Data are above the average grad*T* line.

TDS(z) (A-Fig. 5.3.1.125): Data are available only from shallow depth.

Interpretation: Downward flow down to z = (-250) m asl, than upward flow in greater depth.

#5

p(z) (A-Fig. 5.3.1.14-16): Data are available only from water wells of the Great Plain Aquifer, which show slightly superhydrostatic γ.

T(z) (A-Fig. 5.3.1.91): Data scatter around the average.

TDS(z) (A-Fig. 5.3.1.126): 2 data are available from the Great Plain Aquifer.

Interpretation: Upward flow, no significant anomalies.

#6

p(z) (A-Fig. 5.3.1.17-18): Data are available only from water wells of the Great Plain Aquifer with slightly superhydrostatic γ.

T(z) (A-Fig. 5.3.1.92): Data scatter around the average.

Interpretation: Upward flow, no significant anomalies.

#7

p(z) (A-Fig. 5.3.1.19-20): Water well data from the Great Plain Aquifer and Algyő Aquitard down to at least z = (-900) m asl are mostly subhydrostatic. Above z = 0 m asl: subhydrostatic γ, z = 0-(-50) m asl: superhydrostatic γ, or completely subhydrostatic γ above z = (-50) m asl. z = (-600)-(-900) m asl: subhydrostatic γ.

T(z) (A-Fig. 5.3.1.93): Temperature data in the Algyő Aquitard are above the average, but grad*T* is around the average.

TDS(z) (A-Fig. 5.3.1.127): In the Algyő Aquitard increased concentrations can be observed compared to the shallow values.

Interpretation: Possessing the highest topographical elevation in the DSA, the region of Debrecen represents a recharge area in the upper, gravitational fluid flow system. Based on the potential maps (see also Chapter 5.3.2) overpressured upward flow can be observed up to z ≈ (-1200) m asl, thus the zone between z = (-900) and (-1200) m asl may represent the transient zone between the gravitational and overpressured fluid flow systems characterized by accumulation of heat and dissolved solids (due to the juncture of converging flows). Incidentally, also the effect of decennial intensive water production might contribute to the subhydrostatic pressure conditions above z = (-900) m asl.

#8

p(z) (A-Fig. 5.3.1.22-24): Water well data from the Great Plain Aquifer and Algyő Aquitard down to z ≈ (-1100) m asl are mostly subhydrostatic. Above z = (-100) m asl: subhydrostatic γ, then z = (-600)-(-1100) m asl: approximately hydrostatic γ.

T(z) (A-Fig. 5.3.1.94): Temperature data in the Algyő Aquitard and Pre-Pannonian Aquifer are above the average, but grad*T* is lower than the average.

TDS(z) (A-Fig. 5.3.1.128): In the Algyő Aquitard increased concentrations can be observed compared to the shallow values.

Interpretation: Possessing the highest topographical elevation in the DSA, the region of Debrecen represents a recharge area in the upper, gravitational fluid flow system. Based on the potential maps (see also Chapter 5.3.2) overpressured upward flow can be observed up to z ≈ (-1200) m asl, thus the hydrostatic zone between z = (-600) and (-1100) m asl may

represent the transient zone between the gravitational and overpressured fluid flow systems characterized by accumulation of heat and dissolved solids (due to the juncture of converging flows). Incidentally, also the effect of decennial intensive water production might contribute to the subhydrostatic conditions.

#9

p(z) (A-Fig. 5.3.1.25-26): Data from the Great Plain Aquifer's water wells show slightly superhydrostatic γ. The two deeper superhydrostatic data /around z = (-550) m asl/ are not gaseous. One data from the Pre-Pannonian Aquifer /z ≈ (-2100) m asl, p ≈ 33 MPa) can be found below the thick sequence of Algyő and Endrőd Aquitards, and along a Pannonian fault started from the Pre-Neogene basement.

T(z) (A-Fig. 5.3.1.95): Data and grad*T* are around the average (50°C/km) in the Great Plain Aquifer, then higher absolute temperature data and approximately average grad*T* below the Algyő and Endrőd Aquitards.

TDS(z) (A-Fig. 5.3.1.129): Values are increasing with depth, and particularly at the bottom of the Great Plain Aquifer.

Interpretation: Algyő and Endrőd Aquitards represent a continuous and effective aquitard unit accumulating potential energy and heat below the top of the Algyő Aquitard, while the fault may allow of pressure dissipation toward the slightly superhydrostatic Great Plain Aquifer.

#10

p(z) (A-Fig. 5.3.1.27-28): Data from the Great Plain Aquifer's water wells show slightly superhydrostatic γ. The two deeper superhydrostatic data /around z = (-1000)-(-1200) m asl/ are not gaseous. One data from the Pre-Pannonian Aquifer /z ≈ (-2100) m asl, p ≈ 36 MPa) can be found below the thick sequence of Algyő and Endrőd Aquitards, and along a Pannonian fault started from the Pre-Neogene basement and crossing also the region of p(z) profile #9.

T(z) (A-Fig. 5.3.1.96): Data and grad*T* are around the average in the Great Plain Aquifer, then one higher absolute temperature data can be found in the Pre-Neogene basement.

TDS(z) (A-Fig. 5.3.1.130): One salient data can be found in at the bottom of the Great Hungarian Plain.

Interpretation: Algyő and Endrőd Aquitards represent a continuous and effective aquitard unit accumulating potential energy and heat below the top of the Algyő Aquitard, while the fault may allow of pressure dissipation toward the slightly superhydrostatic Great Plain

Aquifer. Hydraulic communication is probable among the regions of profiles #9 and #10, at least along the fault.

#11

p(z) (A-Fig. 5.3.1.29-30): Water well data from the Great Plain Aquifer are subhydrostatic, with subhydrostatic γ. One overpressured data in the Pre-Pannonian Aquifer.

T(z) (A-Fig. 5.3.1.97): Temperature data in the Great Plain Aquifer are around the average.

Interpretation: See the combined interpretation of profiles #11 and #12 at the interpretation of profile #12.

#12

p(z) (A-Fig. 5.3.1.31-32): Two water well data and their γ in the Great Plain Aquifer are subhydrostatic. Overpressured data can be found in the Pre-Pannonian Aquifer.

Interpretation: It is worth jointly interpreting profiles #11 and #12. These nearby areas in the north of the northern main fault zone of the Derecske Trough may appoint slightly superhydrostatic conditions below the Algyő Aquitard, and show relatively lower overpressures /$p \approx$ 31-32 MPa at $z \approx$ (-2500) m asl/ than the adjacent profiles #13, #14, and #15 in the south of the Trough.

#13

p(z) (A-Fig. 5.3.1.33-34): Water well data from the Great Plain Aquifer are subhydrostatic with subhydrostatic γ. Highly overpressured data were measured in the Algyő Aquitard and Pre-Neogene basement. In the latter, scatter of data is significant also within the single wells in about the same depth, thus γ could not be determined unambiguously.

T(z) (A-Fig. 5.3.1.98): Temperature data at the bottom of the Algyő Aquitard and in the Pre-Neogene basement are mostly above the average, while grad*T* is signficantly higher (103°C/km) than the average.

TDS(z) (A-Fig. 5.3.1.131): Higher values can be found only below the Algyő Aquitard /TDS = 17,200 mg/L at z = (-2480) m asl/.

Interpretation: Scatter of data in the Pre-Neogene basement can be explained by that it is highly fractured and faulted according to the seismic sections. Algyő Aquitard acts as an effective barrier zone maintaining significant overpressure, as well as salt and heat accumulations in the basement. For further interpretation see also profile #15.

#14

p(z) (A-Fig. 5.3.1.35-36): Water well data and γ in the Great Plain Aquifer are subhydrostatic. One highly overpressured data in the Pre-Neogene basement.

TDS(z) (A-Fig. 5.3.1.132): One sample shows highly elevated concentration in the Pre-Neogene basement /TDS = 20,900 mg/L at z = (-3060) m asl/.

Interpretation: See the combined interpretation of profiles #13, #14, and #15 at the interpretation of profile #15.

#15

p(z) (A-Fig. 5.3.1.37-39): Shallow /down to z = (-150) m asl/ water well data and γ in the Great Plain Aquifer are subhydrostatic. There are four data from hydrocarbon wells along Pannonian basement faults in the lower part of the Great Plain Aquifer /below z = (-1100) m asl/, which are slightly overpressured, but three of them are gaseous data. Their γ is minimally superhydrostatic. One significantly overpressured data can be found at the bottom of the Algyő Aquitard.

T(z) (A-Fig. 5.3.1.99): Data and grad*T* are around the average from the Great Plain Aquifer to the Pre-Neogene basement. Incidentally, temperature data from those hydrocarbon wells, which represent slightly overpressured data in the Great Plain Aquifer /between z = (-1100)-(-1400) m asl/, show higher values than the average.

TDS(z) (A-Fig. 5.3.1.133): Higher values can be found only in the hydrocarbon wells representing overpressured conditions /TDS = 3,100-4,600 mg/L at z = (-1100)-(-1200) m asl/.

Interpretation: Since one data among the overpressured hydrocarbon wells in the Great Plain Aquifer is not gaseous, but also superhydrostatic, the system should be superhydrostatic as well even if the three other data were measured in gas column(s). Furthermore, it is also worth jointly interpreting profiles #13, #14, and #15. These nearby areas in the south of the Derecske Trough may appoint superhydrostatic γ in the Pre-Neogene basement and Algyő Aquitard as well, though γ in the latter is higher. Additionally, these data show relatively higher overpressures /p ≈ 37 MPa at z ≈ (-2500) m asl/ than the adjacent profiles #11 and #12 in the north of the Trough.

#16

p(z) (A-Fig. 5.3.1.40-41): Subhydrostatic data and superhydrostatic γ in the Great Plain Aquifer's water wells. Data from the Algyő Aquitard and Pre-Neogene basement are highly overpressured with superhydrostatic γ.

T(z) (A-Fig. 5.3.1.100): Data and grad*T* are slightly above the average in the Pre-Neogene basement.

TDS(z) (A-Fig. 5.3.1.134): Only shallow data /down to z = (-100) m asl/ were available.

Interpretation: According to the hydrostratigraphic classification of the wells, Algyő Aquitard is about 1000 m thick, however in seismic sections only the upper 400 m section shows the delta slope facies (it is general in the north of the Derecske Trough). Significant pressure drop could be supposed at the bottom of this section. Since overpressure is significant still at the top of the Algyő Aquitard (gaseous data, but highly overpressured in a great depth), there should be an aquitard zone in the bottom of the Great Plain Aquifer as well.

#17

p(z) (A-Fig. 5.3.1.42-43): Water well data and γ in the Great Plain Aquifer are subhydrostatic. There is significant overpressure in the Pre-Pannonian Aquifer (the higher value!) and Pre-Neogene basement.

T(z) (A-Fig. 5.3.1.101): Two data above the average in the Endrőd Aquitard and Pre-Pannonian Aquifer.

Interpretation: Regarding the higher pressure value in shallower depth in the Pre-Pannonian Aquifer than in greater depth in the Pre-Neogene basement, these values proved to be reliable during data culling. Thus, it could be explained by the presence of two separated pressure systems, which theory is however not supported by the general experiences regarding the Pre-Pannonian Aquifer's and Pre-Neogene basement's hydraulic conditions. On the other hand, by jointly interpreting with profile #16 it can be interpreted as uncertainty of the measurements. For further interpretation see also profile #19.

#18

p(z) (A-Fig. 5.3.1.44-45): Water well data from the Great Plain Aquifer show subhydrostatic γ. Hydrocarbon well data from the bottom of the Great Plain Aquifer /below z = (-1600) m asl/ are slightly overpressured, however γ is approximately hydrostatic. Data in the Algyő Aquitard show superhydrostatic γ close to the lithostatic γ (≈ 25 MPa/km).

T(z) (A-Fig. 5.3.1.102): Data below the average in the Great Plain Aquifer and Algyő Aquitard received poor qualification from DÖVÉNYI et al. (2002).

Interpretation: Overpressured hydrocarbon well data with hydrostatic γ in the Great Plain Aquifer may due to that these were measured in gas pools. The almost lithostatic γ around the top of the Algyő Aquitard may rather refer to the presence of a very low-permeability strata. For further interpretation see also profile #19.

#19

p(z) (A-Fig. 5.3.1.46-47): Shallow water well data from the Great Plain Aquifer show subhydrostatic γ. Among the two slightly overpressured data around the top of the Algyő Aquitard the deeper one is gaseous, and the γ is close to the lithostatic γ (≈ 25 MPa/km).

Interpretation: It is worth also jointly interpreting profiles #16, #17, #18, and #19. Accordingly, significant overpressure can be observed below the top of the Algyő Aquitard, but in shallower depth the pressure system is hydrostatic. Incidentally, several faults are known from the area, while the almost lithostatic γ around the top of the Algyő Aquitard may refer to the presence of a very low-permeability strata.

#20

p(z) (A-Fig. 5.3.1.48): Gaseous overpressured data from the bottom of the Great Plain Aquifer to the bottom of the Pre-Pannonian Aquifer /p = 57 MPa at z = (-3150) m asl/. One or two γ line could be fitted to the points, bur both are highly superhydrostatic.

T(z) (A-Fig. 5.3.1.103): One data can be found below the average in the Algyő Aquitard and another above the average in the Pre-Neogene basement.

TDS(z) (A-Fig. 5.3.1.135): The deepest /z = (-3200)-(-3300) m asl/ hydrochemical data in the Derecske Study Area, but there are not salient concentrations (TDS_{max} = 15,500 mg/L) regarding the depth.

Interpretation: Gaseous data show such significant overpressures that considering the maximum gas column heights known from the study area (110 m) as well, also the water leg should be highly overpressured, while the γ is superhydrostatic. Since the Algyő Aquitard is highly tectonized, fractured, and faulted, it acts as a less effective aquitard unit, which allows of gradual overpressure dissipation and upward hydrocarbon migration into the lower part of the Great Plain Aquifer as well. For further interpretation see also profile #21.

#21

p(z) (A-Fig. 5.3.1.49-50): Only three data from shallow water wells, which are subhydrostatic with superhydrostatic γ. Significantly overpressured data in the Pre-Pannonian Aquifer determine a slightly superhydrostatic γ.

T(z) (A-Fig. 5.3.1.104): Shallow values from the Great Plain Aquifer can be found around the average.

Interpretation: γ in shallow depths cannot be determined unambiguously from three data, but based on the tomographic potential maps, fluids flow upward near to the land surface, then γ becomes hydrostatic above the zone of deep upwelling. Consequently, the

gravitational and overpressured system can be distinguished hydraulically in this area, even if both show discharge features. There is no Pannonian fault in the otherwise thick Neogene strata. It is worth also jointly interpreting profiles #20 and #21. In profile #20 a moderate "break" can be observed at the bottom of the Algyő Aquitard where the Pre-Pannonian Aquifer's system of approximately hydrostatic γ (represented by profile #21 as well) turns into the Algyő Aquitard with a higher γ. It means that the Algyő Aquitard impedes fluid flow effectively, but overpressure can dissipate even gradually where several Pannonian faults exist.

#22

p(z) (A-Fig. 5.3.1.51-52): Water well data from the Great Plain Aquifer are subhydrostatic, while γ is slightly superhydrostatic. Significant overpressure can be observed in the Algyő Aquitard, Pre-Pannonian Aquifer, and Pre-Neogene basement seemingly delineating a superhydrostatic γ. However, data from differing hydrostratigraphic units can be found in similar depths in the profile.

T(z) (A-Fig. 5.3.1.105): Data in the Great Plain Aquifer scatter around the average grad*T*, then in the Algyő Aquitard more data can be found above the average, while large differences can be observed in similar depths (e.g., 50°C/90m) within 3 km horizontal distance.

TDS(z) (A-Fig. 5.3.1.136): Slightly increasing concentrations with depth down to z = (-800) m asl, and one sample from the Pre-Neogene basement /TDS = 13,300 mg/L at z = (-2300) m asl/ can be observed.

Interpretation: The analyzed wells are scattered in or above a less tectonized, but westward ascending Pre-Neogene basement, which may explain the occurrence of data from differing hydrostratigraphic units in similar depths in the p(z) profile. The superhydrostatic γ shows continuous, gradual overpressure dissipation toward the shallower depths through the Algyő Aquitard as well. However, since the Great Plain Aquifer is only slightly superhydrostatic, there should be a low-permeability zone in its bottom, or in the top of the otherwise thin Algyő Aquitard. Dispersion of the temperature data can partly be explained by the geological setting as in case of the pressure data, but the large differences in similar depths and within small horizontal distances need further interpretation as well. If data reliability is acceptable, conductive and convective heat flow properties should be considered. The former can be excluded, because if these phenomena could be explained by differences in the thermal conductivity of rocks (e.g., between two sides of a fault), lateral grad*T* would be very high and thus the difference would level off

quickly. Consequently, difference in the fluid supply (i.e. convectively transported heat) of rocks, or in other words convective heat transport along faults and its variability could generate the observed situation.

#23

p(z) (A-Fig. 5.3.1.53-54): Water well data from the Great Plain Aquifer are mostly subhydrostatic, while γ is slightly superhydrostatic. Gradual, slightly superhydrostatic dissipation of the significant overpressure in the Pre-Neogene basement and Pre-Pannonian Aquifer can be observed. One overpressured data from the Algyő Aquitard is gaseous, but also its water leg should be overpressured considering the degree of excess pressure compared to the hydrostatic γ of water.

T(z) (A-Fig. 5.3.1.106): Data in the Great Plain Aquifer scatter around the average grad*T*, then below the Algyő Aquitard more data can be found above the average, while the deviation from the average decreases with depth in the Pre-Pannonian Aquifer and Pre-Neogene basement.

Interpretation: Algyő Aquitard is thin (maximum 300 m), but effective flow barrier accumulating heat as well.

#24

p(z) (A-Fig. 5.3.1.55-56): Water well data from the Great Plain Aquifer are slightly subhydrostatic. The only one overpressured data at the bottom of the Algyő Aquitard is gaseous, but also its water leg should be overpressured concerning the depth and degree of the excess pressure

T(z) (A-Fig. 5.3.1.107): Data in the Great Plain Aquifer are slightly above the average.

Interpretation: See the combined interpretations at profiles #25 and #26.

#25

p(z) (A-Fig. 5.3.1.57): Shallow water well data from the Great Plain Aquifer show slightly superhydrostatic γ. Four deeper hydrocarbon well data /between z = (-1100)-(-1400) m asl/ from the Great Plain Aquifer are overpressured and show the same slightly superhydrostatic γ, however being gaseous. One overpressured data from the Pre-Neogene basement.

T(z) (A-Fig. 5.3.1.108): Data in the Great Plain Aquifer are above the average.

Interpretation: Superhydrostatic γ of the gaseous pressure data is also supported by the superhydrostatic γ of the shallower water wells. Fault connection can be assumed between the regions of profiles #25 and #24. See also the combined interpretation of profiles #24, #25, and #26 at the interpretation of profile #26.

#26

p(z) (A-Fig. 5.3.1.58-59): Water well data from the Great Plain Aquifer are slightly superhydrostatic. Overpressured data in the Pre-Pannonian Aquifer and Pre-Neogene basement were measured in two wells. Position (i.e. depth) of their hydrostratigraphic units is differing, thus one γ line could not be interpreted.

T(z) (A-Fig. 5.3.1.109): Data in the Pre-Pannonian Aquifer are below the average and show higher grad*T* as well. However, below the bottom of the Endrőd Aquitard, some data fall on the average grad*T* line.

TDS(z) (A-Fig. 5.3.1.137): Slightly increasing concentrations with depth down to z = (-1000) m asl, and two samples from the Pre-Pannonian Aquifer with elevated concentrations can be observed.

Interpretation: Between the two deep and nearby wells a fault could be identified on seismic sections, which was quested based on these hydraulic results. It may be a barrier fault, which impedes fluid flow among the two wells causing the development of strongly different pressure conditions on its two sides. It is worth also jointly interpreting profiles #24, #25, and #26. In Significant overpressure and slightly superhydrostatic gradients below the top of the Algyő Aquitard refer to that this aquitard and particularly its lower section is an effective flow barrier in this region. According to the heat and salt accumulation below the Endrőd Aquitard also it acts as an effective aquitard unit. The overpressured and not gaseous Pre-Pannonian data at z ≈ (-2300) m asl in profile #26 confirms that the gaseous data in the Algyő Aquitard in profile #24 represent really superhydrostatic conditions.

#27

p(z) (A-Fig. 5.3.1.60-61): Water well data from the Great Plain Aquifer are subhydrostatic, while γ is approximately hydrostatic. Two overpressured data from one well in the Pre-Pannonian Aquifer are gaseous, thus γ cannot be determined between them.

T(z) (A-Fig. 5.3.1.110): Data from the Szolnok Aquifer down to the Pre-Neogene basement are mostly below the average, however their grad*T* is much higher (104°C/km) than the average.

TDS(z) (A-Fig. 5.3.1.138): Elevated concentrations in the Pre-Pannonian Aquifer and Pre-Neogene formations, but in the latter it is lower.

Interpretation: Water leg of the gaseous data should be highly overpressured as well regarding the degree of the overpressure and the average gas column heights in the Study Areas. Based on the heat and salt accumulation below the Algyő Aquitard as well, it

should be an effective flow impeding zone. See also the combined interpretation of profiles #27, #28, and #29 at the interpretation of profile #29.

#28

p(z) (A-Fig. 5.3.1.62): Water well data from the Great Plain Aquifer are hydrostatic. Highly overpressured data can be found in the Algyő Aquitard and particularly in the Pre-Pannonian Aquifer (e.g., p ≈ 49.20 MPa at z = 2506 m asl). γ (60.22 MPa/km) above the lithostatic γ is questionable, also because it is usually approximately hydrostatic in the Pre-Pannonian Aquifer.

T(z) (A-Fig. 5.3.1.111): Data from the Szolnok Aquifer down to the Pre-Neogene basement are below or above the average, while their grad*T* is higher than the average, while some relatively higher values can be observed around the Endrőd Aquitard as well.

Interpretation: Overpressured data in the Pre-Pannonian Aquifer seemingly show much higher γ than the lithostatic γ (≈ 25 MPa/km), which is practically impossible. Consequently, these data may rather represent the variable pressure conditions of a fractured, faulted rock framework, while the hydraulic opening of the fractures could be explained just by these overpressures. At the same time, Algyő Aquitard should seal very effectively thus maintaining the overpressure in the underlying strata, and allowing of only diffusive overpressure dissipation, which results in a significant pressure drop already at the bottom of the aquitard (see the relatively only slightly overpressured data in the Algyő Aquitard). Additionally, this may refer to the barrier character of the Endrőd Aquitard and/or Szolnok Aquifer as well. Also heat accumulation below the Algyő Aquitard supports its flow barrier character. See also the combined interpretation of profiles #27, #28, and #29 at the interpretation of profile #29.

#29

p(z) (A-Fig. 5.3.1.63-65): Water well data from the Great Plain Aquifer are subhydrostatic with also subhydrostatic γ down to z = (-100) m asl, then γ becomes superhydrostatic (based on two data). A highly overpressured data from the Pre-Pannonian Aquifer and another from the Pre-Neogene basement delineate a superhydrostatic γ (≈ 22.61 MPa/km).

T(z) (A-Fig. 5.3.1.112): Data from the Szolnok Aquifer down to the Pre-Neogene basement are mostly around the average with some relatively higher values below the Endrőd Aquitard. The two lowest temperature data in the z = (-2600)-(-3200) m asl elevation interval received poor qualification from DÖVÉNYI et al. (2002).

TDS(z) (A-Fig. 5.3.1.139): Only shallow data were available.

Interpretation: It is worth jointly interpreting profiles #27, #28, and #29. P(z) profile #27 and #29 show highly superhydrostatic, but realistic γ in the Pre-Pannonian Aquifer and Pre-Neogene basement, while in the former fractures and faults also scatter the pressure. On the other hand, Algyő Aquitard permits of the maintenance of these large overpressures by effectively impeding fluid flows. However, based on the significant pressure drop already at the bottom of the Algyő Aquitard, as well as on the heat and salt distribution around the Endrőd Aquitard, also this unit should represent a significant flow barrier.

#30

p(z) (A-Fig. 5.3.1.66-68): Hydrostratigraphy is deficient. Water well data from the Great Plain Aquifer show slightly superhydrostatic γ. There is a highly overpressured data from the Pre-Pannonian Aquifer and another from the Pre-Neogene basement, which are gaseous. γ is questionable regarding the lower value was observed at larger depth.

T(z) (A-Fig. 5.3.1.113): Data from the Great Plain Aquifer between z = (-150) and (-350) m asl are above the average.

TDS(z) (A-Fig. 5.3.1.140): Data from the Great Plain Aquifer are relatively low regarding the depth.

Interpretation: Water leg of the gaseous data should be highly overpressured as well regarding the degree of the overpressure and the average gas column heights in the Study Areas. Distribution of the overpressured data could be explained by the gas column origin, or by the variable pressure conditions of a fractured, faulted rock framework, or by uncertainty of the measurements. Anyway, these significant overpressures refer to the sealing character of the overlying strata. See also the combined interpretation of profiles #30 and #31 at the interpretation of profile #31.

#31

p(z) (A-Fig. 5.3.1.69-70): Hydrostratigraphy is deficient. Water well data from the Great Plain Aquifer show minimally superhydrostatic γ. There is only one highly overpressured data from the Pre-Pannonian Aquifer.

T(z) (A-Fig. 5.3.1.114): Shallow data from the Great Plain Aquifer scatter around the average.

Interpretation: By jointly interpreting profiles #30 and #31, overpressure in the Pre-Pannonian Aquifer and Pre-Neogene basement is significant, while the γ may be slightly superhydrostatic.

#32

p(z) (A-Fig. 5.3.1.71-72): Water well data from the Great Plain Aquifer are minimally superhydrostatic. Highly overpressured data at the bottom of the Algyő Aquitard, and in the Pre-Pannonian Aquifer (gaseous data) and Pre-Neogene basement delineate a slightly superhydrostatic γ (slightly below the gaseous data).

T(z) (A-Fig. 5.3.1.115): Data scattering below and above the average at the bottom of the Algyő Aquitard, and in the Pre-Pannonian Aquifer and Pre-Neogene basement delineate a significantly higher grad*T* (87 °C/km) than the average.

TDS(z) (A-Fig. 5.3.1.141): Elevated concentrations in the Pre-Pannonian Aquifer and Pre-Neogene basement scatter in a wide interval /TDS = 8200-17,600 mg/L in z = (-2100)-(-2400) m asl elevation interval/.

Interpretation: γ suits to the trend of profiles #27, #28, and #29, while the way of overpressure dissipation in the Algyő Aquitard is unknown. However, significant pressure drop is necessary trough this unit up to the hydrostatic Great Plain Aquifer, which refers to the sealing character of the Algyő Aquitard even if Pannonian faults are known in this region.

#33

p(z) (A-Fig. 5.3.1.73-74): Two water well data from the Great Plain Aquifer are subhydrostatic with superhydrostatic γ. γ of the overpressured gaseous data in the Endrőd Aquitard, Pre-Pannonian Aquifer, and Pre-Neogene basement cannot be determined unambiguously.

T(z) (A-Fig. 5.3.1.116): Data scatter above the average below the Algyő Aquitard, while grad*T* is also higher than the average.

TDS(z) (A-Fig. 5.3.1.142): Data below the Endrőd Aquitard show elevated concentrations also in relatively shallower depth /TDS_{max} = 42,896 mg/L at z = (-1676) m asl/ representing the highest measured concentration in the DSA as well.

Interpretation: Water leg of the gaseous data should be highly overpressured as well regarding the degree of the overpressure and the average gas column heights in the Study Areas. Algyő Aquitard is thin, but impedes fluid flow effectively maintaining the overpressure in relatively shallow depth in a Pre-Neogene basement high, and accumulating heat and salt in the underlying strata as well.

#34

p(z) (A-Fig. 5.3.1.75-76): Water well data from the Great Plain Aquifer are minimally subhydrostatic. Overpressured data in the Pre-Neogene basement show superhydrostatic γ,

while two gaseous data can be interpreted along gas γ (γ_g) lines sitting on the superhydrostatic water leg.

T(z) (A-Fig. 5.3.1.117): Only two data were available.

Interpretation: Salient overpressure can be observed in relatively shallow depth in a Pre-Neogene basement high, thus the otherwise thin Algyő Aquitard impedes fluid flow effectively

#35

p(z) (A-Fig. 5.3.1.77-78): Water well data from the Great Plain Aquifer show slightly superhydrostatic γ. In case of the overpressured and mostly gaseous data in the Algyő and Endrőd Aquitard γ cannot be determined unambiguously.

T(z) (A-Fig. 5.3.1.118): Data in the Great Plain Aquifer are above the average and represent elevated grad*T*. At the bottom of the Algyő Aquitard and in the Endrőd Aquitard and Pre-Pannonian Aquifer data are mostly above the average, while grad*T* is much higher (84°C/km) than the average.

TDS(z) (A-Fig. 5.3.1.143): Elevated concentrations can be found in the Endrőd Aquitard and Pre-Pannonian Aquifer.

Interpretation: Water leg of the gaseous data should be highly overpressured as well regarding the degree of the overpressure and the average gas column heights in the Study Areas. Algyő Aquitard is thin, but impedes fluid flow effectively maintaining the overpressure in relatively shallow depth in a Pre-Neogene basement high, and accumulating heat and salt in the underlying strata as well.

#36

p(z) (A-Fig. 5.3.1.79-81): Water well data from the Great Plain Aquifer show slightly subhydrostatic γ down to z = (-100) m asl, then superhydrostatic. In case of the overpressured and mostly gaseous data from the Algyő Aquitard down to the Pre-Neogene basement γ cannot be determined unambiguously.

T(z) (A-Fig. 5.3.1.119): Data in the Great Plain Aquifer are above the average, but represent lower grad*T*. From the bottom of the Algyő Aquitard down to the Pre-Neogene basement data are mostly above the average, while grad*T* equals to the average. Additionally, relatively higher values can be observed at the bottom of the Algyő Aquitard than in the Endrőd Aquitard.

TDS(z) (A-Fig. 5.3.1.144): Elevated concentrations can be found in the Pre-Pannonian Aquifer and Pre-Neogene basement.

Interpretation: Water leg of the gaseous data should be highly overpressured as well regarding the degree of the overpressure and the average gas column heights in the Study Areas. Algyő Aquitard is thin, but impedes fluid flow effectively maintaining the overpressure in relatively shallow depth in a Pre-Neogene basement high, and accumulating heat and salt in the underlying strata as well.

#37

p(z) (A-Fig. 5.3.1.82-83): Two water well data from the Great Plain Aquifer show subhydrostatic γ. In case of the overpressured and mostly gaseous data from the Endrőd Aquitard down to the Pre-Neogene basement γ cannot be determined unambiguously.

T(z) (A-Fig. 5.3.1.120): Two data in the Great Plain Aquifer are below the average. From the bottom of the Algyő Aquitard down to the Pre-Neogene basement data are below or above the average, while grad*T* is much higher (120°C/km) than the average.

TDS(z) (A-Fig. 5.3.1.145): Elevated concentrations can be found in the Pre-Pannonian Aquifer and Pre-Neogene basement.

Interpretation: Water leg of the gaseous data should be highly overpressured as well regarding the degree of the overpressure. Algyő Aquitard impedes fluid flow effectively maintaining the overpressure in relatively shallow depth in a Pre-Neogene basement high, and accumulating heat and salt in the underlying strata as well.

#38

p(z) (A-Fig. 5.3.1.84-86): Water well data from the Great Plain Aquifer show subhydrostatic γ down to z = (-100) m asl, then slightly superhydrostatic. In case of the overpressured and mostly gaseous data from the bottom of the Algyő Aquitard down to the Pre-Neogene basement γ cannot be determined unambiguously.

T(z) (A-Fig. 5.3.1.121): From the bottom of the Algyő Aquitard down to the Pre-Neogene basement data are below or above the average, while grad*T* is much higher (130°C/km) than the average.

TDS(z) (A-Fig. 5.3.1.146): Data from the Great Plain Aquifer scatter around the shallow average. Elevated concentrations can be found in the Pre-Pannonian Aquifer and Pre-Neogene basement.

Interpretation: Water leg of the gaseous data should be highly overpressured as well regarding the degree of the overpressure. Algyő Aquitard impedes fluid flow effectively maintaining the overpressure in relatively shallow depth in a Pre-Neogene basement high, and accumulating heat and salt in the underlying strata as well.

5.3.1.2 Békés-Battonya Study Area

Numbering is continuous regarding the profiles in the Derecske Study Area.

#39

p(z) (A-Fig. 5.3.1.148-149): Data from the Great Plain Aquifer show slightly superhydrostatic γ.

T(z) (A-Fig. 5.3.1.217): Data in the Great Plain Aquifer are below the average grad*T*.

TDS(z) (A-Fig. 5.3.1.231): Data were available only from shallow depth.

Interpretation: Upward flow, no significant anomalies.

#40

p(z) (A-Fig. 5.3.1.150-151): Shallow data from the Great Plain Aquifer show slightly superhydrostatic γ. Overpressured data were available from one well in the Pre-Pannonian Aquifer showing γ = 89.90 MPa/km.

T(z) (A-Fig. 5.3.1.218): Data from the Great Plain Aquifer down to the Pre-Pannonian Aquifer are below the average grad*T*, while their grad*T* is questionable, but usually higher than the average.

TDS(z) (A-Fig. 5.3.1.232): Data were available only from shallow depth.

Interpretation: Overpressured data in the Pre-Pannonian Aquifer seemingly show much higher γ than the lithostatic γ (≈ 25 MPa/km), which is practically impossible. Consequently, these data may rather represent the variable pressure conditions of a fractured, faulted rock framework, while the hydraulic opening of the fractures could be explained just by these overpressures. At the same time, overlying strata should seal very effectively, thus maintain the overpressure.

#41

p(z) (A-Fig. 5.3.1.152-153): Data from the Great Plain Aquifer show slightly subhydrostatic γ. Highly overpressured data /p = 70 MPa at z = (-3600) m asl/ in the Pre-Neogene basement delineate a slightly superhydrostatic γ.

T(z) (A-Fig. 5.3.1.218): Data from the Great Plain Aquifer down to the Pre-Neogene basement scatter around the average, while grad*T* is lower than the average below the Endrőd Aquitard.

TDS(z) (A-Fig. 5.3.1.232): Maximum values can be found at the bottom of the Great Plain Aquifer.

Interpretation: Strata between the Great Plain Aquifer and Pre-Neogene basement should impede fluid flow effectively maintaining the significant overpressure in the basement.

#42

p(z) (A-Fig. 5.3.1.154-155): Water well data from the Great Plain Aquifer are subhydrostatic, but delineate a slightly superhydrostatic γ. Deeper /z = (-1800)-(-1950) m asl/ water well data from the same unit and the Algyő Aquitard show superhydrostatic γ. One highly overpressured data from the Endrőd Aquitard /p = 54.46 MPa at z ≈ (-2850) m asl/.

T(z) (A-Fig. 5.3.1.219): Data from the Great Plain Aquifer down to the Pre-Neogene basement scatter around the average. Grad*T* seems to be high (92°C/km) around the Endrőd Aquitard.

Interpretation: Strata between the Great Plain Aquifer and Pre-Neogene basement should impede fluid flow effectively.

#43

p(z) (A-Fig. 5.3.1.156-157): Shallow water well data from the Great Plain Aquifer show slightly superhydrostatic γ. One deep /z ≈ (-1650) m asl/ water well data from the same unit is slightly overpressured. One highly overpressured data in the Endrőd Aquitard /p = 59.41 MPa at z ≈ (-2700) m asl/.

T(z) (A-Fig. 5.3.1.221): Data from the Great Plain Aquifer down to the Pre-Neogene basement are above the average, particularly below the Algyő Aquitard.

Interpretation: Strata between the Great Plain Aquifer and Pre-Neogene basement should impede fluid flow effectively maintaining overpressure in the Endrőd Aquitard of a degree similar to profile #42.

#44

p(z) (A-Fig. 5.3.1.158-159): Shallow water well data from the Great Plain Aquifer show slightly superhydrostatic γ. Deeper /z = (-1400)-(-1600) m asl/ water well data from the Great Plain Aquifer are overpressured, while γ is superhydrostatic as well. One highly overpressured data in the Endrőd Aquitard /p = 57.91 MPa at z ≈ (-2650) m asl/.

T(z) (A-Fig. 5.3.1.222): Data rise above the average only in the Endrőd Aquitard, but with a high grad*T* (81°C/km).

Interpretation: Strata between the Great Plain Aquifer and Pre-Neogene basement should impede fluid flow effectively maintaining overpressure in the Endrőd Aquitard of a degree similar to profile #42 and #43.

#45

p(z) (A-Fig. 5.3.1.160-161 Shallow water well data from the Great Plain Aquifer show slightly superhydrostatic γ. One overpressured data in the Algyő Aquitard is observable along a Pannonian fault originated in the Pre-Neogene basement.

T(z) (A-Fig. 5.3.1.223): Data are above the average, but their grad*T* approximately equals to the average.

Interpretation: Significant pressure drop can be observed already at the bottom of Algyő Aquitard that may refer to the barrier character of the Endrőd Aquitard as well.

#46

p(z) (A-Fig. 5.3.1.162-163): Subhydrostatic data and γ down to at least z = (-50) m asl, then slightly superhydrostatic data at the bottom of the Great Plain Aquifer. Slightly overpressured data in the Algyő Aquitard between z = (-1500) and (-1700) m asl show subhydrostatic γ.

T(z) (A-Fig. 5.3.1.224): Significantly higher values and grad*T* than the average in the Algyő Aquitard.

TDS(z) (A-Fig. 5.3.1.234): Slight increase of concentrations can be observed toward down to the bottom of the Algyő Aquitard, but also these values are very low regarding the depth (compared to the DSA).

Interpretation: Recharge conditions down to at least z = (-50) m asl. Heat accumulation may be related to hydrocarbon pools.

#47

p(z) (A-Fig. 5.3.1.164-165): Subhydrostatic data and γ down to z = (-150) m asl, then γ is minimally superhydrostatic form z = (-300) m asl. Overpressured data in the Szolnok Aquifer and Endrőd Aquitard between z = (-1700) and (-2100) m asl. Pre-Neogene basement is located in greater depth in those wells where the two deepest data derived from, thus also the Szolnok Aquifer is in a greater depth in these cases. γ cannot be interpreted unambiguously.

TDS(z) (A-Fig. 5.3.1.235): Increasing concentrations can be observed with depth from the bottom of the Algyő Aquitard, but also these values are very low regarding the depth (compared to the DSA).

Interpretation: Recharge conditions down to z = (-150) m asl. Algyő Aquitard hardly impedes fluid flow.

#48

p(z) (A-Fig. 5.3.1.166-167): Subhydrostatic data with minimally superhydrostatic γ down to z = (-200) m asl. One overpressured data in the Great Plain Aquifer from a hydrocarbon well is possibly gaseous.

T(z) (A-Fig. 5.3.1.225): Shallow data scatter around the average. Data and grad*T* (79°C/km) are highly above the average from the Szolnok Aquifer down to the Pre-Neogene basement.

TDS(z) (A-Fig. 5.3.1.236): Very low and similar concentrations in the total depth interval even in the Pre-Neogene basement compared to the DSA.

Interpretation: Discharge or midline conditions down to z = (-200) m asl.

#49

p(z) (A-Fig. 5.3.1.168-169): Shallow water well data show slightly superhydrostatic γ. Two minimally overpressured data in the Szolnok Aquifer.

Interpretation: Strata above the Endrőd Aquitard show aquifer characters.

#50

p(z) (A-Fig. 5.3.1.170-171): γ is subhydrostatic, particularly down from z = (-700) m asl, though most of the data is superhydrostatic there. In the Algyő and Endrőd Aquitards, as well as in the Pre-Neogene basement data are approximately hydrostatic with some superhydrostatic and gaseous exceptions in the Algyő Aquitard.

TDS(z) (A-Fig. 5.3.1.237): Very low and similar concentrations in the total depth interval even in the Pre-Neogene basement compared to the DSA.

Interpretation: Recharge conditions. Above the elevated Pre-Neogene basement Algyő and Endrőd Aquitards hardly or not impede fluid flow.

#51

p(z) (A-Fig. 5.3.1.172-173): Subhydrostatic data with hydrostatic γ down to z = (-400) m asl. In the Algyő and Endrőd Aquitards, as well as in the Pre-Neogene basement data are approximately hydrostatic with some superhydrostatic and gaseous exceptions in the Algyő Aquitard and subhydrostatic exceptions in the Endrőd Aquitard and Pre-Neogene basement.

TDS(z) (A-Fig. 5.3.1.238): Very low concentrations even in the Pre-Neogene basement compared to the DSA. Some salient concentrations (positive anomalies) can be observed in shallow depth /z = (-200)-(-400) m asl.

Interpretation: Midline conditions. Above the elevated Pre-Neogene basement Algyő and Endrőd Aquitards hardly or not impede fluid flow.

#52

p(z) (A-Fig. 5.3.1.174-175): Subhydrostatic data with subhydrostatic γ down to at least z = (-100) m asl. Deeper data at the bottom of the Great Hungarian Plain and Algyő Aquitard show slightly superhydrostatic γ.

TDS(z) (A-Fig. 5.3.1.239): Very low and similar concentrations in the total depth interval compared to the DSA.

Interpretation: Recharge conditions down to z = (-100) m asl. Above the elevated Pre-Neogene basement Algyő and Endrőd Aquitards hardly or not impede fluid flow.

#53

p(z) (A-Fig. 5.3.1.176-177): Shallow water well data show slightly superhydrostatic γ. In the Endrőd Aquitard, Pre-Pannonian Aquifer and Pre-Neogene basement also sub- and superhydrostatic data can be found, while γ cannot be determined unambiguously.

T(z) (A-Fig. 5.3.1.226): Data and grad*T* are above the average in the Great Plain Aquifer.

TDS(z) (A-Fig. 5.3.1.240): One sample from the Great Plain Aquifer shows elevated TDS concentrations compared to the deeper samples of low concentrations.

Interpretation: Above the elevated Pre-Neogene basement Algyő and Endrőd Aquitards hardly or not impede fluid flow.

#54

p(z) (A-Fig. 5.3.1.178-179): Shallow water well data are mostly subhydrostatic with slightly superhydrostatic γ. One slightly overpressured data at the bottom of the Great Plain Aquifer can be found as well.

T(z) (A-Fig. 5.3.1.227): Data and grad*T* scatter around the average in the Great Plain Aquifer.

Interpretation: Basically midline conditions can be observed in the Great Plain Aquifer.

#55

p(z) (A-Fig. 5.3.1.180-181): Shallow water well data show subhydrostatic γ down to z = (-150) m asl, then slightly superhydrostatic γ between z = (-300)-(-400) m asl. Slightly overpressured data at the bottom of the Great Plain Aquifer are gaseous. Data in the Algyő and Endrőd Aquitards are approximately hydrostatic and show slightly subhydrostatic γ.

TDS(z) (A-Fig. 5.3.1.241): Two shallow samples show increasing concentrations with depth.

Interpretation: Recharge conditions down to z = (-150) m asl. Algyő and Endrőd Aquitards hardly or not impede fluid flow.

#56

p(z) (A-Fig. 5.3.1.182-183): Shallow water well data shos subhydrostatic γ down to z = (-50) m asl, then γ is superhydrostatic between z = (-400)-(-800) m asl. Data in the Algyő and Endrőd Aquitards, as well as the Pre-Pannonian Aquifer are approximately hydrostatic with some subhydrostatic exceptions, which are PWS data (thus less reliable).

TDS(z) (A-Fig. 5.3.1.242): Very low and similar concentrations in the total depth interval compared to the DSA.

Interpretation: Recharge conditions down to z = (-50) m asl. Algyő and Endrőd Aquitards hardly or not impede fluid flow.

#57

p(z) (A-Fig. 5.3.1.184-185): Data are available only from the Great Plain Aquifer, which are approximately hydrostatic, but show slightly superhydrostatic γ. The deeper data are gaseous as well, while the subhydrostatic value is a PWS data (thus less reliable).

TDS(z) (A-Fig. 5.3.1.243): Very low and similar concentrations in the total depth interval compared to the DSA.

Interpretation: Recharge conditions can be observed in the Great Plain Aquifer.

#58

p(z) (A-Fig. 5.3.1.186-187): Shallow water well data show subhydrostatic γ down to z = (-50) m asl. One data from the Pre-Pannonian Aquifer is hydrostatic.

TDS(z) (A-Fig. 5.3.1.244): Slightly increasing concentrations with depth, but the concentrations are very low compared to the DSA.

Interpretation: Recharge conditions down to z = (-50) m asl. Algyő and Endrőd Aquitards hardly or not impede fluid flow.

#59

p(z) (A-Fig. 5.3.1.188-189): Shallow water well data show subhydrostatic γ down to z = (-170) m asl. The deeper superhydrostatic data in the Great Plain Aquifer /z = (-450)-(-650) m asl/ derived from hydrocarbon wells and show superhydrostatic γ. Data in the Algyő and Endrőd Aquitards, Pre-Pannonian Aquifer, and Pre-Neogene basement are hydrostatic or gaseous and superhydrostatic. γ cannot be determined unambiguously, however scatter of the (also pressure and hydrostratigraphic) data refers to fractured/faulted rock framework.

TDS(z) (A-Fig. 5.3.1.245): One sample show salient concentrations in relatively shallow depth /z ≈ (-600) m asl/.

Interpretation: Recharge conditions down to z = (-170) m asl. Algyő and Endrőd Aquitards hardly or not impede fluid flow.

#60

p(z) (A-Fig. 5.3.1.190-191): Shallow water well data show subhydrostatic γ down to z = (-100) m asl. Data in the Endrőd Aquitard are sub- or mostly superhydrostatic and show some scatter in a narrow depth interval /z = (-850)-(-890) m asl/.

TDS(z) (A-Fig. 5.3.1.246): Data of low concentrations in the Endrőd Aquitard scatter moderately in a narrow depth interval /z = (-890)-(-950) m asl/.

Interpretation: Recharge conditions down to at least z = (-100) m asl. Endrőd Aquitard is known to be mostly calcareous and highly fractured in this region, which could explain the scatter of pressure and hydrochemical data.

#61

p(z) (A-Fig. 5.3.1.192-193): Data from the Great Plain Aquifer show approximately hydrostatic γ.

Interpretation: Midline conditions can be observed in the Great Plain Aquifer.

#62

p(z) (A-Fig. 5.3.1.194-195): Data from the Great Plain Aquifer show slightly subhydrostatic γ down to z = (-150) m asl, then in greater depth slightly superhydrostatic γ.

Interpretation: Local recharge conditions in the shallow Great Plain Aquifer, then upward flow from about z = (-170) m asl.

#63

p(z) (A-Fig. 5.3.1.196-197): Data from the Great Plain Aquifer show slightly superhydrostatic γ.

Interpretation: Moderate upward flow in the Great Plain Aquifer.

#64

p(z) (A-Fig. 5.3.1.198-199): Data from the Great Plain Aquifer show approximately hydrostatic γ down to z = (-200) m asl, then superhydrostatic γ in greater depth.

Interpretation: Midline conditions in the shallow Great Plain Aquifer.

#65

p(z) (A-Fig. 5.3.1.200-201): Data from the Great Plain Aquifer show slightly superhydrostatic γ.

TDS(z) (A-Fig. 5.3.1.247): Low concentrations, but increase with depth.

Interpretation: Moderate upward flow in the Great Plain Aquifer.

#66

p(z) (A-Fig. 5.3.1.202-203): Data from the Great Plain Aquifer show slightly superhydrostatic γ.

Interpretation: Upward flow conditions can be observed in the Great Plain Aquifer.

#67

p(z) (A-Fig. 5.3.1.204-205): Data from the Great Plain Aquifer show subhydrostatic γ. Moderately overpressured data in the Pre-Neogene basement are gaseous with the exception of the three deepest data.

T(z) (A-Fig. 5.3.1.228): Data from the Great Plain Aquifer toward the Pre-Neogene basement show increase but below the average grad*T*.

TDS(z) (A-Fig. 5.3.1.248): Low concentrations, but increase with depth.

Interpretation: Recharge conditions in the shallow Great Plain Aquifer. Not gaseous overpressured data may represent the superhydrostatic water leg. Algyő Aquitard impedes fluid flow more effectively than around the Battonya High (see e.g., profiles #51-59).

#68

p(z) (A-Fig. 5.3.1.206-207): Data from the Great Plain Aquifer show minimally superhydrostatic γ. Overpressured data in the Pre-Neogene basement delineate a superhydrostatic γ.

Interpretation: Upward flow conditions. Algyő Aquitard impedes fluid flow more effectively then around the Battonya High (see e.g., profiles #51-59).

#69

p(z) (A-Fig. 5.3.1.208-209): Data from the Great Plain Aquifer show subhydrostatic γ.

Interpretation: Recharge conditions can be observed in the Great Plain Aquifer.

#70

p(z) (A-Fig. 5.3.1.210-211): Data from the Great Plain Aquifer show slightly superhydrostatic γ. In the Szolnok Aquifer significant overpressures can be observed with abnormally high γ values (the highest superhydrostatic γ is 51.42 MPa/km) within each hydrocarbon well.

T(z) (A-Fig. 5.3.1.229): Data from the Great Plain Aquifer toward the Pre-Neogene basement are around the average grad*T*.

TDS(z) (A-Fig. 5.3.1.249): Very low and similar concentrations in the total depth interval compared to the DSA.

Interpretation: Overpressured data in the Szolnok Aquifer seemingly show much higher γ than the lithostatic γ (≈ 25 MPa/km), which is practically impossible. Consequently, these

data may rather represent the variable pressure conditions of a fractured, faulted rock framework, while the opening of the fractures could be explained just by these overpressures. The Szolnok Aquifer represent the determining low-permeability conditions in this region, thus hydraulic behaviour of the Algyő Aquitard is less significant.

#71

p(z) (A-Fig. 5.3.1.212): Data from the Great Plain Aquifer show slightly superhydrostatic γ.

T(z) (A-Fig. 5.3.1.230): Data from the Great Plain Aquifer toward the Pre-Pannonian Aquifer mostly scatter below the average grad*T*.

TDS(z) (A-Fig. 5.3.1.250) Very low and similar concentrations in the total depth interval compared to the DSA.

Interpretation: Basically midline conditions can be observed in the Great Plain Aquifer.

#72

p(z) (A-Fig. 5.3.1.213-214): Data from the Great Plain Aquifer show slightly superhydrostatic γ.

Interpretation: Upward flow conditions can be observed in the Great Plain Aquifer.

#73

p(z) (A-Fig. 5.3.1.215-216): Data from the Great Plain Aquifer show slightly subhydrostatic γ down to z = (-100) m asl, then superhydrostatic. In the Szolnok Aquifer significant overpressures can be observed with abnormally high γ values (the highest γ is 67.29 MPa/km) within each hydrocarbon well.

TDS(z) (A-Fig. 5.3.1.251): Very low and similar concentrations in the total depth interval compared to the DSA.

Interpretation: Recharge conditions can be observed in the Great Plain Aquifer. Overpressured data in the Szolnok Aquifer seemingly show much higher γ than the lithostatic γ (≈ 25 MPa/km), which is practically impossible. Consequently, these data may rather represent the variable pressure conditions of a fractured, faulted rock framework, while the opening of the fractures could be explained just by these overpressures. The Szolnok Aquifer represent the determining low-permeability conditions in this region, thus hydraulic behaviour of the Algyő Aquitard is less questionable.

#74

TDS(z) (A-Figs. 5.3.1.252): Very low concentrations (compared to the DSA) with a moderate increase below the Endrőd Aquitard.

Interpretation: Algyő Aquitard may impede fluid flow effectively.

#75

TDS(z) (A-Figs. 5.3.1.253): Two shallow data with salient TDS concentrations, as well as one sample with low concentration from the Pre-Neogene basement were available.

Interpretation: Elevated TDS concentrations in shallow depth compared to the deeper values are not unique in this profile, but common in the region (see also e.g., profiles #51 and #53), thus it could not be explained simply by surface contamination.

5.3.2 Tomographic fluid-potential, isotherm, and iso-concentration (TDS) maps

Topographical maps (A-Fig. 5.3.2.1 and 5.3.2.30), as well as tomographic fluid-potential /h(x,y)/ (A-Fig. 5.3.2.2-11 and 5.3.2.31-40), isotherm /T(x,y)/ (A-Fig. 5.3.2.12-20 and 5.3.2.41-48), and iso-concentration /TDS(x,y)/ maps (A-Fig. 5.3.2.21-29 and 5.3.2.49-56) are presented in the followings in reference to the studied elevation intervals. Maps are displayed in the Figure and Table Appendix volume type by type, thus first the h(x,y), then the T(x,y), and thirdly the TDS(x,y) maps, since maps representing the same type of data have to be compared with each other, for instance T(x,y) maps with T(x,y) maps. It has particular significance in case of the h(x,y) maps, because also the vertical driving force directions can be deduced by contrasting the subsequent ('adjacent') maps. However, descriptions of the maps are presented in the order of the elevation intervals in order to avoid repetitions. The observable anomalies numbered alphabetically (i.e. A-Z, then AA-AZ, BA-BZ, and CA-CE) are listed in A-Table 5.3 summarizing the types of anomalies (i.e. hydraulic, temperature, TDS), and also their coincidence with faults and hydrocarbon occurrences. Numbering is consistent irrespectively of data type, but with reference to the position. Thus, for instance if a potential and thermal anomaly coincide, their letter-sign will be the same. Additionally, anomalies observed in differing elevation intervals (i.e. maps) were signed by the same letter(s) only if the continuity between them could be supported also by cross-sections, such as in case of anomaly #AC. Eventually, particluarly in case of the h(x,y) maps in the deeper elevation intervals it is usual that data clustered into a few locations, and all of these groups represent anomalies considering Δh within the anomalies. Thus these are not misinterpreted anomalies due to the small number of data. The effect of gas accumulations being capable of inducing potential anomalies were decided based on the rate of hydraulic heads and Δh within the anomaly, as well as on the maximum h surplus that can be caused by the gas /$\Delta h_{wg(max)}$=254 m asl/ (see also Appendix 2). Then anomalies probably caused by gas accumulations were called as *gaseous anomalies*, and otherwise as *real anomalies*.

5.3.2.1 Derecske Study Area

#1 /z = 134-0 m asl/ (data from the Great Plain Aquifer)

h(x,y) (A-Fig. 5.3.2.2): It completely reflects the effect of topography (A-Fig. 5.3.2.1), namely coincidence of topographical and potential highs, lows, and direction of gradients can be observed. Regional flow direction according to the topographical tilt is oriented from NE to SW (NE-SW). Low lateral hydraulic gradient (average gradh_h≈50m/80km=6.25*10^{-4}) is relatively higher in the NE where topographical gradient is higher as well. Regarding the local scale phenomena, some potential mounds reflecting recharge areas around topographic highs (anomalies #A and #B), and a potential bay at a topographical depression referring to discharge conditions (anomaly #C) are listed in A-Table 5.3.A to name but a few.

TDS(x,y) (A-Fig. 5.3.2.21): Data are available only from z = 104 m asl. Roughly uniform distribution of TDS (average TDS≈500 mg/L) can be observed with some local maximums. In the SW part of the area higher concentrations (TDS>2000 mg/L) refer to discharge conditions. Among the local positive maximums (anomalies #D-G) # F and #G (TDS>1000 mg/L) show lower concentrations in the next map /TDS(x,y) #2/, thus these may refer to local surface or near-surface phenomena (e.g., salinization, contamination).

Interpretation: Gravity-driven flow system can be identified characterized by a regional NE-SW flow direction and superimposed local systems generated by local topographic highs and lows.

#2 /z = 0-(-200) m asl/ (data from the Great Plain Aquifer)

h(x,y) (A-Fig. 5.3.2.3): It reflects the effect of topography. Regional flow direction according to the topographical tilt is NE-SW. Lateral hydraulic gradient is lower than in the previous map slide (h(x,y) #1) (average gradh_h≈35m/80km=4.38*10^{-4}). Vertical hydraulic gradient (compared to the previous map h(x,y) #1) shows slight downward flow in the N-NE part of the area (gradh_v≈15m/200m=7.5*10^{-2}), while mostly through-flow conditions in the rest of the area. The downward flow pattern in the N-NE is also supported by that the vertical grad$h$ (≈5m/160m=3.13*10^{-2}) is higher with at least one order of magnitude than the horizontal (gradh_h≈20m/20km=10^{-3}). Upward flow conditions can be observed locally for instance at anomalies #H, I, K, and L.

T(x,y) (A-Fig. 5.3.2.12): It indirectly reflects the effect of topography due to its direct dependence on fluid-potential distribution (i.e. for instance coincidence of topographical and potential highs with temperature lows, and vice versa).

TDS(x,y) (A-Fig. 5.3.2.22): It indirectly reflects the effect of topography due to its direct dependence on fluid-potential distribution (i.e. for instance coincidence of topographical and potential highs with concentration lows, and vice versa).

Interpretation: Gravitational flow system with a regional recharge area at the NE. Temperature and chemical composition of water follow the potential, and consequently the topographic relief.

#3 /z = (-200)-(-600) m asl/ (data from the Great Plain Aquifer)

h(x,y) (A-Fig. 5.3.2.4): It shows less mosaic pattern, thus only slightly reflects the effect of topography (i.e. local undulations of topography became insignificant). Regional flow direction according to the regional topographical tilt is NE-SW. Lateral hydraulic gradient increased in two narrow zones (gradh_h≈10m/3km=3*10^{-3}), which coincides with the northern and southern fault zones of the Derecske Trough, as well as with their elongations. However, gradh_h is minimal in the SW part of the area. Vertical gradient (compared to the previous map h(x,y) #2) shows slight downward flow in the NE part of the area (gradh_v≈15m/200m=7.5*10^{-2}), while upward flow conditions in the SW.

T(x,y) (A-Fig. 5.3.2.13): It shows more mosaic temperature distribution, thus diminishing effect of topography. At the anomaly #R relatively higher temperatures can be observed (positive anomaly) where fluid-potentials reflect to downward flow conditions but only based on a few temperature data. The positive anomaly #T can be observed along a fault first signed in map h(x,y) #5, but it can be observed also in this elevation interval.

TDS(x,y) (A-Fig. 5.3.2.23): Only a few data are available in the E-SE. In the northern third of the area concentrations are higher with more 1000 mg/L than in the previous map (TDS (x,y) #2). At anomaly #R a salient positive anomaly (TDS>10,000mg/L) based on one data can be observed where fluid-potentials reflect to downward flow conditions. Anomaly #T can be observed along the same fault, which induces positive thermal anomaly as well.

Interpretation: Effect of topography is less explicit, it is rather effective only regionally. Thus regional downward flow at the NE, upward flow at the SW can be observed, while the rest of the area shows through-flow conditions. The potential escarpments along the Derecske Trough's northern and southern fault zones may refer to the vertically conduit, but transversally barrier function of these zones. The Pre-Neogene – Pannonian fault around anomaly #T should be a conduit fault forwarding upward flow based on the positive thermal and chemical anomalies (it will also be proved hydraulically in lower map slides).

#4 /z = (-600)-(-1200) m asl/ (data from the Great Plain Aquifer)

h(x,y) (A-Fig. 5.3.2.5): Compared to the previous map (h(x,y) #3) *h* values are significantly higher (~10-100 m increase) and upward flow direction can be observed everywhere. Among the potential highs/mounds only #AC may be caused by gas accumulations.

T(x,y) (A-Fig. 5.3.2.14): Beside the increasing temperature conditions particularly in the northern part of the area, positive anomalies show usual coincidence with potential highs (see also A-Table 5.3.A). Where the lateral thermal gradient is saliently high (e.g., in the east of anomaly #Y, in the northeast of anomaly #AE) barrier faults could be made probable. The positive anomaly #AB still exists (as in the previous map at anomaly #R).

TDS(x,y) (A-Fig. 5.3.2.24): Maximums coincide with temperature maximums. The positive anomaly #AB still exists (as in the previous map at anomaly #R), though the maximum was shifted eastward.

Interpretation: Ubiquitous upward flow represents the overpressure-driven, lower flow system, which underpins hydraulically the gravitational flow system. The transient zone between the two flow systems may be found in the lower part of the previous map's (h(x,y) #3; z = (-200)-(-600) m asl) and in the upper part of this map's elevation interval. The two flow systems can be hydraulically separated in the NE part of the area where the gravitational downward and overpressured upward flow encounter in a potential minimum zone also causing the accumulation of heat and dissolved salts in this zone (e.g., at anomalies #R and #AB). Where both flow systems represent upward flow conditions they can be distinguished only in one local site. Namely, at p(z) profiles #20-21 (A-Fig. 5.3.1.48-50) where a hydrostatic transient zone can be observed between the gravitational and overpressured upward flows.

#5 /z = (-1200)-(-1800) m asl/ (data from the Great Plain Aquifer and Algyő Aquitard)

h(x,y) (A-Fig. 5.3.2.6): Potential highs/mounds at anomalies #AC and AF may be caused by gas accumulations, while salient potential highs at anomalies #AH do not contain only gaseous data, thus these anomalies cannot be caused simply by the gas accumulations (regarding also the rate of h>1200 m asl). There are two data points at anomaly #AG showing large lateral hydraulic gradient (gradh_h>500m/1km=0.5). The higher value (h≈700 m asl) was measured in the Algyő Aquitard, while the lower data (h≈170 m asl) in the Great Plain Aquifer and in a shallower depth by about 180 m. Thus the gradient may refer to a rather horizontal barrier in the top of the Algyő Aquitard or at the bottom of the Great Plain Aquifer. Effect of the gas inflows cannot be determined distinctly here.

T(x,y) (A-Fig. 5.3.2.15): All of the temperature data were measured in the Algyő Aquitard and show higher values on average in the south of the Derecske Trough. The negative anomaly #AJ in the Trough is based on one data, though having a relatively good ranking (7 – good). Slight temperature decrease can be observed in the northeastern part of the area compared to the previous elevation interval (T(x,y) #4, anomaly #AB). Hydrocarbon accumulations can be found around positive temperature anomalies and/or along faults.

TDS(x,y) (A-Fig. 5.3.2.25): Only a few data are available in the western part of the area showing similar distribution to the temperature values. Data from the Algyő Aquitard show salient positive anomalies (TDS>34,000 mg/L) at #AH and #AL. Hydrocarbon accumulations can be found around positive anomalies or high concentration gradients.

Interpretation: Overpressured flow system represents significant positive anomalies, while these anomalies usually coincide with positive temperature and water chemical anomalies, as well as with hydrocarbon accumulations. Algyő Aquitard seems to be an effective flow barrier accumulating potential energy (e.g. anomaly #AG), heat (in the south of the Trough), salinity (particularly at the bottom of the Aquitard for instance by membrane filtration), and hydrocarbons as well. The apparent temperature decrease in the northeastern part of the area may be due to the relative temperature increase in the transient zone of the two regional flow systems in the previous elevation interval.

#6 /z = (-1800)-(-2200) m asl/ (data from the Algyő Aquitard particularly within the Derecske Trough, and from the Pre-Pannonian Aquifer and Pre-Neogene basement above basement highs)

h(x,y) (A-Fig. 5.3.2.7): Potential high/mound at anomaly #AO is a real anomaly (at the only one gaseous data h>1000m), while another one at anomaly #AF is a gaseous and rather negative anomaly. The positive anomaly #AN can be observed along a Pre-Neogene – Pannonian fault (see also maps #3), irrespectively of the gas occurrence since there is a non-gaseous data as well, and h>1200 m asl. High lateral hydraulic gradient (gradh_h≈1200m/5km=0.24) can be observed along faults at anomaly #AP where rates of h exclude the 'gas-induced anomaly' question. A potential 'plateau' as the average of several data points showing mosaic pattern locally at anomaly #AH can be observed (rates of h exclude the 'gas-induced anomaly' question) at the bottom of the Algyő Aquitard. The salient lateral hydraulic gradient (gradh_h≈600m/2.5km=0.24) at the north-northwestern tip of the anomaly may refer to structural causes (i.e., Pre-Neogene basement slope is dipping eastward, while Algyő Aquitard is thinning westward; faults are not known).

T(x,y) (A-Fig. 5.3.2.16): The temperature difference between the areas in the north and in the south of the Derecske Trough observed in the previous elevation interval (T(x,y) #5) disappeared. A negative-positive anomaly couple can be observed at #AP. At the eastern, positive anomaly Algyő Aquitard is thicker and less faulted than at the western, relatively negative anomaly. Mosaic pattern of temperature distribution is also characteristic at anomaly #AH.

TDS(x,y) (A-Fig. 5.3.2.26): In the western part of the area lower concentrations can be observed than in the previous elevation interval (TDS(x,y) #5).

Interpretation: Overpressured flow system is represented regionally. Hydraulic effect of conduit faults (e.g., at anomaly #AN), and the Algyő Aquitard (e.g., at anomaly #AH) can be identified, and mostly supported by the temperature, and partly by the hydrochemical concentration values as well.

#7 /z = (-2200)-(-2500) m asl/ (data from the Algyő Aquitard in the Derecske Trough, and from the Pre-Pannonian Aquifer and Pre-Neogene basement above basement highs)

h(x,y) (A-Fig. 5.3.2.8): Elevated h values represent higher lateral gradient (gradh_h≈1100m/3km=0.4) and salient vertical hydraulic gradient (gradh_v≈ (-1600)m/8km=(-0.2)) as well compared to the previous elevation interval (h(x,y) #6) at anomalies #AO and #AS. In these sites data in the north of the Derecske Trough's northern fault zone show lower values (#AS) than data in the south of it (#AO). The southern positive maximum (#AO) can be considered as a real anomaly, while the other one (#AS) as the result of a barrier fault zone (i.e. the northern fault zone of the Trough). The potential plateau in the previous map at anomaly #AH broke up but probably only due to the lack of the data.

T(x,y) (A-Fig. 5.3.2.17): The apparent negative anomaly in the NE part of the area only represents slighter temperature increase compared to the previous depth interval (T(x,y) #6) and the rest of the Study Area. An anomalously high data (ranked by 8 as good) can be found along a fault at anomaly #AU, which was previously determined as a conduit fault.

TDS(x,y) (A-Fig. 5.3.2.27): Since only a few data were available, interpolation is not reliable. Accordingly, in spite of the apparent decrease compared to the previous map (TDS(x,y) #6) signed by the iso-concentration lines, the data points represent higher values. High lateral concentration gradient can be observed between two wells at anomaly #AO.

Interpretation: Overpressured flow system is represented regionally, while a slight difference in hydraulic heads starts to emerge between the areas in the north and in the south of the Derecske Trough (higher *h* values can be found in the south).

#8 /z = (-2500)-(-3000) m asl/ (data from the Algyő Aquitard in the Derecske Trough, and from the Pre-Pannonian Aquifer and Pre-Neogene basement above basement highs)

h(x,y) (A-Fig. 5.3.2.9): In the north of the Derecske Trough lower *h* values can be observed than in the south of it, as well as a slight lateral hydraulic gradient (gradh_h≈300m/4km=7.5*10^{-2}) towards the Trough, thus fluid tends to flow northwestward (away from the Trough). However, the vertical gradient is salient (gradh_v≈(-850)m/750m= (-1.13) at least) compared to the last elevation interval which represents data from this region (h(x,y) #6, z = (-1800)-(-2200) m asl). A potential high at anomaly #AP also represent significant vertical hydraulic gradient (gradh_v≈(-700)m/400m=(-1.75)) compared to the previous map (h(x,y) #7), as well as high lateral gradients northward (gradh_h≈800m/4km=0.2 decrease) and eastward (gradh_h≈500m/8km=0.06 decrease) too. Another potential mound at anomaly #AV also show salient vertical hydraulic gradient (gradh_v≈(-400)m/400m=(-1)) compared to the previous map (h(x,y) #7), as well as high lateral hydraulic gradient (gradh_h≈200m/1km=0.2).

T(x,y) (A-Fig. 5.3.2.18): Slight increase in temperature values can be observed compared to the previous map (T(x,y) #7). Temperature minima also can be found at some sites around data with good ranking (e.g., anomalies #AY and #AP).

TDS(x,y) (A-Fig. 5.3.2.28): Data were available only from three wells showing significantly higher TDS values (10,000-15,000 mg/L excess) in the concerned area than in the previous elevation interval (TDS(x,y) #7).

Interpretation: Intense upward flow can be observed, while the difference in hydraulic heads between the areas in the north and in the south of the Derecske Trough (higher *h* values can be found in the south) is more explicit.

#9 /z = (-3000)-(-3400) m asl/ (data from the Pre-Pannonian Aquifer and Pre-Neogene basement)

h(x,y) (A-Fig. 5.3.2.10): Data were available only from three sites representing salient vertical hydraulic gradients (gradh_v≈(-800)m/450m=(-1.8)) compared to the previous map (h(x,y) #8).

T(x,y) (A-Fig. 5.3.2.19): As a result of the significant increase compared to the previous map (T(x,y) #8), temperature exceeds the 200°C as well (e.g., anomalies #AP and #AZ). Temperature maximums are concentrated around the Derecske Trough. The apparent

negative anomaly at #AP only represents slighter temperature increase compared to the previous elevation interval (T(x,y) #8) and the rest of the Study Area.

TDS(x,y) (A-Fig. 5.3.2.29): Data were available only from three sites and down to z = (-3250) m asl. All of the values are above 11,000 mg/L.

Interpretation: Intense upward flow can be observed.

#10 /z = (-3400)-(-4000) m asl/ (data from the Pre-Pannonian Aquifer particularly in the Derecske Trough, and from the Pre-Neogene basement)

h(x,y) (A-Fig. 5.3.2.11): Data were available only from three wells. Vertical hydraulic gradient compared to the previous map (h(x,y) #9) is more significant in the north of the Trough (gradh_v≈(-400)m/900m=(-0.4)) than within it (gradh_v≈(-100)m/450m=(-0.2)).

T(x,y) (A-Fig. 5.3.2.20): Three of the four data is above 200°C.

Interpretation: Intense upward flow can be found, while the difference in hydraulic heads between the areas in the north and in the south of the Derecske Trough's northern fault zone (higher *h* values can be found in the south) is still observable.

5.3.2.2 Békés-Battonya Study Area

Numbering is continuous regarding the maps and anomalies in the Derecske Study Area.

#11 /z = 100-75 m asl/ (data from the Great Plain Aquifer)

h(x,y) (A-Fig. 5.3.2.31): It completely reflects the effect of topography (A-Fig. 5.3.2.30), namely coincidence of topographical and potential highs, lows, and direction of gradients can be observed. Regional flow direction according to the topographical tilt is oriented from SE to NW (SE-NW). The lateral hydraulic gradient is usually low (maximum gradh_h≈20m/70km=2.9*10^{-4}), while in the northwestern part of the area it is minimal (*h*=80-85 m asl regionally). Regarding the local scale phenomena, a potential mound reflects recharge area around a topographic high at anomaly #BB, while a potential basin at a topographical depression refers to discharge conditions at anomaly #BC, to name but a few.

Interpretation: Gravity-driven flow system can be identified characterized by a regional SE-NW flow direction and superimposed local systems generated by local topographic highs and lows.

#12 /z = 75-0 m asl/ (data from the Great Plain Aquifer)

h(x,y) (A-Fig. 5.3.2.32): It reflects the effect of topography. Regional flow direction according to the topographical tilt is SE-NW. Lateral hydraulic gradient is low similar to the previous elevation interval (h(x,y) #11) (average gradh_h≈5m/10km=5*10^{-4}). Vertical hydraulic gradient (compared to the previous map h(x,y) #11) shows slight downward flow in the S-SE part of the area (gradh_v≈3m/50m=0.06), while mostly through-flow conditions in the rest of the area. The downward flow pattern in the S-SE is also supported by that the vertical grad*h* is higher with at least two orders of magnitude than the horizontal. Upward flow conditions can be observed locally related to a local topographic depression for instance at anomaly #BE, while downward flow conditions at anomaly #BD.

Interpretation: Gravitational flow system with a regional recharge area at the SE and superimposed local systems generated by local topographic highs and lows.

#13 /z = 0-(-200) m asl/ (data from the Great Plain Aquifer)

h(x,y) (A-Fig. 5.3.2.33): Regional flow direction according to the regional topographical tilt is still SE-NW. Lateral hydraulic gradient is even lower where *h*<90 m asl (in most of the area) (gradh_h≈10m/45km=2.2*10^{-4}). Vertical hydraulic gradient (compared to the previous map h(x,y) #12) shows slight downward flow in the SE part of the area (gradh_v≈3m/150m=0.02), while moderately upward flow conditions in the N-NW. More explicit upward flow can be observed for instance at anomaly #BF.

T(x,y) (A-Fig. 5.3.2.41): Only a few data were available in the southwestern part of the area. These indirectly reflect the effect of topography due to its direct dependence on fluid-potential distribution as thermal maximums can be found at areas characterized by upward flow conditions (e.g., at anomaly #BF).

TDS(x,y) (A-Fig. 5.3.2.49): Only a few data were available. Concentration increase can be observed regionally from the SE towards the NW following the potential and thus topographical pattern.

Interpretation: Effect of topography is still observable, thus regional downward flow at the SE, upward flow at the N-NW can be seen, while the rest of the area shows through-flow conditions. Temperature and chemical composition of water follow the potential, and consequently the topographic relief.

#14 /z = (-200)-(-600) m asl/ (data from the Great Plain Aquifer)

h(x,y) (A-Fig. 5.3.2.34): Compared to the previous map (h(x,y) #13) *h* values are generally higher (~10-15 m increase) and upward flow direction can be observed everywhere. Lateral hydraulic gradient increased along the margins of the Battonya High

(gradh_h≈10m/10km=10^{-3}) inducing flows towards the basins (i.e., towards NE, N, and W), while vertical gradient also rose in the southeastern part of the area (above the top of the Battonya High) (gradh_v≈(-15)m/300m=(-5*10^{-2})). There are only three gaseous data in the SE the anomaly-inducing effect of which is negligible since non-gaseous data show even higher *h* values there.

T(x,y) (A-Fig. 5.3.2.42): In the eastern part of the area only 3 data were available. In the west, beside the generally increasing temperature conditions thermal maximum can be observed along the Battonya High (at anomaly #BK), while relative minimum in the west of it (in the Makó Basin).

TDS(x,y) (A-Fig. 5.3.2.50): Compared to the previous map (TDS(x,y) #13) TDS concentration only slightly increased at anomalies #BI, BJ, and BK, due to the elevated HCO_3^- content (400-1500 mg/L). The latter maximum coincides with a temperature maximum as well, while a minimum zone in the Makó Trough also coincides with a temperature minimum. Observed concentrations are usually lower with at least one order of magnitude than in the DSA in similar depths, while the positive anomalies are relative compared to the surrounding data.

Interpretation: Ubiquitous upward flow represents the overpressure-driven, lower flow system, which underpins hydraulically the gravitational flow system. The transient zone between the two flow systems may be found in this elevation interval (i.e., z = (-200)-(-600) m asl). The two flow systems can be hydraulically separated in the SE part of the area where the gravitational downward and overpressured upward flow encounter in a potential minimum zone also causing the accumulation of heat and dissolved salts in this zone (see also the next maps h/T/TDS(x,y) #15). Where both flow systems represent upward flow conditions they can be distinguished only in one local site. Namely, at p(z) profiles #48-49 (A-Fig. 5.3.1.166-169) where a hydrostatic transient zone can be observed between the gravitational and overpressured upward flows (in z = 0-(-200) m asl elevation interval). Consequently, the lateral SE-NW flow direction along the Battonya High is rather due to the same tilt of the Pre-Neogene basement high than to topographical effects.

#15 /z = (-600)-(-1200) m asl/ (most of the data from the Great Plain Aquifer, while above the Battonya High from the Algyő and Endrőd Aquitards, and the Pre-Pannonian Aquifer as well)

h(x,y) (A-Fig. 5.3.2.35): Compared to the previous map (h(x,y) #14) *h* values are usually higher, but in the northwestern part of the Battonya High (at anomaly #BP) also *h* decrease and a closed potential depression can be observed mostly in the Great Plain Aquifer. However, the lateral gradient along the 'margins' of this negative potential anomaly is

relatively high (gradh_h≈20m/1km=0.02) that could be explained also by the coincidence of these 'margins' with the Battonya High's bounding faults. Accordingly, these faults may be conduits for upwelling fluids and thus could contribute to the high lateral hydraulic gradient around the potential depression. Additionally, most of the data is gaseous and if we considered the maximum *h* surplus caused by the gas ($\Delta h_{wg(max)}$=254 m asl, which is probably lower in the BBSA (see also Appendix 2)), the negative potential anomaly would be even more negative. Where the Pre-Neogene basement approaches its shallowest depth /z = (-950)-(1000) m asl/ a potential mound also can be found (h>200m) in the Endrőd Aquitard (anomaly #BO), however it could be a gaseous anomaly as well.

T(x,y) (A-Fig. 5.3.2.43): Only a few data were available, which show slight temperature increase and a local maximum (based on two data) at anomaly #BN representing similar values to that of the maximum in the previous elevation interval (T(x,y) #14).

TDS(x,y) (A-Fig. 5.3.2.51): Data were available practically only from the Battonya High Area and show concentration decrease compared to the previous map (TDS(x,y) #14), and thus anomalously low concentrations (50-500 mg/L) regionally. The three further data from other regions represent similar conditions (maximum 1200 mg/L).

Interpretation: Around the Battonya High anomalously low fluid potentials can be observed, while the whole Study Area is characterized by anomalously low TDS concentrations.

#16 /z = (-1200)-(-1800) m asl/ (above the Battonya High data from the Lower Pannonian succession, Pre-Pannonian Aquifer, and Pre-Neogene basement, while in the adjacent basins from the Great Plain Aquifer)

h(x,y) (A-Fig. 5.3.2.36): Compared to the previous map (h(x,y) #15) *h* values are usually higher, but the closed potential depression at the Battonya High (at anomaly #BP) is more extensive in the Algyő Aquitard and Pre-Pannonian Aquifer. Also the lateral hydraulic gradient along its 'margins' remained relatively high (gradh_h≈20m/1km=0.02). Additionally, several data is gaseous and lead to the same conclusions as in the previous map (h(x,y) #15).

T(x,y) (A-Fig. 5.3.2.44): Salient temperature increase can be observed regionally, as well as local maximums at the northwestern tip of the Battonya High (at anomaly #BS) (>110°C) and at anomaly # BQ. The negative anomaly in the northwest of anomaly #BS is caused by only one data, thus it is not sufficiently established.

TDS(x,y) (A-Fig. 5.3.2.52): Data around the Battonya High Area and in the east of it still show anomalously low concentrations (<600 mg/L). Local (relative) maximums can be observed at anomalies #BQ and #BT (~3000 mg/L).

Interpretation: Around the Battonya High anomalously low fluid potentials can be observed, while the whole Study Area is characterized by anomalously low TDS concentrations with two exceptional local sites.

#17 /z = (-1800)-(-2200) m asl/ (above the Battonya High data from the Lower Pannonian succession, Pre-Pannonian Aquifer, and Pre-Neogene basement, while in the adjacent basins from the Great Plain Aquifer)

h(x,y) (A-Fig. 5.3.2.37): Compared to the previous map (h(x,y) #16) *h* values are much higher (by about >200 m). There is no data from the area of the closed potential depression appearing on the Battonya High (at anomaly #BP) in the two previous (upper) elevation intervals. At anomaly #BU the shallower and thus lower *h* values (<100 m asl) are separated by a fault zone from the deeper (by about 200 m) and much higher data (*h*>500 m asl) (see also p(z) profile #47, A-Fig. 5.3.2.164-165).

T(x,y) (A-Fig. 5.3.2.45): Salient temperature increase can be observed regionally with a similar temperature distribution to the previous map (T(x,y) #16). The negative anomaly #BX is caused by only one data, thus it is not sufficiently established.

TDS(x,y) (A-Fig. 5.3.2.53): Only a few data around the Battonya High Area and in the east of it still show anomalously low concentrations (<800 mg/L). Local relative maximum (>2500 mg/L) can be observed at anomaly #BX based on one data, thus it is not sufficiently established.

Interpretation: The first elevation interval where significant increase in hydraulic head values appears. The whole Study Area is characterized by anomalously low TDS concentrations, while the Battonya High represents a thermal maximum as well.

#18 /z = (-2200)-(-2500) m asl/ (data from the Lower Pannonian strata, Pre-Pannonian Aquifer, and Pre-Neogene basement)

h(x,y) (A-Fig. 5.3.2.38): Compared to the previous map (h(x,y) #17) *h* values are significantly higher (by about >1000 m in some places). Though most of the data is gaseous at the Szarvas High, the positive anomaly should be a real anomaly. The highest *h* value in this map can be found at anomaly #CA (Fábiánsebestyén-Nagyszénás-Orosháza Area) (*h*=2635 m asl) in the Algyő Aquitard, however the gradient is unknown in the lack of further data. Data along the Battonya High's margins were measured after 1990, thus

probably represents by their relatively lower *h* values (400-500 m asl) the effect of hydrocarbon production as well.

T(x,y) (A-Fig. 5.3.2.46): Only a few data were available. Temperature regionally increases northward (from about 120 to 160°C).

TDS(x,y) (A-Fig. 5.3.2.54): Only a few data were available, which regionally show anomalously low concentrations (<600 mg/L).

Interpretation: Saliently high hydraulic heads in the Szolnok Aquifer and Algyő Aquitard can be observed at the Szarvas and Békés Highs, as well as the Fábiánsebestyén-Nagyszénás-Orosháza Area. The whole Study Area is characterized by anomalously low TDS concentrations, while the Battonya High represents thermal maximum as well.

#19 /z = (-2500)-(-3100) m asl/ (data from the Lower Pannonian strata, Pre-Pannonian Aquifer, and Pre-Neogene basement)

h(x,y) (A-Fig. 5.3.2.39): Salient potential highs (h>3000 m asl) can be observed at anomalies #BY (Szarvas High) and #BZ (Békés High) in the Szolnok Aquifer, as well as at anomaly #CA (Fábiánsebestyén-Nagyszénás-Orosháza Area) and #CC in the Endrőd Aquitard and Pre-Pannonian Aquifer.

T(x,y) (down to z = (-3000) m asl) (A-Fig. 5.3.2.47): Slight temperature increase in most of the area can be observed. The negative anomaly #CC is caused by only one data, thus it is not sufficiently established.

TDS(x,y) (down to z = (-3000) m asl) (A-Fig. 5.3.2.55): Concentrations slightly increased, but the maximum is still anomalously low (~1300 mg/L).

Interpretation: Saliently high hydraulic heads in the Szolnok Aquifer, Endrőd Aquitard, and Pre-Pannonian Aquifer can be observed at the Szarvas and Békés Highs, as well as in the Fábiánsebestyén-Nagyszénás-Orosháza Area. The whole Study Area is characterized by anomalously low TDS concentrations.

#20 /z = (-3100)-(-5000) m asl/ (data from the Pre-Pannonian Aquifer and Pre-Neogene basement)

h(x,y) (A-Fig. 5.3.2.40): Data were available only from three wells and some approximate the 4000 m *h*[5].

T(x,y) (z = (-3000)-(-4000) m asl) (A-Fig. 5.3.2.48): Temperature increase can be observed regionally. The thermal maximum (>200°C) at the Battonya High (anomaly #CE) is caused by only one data, and thus it is not sufficiently established.

[5] ≈ 9000 m (theoretical) water column!

TDS(x,y) (z = (-3000)-(-4553) m asl) (A-Fig. 5.3.2.56): Concentrations are anomalously low (<600 mg/L) regionally, and the only one higher value (~820 mg/L) is based on one data, thus it is not sufficiently established.

Interpretation: Saliently high hydraulic heads, higher than average temperature conditions, and anomalously low TDS concentrations can be observed regionally.

5.3.3 Hydraulic, geothermal, and hydrochemical cross-sections

Numbering of the hydraulic /h(s,z)/, geothermal /T(s,z)/, and hydrochemical cross-sections /TDS(s,z)/ (A-Fig. 5.3.3.1-39) is consistent irrespectively of data type, but with reference to the trace line. Also the order of the sections' representation follows the trace lines in the text, as well as in the Figure and Table Appendix in contrast with the profiles and maps, which were presented data type by data type, since comparison of the sections with each other was less significant. Phenomena in the sections are appointed by their distance along the section (i.e., along the horizontal axis s, from s=0) expressed in kilometers (its hereafter used abbreviation is 'skm' as section kilometer(s)), as well as their elevation (i.e., along the vertical axis z). The numbered anomalies are listed in A-Table 5.4 summarizing the types of anomalies (i.e. hydraulic, temperature, TDS), and also their coincidence with faults and hydrocarbon occurrences. Additionally, their numbering /1-48/ is consistent irrespectively of data type, but with reference to the position. Thus, for instance if a potential and thermal anomaly coincide, their number will be the same. Additionally, some anomalies were cross-cut by more cross-sections as well. These were signed by the same number(s) in all of the sections. The effect of gas accumulations being capable of inducing potential anomalies were decided based on the rate of hydraulic heads and Δh within the anomaly, as well as on the maximum h surplus that can be caused by the gas /$\Delta h_{wg(max)}$=254 m asl/ (see also Appendix 2). Then anomalies probably caused by gas accumulations were called as *gaseous anomalies*, and otherwise as *real anomalies*. Faults terminated in the Pre-Neogene basement and cross-cut also the Algyő Aquitard are called as b-Pa2 faults, while those which terminate below the top of the Algyő Aquitard as b-Pa1 faults, and which cross-cut only the Upper Pannonian strata as Pa2 faults. Hydraulic cross-sections are described first regarding the gravitational, and secondly the overpressured flow system.

5.3.3.1 Derecske Study Area

#1

h(s,z) (A-Fig. 5.3.3.1): In the uppermost 1000 m thick zone effected by surface topography the regional gravitational flow direction tends from east to west, and characterized by low hydraulic gradients. Through-flow conditions occur at around the 25-35th and 40-50th skm, while along the rest of the section upward flow can be observed. Local discharge areas can be found for instance at the 11-16th skm, whilst local recharge area at the 59th skm. In the mostly overpressured zone below z = (-1000) m asl significant increase can be observed in hydraulic heads (high gradh_v) below the Algyő Aquitard. (From the Aquitard itself hardly any data were available.) At anomaly #7 high lateral gradient ($\Delta h \approx 700$m) between the two sides of a b-Pa2 fault refer to its barrier character.

T(s,z) (A-Fig. 5.3.3.2): Aside from the local anomalies, vertical temperature gradient is roughly uniform.

TDS(s,z) (A-Fig. 5.3.3.3): Jump-like increase in TDS can be observed below the Algyő Aquitard, then in the Pre-Neogene basement.

Interpretation: In the uppermost 1000 m thick zone affected by surface topography gravity-driven flow system can be identified characterized by a regional E-W flow direction and superimposed local systems generated by local topographic highs and lows. Below the Algyő Aquitard significant increase can be observed in the hydraulic heads (i.e. salient overpressure) and TDS concentrations as well. Fluid-potential anomalies usually coincide with thermal and hydrochemical anomalies, as well as with faults and hydrocarbon accumulations.

#2

h(s,z) (A-Fig. 5.3.3.4): In the uppermost 1000-1500 m thick zone effected by surface topography the regional gravitational flow direction is roughly N(E)-S(W) along the section. In the north of the 50th skm downward flow can be observed down to about z = (-600) m asl, then upward flow. Through-flow (hydrostatic) conditions occur at the 48-58th skm from the land surface down to about 1500 m depth. In this region potential anomaly was caused by gas accumulations, while after the correction of hydraulic heads (Appendix 2) a regional negative anomaly still remained (anomaly #10). In the south of the 50th skm ubiquitous upward flow can be observed with the exception of the region of p(z) profile #19 (at around the 29th skm) where hydrostatic conditions dominate. Significant increase in

hydraulic heads (high gradh_v) can be observed below the Algyő Aquitard. (From the Aquitard itself hardly any data were available.)

T(s,z) (A-Fig. 5.3.3.5): Aside from the local anomalies, vertical temperature gradient is roughly uniform.

TDS(s,z) (A-Fig. 5.3.3.6): Salient increase in TDS can be observed below the Algyő Aquitard, then in the Pre-Neogene basement.

Interpretation: In the uppermost 1000-1500 m thick zone affected by surface topography gravity-driven flow system can be identified characterized by a regional N(E)-S(W) flow direction along the section, which based on the tomographic fluid-potential maps is NE-SW in deed. In the flow-converging zone along the northern third of the section the lateral flow direction tends to (south)west according to the tomographic fluid-potential maps. Below the Algyő Aquitard significant increase can be observed in the hydraulic heads (i.e. salient overpressure) and TDS concentrations as well. Fluid-potential anomalies usually coincide with thermal and hydrochemical anomalies, as well as with faults and hydrocarbon accumulations. The negative potential anomaly #10, which represents an approximately hydrostatic zone from the land surface down to 1500 m depth, could be explained by the thickening of the high-permeability Great Plain Aquifer in the Derecske Trough, as well as by the effect of hydrocarbon production, since also data of producing wells were applied during the correction described in Appendix 2 (otherwise required data would have been missing).

#3

h(s,z) (A-Fig. 5.3.3.7): In the uppermost 1000-1500 m thick zone effected by surface topography the regional gravitational flow direction is roughly N(E)-S(W) along the section. Local recharge and discharge areas also evolved due to the local topographic conditions. In the north of the 55th skm downward flow can be observed down to about z = (-600) m asl, then upward flow. At the 66-72th skm in z = (-500)-(-1200) m asl elevation interval also a closed potential depression can be observed with hydraulic head values lower than 100 m asl (anomaly #16). Through-flow (hydrostatic) conditions occur at about the 23-28th skm near the land surface. Otherwise in the south of the 55th skm upward flow can be observed. Significant increase in hydraulic heads (high gradh_v) can be observed within and below the Algyő Aquitard. In the same depth /~z = (-2300)-(-3300) m asl/ lower hydraulic heads can be found in the north of the Derecske Trough (at the 49th skm at z ≈ (-2900) m asl h≈1600 m asl) than in the south of it (e.g., at the 26th skm at z ≈ (-2900) m asl h≈2000 m asl), though data were available only from one well in the north. At the

28th skm within anomaly #17 high lateral gradient ($\Delta h \approx 900$ m) and hydrocarbon occurrence can be observed as well along a fault, which thus may be a barrier fault. Additionally, also the low permeability of Algyő Aquitard could contribute to the energy loss in the north of the fault where data were measured in it.

T(s,z) (A-Fig. 5.3.3.8): Aside from the local anomalies, vertical temperature gradient is roughly uniform. In the north of the 55th skm in the zone of converging flows /~z = (-500)-(-1200) m asl/ higher temperatures can be observed (~60-70°C in z ≈ (-500) m asl) than further south in the same depth (~50°C).

TDS(s,z) (A-Fig. 5.3.3.9): Only a few data were available. Salient increase in TDS can be observed below the Algyő Aquitard.

Interpretation: In the uppermost 1000-1500 m thick zone affected by surface topography gravity-driven flow system can be identified characterized by a regional N(E)-S(W) flow direction along the section, which based on the tomographic fluid-potential maps is NE-SW in deed. In the flow-converging zone along the northern termination of the section heat and TDS accumulation can be also observed, while the lateral flow direction tends to west-southwest according to the tomographic fluid-potential maps. Below the Algyő Aquitard significant increase can be observed in the hydraulic heads (i.e. salient overpressure) and TDS concentrations as well. Fluid-potential anomalies usually coincide with thermal and hydrochemical anomalies, as well as with faults and hydrocarbon accumulations.

#4

h(s,z) (A-Fig. 5.3.3.10): In the uppermost 1000 m thick zone effected by surface topography the regional gravitational flow direction is NE-SW. Local recharge and discharge areas also evolved due to the local topographic conditions. In the north of the 32th skm downward flow can be observed down to about z = (-800) m asl, then upward flow. In the south of the 32th skm ubiquitous upward flow can be observed with the exception of the region of p(z) profile #19 (at around the 7th skm) where hydrostatic conditions dominate. Significant increase in hydraulic heads (high gradh_v) can be observed within and below the Algyő Aquitard. At anomalies #7 and #25 high lateral gradients (grad$h_h \approx 1100\text{m}/400\text{m} = 2.75$, and $\Delta h \approx 500$ m, respectively) can be observed along faults referring to their transversally barrier character.

T(s,z) (A-Fig. 5.3.3.11): Aside from the local anomalies, vertical temperature gradient is roughly uniform. Anomaly #6 is more pronounced in the cross-section T(s,z) #1 /anomaly #6/, and in T(s,z) #2 /anomaly #6/, while in this section it rather seems to be a negative

anomaly. At anomaly #7 where high lateral hydraulic gradient refers to the flow barrier behaviour of a fault, also some lateral thermal gradient can be observed ($\Delta T \approx 20°C$).

TDS(s,z) (A-Fig. 5.3.3.12): Salient increase in TDS can be observed below the Algyő Aquitard. Significant maximums can be found in near-surface depth at anomalies #47 and #48 (TDS>1000 and >2400 mg/L, respectively), which then show concentration decrease with depth and alignment with the environmental average. Thus local surface effects may cause these anomalies.

Interpretation: In the uppermost 1000 m thick zone affected by surface topography gravity-driven flow system can be identified characterized by a regional NE-SW flow direction. Below the Algyő Aquitard significant increase can be observed in the hydraulic heads (i.e. salient overpressure) and TDS concentrations as well. Fluid-potential anomalies usually coincide with thermal and hydrochemical anomalies, as well as with faults and hydrocarbon accumulations.

#5

h(s,z) (A-Fig. 5.3.3.13): In the uppermost 1000 m thick zone effected by surface topography the regional gravitational flow direction is NE-SW. Local recharge and discharge areas also evolved due to the local topographic conditions. In the north of the 88th skm downward flow can be observed down to about z = (-600) m asl, then upward flow. In the south of the 88th skm ubiquitous upward flow can be observed, while in the south of the 45th skm through-flow conditions. Significant increase in hydraulic heads can be observed within and below the Algyő Aquitard, for instance at the 23th skm grad$h_v \approx$900m/100m=9. In the same depth /~z = (-2300)-(-3300) m asl/ lower hydraulic heads can be found in the north of the Derecske Trough than in the south of it though data were available only from one well in the north.

T(s,z) (A-Fig. 5.3.3.14): Aside from the local anomalies, vertical temperature gradient is roughly uniform.

TDS(s,z) (A-Fig. 5.3.3.15): Salient increase in TDS can be observed below the Algyő Aquitard.

Interpretation: In the uppermost 1000 m thick zone affected by surface topography gravity-driven flow system can be identified characterized by a regional NE-SW flow direction. Below the Algyő Aquitard significant increase can be observed in the hydraulic heads (i.e. salient overpressure) and TDS concentrations as well. Fluid-potential anomalies usually coincide with thermal and hydrochemical anomalies, as well as with faults and hydrocarbon accumulations.

#6

h(s,z) (A-Fig. 5.3.3.16): The cross-section is perpendicular to the regional gravitational NE-SW flow direction, thus in the uppermost 1000 m thick zone effected by surface topography beside some local recharge and discharge areas through-flow conditions dominate. Significant increase in hydraulic heads can be observed below the Algyő Aquitard, for instance at the 33th skm gradh_v≈1000m/700m=1.43.

T(s,z) (A-Fig. 5.3.3.17): Aside from the local anomalies, vertical temperature gradient is roughly uniform.

TDS(s,z) (A-Fig. 5.3.3.18): Salient increase in TDS can be observed below the Algyő Aquitard. Significant maximum can be found in near-surface depth at anomaly #43 (TDS>1200 mg/L), which then shows concentration decrease with depth and alignment with the environmental average. Thus local surface effects may cause this anomaly.

Interpretation: In the uppermost 1000 m thick zone affected by surface topography gravity-driven flow system can be identified characterized mostly by through-flow conditions due to the normal strike of the section regarding the regional NE-SW flow direction. Below the Algyő Aquitard significant increase can be observed in the hydraulic heads (i.e. salient overpressure) and TDS concentrations as well. Fluid-potential anomalies usually coincide with thermal and hydrochemical anomalies, as well as with faults and hydrocarbon accumulations.

#7

h(s,z) (A-Fig. 5.3.3.19): In the uppermost 1000 m thick zone affected by surface topography the regional gravitational flow direction is NE-SW. In the north of the 60th skm downward flow can be observed down to about z = (-800) m asl, then upward flow. In the south of the 60th skm ubiquitous upward flow can be observed. Significant increase in hydraulic heads can be observed within and below the Algyő Aquitard, for instance at the 55th skm gradh_v≈700m/300m=2.33. At anomaly #45 high lateral gradient (Δh≈700m) between the western side of a b-Pa2 fault and data in the east of it in a distance of about 5 km containing further b-Pa2 faults as well refer to their barrier character.

T(s,z) (A-Fig. 5.3.3.20): Aside from the local anomalies, vertical temperature gradient is roughly uniform.

TDS(s,z) (A-Fig. 5.3.3.21): Salient increase in TDS can be observed below the Algyő Aquitard. Significant maximum can be found in near-surface depth at anomaly #44 and #48 (TDS>1200, and >2400 mg/L, respectively), which then show concentration decrease

with depth and alignment with the environmental average. Thus local surface effects may cause these anomalies.

Interpretation: In the uppermost 1000 m thick zone affected by surface topography gravity-driven flow system can be identified characterized by a regional NE-SW flow direction. In the flow-converging zone along the northeastern termination of the section the lateral flow direction tends to west-southwest according to the tomographic fluid-potential maps. Below the Algyő Aquitard significant increase can be observed in the hydraulic heads (i.e. salient overpressure) and TDS concentrations as well. Fluid-potential anomalies usually coincide with thermal and hydrochemical anomalies, as well as with faults and hydrocarbon accumulations.

5.3.3.2 Békés-Battonya Study Area

Numbering is continuous regarding the cross-sections and anomalies in the Derecske Study Area.

#8

h(s,z) (A-Fig. 5.3.3.22): In the uppermost 200-500 m thick zone affected by surface topography the regional gravitational lateral flow direction tends from southeast to northwest, and characterized by low hydraulic gradients. All along the section downward flow can be observed down to about z = (-200)-(-300) m asl, then upward flow. Significant increase in hydraulic heads cannot be observed within or below the Algyő Aquitard, however mostly negative potential anomalies can be found running from the Pre-Neogene basement up to the Great Plain Aquifer (anomalies #49-51). Though most of their data is gaseous, considering the maximum *h* surplus caused by the gas ($\Delta h_{wg(max)}$=254 m asl, which is probably lower in the BBSA (see also Appendix 2)), the negative anomalies would be even more negative.

T(s,z) (A-Fig. 5.3.3.23): Aside from the local anomalies, vertical temperature gradient is roughly uniform. Isotherms between the 10^{th} and 30^{th} skm are ascending together with the Pre-Neogene basement.

TDS(s,z) (A-Fig. 5.3.3.24): Observed concentrations are usually lower with at least one order of magnitude than in the DSA in similar depths. The salient values at anomalies #47 and #48 (TDS>1200 mg/L) are high values only compared to the surroundings, while

located in the transient zone of the gravitational downward and overpressured upward flows.

Interpretation: In the uppermost 200-500 m thick zone affected by surface topography gravity-driven flow system can be identified regionally characterized by SE-NW lateral and downward vertical flow directions. In the upward flow domain below z = (-200)-(-300) m asl hydraulic heads and TDS concentrations are usually anomalously low. Fluid-potential anomalies usually coincide with thermal and hydrochemical anomalies, as well as with faults and hydrocarbon accumulations.

#9

h(s,z) (A-Fig. 5.3.3.25): In the uppermost 200 m thick zone effected by surface topography downward flow can be observed in the (N)E of the 30th skm (at the Battonya High), between the 10-30th skm downward flow with some (south)westward lateral component, while in the (south)western end of the section upward flow conditions. In the thickening Great Plain Aquifer in the Makó Trough /(S)W part of the section/ vertical hydraulic gradient is reduced. Significant increase in hydraulic heads cannot be observed within or below the Algyő Aquitard, however an extensive negative potential anomaly (#51) can be found running from the Pre-Neogene basement up to the Great Plain Aquifer at the Battonya High. Though most of its data is gaseous, considering the maximum *h* surplus caused by the gas ($\Delta h_{wg(max)}$=254 m asl, which is probably lower in the BBSA (see also Appendix 2)), the negative anomalies would be even more negative.

T(s,z) (A-Fig. 5.3.3.26): Only a few data were available showing roughly uniform vertical temperature gradient.

TDS(s,z) (A-Fig. 5.3.3.27): Observed concentrations are usually lower with at least one order of magnitude than in the DSA in similar depths. Also the positive anomalies are relative compared to the surrounding data.

Interpretation: In the uppermost 200 m thick zone affected by surface topography gravity-driven flow system can be identified. In the upward flow domain below z = (-200) m asl hydraulic heads and TDS concentrations are usually anomalously low.

#10

h(s,z) (A-Fig. 5.3.3.28): In the uppermost 300-400 m thick zone affected by surface topography downward flow can be observed in the SW of the 28th skm above the Battonya High, while in the NE of it (in the Békés Basin) upward flow conditions. Significant increase in hydraulic heads cannot be observed within or below the Algyő Aquitard, however an extensive negative potential anomaly (#50) can be found running from the Pre-

Neogene basement up to the Great Plain Aquifer at the Battonya High. Though most of its data is gaseous, considering the maximum *h* surplus caused by the gas ($\Delta h_{wg(max)}$=254 m asl, which is probably lower in the BBSA (see also Appendix 2)), the negative anomalies would be even more negative.

T(s,z) (A-Fig. 5.3.3.29): Only a few data were available

TDS(s,z) (A-Fig. 5.3.3.30): Observed concentrations are usually lower with at least one order of magnitude than in the DSA in similar depths. Also the positive anomalies are relative compared to the surrounding data.

Interpretation: In the uppermost 200 m thick zone affected by surface topography gravity-driven flow system can be identified. In the upward flow domain below z = (-200) m asl hydraulic heads and TDS contents are usually anomalously low. Fluid-potential anomalies usually coincide with thermal and hydrochemical anomalies, as well as with faults and hydrocarbon accumulations.

#11

h(s,z) (A-Fig. 5.3.3.31): All along the section upward flow can be observed with a low vertical hydraulic gradient in the Great Plain Aquifer. Below the top of the Endrőd Aquitard hydraulic heads show significant increase (*h*>2700 m asl at z ≈ (-3000) m asl).

T(s,z) (A-Fig. 5.3.3.32): Vertical temperature gradient is roughly uniform.

TDS(s,z) (A-Fig. 5.3.3.33): Observed concentrations are lower than in the DSA in similar depths, but higher than along sections TDS(s,z) #8-10.

Interpretation: All along the section upward flow can be observed, thus gravity- and overpressure driven flow systems cannot be separated hydraulically. Fluid-potential anomalies usually coincide with thermal and hydrochemical anomalies, as well as with faults and hydrocarbon accumulations.

#12

h(s,z) (A-Fig. 5.3.3.34): In the uppermost 300-400 m thick zone affected by surface topography the gravitational flow system represents through-flow conditions in the NW third of the section, downward flow between 30-38th skm due to a local topographic high, and upward flow in the SE of it (in the Békés Basin). In the z = (-200)-(-3000) m asl elevation interval's ubiquitous upward flow domain vertical hydraulic gradients are low due to the great thickness of the Great Plain Aquifer. Significant increase in hydraulic heads can be observed within and below the Algyő Aquitard.

T(s,z) (A-Fig. 5.3.3.35): Only a few data were available.

TDS(s,z) (A-Fig. 5.3.3.36): Only a few data were available showing at least one order of magnitude lower values than in the DSA in similar depths. Also the positive anomalies are relative compared to the surrounding data.

Interpretation: In the uppermost 300-400 m thick zone affected by surface topography gravity-driven flow system can be identified. TDS concentrations are usually anomalously low. Fluid-potential anomalies usually coincide with thermal and hydrochemical anomalies, as well as with faults and hydrocarbon accumulations.

#13

h(s,z) (A-Fig. 5.3.3.37): In the uppermost 300-400 m thick zone affected by surface topography the gravitational flow system represents upward flow conditions in the SW third of the section, then downward flow around the 30th skm due to a local topographic high, and through-flow conditions in the NE of the 42th skm. In the relatively thick (~2000 m) Great Plain Aquifer the vertical hydraulic gradient is low. Significant increase in hydraulic heads can be observed within and below the Algyő Aquitard.

T(s,z) (A-Fig. 5.3.3.38): Aside from the local anomalies, vertical temperature gradient is roughly uniform.

TDS(s,z) (A-Fig. 5.3.3.39): Only a few data were available showing at least one order of magnitude lower values than in the DSA in similar depths. Also the positive anomaly (#63) is relative compared to the surrounding data.

Interpretation: In the uppermost 300-400 m thick zone affected by surface topography gravity-driven flow system can be identified. TDS concentrations are usually anomalously low. Fluid-potential anomalies usually coincide with thermal and hydrochemical anomalies, as well as with faults and hydrocarbon accumulations.

6 DISCUSSION

6.1 Regional hydrogeological characterization of the Study Areas

6.1.1 Regional hydraulics

Status assessment of regional hydrogeological characteristics of the hydrostratigraphic units building-up both Study Areas (i.e. DSA and BBSA) will be summarized in the followings, since hydraulic behaviour of these units determines the fluid-potential distribution within the impelling force field (see also Fig. 3.4, A-Table 5.1-2).

In the upper several hundred meters of the **Great Plain Aquifer** (total thickness is about 1000 m in the DSA, 400 m in the BBSA) topography driven and hierarchically nested gravitational flow systems can be observed. Namely, topographic maximums coincide with recharge areas (i.e. downward flow direction), while topographic minima with discharge areas (i.e. upward flow direction). Regionally, the northeastern part of the Derecske Study Area representing a surface topographic high (around the NE tip of the Derecske Trough) makes up a recharge area, while the main discharge area can be found in the southwestern part of the Study Area, and through-flow conditions are also usual in a NW-SE striking zone between the main recharge and discharge area (Fig. 6.1). On the other hand, the Battonya High representing equally a Pre-Neogene and a surface topographic high makes up a recharge area, while the marginal flanks of the High show through-flow conditions (Fig. 6.2). Finally, the Makó Trough and Békés Basin representing similarly Pre-Neogene and surface topographic depressions constitute discharge areas (Fig. 6.2). Additionally, also local recharge and discharge areas can be found in both Study Areas (i.e. DSA and BBSA) related to local topographic highs and lows, respectively.

The upper, gravitational flow domain is hydraulically “perched” by a regional overpressured flow system, first described in the Great Hungarian Plain by TÓTH and ALMÁSI (2001). In this lower flow domain the dominant fluid flow direction is upward, or in other words, the vertical pressure gradient is superhydrostatic, i.e. pressure increases with depth towards the Pre-Neogene basement. Appearance of the overpressured system, i.e. that of the spatially uniform upward flow (everywhere in the Study Areas) can be observed generally down from the top of the Algyő Aquitard pending its depth within the z = (-1200)-(2000) m asl elevation interval, with the exception of the Battonya High Area where it appears below z = (-2000) m asl within the Pre-Neogene basement.

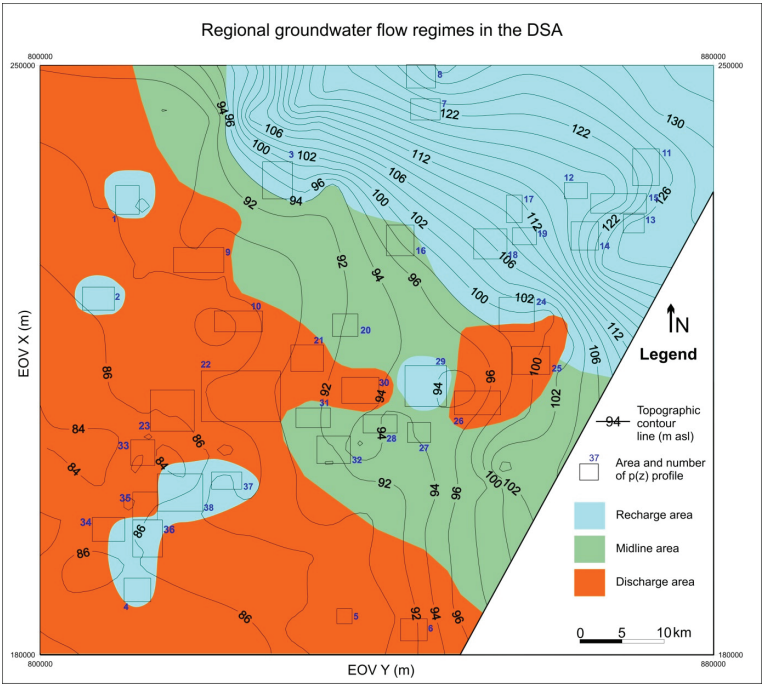

Figure 6.1 Distribution of regional groundwater regimes in the Derecske Study Area inferred from fluid-potential maps between the land surface and z = (-200) m asl, and from p(z) profiles. Topographic contour lines are also presented.

Aside from the topography driven local recharge and discharge areas, the regionally unconfined Great Plain Aquifer is mostly characterized by approximately hydrostatic conditions ($\gamma \approx 9.81 \pm 0.5$ MPa/km) and also low lateral hydraulic gradients due to its large thickness and high regional hydraulic conductivity. In addition, from the underlying overpressured flow domain only a small amount of fluid can enter the unit with significant energy loss through the underlying aquitards. Consequently, where after all significant overpressure can be observed in the Great Plain Aquifer and the fluid-potential anomaly inducing effect of gases can be excluded, presumably conduit faults interconnect the shallow hydrostatic and deep overpressured zones.

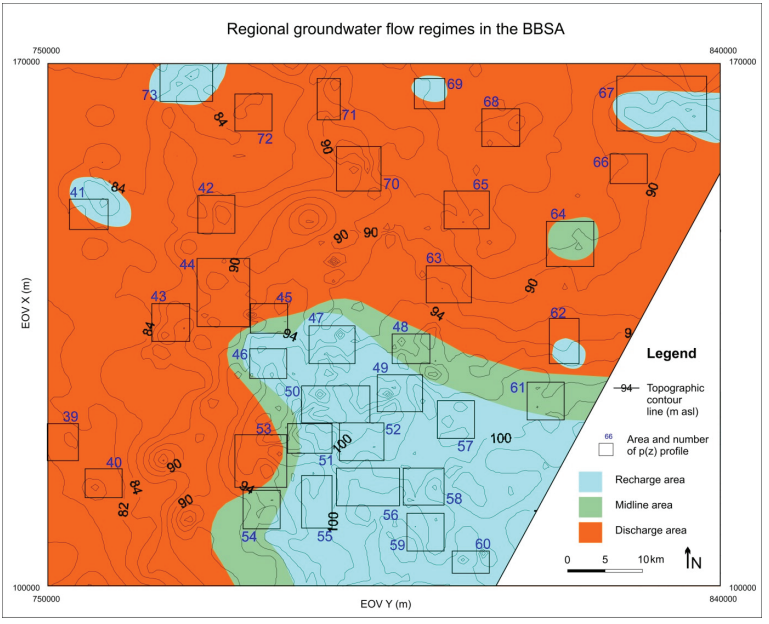

Figure 6.2 Distribution of regional groundwater regimes in the Békés-Battonya Study Area inferred from fluid-potential maps between the land surface and z = (-200) m asl, and from p(z) profiles. Topographic contour lines are also presented.

The gravitational and overpressured flow systems can be separated hydraulically only in two cases. On one hand, where an approximately hydrostatic zone can be observed (mostly in the p(z) profiles) between the gravitational and overpressured upward flows (e.g., p(z) profiles #20-21 (A-Fig. 5.3.1.48-50)). On the other hand, in the recharge areas of the gravitational system where gravitational downward flow meets with overpressured upward flow. Regional examples for this vertical converging zone can be found in both Study Areas in the Great Plain Aquifer, namely in the NE part of the Derecske Study Area in the z = (-400)-(-1000) m asl elevation interval (at the regional recharge area in Fig. 6.1; in cross-sections in A-Fig. 5.3.3.4,-7,-10, and -19), and along the Battonya High in the z = (-200)-(-400) m asl elevation interval (at the regional recharge area in Fig. 6.2; in cross-sections in A-Fig. 5.3.3.22,-25, and -28). Accordingly, the zone's penetration depth and thickness is greater in the DSA due to the higher topographic gradient (maximum differences

in topographical elevations of the Study Areas are 50 m and 20 m within the DSA and BBSA, respectively). Additionally, these potential minimum zones ensure ideal conditions for hydraulic hydrocarbon entrapment regarding vertical fluid flows. Though further lateral migration is possible, these zones build-up the upper boundary for the upward migrating hydrocarbons. However, in the Study Areas only a few hydrocarbon accumulations are known below, but near by the bottom of these zones (e.g., at anomalies #10 and #23 (e.g., A-Fig. 5.3.3.19)) probably due to their shallow depth and the approximately hydrostatic conditions usually existing below these zones as well. Consequently, upward migrating catagenetic hydrocarbons may be trapped by other kind of traps in greater depth before approach these zones. Thus practical significance of these hydraulic entrapment zones might be greater from the biogenetic gases' point of view. Additionally, gravitational discharge areas where there is no upper hydraulic boundary of upward hydrocarbon migration could be targets for near-surface geochemical hydrocarbon exploration[6].

Flow impeding effect of the **Algyő Aquitard** always manifests in a "break" or "step-like" pressure drop in the p(z) profiles pending its relative hydraulic conductivity, i.e. heterogeneity (faults, intercalated sand lenses, etc.), which shows significant spatial variability. Aside from some local regions, hydraulic behaviour or hydraulic conductivity of the Algyő Aquitard proved to be the most decisive among the hydrostratigraphic units in the overpressure's dissipation.

Szolnok Aquifer usually acts as a flow conduit, however in the deep sub-basins more affected by mechanical and chemical compaction, as well as far from the sediment sources its permeability could decrease to such a degree that it rather behaves as an aquitard unit (e.g., around Szarvas /p(z) #73, A-Fig. 5.3.1.215/ and Békés Highs /p(z) #70, A-Fig. 5.3.1.210/).

Endrőd Aquitard is usually strongly overpressured and represents a subsequent step in pressure increase similarly to the Algyő Aquitard. However, it is more homogeneous with the exception of the Battonya High Area. Being a usual source rock, hydrocarbon generation may also contribute to the build-up of excess pressures locally.

The **Pre-Pannonian Aquifer** and **Pre-Neogene** formations show similar hydraulic behaviour in both Study Areas. Namely, these units are regionally highly overpressured, while the dissipation of overpressure is gradual within the units characterized by only slightly superhydrostatic vertical pressure gradients. It refers to their relatively high permeability, and to the presence of effective aquitard units as well in the overlying strata, which force the

[6] Theory of near-surface geochemical hydrocarbon exploration can be found in e.g., LAUBMEYER (1933), PHILP and CRISP (1982), TÓTH (1996), SCHUMACHER (2000).

lateral flow in these high-permeability units. However, barrier strata and faults can locally scatter the pressure data (e.g., p(z) #13, A-Fig. 5.3.1.33).

In conclusion, hydraulic behaviour of the Great Plain Aquifer, as well as the Pre-Pannonian Aquifer and the Pre-Neogene formations is mostly uniform regionally in both Study Areas. On one hand, the Pre-Pannonian Aquifer and the Pre-Neogene formations are highly overpressured (excess pressure is about 30-60 MPa above the hydrostatic – even more than 200%) and characterized by only slightly superhydrostatic vertical pressure gradients (~11-14 MPa/km). On the other hand, the Great Plain Aquifer is unconfined and containing gravitational flow systems, which show approximately hydrostatic conditions ($\gamma \approx 9.81 \pm 0.5$ MPa/km) compared to the overpressured system. These phenomena refers to the relatively high hydraulic conductivity (or permeability) of these units. However, the Endrőd Aquitard, Szolnok Aquifer, and Algyő Aquitard represent spatially variable heterogeneities and thus vertical pressure gradients (even >20 MPa/km). Consequently, these three units, and particularly the Algyő Aquitard, control the "mode" or "way" of overpressure dissipation between the two boundaries of the subsurface fluid flow domain, namely the overpressured Pre-Pannonian strata and the approximately hydrostatic Great Plain Aquifer.

6.1.2 Regional geothermics

Aside from the local anomalies, vertical temperature gradient is roughly uniform in both Study Areas representing the Pannonian Basin's average of 50°C/km, which already indicates positive anomaly compared to the world average of 30°C/km, or exceeding that (up to 149°C/km) (see also Fig. 6.8.A). Regarding the anomalies, heat accumulation can be observed in the potential minimum zones ("hydraulic traps") of converging gravitational downward and overpressured upward flows (see also Chapter 6.1.1.). In addition, the Battonya High Area represents a positive anomaly /$\Delta T \approx$ +(20-40)°C/ compared to its surroundings in the total studied elevation interval. It could be explained by that the asthenosphere reaches its relatively shallower depth (<60 km) within the Pannonian Basin at the Battonya High Area where consequently the heat flow maximum of the Southern Great Hungarian Plain (100-110 mW/m^2) can be found as well (HORVÁTH et al., 2004).

6.1.3 Regional hydrochemistry

In the DSA TDS content shows jump-like increase (from the order of magnitude of 1000 mg/L to 10,000 mg/L) below the Algyő Aquitard, while salt accumulation can be observed in the potential minimum zone ("hydraulic trap") of converging gravitational downward and overpressured upward flows (see also Chapter 6.1.1.). On the other hand, in the BBSA data show at least one order of magnitude lower values than in the DSA in the total studied elevation interval (see also Fig. 6.8.B). Additionally, in the z = (-200)-(-600) m asl elevation interval (in the flow converging zone) a TDS maximum (1000-1500 mg/L) can be observed due to the high concentrations of HCO_3^- (≈ 1000 mg/L). Accordingly, the upwelling NaCl-type (ERDÉLYI, 1976; MÁDL-SZŐNYI and TÓTH, 2009) but less saline groundwater may enrich in HCO_3^- by mixing with the gravitational system's $NaHCO_3$-type or (Ca,Mg)-$(HCO_3)_2$-type water (MÁDL-SZŐNYI and TÓTH, 2009). However, origin of the overpressured system's groundwater of anomalously low concentrations could not be explained based on the results of this thesis. Thus this question requires further studies, while also the data's unreliability has to be kept in mind.

6.2 Diagnostic relationships among the h/T/TDS anomalies, hydrocarbon occurrences, and geological heterogeneities

Beyond the regional hydrogeological characteristics of the Study Areas described in Chapter 6.1, several anomalies can be found in the fluid-potential (*h*), geothermal (*T*), and hydrochemical (TDS) field as well. Their coincidence with each other, as well as with faults and hydrocarbon occurrences supports the diagnostic (~cause and effect) relationships among them. Anomalies and coincidences are listed in A-Tables 5.3-4, while the numbers of their pieces in Fig. 6.3. Regarding the numbers it is important to notice that the lack of coincidences usually due to the lack of data instead of the lack of anomalies. Consequently, these numbers cannot be evaluated realistically by mathematical statistical methods.

As it can be seen from the numbers (Fig. 6.3), 65 fluid-potential, thermal, and/or hydrochemical anomalies can be found in the DSA, and 34 in the BBSA. In the DSA, most of them are positive anomalies, while the BBSA represents several negative hydraulic anomalies and a regional negative hydrochemical anomaly as well. Additionally, all of the hydrocarbon occurrences in the BBSA coincide with fluid-potential anomalies, and in the larger part of the cases not the hydrocarbon causes the potential anomaly, particularly in greater depths. Whilst

more faults are known in the DSA than in the BBSA, almost every fault coincides with a fluid-potential anomaly, and consequently also the co-occurrence of potential anomalies, faults, and hydrocarbons is frequent. Furthermore, temperature and salinity anomalies show more correspondence with potential anomalies than with faults or hydrocarbon occurrences, while less correlation with the others is represented by the salinity.

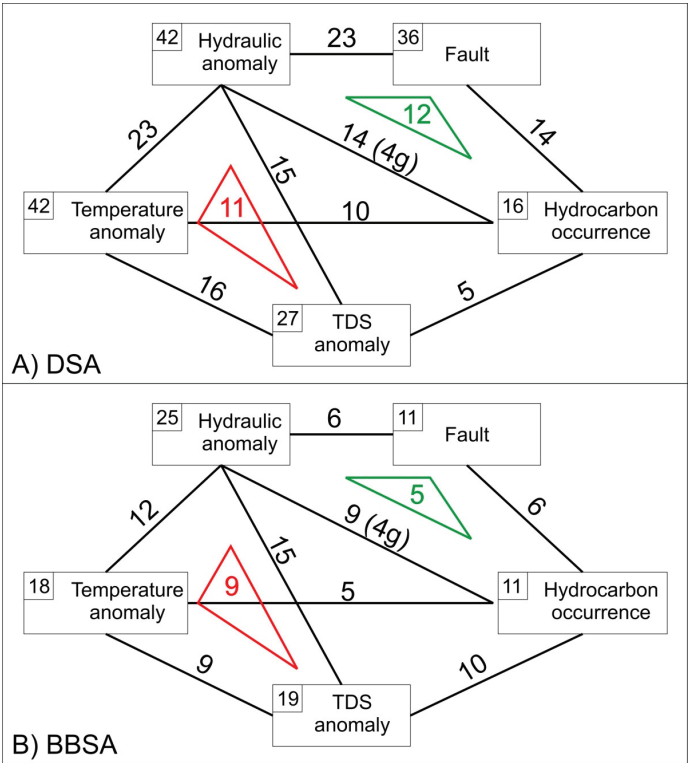

Figure 6.3 Number of anomalies (within the upper left corner of the rectangles) and coincidences (along the lines) in the **A)** DSA and **B)** BBSA. Red numbers show the joint occurrences of hydraulic, temperature and TDS anomalies, while green numbers represent that of the hydraulic anomalies, faults, and hydrocarbon occurrences. Regarding the number of coincidences between hydraulic anomalies and hydrocarbon occurrences, numbers in the brackets /e.g., (4g)/ show the number of gas-induced potential anomalies. In the BBSA TDS anomalies were defined by comparing to the regional negative anomaly.

Based on these facts, the following relations of cause and effect (Fig. 6.4) received diagnostic substantiation. First of all, faults and sedimentological heterogeneities, i.e. the geological build-up determines the mode of overpressure dissipation, thus the migration pathways of fluids from the Pre-Neogene basement towards the approximately hydrostatic Great Plain Aquifer (see also Chapter 6.1 – the hydraulic role of the Endrőd AT, Szolnok AF, and Algyő AT) (Fig. 6.4 – arrow #1). In other words, geological build-up defines the subsurface fluid-potential or energy distribution, and in this way the hydrodynamic conditions, which also involve the fluid-potential anomalies generated by faults and sedimentological heterogeneities (Fig. 6.4 – arrow #2). In the Study Areas of this thesis, shallow potential anomalies are usually induced by local topographic highs and lows, while the deep anomalies and some shallow one as well are caused by faults and sedimentological heterogeneities in the overpressured flow domain. In other words, significant anomalies related to geological heterogeneities can be found up to the top of the overpressured flow system.

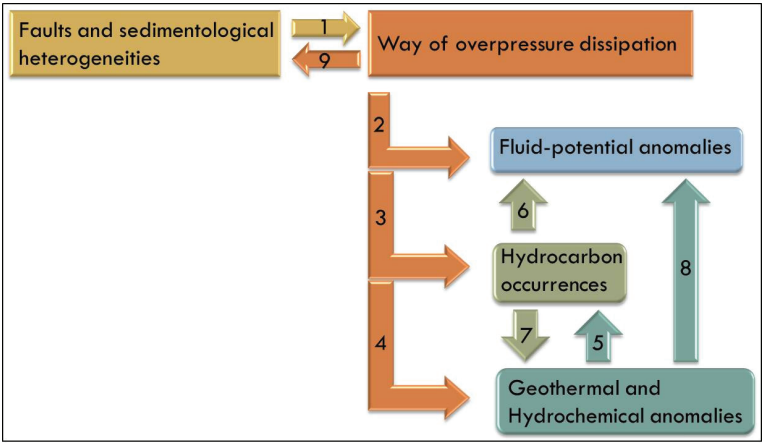

Figure 6.4 Diagnostic relationships among *h*/*T*/TDS anomalies, hydrocarbon occurrences, and geological heterogeneities. Numbered arrows are discussed in the text.

Subsequently, hydrocarbons frequently occur around fluid-potential anomalies representing high hydraulic gradients and (relative) potential minimum "nooks" (Fig. 6.4 – arrow #3). Common coincidence of thermal and hydrochemical anomalies with potential

anomalies can be explained by the same way (Fig. 6.4 – arrow #4), while these anomalies can also contribute to hydrocarbon entrapment considering the screening mechanisms of hydraulic traps (see also Chapter 4.3.3.2) (Fig. 6.4 – arrow #5). However, also hydrocarbon accumulations and particularly gases can cause apparent fluid-potential anomalies (see also Chapter 4.3.1 and Appendix 2) (Fig. 6.4 – arrow #6), as well as local temperature and chemical anomalies (Fig. 6.4 – arrow #7). Furthermore, also other geological factors and processes could generate thermal and chemical anomalies, however frequency of coincidence of them with fluid-potential anomalies is significant. Finally, it is worth mentioning that also spatial differences in temperature or salinity (i.e. concentration) could generate fluid flow (so called "coupled flows") and thus potential anomalies (Fig. 6.4 – arrow #8). However in the Pannonian Basin and particularly in regional scale these are irrelevant considering the temperature and hydrochemical conditions, as well as the two main fluid flow driving forces, namely the elevational differences of the topography (i.e. gravity) and the overpressure.

To sum up, in the cause and effect, as well as usually back and forth acting relation system of the development of *h*, *T*, and TDS anomalies and hydrocarbon occurrences the way of overpressure dissipation plays the primary determining role, which is defined by the geological build-up, and particularly by its discontinuities and heterogeneities. Finally, also this relationship is bidirectional, since also potential (pressure) distribution can effect on the geological build-up according to Terzaghi's law (TERZAGHI, 1923) (see also Chapter 2.2.2.) (Fig. 6.4 – arrow #9). Namely, in case of constant total vertical stress, pore pressure increase causes decrease in the effective stress, thus weakening of the rock framework, which can lead to the opening of hydraulic fissures and fractures, as well as opening or reactivation of faults.

6.3 Hydrogeologically distinct regions and basic types of p(z) profiles

Based on the diagnostic relationships described in the previous chapter, 7 regions were distinguished within the Study Areas that can be characterized by 7 basic types of p(z) profiles traced back to the differences in the geological build-up and consequently in the way of overpressure dissipation. /Their numbering (#1-7) is consistent in the text and in every figure./ From the 7th, Békés Basin region only shallow hydraulic data were available, thus conclusions were drawn rather based on geological analogies, since geological build-up is better known (see also Chapter 6.4.2). The average p(z) profiles referring to each regions can be seen in Fig. 6.5.A, while the generalized basic types of p(z) profiles without numerical quantification due to the differing elevations of the hydrostratigraphic units in Fig. 6.5.B. The

latter also expresses more explicitly the typical hydraulic behaviour (~ vertical pressure gradient) of each unit irrespectively of their depth position. Additionally, in the p(z) type profiles (Fig. 6.5.B) the Endrőd Aquitard was not indicated in order to simplify the profiles, since in the Battonya High Area it shows aquifer character not differentiating from the Pre-Pannonian formations, while otherwise effect of the Algyő Aquitard proved to be more significant. Ranging of the p(z) profiles into the basic types can be seen in Fig. 6.6, while the hydraulically distinct regions in Fig. 6.7. Finally, the fundamental geological characteristics, which proved to be the determining factors in the differentiation, are summarized in Table 6.1. Parameters enhancing the hydraulic conductivity of the certain hydrostratigraphic units are signed by green cells, while parameters diminishing that by red cells. Additionally, the feasible entrapment zones characterizing the certain regions and basic p(z) profile types are also represented in Fig. 6.5.B and Table 6.1. In this case "zones" signify hydrostratigraphic units, while based on the also indicated Pre-Neogene basement depth and on the usual geological characteristics of the Pannonian strata also the depth interval can be approximately deduced. In other words, these figures represent the upper boundary of vertical hydrocarbon migration, thus the depth interval (i.e. above the boundary) where it does not pay to search for hydrocarbon accumulation. Furthermore, looking at the areal distribution of the p(z) type-profiles conclusions could be drawn about the possibilities of lateral migration as well (Fig. 6.5). Finally, the also characteristic T(z) and TDS(z) profiles of the distinct regions can be seen in Fig. 6.8.

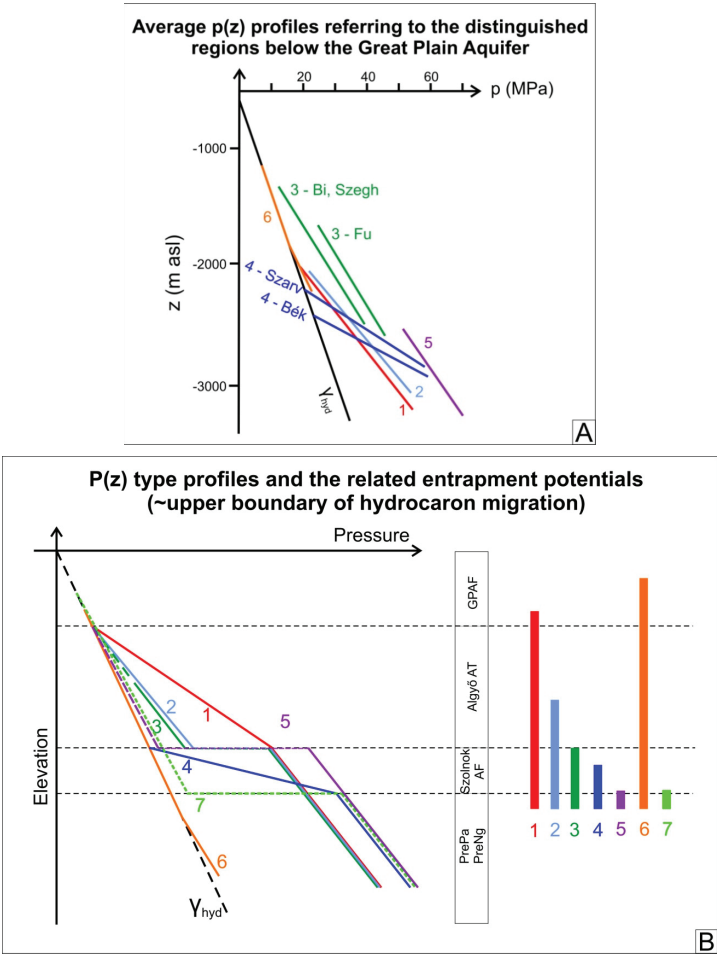

Figure 6.5 The average p(z) profiles referring to each regions (**A**), and the generalized basic types of p(z) profiles (**B**). Endrőd Aquitard is not indicated in the p(z) type profiles (**B**), since where it shows aquitard character usually no data were available from the unit. Abbreviations: γ_{hyd} – hydrostatic vertical pressure gradient (=9.81 MPa/km); 1 – Derecske-North; 2 – Derecske-South; 3 – Furta (Fu), Biharnagybajom (Bi), Szeghalom (Szegh) Highs; 4 – Szarvas (Szarv) and Békés (Bék) Highs; 5 – Fábiánsebestyén-Nagyszénás-Orosháza Area; 6 – Battonya High; 7 – Békés Basin; PreNg – Pre-Neogene; PrePa – Pre-Pannonian; AF – aquifer; AT – aquitard; GPAF – Great Plain Aquifer. In the Fábiánsebestyén-Nagyszénás-Orosháza Area hydrocarbon accumulations are not known, but the upper migration boundary could be determined based on geological analogies.

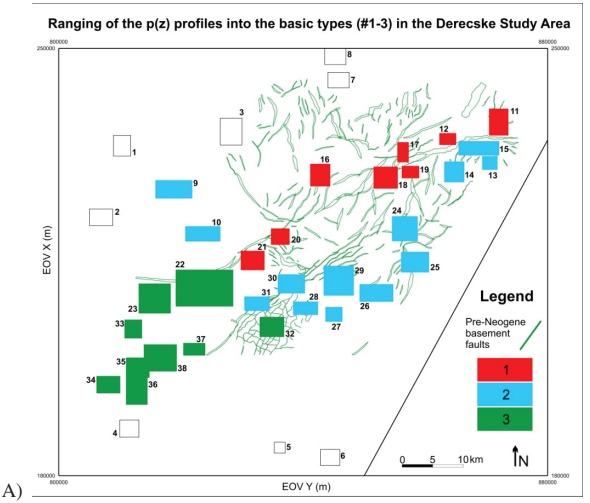

A)

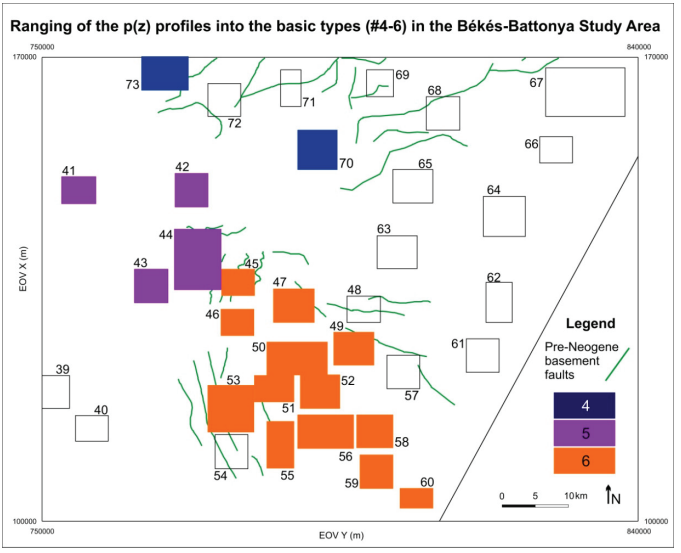

B)

Figure 6.6 Ranging of the p(z) profiles into the basic types in the DSA (**A**) and BBSA (**B**). White polygons represent areas possessing only shallow data (from the Great Plain Aquifer). Legend: 1 – Derecske-North; 2 – Derecske-South; 3 – Furta, Biharnagybajom, Szeghalom Highs; 4 – Szarvas and Békés Highs; 5 – Fábiánsebestyén-Nagyszénás-Orosháza Area; 6 – Battonya High; 7 – Békés Basin.

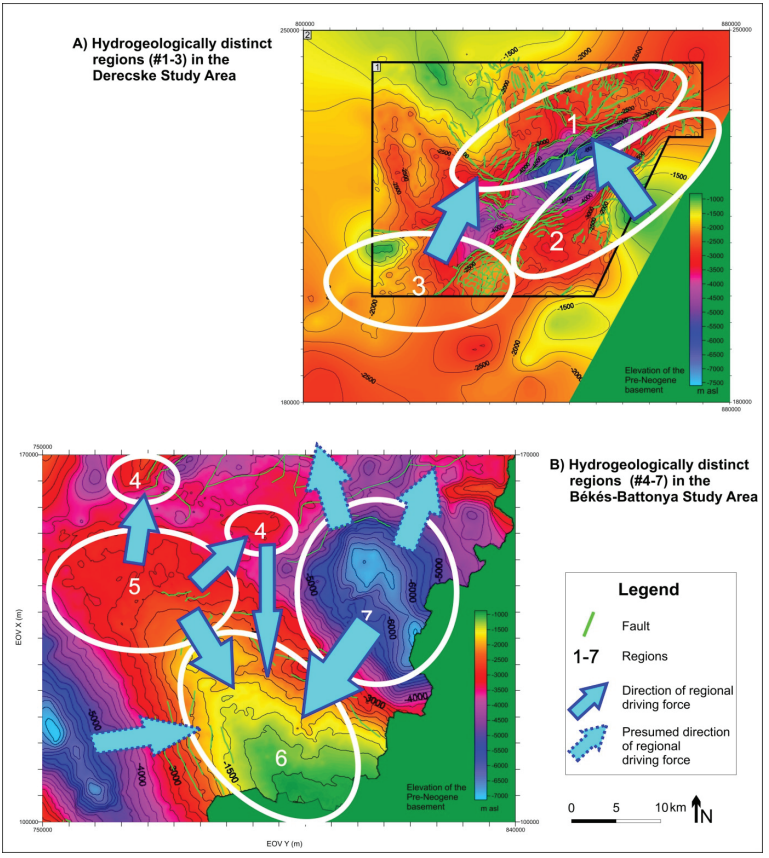

Figure 6.7 Hydrogeologically distinct regions and directions of lateral driving force in the Study Areas represented on the elevation maps of the Pre-Neogene basement /i.e. in the DSA (**A**) on the combined map of the MOL Plc. (1) (MOL Plc., 2009*) and the map constructed from borehole data (2); in the BBSA (**B**) on the map of the MOL Plc. (MOL Plc., 2011*)/. Regions: 1 – Derecske-North; 2 – Derecske-South; 3 – Furta, Biharnagybajom, Szeghalom Highs; 4 – Szarvas and Békés Highs; 5 – Fábiánsebestyén-Nagyszénás-Orosháza Area; 6 – Battonya High; 7 – Békés Basin. Driving force towards the Battonya High (6) from the west could be presumed based on the known geological analogies between the Békés Basin and the Makó Trough.

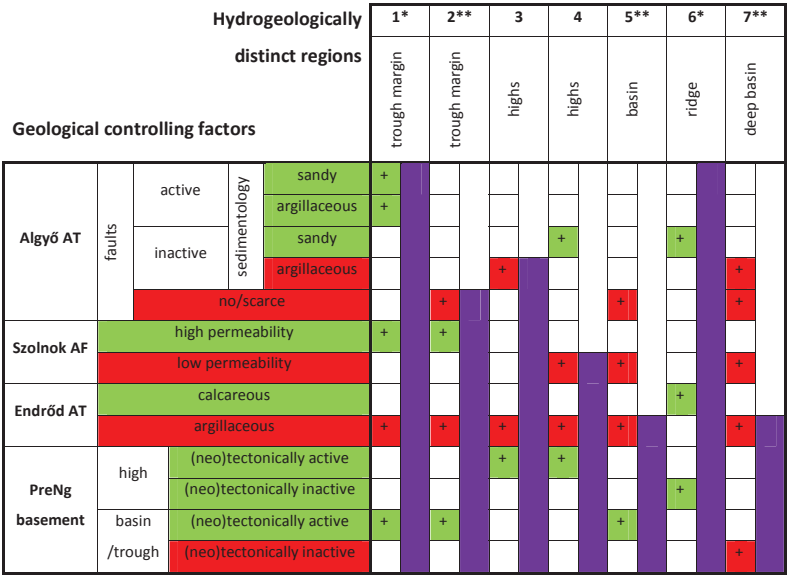

Table 6.1 The fundamental geological characteristics, which proved to determine the hydraulic differentiation of the regions. Legend: green cell – conduit/aquifer character; red cell – barrier/aquitard character; purple cell – formation-based upper boundary of hydrocarbon migration (~occurrence of accumulations); * – possibility of hydraulic entrapment is also given; ** – "compaction vs. overpressure" problem could emerge. See the text for further details. Abbreviations of regions: 1 – Derecske-North; 2 – Derecske-South; 3 – Furta, Biharnagybajom, Szeghalom Highs; 4 – Szarvas and Békés Highs; 5 – Fábiánsebestyén-Nagyszénás-Orosháza Area; 6 – Battonya High; 7 – Békés Basin. In the Fábiánsebestyén-Nagyszénás-Orosháza Area hydrocarbon accumulations are not known, but the upper migration boundary could be determined based on geological analogies.

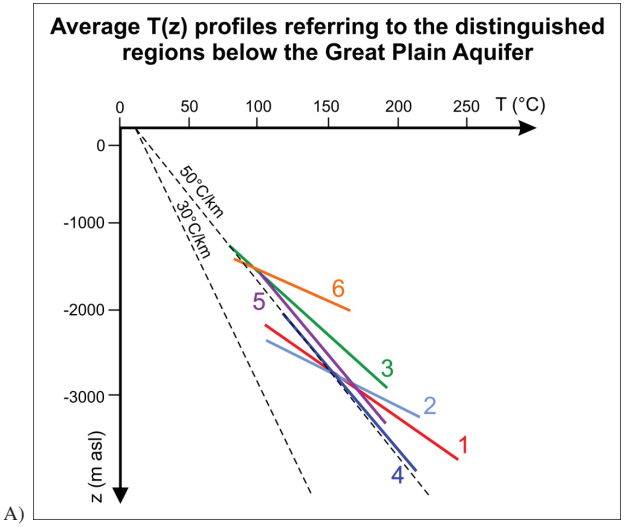

A)

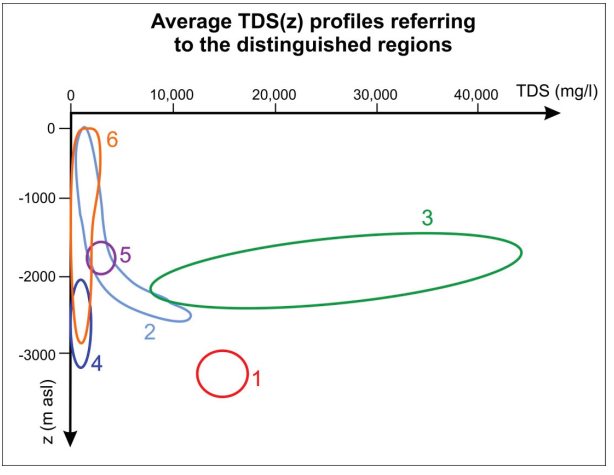

B)

Figure 6.8 Characteristic geothermal gradients (**A**) and TDS distribution (**B**) in the primarily hydraulically distinct regions. Regions: 1 – Derecske-North; 2 – Derecske-South; 3 – Furta, Biharnagybajom, Szeghalom Highs; 4 – Szarvas and Békés Highs; 5 – Fábiánsebestyén-Nagyszénás-Orosháza Area; 6 – Battonya High.

In the followings the distinguished regions and p(z) type-profiles are presented by summarizing the results of this thesis, and information from the literature (see also Chapter 3) where it is necessary.

Factors enhancing hydraulic conductivity were signed by "**C**" as conduit, while diminishing factors by "**B**" as barrier within brackets. Tectonic activity usually boosts permeability, since on one hand, in low-permeability formations only active faults could be effective flow conduits, while inactive faults could be act as flow pathways in high-permeability strata or filled by coarser grained intrusions (see also Chapter 2.1.1.). On the other hand, compressional tectonic field could generate overpressure (e.g., OLIVER, 1986; GE and GARVEN, 1992, 1994; GARVEN, 1995; JU and YANG, 2010) as well, which can contribute to the opening of faults and fractures (see also Chapter 2.2.2. and 6.2.). In case of the Pre-Neogene basement being in a deeper position also compaction ("**Co**" in the text), or else the "compaction versus overpressure problem" ("**CovsOp**" in the text) (see also Chapter 2.2.2.) has to be taken into account, since beside tectonic activity also compaction could generate significant overpressure ("**OpG**" as overpressure generating factor in the text). Even if the Pre-Neogene basement emerges into a shallower depth, it could be highly overpressured ("**Op**") if there are regionally extensive low-permeability strata in the Pannonian succession. Finally, also topographical conditions are interesting from the point of view of shallow hydraulic entrapment potential.

1. Derecske – North

- **Area** (Fig. 6.6.A and 6.7): Northern rim and northern surroundings of the Derecske Trough.
- **Topography** (Fig. 3.1): Topographical high in the NE is a recharge area of the gravitational flow system (Fig. 6.1).
- **Geological build-up** (Table 6.1): Pre-Neogene basement is in a relative great depth /z ≈ (-2500) m asl/ (Co)(Op) and tectonically active due to the bounding strike-slip fault zones of the Trough (C)(OpG). Endrőd Aquitard is more pelitic (B), while the Szolnok Aquifer is coarser grained (C). Algyő Aquitard is more heterogeneous sedimentologically and structurally as well (C). On one hand, according to seismic sections the total thickness of the delta slope facies is smaller and less pronounced than in the south of the Trough. On the other hand, several active faults, namely flower structures of the northern bounding fault zone of the Trough cross-cut the Aquifer, particularly around p(z) profiles #20.

- **Way of overpressure dissipation** (Fig. 6.5 and 6.6.A): p(z) type-profile #1 – "break" at the bottom of the Algyő Aquitard. Significant overpressure in the Pre-Neogene basement and Pre-Pannonian Aquifer (~40-50 MPa; with 20-25 MPa excess pressure above the hydrostatic value) gradually, i.e. diffusively dissipates through the relatively high-permeability Algyő Aquitard, the aquitard character of which is supported nevertheless by the maintained overpressure below the unit.
- **Temperature conditions** (Fig. 6.8.A): Geothermal gradient is higher than the Pannonian Basin's average of 50°C/km.
- **Hydrochemical conditions** (Fig. 6.8.B): Suited into the increasing concentration trend with depth of the Derecske – South region.
- **Entrapment potential** (Fig. 6.5.B and Table 6.1): Hydrocarbon occurrences are known from the total depth interval of the Algyő Aquitard, and also from the bottom zone of the Great Plain Aquifer. In shallower depth also the possibility for hydraulic entrapment is given in the flow converging zone around the boundary of the gravitational and overpressured flow system.

2. Derecske – South

- **Area** (Fig. 6.6.A and 6.7): Southern rim and southern surroundings of the Derecske Trough.
- **Topography** (Fig. 3.1): Topographical high in the NE is a recharge area of the gravitational flow system (Fig. 6.1).
- **Geological build-up** (Table 6.1): Pre-Neogene basement is in a relative great depth ($z <$ (-2500) m asl) (Co)(Op) and tectonically active due to the bounding strike-slip fault zones of the Trough (C)(OpG). Endrőd Aquitard is more pelitic (B), while the Szolnok Aquifer is coarser grained (C). Algyő Aquitard is more homogeneous (B), since fault density is much lower. In addition, according to seismic sections the total thickness of the delta slope facies is greater than in the north of the Trough.
- **Way of overpressure dissipation** (Fig. 6.5 and 6.6.A): p(z) type-profile #2 – "jump" at the bottom of the Algyő Aquitard. Significant overpressure in the Pre-Neogene basement and Pre-Pannonian Aquifer (~50-60 MPa; with 20-30 MPa excess pressure above the hydrostatic value), then jump-like pressure drop at the bottom of the Algyő Aquitard. Accordingly, overpressure can dissipate only concentrated along a few faults, while the low-permeability matrix of the Aquitard effectively maintenances the overpressure below. In addition, comparing the p(z) profiles generalized in this type-profile #2, elevation of the

bottom of the Algyő Aquitard varies between z = (-2050)-(-2400) m asl, which can be interpreted regionally as a transient zone characterized by the scatter of data, while the effective barrier zone follows above.

- **Temperature conditions** (Fig. 6.8.A): Geothermal gradient is slightly higher than in the Derecske – North region, while heat accumulation can be observed at the bottom of the Algyő Aquitard.
- **Hydrochemical conditions** (Fig. 6.8.B): Increasing concentrations with depth by the same trend as in the Derecske – North region.
- **Entrapment potential** (Fig. 6.5.B and Table 6.1): Hydrocarbon occurrences are known from the bottom zone of the Algyő Aquitard. In shallower depth also the possibility for hydraulic entrapment is given in the flow converging zone around the boundary of the gravitational and overpressured flow system.

3. Furta, Biharnagybajom, and Szeghalom Highs

- **Area** (Fig. 6.6.A and 6.7): Southwestern rim and in the SW of the Derecske Trough.
- **Topography** (Fig. 3.1): Topographical depression.
- **Geological build-up** (Table 6.1): Pre-Neogene basement is in a relative shallow depth (z > (-2500) m asl) (Op), while tectonically less active than the Derecske Trough. Endrőd Aquitard is more pelitic (B), while the Szolnok Aquifer is pinching out along the margins of the basement highs. Algyő Aquitard is thinner, but more pelitic and cross-cut by some faults, most of which may be inactive atectonic structures (B).
- **Way of overpressure dissipation** (Fig. 6.5 and 6.6.A): p(z) type-profile #3 – "jump" at the bottom of the Algyő Aquitard. Significant overpressure in the Pre-Neogene basement and Pre-Pannonian Aquifer (~50-60 MPa; with 20-30 MPa excess pressure above the hydrostatic value) emerges into shallow depth with the basement highs, then only a few data are available from the bottom of the Algyő Aquitard representing jump-like pressure drop. Consequently, the Algyő Aquitard should impede fluid flows effectively in spite of its small thickness (~200-600m), and probably due to its low-permeability matrix cross-cut only by some inactive faults.
- **Temperature conditions** (Fig. 6.8.A): Geothermal gradient is slightly lower than in the Derecske – North and South regions, however the temperature values are higher also in the Great Plain Aquifer, while salient heat accumulation can be observed in the Algyő Aquitard.

- **Hydrochemical conditions** (Fig. 6.8.B): Higher concentrations than in the Derecske – North and South regions, particularly below the Algyő Aquitard.
- **Entrapment potential** (Fig. 6.5.B and Table 6.1): Hydrocarbon occurrences are not known from the Pannonian strata, but otherwise from the Pre-Pannonian Miocene and Pre-Neogene formations.

4. Szarvas and Békés Highs

- **Area** (Fig. 6.6.B and 6.7): Szarvas High in the north of a Mesozoic nappe boundary, and Békés High at the N(W) margin of the Békés Basin.
- **Topography** (Fig. 3.2): Topographical depressions.
- **Geological build-up** (Table 6.1): Pre-Neogene basement is in a relative shallow depth ($z > (-3000)$ m asl) (CovsOp), while tectonically less active. Endrőd Aquitard is more pelitic (B), while the Szolnok Aquifer is very low-permeability probably due to its finer grained character deposited far from the sediment sources in the NE and NW, as well as to mechanical and chemical compaction. Sand content of the Algyő Aquitard is higher, thus the cross-cutting, mostly inactive growth faults might be flow conduits containing coarser grained filling (C).
- **Way of overpressure dissipation** (Fig. 6.5 and 6.6.B): p(z) type-profile #4 – "jump" within the Szolnok Aquifer. Significant overpressure in the Pre-Neogene basement and Pre-Pannonian Aquifer (~60-70 MPa; with 30-40 MPa excess pressure above the hydrostatic value), then pressure drop within the low-permeability Szolnok Aquifer and approximately hydrostatic conditions above it. Considering the practically impossible higher than lithostatic vertical pressure gradients and scatter of the data in the Szolnok Aquifer, fluid flow could be materialized most probably in (natural) hydraulic fractures. As a result, hydraulic behaviour of the Algyő Aquitard is insignificant, but otherwise it is a less effective barrier zone here.
- **Temperature conditions** (Fig. 6.8.A): Geothermal gradient represents the Pannonian Basin's average of 50°C/km, while some higher temperature values are known from the Szolnok Aquifer.
- **Hydrochemical conditions** (Fig. 6.8.B): Lower concentrations than in the DSA's regions (#1-3).
- **Entrapment potential** (Fig. 6.5.B and Table 6.1): Hydrocarbon occurrences are not known from above the Szolnok Aquifer.

5. Fábiánsebestyén-Nagyszénás-Orosháza Area

- **Area** (Fig. 6.6.B and 6.7): In the NW foreland of the Battonya High, along and in the south of a Mesozoic nappe boundary.
- **Topography** (Fig. 3.2): Topographical depression.
- **Geological build-up** (Table 6.1): Pre-Neogene basement is in a relative great depth (z < (-3000) m asl) (CovsOp), cross-cut by a Mesozoic nappe boundary (OpG). Endrőd Aquitard is more pelitic (B), while the Szolnok Aquifer might be low-permeability as well (B). The Algyő Aquitard is more pelitic and faults are hardly known (B).
- **Way of overpressure dissipation** (Fig. 6.5 and 6.6.B): p(z) type-profile #5 – "jump" at latest at the bottom of the Algyő Aquitard. Most significant overpressures in the Pre-Neogene basement and Pre-Pannonian Aquifer of the Study Areas (>60-70 MPa; with 40-50 MPa excess pressure above the hydrostatic value), then the largest pressure drop at the bottom of the low-permeability Algyő Aquitard.
- **Temperature conditions** (Fig. 6.8.A): Geothermal gradient represents the Pannonian Basin's average of 50°C/km, while higher temperature values are known from the Great Plain and Szolnok Aquifers, as well as from the Endrőd Aquitard. Also water vapour occurrences are known from the Pre-Neogene basement (PAP, 1993).
- **Hydrochemical conditions** (Fig. 6.8.B): Lower concentrations than in the DSA's regions (#1-3), however waters with high H_2SiO_3 content have already been described in the Pre-Neogene basement (PAP, 1993).
- **Entrapment potential** (Fig. 6.5.B and Table 6.1): Hydrocarbon occurrences are not known, and cannot be expected in shallower strata than the Szolnok Aquifer.

6. Battonya High

- **Area** (Fig. 6.6.B and 6.7): Battonya High and its surroundings.
- **Topography** (Fig. 3.2): Topographical high, thus recharge area of the gravitational flow system (Fig. 6.2).
- **Geological build-up** (Table 6.1): Pre-Neogene basement is in a shallow depth (z > (-1500) m asl) (Op), while tectonically less active (emerges, but there are only a few Pannonian faults). Endrőd Aquitard is more calcareous and fissured (C), while the Szolnok Aquifer is pinching out along the margins of the basement high. Sand content of the Algyő Aquitard is higher, thus the cross-cutting, mostly inactive growth faults might be flow conduits containing coarser grained filling (C).

- **Way of overpressure dissipation** (Fig. 6.5 and 6.6.B): p(z) type-profile #6 – approximately hydrostatic conditions. Overpressure appears form about z = (-2000) m asl, while in shallower depth the total Pre-Neogene – Pannonian succession is in approximately hydrostatic conditions due to the lack of regionally effective aquitards in the Pannonian strata. Consequently, in this region appearance of the overpressure is depth-dependent due to the high-permeability Pannonian succession, while in all of the other regions (#1-5) it seems to coincide with the top of the usually low-permeability Algyő Aquitard, which otherwise can be generally found in the same depth (z ≈ (-2000) m asl). Additionally, a closed potential depression can be observed in the central part of the High in the z = (-600)-(-1800) m asl elevation interval. The results of this thesis cannot explain the formation of this regional scale negative potential anomaly, however some considerations could be taken in the following way. i) Effect of hydrocarbon production can be excluded, since pressure data were used from the first exploration wells in each field. ii) Correction of hydraulic head calculations by water density would cause even more negative anomaly, while density correction by taking into account the low TDS and high temperature values of the region would result in a lower density, thus higher *h* values. However, pressure data would remain hydrostatic or subhydrostatic even in these cases. iii) Being a recharge area of the gravitational system, the effect of insufficient amount of infiltration can also arise /on the analogy of the effect of an aquitard sandwiched between two aquifers with basal aquifer outcropping at low elevation (TÓTH, 1980 Fig. 5; TÓTH, 2009, pp. 55-57, Fig. 3.12)/, but this closed potential depression can be already found in the overpressured flow system. iv) Since the Pannonian strata of the Békés Basin (see also p(z) type-profile #7) and Makó Trough are usually low-permeability due to their finer grained character (far from the NW and NE sediment sources), as well as to mechanical and chemical compaction, lateral recharge of the Battonya High from these basins is at least restricted and being able to partly explain the presence of the potential minimum zone. v) The currently uplifting Battonya High has already sustained significant erosion (~1000 m) (KÁROLY KISS, MOL Plc., personal communication, 2011), which could have transient pressure increasing ("memory") or decreasing ("unloading/rebound and/or cooling/aquathermal") effect (e.g., BARKER, 1972; TÓTH and MILLAR, 1983; NEUZIL and POLLOCK, 1983; TÓTH and CORBET, 1986; CORBET and BETHKE, 1992; PARKS and TÓTH, 1995; BEKELE et al., 2003) on the High's potential distribution as well. However, in both cases presence of at least one regionally extensive low-permeability strata is required. In case of the Battonya High, this flow barrier zone

should be located above the potential minimum zone, within the Great Plain Aquifer around z = (-600) m asl, where a relative potential maximum zone (correlated to the shallower and deeper values as well) can just be found. Also the development of this maximum zone could be explained by a low-permeability formation there. However, it is not known such strata for the time being.

- **Temperature conditions** (Fig. 6.8.A): Geothermal gradient is higher than the Pannonian Basin's average of 50°C/km, and also the temperature values are significantly higher in shallow depths as well. This phenomenon cannot be explained by the high-permeability Pannonian strata, but by the relatively shallow depth (<60 km) of the asthenosphere (see also Chapter 6.1.2.).
- **Hydrochemical conditions** (Fig. 6.8.B): Lower concentrations than in the DSA's regions (#1-3) and similar values irrespectively of depth can be observed. The anomalously low concentrations cannot be explained based on the results of this study. For further considerations see also chapter 6.1.3. However, it is possible that the negative fluid-potential and hydrochemical anomaly are connected to each other, and the reasons should not be searched only in the current processes, but also in the geological evolution history of the area.
- **Entrapment potential** (Fig. 6.3.B and Table 6.1): Hydrocarbon occurrences are known from the total Pre-Neogene – Pannonian succession due to the lack of vertical flow barrier(s). In shallower depth also the possibility for hydraulic entrapment is given in the flow converging zone around the boundary of the gravitational and overpressured flow system.

7. Békés Basin

- **Area** (Fig. 6.6.B and 6.7): Békés Basin
- **Topography** (Fig. 3.2): Topographical depression.
- **Geological build-up** (Table 6.1): Pre-Neogene basement is in a great depth (z < (-6000) m asl) (CovsOp), while tectonically less active (subsides, but there are only a few Pannonian faults along the margins). Endrőd Aquitard is more pelitic (B), while the Szolnok Aquifer is very low-permeability (B) and pinches out towards the basin margins. The Algyő Aquitard is more pelitic and faults are hardly known (B).
- **Way of overpressure dissipation** (Fig. 6.5): p(z) type-profile #7 – "jump" can be supposed already in the Szolnok Aquifer. Hydraulic data were available only from the Great Plain Aquifer (down to z = (-2100) m asl) and represent slightly superhydrostatic

conditions in the bottom zone of the Aquifer. Considering the thickness of the Neogene succession (maximum ~7000 m), as well as the low-permeability character of at least the aquitards, the Pre-Neogene basement should be highly overpressured. Hydrodynamic conditions of the Szolnok Aquifer should be similar to that of the Szarvas and Békés Highs. However, based on the p(z) profiles drawn along the basin's margins and on the potential maps of the adjacent areas as "boundary conditions", vertical and lateral driving forces can be presumed. Accordingly, lateral flows might be directed from the basin centers towards the margins, and particularly towards the Battonya High representing the lowest fluid-potential conditions in the Study Areas. However, "compaction versus overpressure problem" (see also Chapter 2.2.2.) also has to be taken into account particularly in this region regarding the potential amount of movable fluids.

- **Temperature conditions**: No data were available, however temperatures higher than the average could be expected, considering the shallow depth (<60 km) of the asthenosphere in the Southeastern Great Hungarian Plain.
- **Hydrochemical conditions**: No data were available, however relatively lower concentrations could be expected similarly to its surroundings. In addition, occasionally high (dissolved) methane content of water wells is a well-known phenomenon in the region, though shallow biogenic extraction cannot be excluded.
- **Entrapment potential** (Fig. 6.5.B and Table 6.1): Hydrocarbon occurrences are not known so far. However, it is worth mentioning that mobilization of hydrocarbons generated in the Endrőd Aquitard (or deeper units) also poses the question of "compaction versus overpressure problem" (see also Chapter 2.2.2.). If migration could materializes from the Endrőd Aquitard towards the Szolnok Aquifer or within it, impelling forces would drive hydrocarbons towards the basin margins and particularly towards the Battonya High where the Szolnok Aquifer pinching out could provide stratigraphic traps as well. However, also secondary migration in the Szolnok Aquifer would be questionable considering the above discussions. Finally, if migration could not be realized, *in situ* accumulation could be expected. Furthermore, also the Algyő Aquitard might be an effective flow barrier having small grain size, large thickness, and no cross-cutting faults. Consequently, methane occurrences in water wells may have biogenic source with greater chance.

6.4 Methodological development

Beside the results delineated in the above chapters, a further outcome of this Ph.D. research work is the development of a hydrogeologically based methodology for determining fluid migration pathways and trap forming potentials, which method was worked out, modulated, and also controlled through the working process. Namely, methodology was worked out in the DSA where several data were available, then controlled in the BBSA where the successful application confirmed the justification of the method. Since in the Békés Basin where hardly any hydraulic, temperature, and hydrochemical data were available, and conclusions were drawn mostly based on geological analogies, opportunity for the inverse application of the method was also given.

6.4.1 Methodology #I – for areas providing sufficient data

Figure 6.9.A represents the workflow chart of the methodology (#I) which can be usable in research areas where enough data, and particularly hydraulic data are available. This method is based on the processing of (I) geological data derived from boreholes and seismic interpretations, as well as of (II) hydraulic data of water and hydrocarbon wells complemented by temperature and hydrochemical data as well.

I) On one hand, hydrostratigraphic model should built up ideally on a facies- and permeability-based geological model. However, in the lack of these data the present study's hydrostratigraphy was based on formation classification, which otherwise refers to the facieses and permeability conditions as well (TÓTH and ALMÁSI, 2001). Spatial position and activity of faults also have to be known in order to determine the strata's heterogeneity, which finally controls the way of overpressure dissipation in the Study Areas.

II) On the other hand, during hydraulic data processing and interpretation three methods can be used to "visualize" the subsurface fluid-potential field. These are the followings in the order of building on each other: construction of i) pressure-elevation profiles determining vertical flow directions (and in special cases the lateral as well), ii) tomographic fluid potential maps determining lateral flow directions (and vertical as well between the maps), and iii) hydraulic cross-sections determining the lateral and vertical flow directions along the section. Regarding the methodological developments, improvements were carried out in case of the p(z) profiles allowing of studying the faults' and low-permeability formations' regional scale hydraulic behaviour (see also Chapter 4.3.3.1). Additionally, it

turned out particularly during the analysis of anomalies that these hydrogeological research techniques (i-iii) also effectively complement each other. For instance, in some cases the cross-sections provided more information about anomalies, because more data were available vertically, while in other cases the fluid-potential maps showed more information, since further data were available horizontally from outside of the section's trace line. Similarly, also temperature and hydrochemical data can be analyzed in this way in order to support the hydraulic results. Consequently, by using these methods the way of overpressure dissipation can be analyzed, thus the fluid-potential field as well, which shows diagnostic relationships among fluid-potential, geothermal, and hydrochemical anomalies, as well as hydrocarbon accumulations, faults, and sedimentological heterogeneities.

Finally, all of these phenomena and relationships can be demonstrated in the best way by the p(z) type-profiles, which represent differing geological settings characterized by differing and typical fluid-potential, geothermal, and hydrochemical features, as well as hydrocarbon traps. Consequently, it could serve as a starting point for further groundwater, geothermal or hydrocarbon explorations in the Great Hungarian Plain, since in view of the geological build-up of an area its hydrodynamic conditions and entrapment potential can be determined based on the correlations and diagnostic relationships represented by the p(z) type-profiles. Moreover, in case of sufficient data quantity and quality the method can be used anywhere, just first of all the p(z) type profiles being typical of the given area, as some kind of calibrator curves should be determined. Thus this methodology can be used most effectively in the initial phase of a research project, or as a status assessment serving the base for numerical modeling of past or present processes, to name but a few.

6.4.2 Methodology #II – for areas not providing sufficient (hydraulic) data

In areas being out of hydraulic data, but providing some basic geological data (e.g., seismic interpretations) the methodology #I described in Chapter 6.4.1. can be applied inversely based on geological analogies (Fig. 6.9.B). Since the p(z) type-profiles can be generated from two ways (i.e., from geological and/or from hydraulic data) (Fig. 6.9.A), only one direction should be enough to determine the boundary conditions of fluid migration, such as the hydraulic/hydrodynamic entrapment potential. In the present Ph.D. work, it was necessary partly in the Békés Basin.

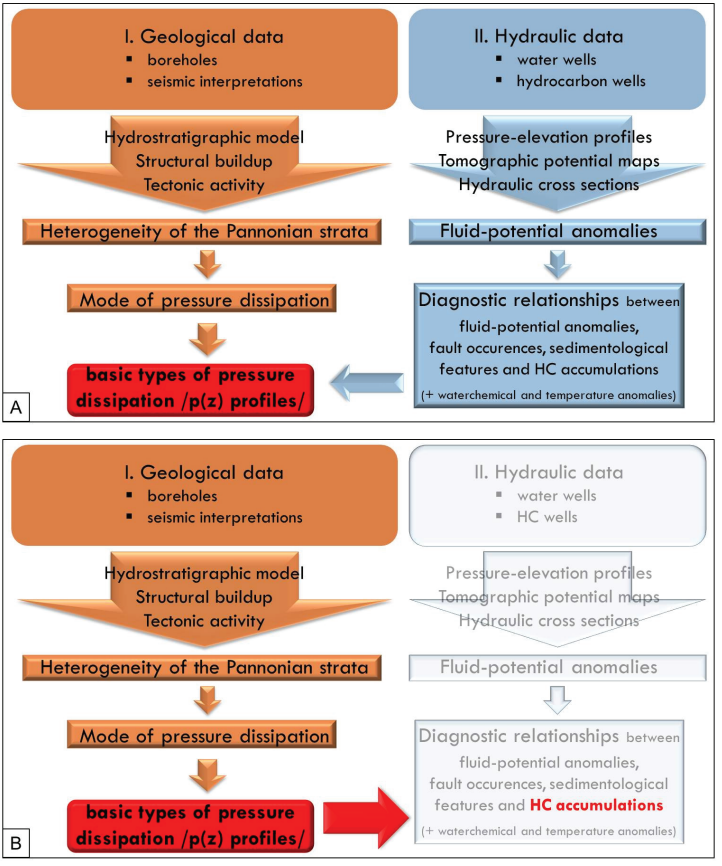

Figure 6.9 Workflow chart of methodology #I (**A**) and #II (**B**). #I can be usable in research areas where enough hydraulic data are available, otherwise #II. Abbreviation: HC – hydrocarbon.

The previously presented Table 6.1 (see also Chapter 6.3.), which summarizes the geological features of the distinguished regions, in other words also contains as a syllabus the minimally necessary information (in the headings) required to draw the conclusions about a region (in the rows). These are expounded in the followings.

1) Topography – analysis of hydraulic entrapment potential: gravitational downward flow can be expected at topographical highs.

2) Depth and morphology of the Pre-Neogene basement
    - Relatively deep (~ z < (-3000) m asl in the DSA and BBSA) → significant mechanical compaction, "problem of mechanical compaction versus overpressure" (see also Chapter 2.2.2), can be expected
    - Relatively shallow (~ z > (-3000) m asl in the DSA and BBSA) → significant overpressure in shallower depths than as usual can be expected if effective aquitards can be found in the Neogene sedimentary basin fill
3) Characteristics of the Endrőd Formation/Aquifer
    - More pelitic → more plastic, permeability is lower
    - More calcareous → more rigid, thus fissured and fractured, permeability is higher
4) Characteristics of the Szolnok Formation/Aquifer
    - Coarser grained (closer to the sediment sources) → aquifer character
    - Finer grained (far from the sediment sources) → aquitard character
    - In shallower depth (mostly mechanical compaction) → rather aquifer character
    - In greater depth (mechanical and chemical compaction) → rather aquitard character
5) Characteristics of the Algyő Formation/Aquifer
    - More homogeneous → effective aquitard
    - More heterogeneous → less effective aquitard
        - High-permeability lenses, intercalations, higher sand content → less effective aquitard
        - Few/no faults → more effective aquitard
        - Active faults (conduits) → less effective aquitard
        - Inactive faults in low-permeability environment (barriers) → more effective aquitard
        - Inactive faults with coarser grained filling in low-permeability environment (conduits) → less effective aquitard

In conclusion, being in possession of the topographic map, some seismic interpretations (usually the first data during hydrocarbon exploration), and possibly some borehole data of a research area it is possible to forecast the fluid-potential (pressure) distribution and hydraulic/hydrodynamic entrapment potential on a formation, facies, or depth interval base.

7 SYNTHESIS

The primary goal of the present Ph.D. work was to investigate the hydraulic role of faults and low-permeability formations in subsurface fluid flow systems in differing study areas in order to develop a hydrogeology-based methodology, which can be usable also in other research areas for hydraulic and/or hydrodynamic (hydrocarbon/geothermal) reservoir prognosis. Study areas were chosen in the Great Hungarian Plain (Pannonian Basin, Hungary) where regional hydraulics has already been studied by TÓTH and ALMÁSI (2001), and also the MOL Plc. represents research interest. Consequently, a regional scale Pre-Neogene basement high (Battonya High), as well as two regional scale depressions (Derecske Trough, Békés Basin) were studied.

As a result, regarding the amount and distribution of well-data, as well as the number of faults, regional scale conclusions could be drawn. Consequently, hydraulic role of certain faults could be identified only in a few cases, while the regional significance of fault zones' hydraulic function led to further issues, such as the hydraulic behaviour of low-permeability formations, the generalizable geological controlling factors of fluid-potential distribution in an overpressured sedimentary basin, and the related geothermal, hydrochemical, and accumulation phenomena. Finally, based on the exploration of the diagnostic relationships among these issues and the deduced pressure-elevation type-profiles as outcomes of the regional scale hydrogeological characterization of the Study Areas, a hydrogeology-based methodology was worked out, which can be usable in the initial research phase of groundwater/geothermal/hydrocarbon exploration, or as a field data-based preparation for hydrodynamic modeling.

The itemized statements and results (i.e. Theses #1-20) are the followings.

1. Hydraulic behaviour of the ***Great Plain Aquifer*** (in the sallowest position), as well as the ***Pre-Pannonian Aquifer*** and the ***Pre-Neogene formations*** (in the deepest position) is mostly uniform regionally in both Study Areas. On one hand, the Pre-Pannonian Aquifer and the Pre-Neogene formations are highly overpressured (excess pressure is about 30-60 MPa above the hydrostatic – even more than 200%) and characterized by only slightly superhydrostatic vertical pressure gradients ($\gamma \approx$ 11-14 MPa/km). On the other hand, the Great Plain Aquifer is unconfined and containing gravitational flow systems, which show approximately hydrostatic conditions ($\gamma \approx 9.81 \pm 0.5$ MPa/km)

compared to the overpressured system. These phenomena refers to the ***relatively high hydraulic conductivity*** (or permeability) of these units.

2. However, the intervening ***Endrőd Aquitard***, ***Szolnok Aquifer***, and ***Algyő Aquitard*** represent ***spatially variable heterogeneities***. Consequently, these three units ***control the "mode" or "way" of overpressure dissipation*** between the two boundaries of the subsurface fluid flow domain, i.e. the lowest overpressured Pre-Pannonian strata and the uppermost approximately hydrostatic Great Plain Aquifer. Namely, when the aquifer character prevails, the vertical pressure gradient is relatively low, but it increases (even above 20 MPa/km) with the decreasing hydraulic conductivity.
3. Aside from some local regions, hydraulic behaviour of the ***Algyő Aquitard proved to be the most decisive*** among the hydrostratigraphic units in the overpressure dissipation. Flow impeding effect of this aquitard always manifests in a "break" or "step-like" (upward) pressure drop in the pressure-elevation profiles pending on its relative hydraulic conductivity, i.e. heterogeneity (faults, intercalated sand lenses, etc.), which shows significant spatial variability.
4. ***Appearance of the overpressured system***, i.e. that of the spatially uniform upward flow (everywhere in the Study Areas) can be observed generally down ***from the top of the Algyő Aquitard*** pending its depth within the z = (-1200)-(2000) m asl elevation interval. However, the Battonya High Area represents a regional scale exception where the overpressured system appears only down from about z = (-2000) m asl within the Pre-Neogene basement, while the total overlying succession is in approximately hydrostatic, or even subhydrostatic condition. Consequently, appearance of the overpressured system proved to be rather depth-, than formation-dependent in the Battonya High Area.
5. ***Fluid-potential minimum zones*** were identified along the Battonya High in the z = (-200)-(-400) m asl elevation interval, and in the NW part of the Derecske Study Area in the z = (-400)-(-1000) m asl elevation interval where the overpressured upward flows meet with the gravitational recharge areas' downward flows. These regional flow converging zones serve as ***hydraulic traps*** for heat and dissolved salts, while hydrocarbon accumulations are known from below, but near by the bottom of these zones building up the upper boundary of upward fluid migration. The zones' penetration depth and thickness is greater in the Derecske Study Area due to the higher topographic gradient (maximum differences in topographical elevations of the Study Areas are 50 m and 20 m within the DSA and BBSA, respectively). On the other hand, gravitational

discharge areas where there is no upper hydraulic boundary of upward fluid migration could be targets for near-surface geochemical hydrocarbon exploration. For instance, in the Békés Basin occasionally high (dissolved) methane content of water wells is a well-known phenomenon, and though the shallow (i.e., above the Algyő Aquitard) biogenic origin of gases cannot be excluded, it may refer to upward flow conditions in the total flow domain.

6. Aside from the local anomalies, vertical ***temperature*** gradient is roughly uniform in both Study Areas representing the Pannonian Basin's average of 50°C/km, which already indicates positive anomaly compared to the world average of 30°C/km, or higher geothermal gradients as well (up to 149 °C/km). Regarding the anomalies, heat accumulation can be observed in the fluid-potential minimum zones (hydraulic traps) of converging gravitational downward and overpressured upward flows. In addition, the Battonya High Area represents a positive anomaly /$\Delta T \approx +(20\text{-}40)$°C/ compared to its surroundings in the total studied elevation interval /z = 0-(-4000) m asl/. It could be explained by that the asthenosphere reaches its relatively shallower depth (<60 km) within the Pannonian Basin at the Battonya High Area where consequently the 'heat flow maximum of the Southern Great Hungarian Plain' (100-110 mW/m^2) can be found as well (HORVÁTH et al., 2004).

7. In the Derecske Study Area the ***total dissolved solid content*** (TDS) increasing with depth shows jump-like (from the order of magnitude of 1000 mg/L to 10,000 mg/L) increase below the Algyő Aquitard, while salt accumulation can be observed in the fluid-potential minimum zone (hydraulic trap) of converging gravitational downward and overpressured upward flows. On the other hand, in the Békés-Battonya Study Area data show at least one order of magnitude lower TDS values than in the Derecske Study Area in the total studied elevation interval. Additionally, in the z = (-200)-(-600) m asl elevation interval a TDS maximum (1000-1500 mg/L) can be observed due to the high concentrations of HCO_3^- (≈ 1000 mg/L). Accordingly, the upwelling NaCl-type (ERDÉLYI, 1976; MÁDL-SZŐNYI and TÓTH, 2009) but less saline groundwater may enrich in HCO_3^- by mixing with the gravitational system's $NaHCO_3$-type or (Ca,Mg)-$(HCO_3)_2$-type water (MÁDL-SZŐNYI and TÓTH, 2009). However, origin of the overpressured system's groundwater of anomalously low TDS content could not be explained based on the results of this dissertation. Thus this question requires further studies, while also the data's unreliability has to be kept in mind.

8. In both Study Areas, several ***anomalies*** could be identified in the fluid-potential, geothermal, and hydrochemical field as well, usually around faults and hydrocarbon occurrences. Their frequent coincidence with each other supports the ***diagnostic relationship***s among them. In the cause and effect, as well as usually back and forth acting relation system of their development and that of the hydrocarbon occurrences, the way of overpressure dissipation plays the primary determining role, which is defined by the geological build-up, and particularly by its discontinuities and heterogeneities.
9. Based on the regional hydrogeological characterization and the diagnostic relationships seven ***regions*** (#1-7) were distinguished within the Study Areas that can be characterized by seven ***basic types of pressure-elevation profiles*** traced back to the differences in the geological build-up and consequently in the way of overpressure dissipation.
10. In the ***Derecske – North region*** (#1) the significant overpressure (~20-25 MPa excess pressure above the hydrostatic value) gradually, i.e. diffusively dissipates through the densely faulted and thus relatively high-permeability Algyő Aquitard allowing of upward hydrocarbon migration even into the Great Plain Aquifer. On the other hand, in the ***Derecske – South region*** (#2) the more significant overpressure (~20-30 MPa excess pressure above the hydrostatic value) can dissipate only concentrated along a few faults, while the low-permeability matrix of the Algyő Aquitard effectively maintenances the overpressure and retains hydrocarbons below. In shallower depth also the possibility for hydraulic entrapment is given in both regions.
11. Around the ***Furta, Biharnagybajom, and Szeghalom Highs*** (#3) overpressure (~30-40 MPa excess pressure above the hydrostatic value) emerges into shallow depth with the basement highs, then Algyő Aquitard impedes fluid flows effectively in spite of its small thickness (~200-600 m in contrast with the average 800-1000 m), probably due to its low-permeability matrix cross-cut only by some inactive faults.
12. Around the ***Szarvas and Békés Highs*** (#4) overpressure (~40-50 MPa excess pressure above the hydrostatic value) decrease to hydrostatic conditions through the low-permeability Szolnok Aquifer with practically impossible, higher than lithostatic vertical pressure gradients. These gradients and scatter of the data refer to that fluid flow could be materialized most probably in (natural) hydraulic fractures in the Szolnok Aquifer, which impedes upward hydrocarbon migration as well.
13. In the ***Fábiánsebestyén-Nagyszénás-Orosháza Area*** (#5) where the most significant overpressures are known in the Pre-Neogene basement and Pre-Pannonian Aquifer of

the Study Areas (>60-70 MPa), the largest (upward) pressure drop at the bottom of the low-permeability Algyő Aquitard can be observed as well. Hydrocarbon occurrences are not known and cannot be expected in shallower strata than the Szolnok Aquifer.

14. In the ***Battonya High Area*** (#6) overpressure appears form about z = (-2000) m asl, while in shallower depth the total Pre-Neogene – Neogene succession is in approximately hydrostatic conditions containing hydrocarbons as well due to the lack of regionally effective aquitards among the Pannonian strata. Additionally, a closed potential depression can be observed in the central part of the High in the z = (-600)-(-1800) m asl elevation interval. The results of this dissertation cannot explain the formation of this regional scale negative potential anomaly, however some considerations were taken, particularly excluding some options (e.g., effects of fluid production in the area). Also the hydrochemical analysis showed a regional negative anomaly that cannot be explained by the results of this dissertation, while the positive geothermal anomaly could be traced back to the shallow depth of the asthenosphere (<60 km).

15. In the ***Békés Basin*** (#7) hydraulic data were available only from the Great Plain Aquifer (down to z = (-2100) m asl), which represent slightly superhydrostatic conditions in the bottom zone of the Aquifer. Considering the geological analogies with the other regions, the thickness of the Neogene succession (maximum ~7000 m), as well as the low-permeability character of at least the aquitards, the Pre-Neogene basement should be highly overpressured. Hydrodynamic conditions of the Szolnok Aquifer should be similar to that of the Szarvas and Békés Highs. Lateral flows might be directed from the basin centers towards the margins, and particularly towards the Battonya High representing the lowest fluid-potential conditions in the Study Areas. However, the potential amount of movable fluids is questionable, since increasing overpressure could stop mechanical compaction (i.e. increase of effective stress) and fluid release from storage, thus fluid migration. Hydrocarbon occurrences are not known so far. However, if migration could materialize from the Endrőd Aquitard (or deeper units) towards the Szolnok Aquifer, impelling forces would drive hydrocarbons towards the basin margins and particularly towards the Battonya High where pinching out of the Szolnok Aquifer could provide stratigraphic traps as well. If migration could not be realized, *in situ* accumulation could be expected. Finally, also the Algyő Aquitard might be an effective flow barrier having small grain size, large thickness (800-2600 m), and only a few cross-cutting faults.

16. During the working process a hydrogeologically based ***methodology*** was worked out, modulated, and also controlled for ***determining the regional fluid migration pathways and hydraulic/hydrodynamic trap forming potentials***. Namely, a method was worked out in the Derecske Study Area where several data were available, then controlled in the Békés-Battonya Study Area where the successful application confirmed the justification of the method. This method is based on the processing of (I) geological data derived from boreholes and seismic interpretations, as well as of (II) hydraulic data of water and hydrocarbon wells also complemented by temperature and hydrochemical data. Based on the diagnostic relationships, both ways (i.e. (I) and (II)) lead to the generalization of ***pressure-elevation type profiles***, which represent differing geological settings characterized by differing and typical fluid-potential, geothermal, and hydrochemical features, as well as hydrocarbon entrapment potentials.
17. As a basic methodological development, improvement of the ***p(z) profile*** interpretation was carried out, which allowed of the examination of faults' and low-permeability formations' ***regional scale hydraulic*** behaviour.
18. As another methodological object, ***the average groundwater density values being typical of the Study Areas*** were also determined (993 kg/m^3 in the Derecske Study Area, and 985 kg/m^3 in the Békés-Battonya Study Area), which however ***do not cause significant deviations*** (maximum (+39) m or 2%, and (+106) m or 4% deviation in hydraulic heads in the Derecske and Békés-Battonya Study Areas, respectively) from the results of calculations where constant density value is required applying the 1000 kg/m^3 density value. In other words, hydraulic conditions interpreted based on the original and calculated pressure and hydraulic head data were concordant.
19. A further segment of the method development was the ***correction of hydraulic calculations in case of pressure data measured in gas columns***. As a result, the possible maximum error in calculated hydraulic heads in the Study Areas can vary between +113 and +254 m that could cause apparent fluid-potential anomalies in shallower depth than about 2000 m. However, even if ***gas-induced potential anomalies*** can lead to false deductions about the faults and low-permeability strata's hydraulic behaviour, these could be the ***diagnostic indications of hydrocarbon, and particularly gas accumulations*** as well. In addition, the presence of hydrocarbon accumulations could also refer to the conduit behaviour of the ambient faults at least in their past.
20. In areas being out of hydraulic data, but providing some basic geological data the ***method*** (described in thesis #15) ***can be applied inversely based on geological***

analogies. Since the p(z) type-profiles can be generated from two ways (i.e., from geological and/or from hydraulic data), only one direction should be enough to determine the boundary conditions of fluid migration, such as the hydraulic/hydrodynamic entrapment potential. Namely, being in possession of the topographic map, some seismic interpretations (usually the first data during hydrocarbon exploration), and possibly some borehole data of a research area it is feasible to forecast the regional fluid-potential (pressure) distribution and the related spatial ***boundaries of hydrocarbon migration***, thus the regional hydraulic/hydrodynamic entrapment potential on a formation, facies, or depth interval base. In the present Ph.D. work, inverse application of the method was partly necessary in the Békés Basin. Consequently, this methodology applied directly or indirectly can be used most effectively in the ***initial phase of a research project***, or as a ***status assessment*** serving the ***base for numerical modeling*** of past or present processes, to name but a few.

REFERENCES

ADAMS JJ, BACHU S (2002) Equations of state for basin geofluids: algorithm review and intercomparison for brines. Geofluids 2:257-271

ALFÖLDI L, ERDÉLYI M, GÁLFI J, KORIM K, LIEBE P (1978) A geothermal flow system in the Pannonian Basin; case history of a complex hydrogeological study at Tiszakécske – *in* KONDA J (ed) Hydrogeology of great sedimentary basins; conference of Budapest: Memoires - International Association of Hydrogeologists, pp. 716-732

ALMÁSI I (2001) Petroleum Hydrogeology of the Great Hungarian Plain, Eastern Pannonian Basin, Hungary. PhD Thesis, University of Alberta, Department of Earth and Atmospheric Sciences, Edmonton, Alberta, 312 p

ALMÁSI I (2003) Evaluation of the possible mechanisms able to generate and maintain the overpressured regime in the Pannonian Basin, Eastern Hungary. Journal of Geochemical Exploration 78-79:139-142

ANDERSON S, NEWELL R (2004) Prospects for carbon capture and storage technologies. Annual Review of Environment and Resources 29:109-142

AVIS J, ROBERTS R, BEAUHEIM R (2009) Hydraulic testing to characterize low permeability sedimentary formations – proposed Deep Geologic Repository, Tiverton, Ontario. Paper presented at GeoHalifax 2009, 62nd Canadian Geotechnical Conference & 10th Joint CGS/IAH-CNC Groundwater Conference, 20-24 September 2009, pp. 1356-1361

AYDIN A (2000) Fractures, faults, and hydrocarbon entrapment, migration and flow. Marine and Petroleum Geology 17:797-814

BACHU S (2008) CO_2 storage in geological media: role, means, status and barriers to deployment. Progress in Energy and Combustion Science 34:254–273

BACK W (1966) Hydrochemical facies and ground-water flow patterns in northern part of Atlantic Coastal Plain. Hydrochemical facies and ground-water flow patterns in the northern part of the Atlantic Coastal Plain. US Geological Survey Prof. Paper 498-A, 42 p

BADA G, HORVÁTH F, DÖVÉNYI P, SZAFIÁN P, WINDHOFFER G, CLOETINGH S (2007) Present-day stress field and tectonic inversion in the Pannonian Basin. Global and Planetary Change 58:165-180

BARKER C (1972) Aquathermal pressuring – role of temperature in development of abnormal pressure zones. Am. Assoc. Pet. Geol. Bull. 56:2068-2071

BEKELE EB, ROSTRON BJ, PERSON MA (2003) Fluid pressure implications of erosional unloading, basin hydrodynamics and glaciation in the Alberta Basin, Western Canada. Journal of Geochemical Exploration 78-79:143-147

BENNION DB, THOMAS FB, BIETZ RF (1996) Low permeability gas reservoirs: Problems, opportunities and solutions for drilling, completion, stimulation and production. SPE 35577, paper presented at the Gas Technology Conference, Calgary, Alberta, Canada, 28 April – 1 May 1996, pp. 117-131

BÉRCZI I, HÁMOR G, JÁMBOR Á, SZENTGYÖRGYI K (1988) Neogene sedimentation in Hungary – *in* ROYDEN LH, HORVÁTH F (eds) The Pannonian Basin, a study in basin evolution. AAPG Memoir 45:57-67

BÉRCZI I, PHILLIPS RL (1985) Processes and depositional environments within the Neogene delta lacustrine sediments, Pannonian Basin, SE Hungary. Geophysics Transactions 31/1-3:55-74

BERKOWITZ B (2002) Characterizing flow and transport in fractured geological media: A review. Advances in Water Resources 25:861-884

BETHKE CM (1989) Modeling subsurface flow in sedimentary basins. Geologische Rundschau 78:129-154

BJØRLYKKE K (1999) Principal aspects of compaction and fluid flow in mudstones – *in* APLIN AC, FLEET AJ, MACQUAKER JHS (eds) Muds and Mudstones: Physical and Fluid Flow Properties. Geological Society, London, Special Publications, 158:73-78

BREDEHOEFT JD, NEUZIL CE, MILLY PC (1983) Regional flow in the Dakota aquifer; a study of the role of confining layers. USGS Water Supply Paper 2237, 45 p

BREDEHOEFT JD, WESLEY JB, FOUCH TD (1994) Simulation of the origin of fluid pressure, fracture generation, and the movement of fluids in the Uinta basin, Utah. AAPG Bulletin 78:1729-1747

BUDA E (1986) Kőolaj-, földgáz- vagy vízkitörések a magyar szénhidrogénfúrások mélyítése és termeltetése közben [Oil-, gas-, or water blowouts during drilling and production of Hungarian hydrocarbon well]. Kőolaj és Földgáz 19/11:339-343 (in Hungarian)

BUDA E, GÖTZ T, ID. ŐSZ Á (2004) A magyarországi kőolaj-, földgáz-, szén-dioxid-, gőz- és forróvíz-kitörések elhárításának története 1909-2000 között [Prevention history of oil-, gas-, carbon-dioxide-, steam-, and hot water blowouts in Hungary between 1909-2000]. Kőolaj és Földgáz 37/9-10:113-126 (in Hungarian)

BYERLEE J (1990) Friction, overpressure and fault normal compression. Geophysical Research Letters 17:2109-2112

CAINE JS, EVANS JP, FORSTER CB (1996) Fault zone architecture and permeability structure. Geology 24/11:1025-1028

CHEBOTAREV II (1955) Metamorphism of natural waters in the crust of weathering. Geochimica et Cosmochimica Acta 8:137-170

CLAUSER C (1992) Permeability of crystalline rocks. Eos, Transactions American Geophysical Union 73/21, 233 p

CLAYTON JL, KONCZ I, KING JD, TATÁR É (1994) Organic geochemistry of crude oils and source rocks, Békés Basin – *in* TELEKI PG, MATTICK RE, KÓKAI J (eds) Basin analysis in petroleum exploration; A case study from the Békés Basin, Hungary. Kluwer Academic Publishers, printed in the Netherlands, pp. 161 – 185

CLUFF RM, BYRNES A (2010) Relative permeability in tight gas sandstone reservoirs – The „permeability jail" model. SPWLA 51th Annual Logging Symposium, June 19-23, 2010. Available via http://www.discovery-group.com/pdfs/2010_Cluff%20&%20Byrnes%20-20Permeability%20Jail,%20SPWLA%2051st%20Ann%20Symp%20Perth.pdf. Cited 11 October 2011

CORBET TF, BETHKE CM (1992) Disequilibrium Fluid Pressures and Groundwater Flow in the Western Canada Sedimentary Basin. Journal of Geophysical Research 97/B5:7203-7217

CSONTOS L, NAGYMAROSY A, HORVÁTH F, KOVÁC M (1992) Tertiary evolution of the Intra-Carpathian area: a model. Tectonophysics 208:221-241

CZAUNER B (2008) Vetők hidraulikai viselkedésének komplex vizsgálata Berekfürdő térségében. [Complex research of faults' hydraulic behaviour in the region of Berekfürdő] MSc thesis, Budapest, ELTE Institute of Geography and Earth Sciences, Dept. of Physical and Applied Geology, 165 p (in Hungarian)

CZAUNER B, MÁDLNÉ SZŐNYI J (2008) A berekfürdői mélyszerkezet és vízföldtani vonatkozásai [The deep structure at Berekfürdő and its hydrogeological aspects]. Hidrológiai Tájékoztató pp. 32-34 (in Hungarian)

CZAUNER B, MÁDLNÉ SZŐNYI J (2009) Folyadék-potenciál anomáliákhoz kötődő szénhidrogén csapdázódás kutatása a Derecskei-árok térségében – I. RÉSZJELENTÉS. [Research of Petroleum Entrapment Connecting to Fluid-potential Anomalies in the Region of Derecske Trough – I. REPORT] Made for the MOL Hungarian Oil and Gas Company Plc. 28th October 2009, 68 p (in Hungarian)

CZAUNER B, MÁDLNÉ SZŐNYI J (2010) Folyadék-potenciál anomáliákhoz kötődő szénhidrogén csapdázódás kutatása a Derecskei-árok térségében – II. RÉSZJELENTÉS. [Research of Petroleum Entrapment Connecting to Fluid-potential Anomalies in the Region of Derecske Trough – II. REPORT] Made for the MOL Hungarian Oil and Gas Company Plc. 29th October 2010, 479 p (in Hungarian)

CZAUNER B, MÁDLNÉ SZŐNYI J (2011) Folyadék-potenciál anomáliákhoz kötődő szénhidrogén csapdázódás kutatása a Derecskei-árok térségében – ZÁRÓJELENTÉS. [Research of Petroleum Entrapment Connecting to Fluid-potential Anomalies in the Region of Derecske Trough – III., FINAL REPORT] Made for the MOL Hungarian Oil and Gas Company Plc. 20th October 2011, 290 p (in Hungarian)

CZAUNER B, MÁDL-SZŐNYI J (2011) The function of faults in hydraulic hydrocarbon entrapment: Theoretical considerations and a field study from the Trans-Tisza region, Hungary. AAPG Bulletin 95:795-811

CZAUNER B, MÁDL-SZŐNYI J, TÓTH J, POGÁCSÁS GY (2009) Hydraulic potential anomaly indicating thermal water reservoir and gas pool near Berekfürdő, Trans-Tisza Region, Hungary. Central European Geology 51/3:253-266

DAHLBERG EC (1995) Applied hydrodynamics in petroleum exploration. Springer-Verlag, New York, pp. 180-183

DANK V (1988) Petroleum geology of the Pannonian Basin, Hungary: an overview – *in* ROYDEN LH, HORVÁTH F (eds) The Pannonian Basin, a study in basin evolution. AAPG Memoir 45:319-331

DANK V (1990) Kőolajföldtan [Petroleum geology]. Tankönyvkiadó, Budapest, pp. 113, 174, 378-379, 438-443 (in Hungarian)

DARCY H (1856) Les fontaines publiques de la ville de Dijon. Victor Dalmont, Paris

DEMING D (1993) Regional permeability estimates from investigations of coupled heat and groundwater flow, North Slope of Alaska. Journal of Geophysical Research 98:16,271-16,286

DERYAGIN BV, KRYLOV NA (1944) Anomalies observed in the flow of liquids through hard fine-pored filters. Proceedings Conference on Viscosity of Liquids and Colloid Solutions 2. USSR Academy of Sciences Press, Moscow, pp. 52-53

DEWHURST DN, YANG Y, APLIN AC (1999) Permeability and fluid flow in natural mudstones – *in* APLIN AC, FLEET AJ, MACQUAKER JHS (eds) Muds and Mudstones: Physical and Fluid Flow Properties. Geological Society, London, Special Publications, 158:23-43

DISTINGUIN M, LAVANCHY J-M (2007) Determination of hydraulic properties of the Callovo-Oxfordian argillite at the bure site: Synthesis of the results obtained in deep boreholes using several in situ investigation techniques. Physics and Chemistry of the Earth 32:379-392

DÖVÉNYI P, HORVÁTH F (1988) A review of temperature thermal conductivity, and heat flow data for the Pannonian Basin – *in* ROYDEN LH, HORVÁTH F (eds) The Pannonian Basin, a study in basin evolution. AAPG Memoir 45:195-233

DÖVÉNYI P, HORVÁTH F, DRAHOS D (2002) Hungary – *in* HURTER S, HAENEL R (eds) Atlas of Geothermal Resources in Europe. Publication No. 17811 of the European Commission, Office for Official Publications of the European Communities. L-2985, Luxembourg, pp. 36–38

DÖVÉNYI P, HORVÁTH F, LIEBE P, GÁLFI J, ERKI I (1983) Geothermal conditions of Hungary. Geophysical Transactions 29:84

DRISCOLL FG (2003) Groundwater and wells. Johnson Screens, St. Paul, Minnesota, 100 p

ERDÉLYI M (1976) Outlines of the hydrodynamics and hydrochemistry of the Pannonian Basin. Acta Geologica Academiae Scientiarum Hungaricae 20:287-309

FORCHHEIMER P (1901) Wasserbewegung durch Boden. Z. Ver. Deutsch. Ing. 45:1782–1788

FREEZE RA, CHERRY JA (1979) Groundwater. Prentice Hall, Engwood Cliffs, New Jersey, pp. 72-74, 140

FRISCH HL, HAMMERSLEY JM (1963) Percolation processes and related topics. J Soc Indust Appl Math 11: 894-918

GAARENSTROOM L, TROMP RAJ, JONG MC, BRANDENBURG AM (1993) Overpressures in the Central North Sea: implications for trap integrity and drilling safety – *in* Parker JR (ed) Petroleum Geology of Northwest Europe: Proceedings of the 4th Conference, etroleum Geology '86 Ltd. Published by The Geological Society, London, pp. 1305-1313

GAJDOS I, PAP S, SOMFAI A, VÖLGYI L (1983) Az alföldi pannóniai (s.l.) képződmények litosztratigráfiai egységei [Lithostratigraphic units of the Pannonian (s.l.) formations in the Hungarian Plain]. MÁFI, Budapest, 70 p (in Hungarian)

GÁL M (1981) Az Alföld Gyógyfürdői és Fürdői [Thermal Bathes and Bathes in the Great Hungarian Plain). Budapest, 368 p (in Hungarian)

GARVEN G (1995) Continental-scale groundwater flow and geologic processes. Annu. Rev. Earth Planet. Sci. 23:89-117

GE S, GARVEN G (1994) A theoretical model for thrust-induced deep groundwater expulsion with application to the Canadian Rocky Mountains. Journal of Geophysical Research 99/B7: 13851-13868

GE S, GARVEN, G (1992) Hydromechanical modeling of tectonically driven groundwater flow with application to the Arkoma Foreland Basin. Journal of Geophysical Research 97/B6: 9119-9144

GEIGER J, HAJDÚNÉ MOLNÁR K, JÁMBOR Á, KONCZ I, POGÁCSÁS G, RÉVÉSZ I, SOMFAI A, SZALAY Á, SZENTGYÖRGYI K (1991) A Pannon medence fejlődéstörténeti rekonstrukciója és a fejlődéstörténeti modellek alkalmazása a szénhidrogén prognózisban [The evolution of the Pannonian Basin and the application of evolutionary models for hydrocarbon prognosis]. Internal report, Hungarian Institute of Petroleum Exploration and Development, Szeged, Hungary, 1055 p (in Hungarian)

GRASBY SE, HUTCHEON I (2001) Controls on the distribution of thermal springs in the southern Canadian Cordillera. Canadian Journal Earth Sciences 38:427-440

GRENERCZY GY, SELLA GF, STEIN S, KENYERES A (2005) Tectonic implications of the GPS velocity field in the northern Adriatic region. Geophysical Research Letters 32, L16311, doi:10.1029/2005GL022947.

GROW JA, POGÁCSÁS GY, BÉRCZINÉ MAKK A, VÁRNAI P, HAJDU D, VARGA E, PÉRÓ CS (1989) A Békési medence tektonikai és szerkezeti viszonyai [Tectonic and structural features of the Békés Basin]. Magyar Geofizika XXX/2-3:63-97 (in Hungarian)

GUDMUNDSSON A (2001) Fluid overpressure and flow in fault zones: field measurements and models. Tectonophysics 336/1-4:183-197

HAAS J, BUDAI T, CSONTOS L, FODOR L, KONRÁD GY (eds) (2010) Magyarország pre-kainozoos földtani térképe 1:500000 [Pre-Cenozoic geological map of Hungary]. Published by the Geological Institute of Hungary, Budapest

HEM JD (1989) Study and interpretation of the chemical characteristics of natural water. U.S. Geological Survey Water-Supply Paper 2254. United States Government Printing Office, Washington, pp. 69-73

HITCHON B (2000) "Rust" contamination of formation waters from producing wells. Applied Geochemistry 15:1527-1533

HITCHON B, BRULOTTE M (1994) Culling criteria for "standard" formation water analyses. Applied Geochemistry 9:637-645

HORVÁTH F (1993) Towards a mechanical model for the formation of the Pannonian basin. Tectonophysics 226:333-357

HORVÁTH F (2007) A Pannon-medence geodinamikája [Geodynamics of the Pannonian Basin]. Budapest, 238 p

HORVÁTH F, BADA G, WINDHOFFER G, CSONTOS L, DÖVÉNYI P, FODOR L, GRENERCZY GY, SÍKHEGYI F, SZAFIÁN P, SZÉKELY B, TIMÁR G, TÓTH L, TÓTH T (2004) A Pannon-medence jelenkori geodinamikájának atlasza: Euro-konform térképsorozat és magyarázó [Atlas of the present geodynamics of the Pannonian Basin: Euro-conform

map series and commentary]. Available via http://geophysics.elte.hu/atlas/geodin_atlas.htm. Cited 23 October 2011

HORVÁTH F, BODRI L, OTTLIK P (1979) Geothermics of Hungary and the tectonophysics of the Pannonian Basin "Red Spot" – *in* CERMAK V, RYBACH L (eds) Terrestrial heat flow in Europe. Berlin, Federal Republic of Germany, Springer-Verlag, pp. 206-217

HORVÁTH F, CLOETINGH S (1996) Stress-induced late-stage subsidence anomalies in the Pannonian basin. Tectonophysics 266:287-300

HORVÁTH F, DÖVÉNYI P, SZALAY Á, ROYDEN LH (1988) Subsidence, thermal, and maturation history of the Great Hungarian Plain – *in* ROYDEN LH, HORVÁTH F (eds) The Pannonian Basin, a study in basin evolution. AAPG Memoir 45:355-372

HUBBERT MK (1940) The theory of ground-water motion. The Journal of Geology 48:785-944

HUBBERT MK (1953) Entrapment of petroleum under hydrodynamic conditions. AAPG Bulletin 37/8:1954-2026

INGEBRITSEN S, SANFORD W, NEUZIL C (2008) Groundwater in Geologic Processes. 2nd ed., Cambridge University Press, Cambridge UK, pp. 2-6, 15-18,

JÁRAI A (1982) Nagy szén-dioxid-tartalmú gázzal történő művelés a Pusztaföldvár-mező Földvár alsó I. telepében [Working with high carbon-dioxide content gas in the Földvár lower I pool of the Pusztaföldvár field]. Kőolaj és Földgáz 15/12:367-371 (in Hungarian)

JOHNSON RH (1992) Opus Handbook – Formation Waters of Western Canada. Opus Petroleum Engineering Ltd., Calgary, Canada

JONES G, FISHER QJ, KNIPE RJ (eds) (1998) Faulting, fault sealing and fluid flow in hydrocarbon reservoirs. London, Geological Society, Special Publication, 319 p

JU M, YANG J (2010) Preliminary numerical simulation of tectonic deformation-driven fluid flow: Implications for ore genesis in the Dachang district, South China. Journal of Geochemical Exploration 106/1-3:133-136

JUHÁSZ GY (1992) A pannóniai (s.l.) formációk térképezése az Alföldön: elterjedés, fácies és üledékes környezet [Mapping of the Pannonian (s.l.) formations in the Hungarian Plain: spread, facies and depositional environment]. Földtani Közlöny 122(2-4):133-165 (in Hungarian)

JUHÁSZ GY, POGÁCSÁS GY, MAGYAR I, VAKARCS G (2007) Tectonic versus climatic control on the evolution of fluvio-deltaic systems in a lake basin, Eastern Pannonian Basin. Sedimentary Geology 202:72-95

K JUHÁSZ GY, MOLENAAR CM, BÉRCZI I, RÉVÉSZ I, KOVÁCS A, SZANYI B (1989) A Békési-medence pannóniai s.l. üledékösszletének rétegtani viszonyai [Pannonian (s.l.) tratigraphy of the Békés Basin]. Magyar Geofizika XXX/4-5:129-145 (in Hungarian)

KALAYDJIAN FJ-M, BOURBIAUX BJ, LOMBARD JM (1996) Predicting gas-condensate reservoir performance: How flow parameters are altered when approaching production wells.

SPE 36715. Proceedings of the Annual Fall Technical Conference of the SPE-AIME, October 6-9, Denver, Colorado, USA

KALDI J (2005) Geosequestration. AIG (Australian Institute of Geoscientists) NEWS, 80:1–6

KASAP E, HUANG K, SHWE T, GEORGI D (1996) Robust and Simple Graphical Solution for Wireline Formation Tests: Combined Drawdown and Buildup Analyses. SPE 36525, paper presented at the 1996 SPE Annual Technical Conference and Exhibition, Denver, Colorado, USA, 6-9 October 1996

KÉZDI Á (1969) Talajmechanika I (Soil mechanics #I). Tankönyvkiadó, Budapest (in Hungarian)

KING FH (1899) Principles and conditions of the movement of groundwater. US Geological Survey Annual Report 19 (Part II), pp. 59-294

KORIM K (1994) The hydrogeothermal systems in Hungary. International Association of Hydrogeologists, International contributions to hydrogeology, v. 15: Hamburg, Verlag Heinz Heise, pp. 43-55

LAUBMEYER G (1933) A new geophysical prospecting method, especially for deposits of hydrocarbons. Petroleum 29:1-4

LEE J, MICHAELS J (2000) Enhanced wireline formation tests in low-permeability formations: quality control through formation rate analysis. SPE 60293, paper presented at the 2000 SPE Rocky Mountain Regional/Low Permeability Reservoirs Symposium and Exhibition, Denver, Colorado, USA, 12-15 March 2000, pp. 1-7

LEMBERKOVICS V, BÁRÁNY Á, GAJDOS I, VINCZE M (2005) A szekvencia-sztratigráfiai események és a tektonika kapcsolata a Derecskei-árok pannóniai rétegsorában [Connection between the sequence-stratigraphic events and tectonics in the Pannonian sediments of the Derecske Trough]. Földtani Kutatás XLII/1:16-24 (in Hungarian)

LENKEY L (1999) Geothermics of the Pannonian Basin and its bearing on the tectonics of basin evolution. Ph.D. Thesis, Vrije Universiteit, Amsterdam, 215 p

LONERGAN L, WILKINSON JJ, MCCAFFREY KJW (1999) Fractures, fluid flow and mineralization: an introduction – *in* MCCAFFREY KJW, LONERGAN L, WILKINSON JJ (eds) Fractures, fluid flow and mineralization, Geological Society, London, Special Publication 155:1-6

LUSCZYNSKI NJ (1961) Head and flow of ground water of variable density. Journal of Geophysical Research 66/12:4247-4256

MTÓTH T, KEDVES M, SCHUBERT F (2003) Az Alföld metamorf aljzatának exhumációja a szeghalmi-hát környékén: palinológiai bizonyítékok [Exhumation of the metamorphic basement of the Pannonian Basin (Szeghalom Dome, SE Hungary) palynological constraints]. Földtani Közlöny 133/4:547-562 (in Hungarian)

MÁDL-SZŐNYI J, TÓTH J (2009) A hydrogeological type section for the Duna-Tisza Interfluve, Hungary. Hydrogeology Journal 17(4):961-980

MAGYAR I, JUHÁSZ GY, SZUROMINÉ KORECZ A, SÜTŐNÉ SZENTAI M (2001) A pannóniai Tótkomlósi Mészmárga Tagozat kifejlődése és kora a Battonya-pusztaföldvári-hátság környezetében [The Tótkomlós Calcareous Marl Member of the Lake Pannon

sedimentary sequence in the Battonya-Pusztaföldvár region, SE Hungary]. Földtani Közlöny 133(4):521-540 (in Hungarian)

MARTON L (2009) Alkalmazott hidrogeológia (Applied hydrogeology). ELTE Eötvös Kiadó, Budapest, pp. 411-416 (in Hungarian)

MATTHÄI SK, ROBERTS SG (1996) The influence of fault permeability on single-phase fluid flow near fault-sand intersections: results from steady-state high resolution models of pressure-driven fluid flow. AAPG Bulletion 80/11:1763-1779

MATTICK RE, PHILLIPS RL, RUMPLER J (1988) Seismic stratigraphy and depositional framework of sedimentary rocks in the Pannonian Basin in southeastern Hungary – *in* ROYDEN LH, HORVÁTH F (eds) The Pannonian Basin, a study in basin evolution. AAPG Memoir 45:117-145

MAYO AL, KOONTZ W (2000) Fracture flow and groundwater compartmentalization in the Rollins Sandstone, Lower Mesaverde Group, Colorado, USA. Hydrogeology Journal 8/4: 430-446

METZ B, DAVIDSON O, DE CONINCK H, LOOS M, MEYER L (eds) (2005) Intergovernmental Panel on Climate Change (IPCC) Special Report on Carbon Dioxide Capture and Storage. Cambridge University Press, Cambridge

MITCHELL JK (1976) Fundamentals of Soil Behavior. John Wiley, New York, 422 p

MITCHELL JK, YOUNGER JS (1967) Abnormalities in hydraulic flow through fine-grained soils, ASTM Spec. Tech. Publ. 417:106-141

MOL – Hungarian Oil and Gas Company Plc. (2009*) Depth map of the Pre-Neogene basement in the Derecske Trough and its surroundings. *Delivered in digital format in 2009

MOL – Hungarian Oil and Gas Company Plc. (2009*) Depth map of the Pannonian basement in the Derecske Trough and its surroundings. *Delivered in digital format in 2009

MOL – Hungarian Oil and Gas Company Plc. (2009*) Depth map of the bottom of the Algyő Formation in the Derecske Trough and its surroundings. *Delivered in digital format in 2009

MOL – Hungarian Oil and Gas Company Plc. (2009*) Depth map of the top of the Algyő Formation in the Derecske Trough and its surroundings. *Delivered in digital format in 2009

MOL – Hungarian Oil and Gas Company Plc. (2011*) Depth map of the Pre-Neogene basement in the Békés Basin and Battonya High. *Delivered in digital format in 2011

MOL – Hungarian Oil and Gas Company Plc. (2011*) Depth map of the Pannonian basement in the Békés Basin and Battonya High. *Delivered in digital format in 2011

MOL – Hungarian Oil and Gas Company Plc. (2011*) Depth map of the bottom of the Algyő Formation in the Békés Basin and Battonya High. *Delivered in digital format in 2011

MOL – Hungarian Oil and Gas Company Plc. (2011*) Depth map of the top of the Algyő Formation in the Békés Basin and Battonya High. *Delivered in digital format in 2011

MORETTI I, LABAUME P, SHEPPARD SMF, BOULÈGUE J (2000) Compartmentalisation of fluid migration pathways in the Sub-Andean Zone, Bolivia. Tectonophysics 348:5-24

NEUZIL CE (1986) Groundwater Flow in Low-Permeability Environments. Water Resources Research 22/8:1163-1195

NEUZIL CE (1994) How permeable are clays and shales? Water Resources Research 30/2:145-150

NEUZIL CE, POLLOCK DW (1983) Erosional unloading and fluid pressures in hydraulically „tight" rocks. Journal of Geology 91:179-193

O'BRIEN GS, BEAN CJ, MCDERMOTT F (2003) A numerical study of passive transport through fault zones. Earth and Planetary Science Letters 214:633-643

OLIVER J (1986) Fluids expelled tectonically from orogenic belts: Their role in hydrocarbon migration and other geologic phenomena. Geology 14:99-102

OLSEN HW (1965) Deviations from Darcy's law in saturated clays. Soil Sci. Soc. Am. Proc. 29/2:135-140

OSIF TL (1988) The Effect of Salt, Gas, Temperature, and Pressure on the Compressibility of Water. SPE Reservoir Engineering 3:175-181

OTTLIK P, GALFI J, HORVÁTH F, KORIM K, STEGENA L (1981) The low enthalpy geothermal resource of the Pannonian Basin, Hungary – *in* RYBACH L, MUFFLER LJP (eds) Geothermal systems; principles and case histories. Chichester, United Kingdom, John Wiley & Sons, p. 221-245

PAP S (1993) Fábiánsebestyén – Nagyszénás – Orosháza környékének mélyföldtana [Deep geology of Fábiánsebestyén – Nagyszénás – Orosháza area]. Földtani Közlöny 123/1:69-98 (in Hungarian)

PARKS KP, TÓTH J (1995) Field evidence for erosion-induced underpressuring in Upper Cretaceous and Tertiary strata, west central Alberta, Canada. Bulletin of Canadian Petroleum Geology 43/3:281-292

PHILP RP, CRISP PT (1982) Surface geochemical methods used for oil and gas prospecting – a review. Journal of Geochemical Exploration 17:1-34

POGÁCSÁS G, MATTICK RE, TARI G, VÁRNAI P (1994) Structural control on hydrocarbon accumulation in the Pannonian Basin, Hungary – *in* TELEKI PG, MATTICK RE, KÓKAI J (eds) Basin analysis in petroleum exploration; A case study from the Békés Basin, Hungary. Kluwer Academic Publishers, printed in the Netherlands, pp. 221-235

POGÁCSÁS GY (1990) A Pannon medence szeizmikus rétegtani, fácies és tektonikai viszonyai a szénhidrogénkutató geofizikai mérések tükrében [Seismic stratigraphic, facies and tectonic characteristics of the Pannonian Basin based on hydrocarbon explorational geophysical measurements]. Candidate dissertation, Budapest, 147 p

POGÁCSÁS GY, LAKATOS L, ÚJSZÁSZI K, VAKARCS G, VÁRKONYI L, VÁRNAI P, RÉVÉSZ I (1988) Seismic facies, electro facies and Neogene sequence chronology of the Pannonian Basin. Acta Geologica Hungarica 31/3-4:175-207

POGÁCSÁS GY, VAKARCS G, BARVITZ A, LAKATOS L (1989) Postrift strike-slip faults in the Pannonian Basin and their role in the hydrocarbon accumulation. 34th International

Geophysical Symposium, Budapest, Abstracts and papers of the technical program II:601-611

RADÓ S (1974a) Az Észak-Alföld atlasza: Magyarország tervezési-gazdasági körzetei [Atlas of the northern part of the Great Hungarian Plain: Planning and economic regions of Hungary]. Budapest, Ministry of Agriculture and Food, National Land and Cartographic Institute (in Hungarian)

RADÓ S (1974b) A Dél-Alföld atlasza: Magyarország tervezési-gazdasági körzetei [Atlas of the southern part of the Great Hungarian Plain: Planning and economic regions of Hungary]. Budapest, Ministry of Agriculture and Food, National Land and Cartographic Institute (in Hungarian)

RADÓ S (1974c) A központi körzet atlasza: Magyarország tervezési-gazdasági körzetei [Atlas of the central district: Planning and economic regions of Hungary]. Budapest, Ministry of Agriculture and Food, National Land and Cartographic Institute (in Hungarian)

RÉTHÁTI L (1974) Talajvíz a mélyépítésben (Groundwater in civil engineering). Akadémiai Kiadó, Budapest, 497 p (in Hungarian)

RÉVÉSZ I, BÉRCZI I, PHILLIPS RL (1989) A Békési medence alsópannóniai üledékképződése [Lower Pannonian sedimentation in the Békés Basin]. Magyar Geofizika XXX/2-3:98-113 (in Hungarian)

REYNOLDS O (1883) An experimental investigation of the circumstances which determine whether the motion of water shall be direct or sinuous and of the law of resistance in parallel channels. Proceedings of the Royal Society of London 35:84-99

ROBERTS RM, BEAUHEIM RL, DOMSKI PS (1999) Hydraulic Testing of Salado Formation Evaporites at the Waste Isolation Pilot Plant Site: Final Report. SAND98-2537. Albuquerque, NM: Sandia National Laboratories

RÓNAI A (1985) Az Alföld negyedidőszaki földtana. Geologica Hungarica, Series Geologica 21, 446 p

RUMPLER J, HORVÁTH F (1988) Some representative seismic reflection lines from the Pannonian Basin and their structural interpretation – *in* ROYDEN LH, HORVÁTH F (eds) The Pannonian Basin, a study in basin evolution. AAPG Memoir 45:153-169

SAMAHA A, HUANG K, KASAP E (1996) Near Wellbore Permeability and Damage Measurements: Experiments and Numerical Simulations for Interpretation of WFT Data. SPE 35150, paper presented at the 1996 SPE International Symposium On Formation Damage Control, Lafayette, February 1996

SCHUMACHER D (2000) Surface geochemical exploration for oil and gas: New life for an old technology. The Leading Edge 3:258-261

SIMON SZ, MÁDL-SZŐNYI J, MÜLLER I, POGÁCSÁS GY (2011) Conceptual model for surface salinization in an overpressured and a superimposed gravity flow field, Lake Kelemenszék area, Hungary. Hydrogeology Journal 19/3:701-717

SOMFAI A (1994) Hungary – *in* KULKE H (ed) Regional petroleum geology of the world, Part I: Europe and Asia. Berlin, Gebrüder Borntraeger, pp. 277-285

SORKHABI R, TSUJI Y (2005) The place of faults in petroleum traps – *in* SORKHABI R, TSUJI Y (eds) Faults, fluid flow, and petroleum traps. AAPG Memoir, no. 85, pp. 1-31

SORKHABI R, TSUJI Y (eds) (2005) Faults, fluid flow, and petroleum traps. AAPG Memoir, 343 p

STEGENA L (1958) A Nagyalföld geotermikus viszonyai [Geothermal conditions of the Great Hungarian Plain]. Geofizikai Közlöny VII:3-4 (in Hungarian)

STEGENA L (1982) Water migration influences on the geothermics of basins. Tectonophysics 83:91-99

STEGENA L (1989) Thermal effect of hydrogeology in closed basins – *in* BECK AE, GARVEN G, STEGENA L (eds) Hydrogeological regimes and their subsurface thermal effects. Geophysical Monograph 47, IUGG v. 2, Washington, D.C., American Geophysical Union, pp. 81-86

STEGENA L, GÉCZY B, HORVÁTH F (1975) Late Cenozoic evolution of the Pannonian Basin. Tectonophysics 26:71-90

SZALAY Á (1988) Maturation and migration of hydrocarbons in the southeastern Pannonian Basin – *in* ROYDEN LH, HORVÁTH F (eds) The Pannonian Basin; a study in basin evolution. AAPG Memoir 45:347-354

SZALAY Á, KONCZ I (1993) Migration and accumulation of oil and natural gas generated from Neogene source rocks in the Hungarian part of the Pannonian Basin – *in* SPENCER AM (ed) Generation, accumulation, and production of Europe's hydrocarbons III. Special Publication of the European Association of Petroleum Geoscientists, Federal Republic of Germany, pp. 303-309

SZALAY Á, SZENTGYÖRGYI K (1988) A method for lithogenetic subdivision of Pannonian (s.l.) sedimentary rock – *in* ROYDEN LH, HORVÁTH F (eds) The Pannonian Basin, a study in basin evolution. AAPG Memoir 45:89-96

SZENTGYÖRGYI K (1989) A Békési-medence miocén korú képződményei és szénhidrogén-földtani jelentőségük [Miocene formations in the Békés Basin and their petroleum geological significance]. Magyar Geofizika XXX/4-5:113-128 (in Hungarian)

TARI G (1994) Alpine tectonics of the Pannonian basin. PhD thesis, Rice University, Houston, Texas, 501 p

TARI G, DÖVÉNYI P, DUNKL I, HORVÁTH F, LENKEY L, SZAFIÁN P, TÓTH T (1999) Lithospheric structure of the Pannonian basin derived from seismic, gravity and geothermal data – *in* DURAND B, JOLIVET L, HORVÁTH F, SÉRRANE M (eds) The Mediterranean basins: Tertiary extension within the Alpine orogen. Geol. Soc. Spec. Publ. 156, London, pp. 215-250

TARI G, HORVÁTH F, RUMPLER J (1992) Styles of extension in the Pannonian basin. Tectonophysics 208:203-219.

TERZAGHI K (1923) Die Berechnung der Durchlassigkeitsziffer des Tones aus dem Verlauf der hydrodynamischen Spannungserscheinungen. Akademie der Wissenschaften in Wein, Sitzungsberichte, Mathematischnaturwissenschaftliche Klasse Part IIa, 132/3-4:125-138 (Reprinted in Bjerrum L, Cassagrande A, Peck RB, Skempton AW (1960) (eds) From Theory to Practice in Soil Mechanics. John Wiley, New York, pp. 133-146.)

TÓTH J (1980) Cross-formational gravity-flow of groundwater: A mechanism of the transport and accumulation of petroleum (The generalized hydraulic theory of petroleum migration) – *in* ROBERTS WH, CORDELL RJ (eds.) Problems of Petroleum Migration. AAPG Studies in Geology, no. 10, Tulsa, Oklahoma, USA, pp. 121-167

TÓTH J (1984) The role of regional gravity flow in the chemical and thermal evolution of ground water – *in* HITCHON B, WALLICK EI (eds) Proceedings, Practical Applications of Ground Water Geochemistry. First Canadian/American Conference on Hydrogeology, National Water Well Association and Alberta Research Council. Worthington, Ohio, U.S.A., pp 3-39

TÓTH J (1988) Ground water and hydrocarbon migration – *in* BACK W, ROSENSHEIN JS, SEABER PR (eds) Hydrogeology. The Geology of North America, v. O-2., Boulder, Colorado, Geological Society of America, pp. 485-502

TÓTH J (1996) Thoughts of a hydrogeologist on vertical migration and near-surface geochemical exploration for petroleum – *in* SCHUMACHER D, ABRAMS MA (eds) Hydrocarbon migration and its near-surface expression. AAPG Memoir 66:279-283

TÓTH J (1999) Groundwater as a geologic agent: An overview of the causes, processes, and manifestations. Hydrogeology Journal 7/1:1-14

TÓTH J (2003) Fluid-potential patterns and hydrocarbon deposits in groundwater flow-fields induced by gravity and tectonic compression, Hungarian Great Plain, Pannonian Basin. Journal of Geochemical Exploration 78-79:427-431

TÓTH J (2009) Gravitational Systems of Groundwater Flow – Theory, Evaluation, Utilization. University Press, Cambridge, UK, pp. 55-57

TÓTH J, ALMÁSI I (2001) Interpretation of observed fluid potential patterns in a deep sedimentary basin under tectonic compression: Hungarian Great Plain, Pannonian Basin. Geofluids 1:11-36

TÓTH J, CORBET T (1986) Post-Paleocene evolution of regional groundwater flow-systems and their relation to petroleum accumulations, Taber Area, Southern Alberta, Canada. Bulletin of Canadian Petroleum Geology 34/3:339-363

TÓTH J, MILLAR RF (1983) Possible Effects of Erosional Changes of the Topographic Relief on Pore Pressures at Depth. Water Resources Research 19/6:1585-1597

TÓTH J, OTTO CJ (1993) Hydrogeology and oil deposits at Pechelbronn-Soultz-Upper Rhine Graben. Acta Geologica Hungarica 36/4:375-393

UNDERSCHULTZ JR, OTTO CJ, BARTLETT R (2005) Formation fluids in faulted aquifers: examples from the foothills of Western Canada and the North West Shelf of Australia – *in* BOULT P, KALDI J (eds) Evaluating fault and cap rock seals. AAPG Hedberg Series 2, pp. 247-260

URBANCSEK J (1965) Az Alföld negyedkori földtani képződményeinek mélyszerkezete [Quaternary profound structures in the Hungarian Plains]. Hidrológiai Közlöny 45/3:111-124 (in Hungarian)

VAN BALEN RT, CLOETINGH S (1994) Tectonic control of the sedimentary record and stress-induced fluid flow: constraints from basin modeling – *in* PARNELL J (ed) Geofluids:

origin, migration and evolution of fluids in sedimentary basins. Geological Society of London, London, United Kingdom, Geological Society Special Publications 78:9-26

VÁNDORFI R (1965) Az alföldi szénhidrogén-telepek és azok földtani jellemzése [Hydrocarbon accumulations and their geological characterization in the Great Hungarian Plain]. Földtani Közlöny 95/2:164-182 (in Hungarian)

VARSÁNYI I, MATRAY JM, Ó KOVÁCS L (1997) Geochemistry of formation waters in the Pannonian Basin (southeast Hungary). Chemical Geology 140:89-106

VARSÁNYI I, MATRAY JM, Ó KOVÁCS L (1999) Hydrogeochemistry in two adjacent areas in the Pannonian Basin (Southeast-Hungary). Chemical Geology 156:25-39

VARSÁNYI I, Ó. KOVÁCS L (2009) Origin, chemical and isotopic evolution of formation water in geopressured zones in the Pannonian Basin, Hungary. Chemical Geology 264:187-196

VERWEIJ H (2003) Fluid flow systems analysis on geological timescales in onshore and offshore Netherlands. Published by the Netherlands Institute of Applied Geoscience TNO – National Geological Survey, Utrecht, the Netherlands, 278 p

VÖLGYI L (1977) Hazai geotermikus viszonyok szerepe a szénhidrogén prognózisban [The role of geothermics in prediction of prospective areas of hydrocarbon accumulations in Hungary]. Research report for the Hungarian Petroleum Research Company, 52 p (in Hungarian)

VON ENGLEHARDT W, TUNN WLM (1955) The flow of fluids through sandstones. Circ. Ill. State Geol. Surv. 194:1-17

WANG X, LIU C (2005) Start-up pressure gradient of tight gas reservoirs in Daniudi gas field and its application method. Oil & Gas Geology 26/5:698-701

WELTE DH, HANTSCHEL T, WYGRALA BP, WEISSENBURGER KS, CARRUTHERS D (2000) Aspects of petroleum migration modelling. Journal of Geochemical Exploration 69-70:711-714

WHITAKER S (1996) The Forchheimer equation: A theoretical development. Transport in Porous Media 25/1:27-61

WILKINSON D, WILLEMSEN JF (1983) Invasion percolation: a new form of percolation theory. J. Phys. A: Math. Gen. 16:3365-3376

WILLETT SD, CHAPMAN DS (1987) Temperatures, fluid flow, and the thermal history of the Uinta basin. – *in* DOLIGEZ B (ed) Migration of Hydrocarbons in Sedimentary Basins, Paris: Editions Technip., pp. 533-551

WINDHOFFER G, BADA G (2005) Formation and deformation of the Derecske Trough, Pannonian Basin: Insights from analog modeling. Acta Geologica Hungarica 48/4:351-369

WINDHOFFER G, BADA G, NIEUWLAND D, WÓRUM G, HORVÁTH F, CLOETINGH S (2005) On the mechanics of basin formation in the Pannonian basin: Inferences from analogue and numerical modelling. Tectonophysics 410:389-415

WHITTAKER SG, ROSTRON BJ (2003) Geologic Storage of CO_2 in a carbonate reservoir within the Williston Basin, Canada: An update. – *in* GALE J, KAYA Y (eds) Green House Gas Control Technologies, Volume I, Elsevier, pp. 385-390

XIONG W, LEI Q, GAO S, HU Z, XUE H (2009) Pseudo threshold pressure gradient to flow for low permeability reservoirs. Petroleum Exploration and Development (Online English edition of the Chinese language journal) 36/2:232-236

ZENTAI L (1996) A Kárpát-medence domborzata [Topography of the Carpathian Basin]. Available via http://lazarus.elte.hu/hun/summer.jpg. Cited 17 July 2012. (in Hungarian)

ZOUHRI L, GORINI C, DEFFONTAINES B, MANIA J (2004) Relationships between hydraulic conductivity distribution and synsedimentary faults, Rharb-Mamora basin, Morocco; Hydrogeological, geostatistical and modeling approaches. Hydrogeology Journal 12/5:591-600

APPENDIX 1

CORRECTION OF WATER DENSITY

The objective of this work was to determine the density values, which are typical of the two main Study Areas, and can be used to control the hydraulic (pressure – hydraulic head) calculations performed with the constant density value of 1000 kg/m^3.

Water density basically depends on temperature, salinity, and free gas content, while less intensely on pressure, and dissolved gas content. Since usually the amount of dissolved gases is small, their effect on water density and viscosity is considered to be significantly smaller than the effects of salinity and temperature. Thus, the effect of dissolved gases on formation brine properties such as density and viscosity can be neglected for the range of conditions found in sedimentary basins (ADAMS and BACHU, 2002). The role of free gas content is discussed separately in Chapter 4.3.1. Consequently, the cumulated effect of salinity (S), temperature (T), and pressure (p) on water density was attempted to correct. However, there is no available water sample in the Study Areas, which has all of these data simultaneously. Therefore, average T, S, and p values were calculated for the elevation intervals (Table 1.1), which were used during the further data processing as well. Further uncertainties of the calculations and results are discussed in Chapter 4.3.1. In this appendix only the applied calculation methods and data, as well as the results are itemized.

1.1. Applied calculation methods

The displayed methods and equations are appropriate to calculate the change of a reference density (here: 1000 kg/m3) due to the effects of temperature, salinity, and pressure. The induced changes in density by each effect are additive, but there are equations for calculate the coupled effect of T, S, and p as well.

Applied equations are presented in the followings, while the applied data and results can be found in Table 1.1 regarding the elevation intervals where T, S, and p data were averaged. Afterwards, density values calculated by the single equations (Table 1.1) were cumulated in every possible T+S+p combinations (Table 1.2). Subsequently, these combined results were averaged for each elevation interval, and finally the average of these values represents the water densities being typical for the two main Study Areas. The average differences in meter and % that caused by the correction in the calculated hydraulic head values can be found in Table 1.3.

Equation 1 – Effect of temperature (T) (source: www.engineeringtoolbox.com)

$$\rho_1 = \frac{\rho_0}{[1+\alpha(T_1-T_0)]} \tag{1}$$

where

- ρ_1 = final density (kg/m^3)
- ρ_0 = initial density (kg/m^3), $\rho_{0(w)}$ = 998.2 kg/m^3
- α = volumetric temperature expansion coefficient (m^3/m^3°C), $\alpha_{(water)}$ = 0.0002 m^3/m^3°C
- T_1 = final temperature (°C)
- T_0 = initial temperature (°C), $T_{0(w)}$ = 20°C

Equation 2 – Effect of salinity (S) (source: DAVIES, 1987)

$$\rho_1 = \frac{\rho_0}{[1+\alpha(c_1-c)]} \tag{2}$$

where

- ρ_1 = fluid density (kg/m^3)
- ρ_0 = reference fluid density (kg/m^3), $\rho_{0(w)}$ = 998.2 kg/m^3
- α = volumetric expansion coefficient (m^3/m^3°C), $\alpha_{(water)}$ = 0.0002 m^3/m^3(°C)
- c_1 = solute concentration (kg/m^3)
- c_0 = reference solute concentration (kg/m^3), $c_{0(freshwater)}$ = 0 kg/m^3

Equation 3 – Effect of salinity (S) (based on the linear relationship (R^2=0.999) between salinity and density at T=20°C (see also Fig. 1.1))

$$\rho = \frac{S+1296.6}{1.299} \tag{3}$$

where

- ρ = density (kg/m^3)
- S = salinity (TDS) (kg/m^3)

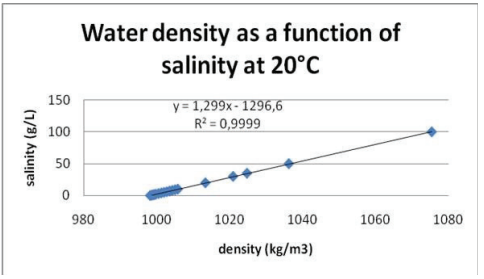

Figure 1.1 Relationship between water salinity and density at T = 20°C

Equation 4 – Effect of pressure (p) (source: FREEZE and CHERRY, 1979)

$$\rho_1 = \rho_0 \exp[\beta(p_1 - p_0)] \tag{4}$$

where

- ρ_1 = final density (kg/m^3)
- ρ_0 = initial density (kg/m^3), $\rho_{0(w)}$ = 998.2 kg/m^3
- β = compressibility of water = 4.4*10^{-10} m^2/N (or 1/Pa)
- p_1 = final pressure (Pa)
- p_0 = reference pressure (Pa), p_0 = 1 atm = 101325 Pa

Equation 5 – Effect of pressure (p) (source: www.engineeringtoolbox.com)

$$\rho_1 = \frac{\rho_0}{\left[\frac{1-(p_1-p_0)}{E}\right]} \tag{5}$$

where

- ρ_1 = final density (kg/m^3)
- ρ_0 = initial density (kg/m^3), $\rho_{0(w)}$ = 998.2 kg/m^3
- E = bulk modulus fluid elasticity, $E(water)$ = 1/β =2.27*10^9 N/ m^2 (or Pa)

- p_1 = final pressure (Pa)
- p_0 = initial pressure (Pa), p_0 = 1 atm = 101325 Pa

Equation 6 – Coupled effect of temperature (T) and salinity (S) (source: McCutcheon et al., 1993)

$$\rho_{(T,S)} = \rho_{(T)} + AS + BS^{\frac{3}{2}} + CS^2$$

$$\rho_{(T)} = 1000\left[1 - \frac{T+288.9414}{508929.2(T+68.12963)}(T-3.9863)^2\right]$$

$$A = 0.824493 - 4.0899 * 10^{-3}T + 7.6438 * 10^{-5}T^2 - 8.2467 * 10^{-7}T^3 + 5.3675 * 10^{-9}T^4$$

$$B = -5.724 * 10^{-3} + 1.0227 * 10^{-4}T - 1.6546 * 10^{-6}T^2$$

$$C = 4.8314 * 10^{-4} \quad (6)$$

where

- ρ = density (kg/m^3)
- T = temperature (°C)
- S = salinity (kg/m^3)

Equation 7 – Coupled effect of temperature (T) and pressure (p) (source: www.engineeringtoolbox.com)

$$\rho_1 = \frac{\rho_0}{\frac{1+\alpha(T_1-T_0)}{1-\frac{(p_1-p_0)}{E}}} \quad (7)$$

where

- ρ_1 = final density (kg/m^3)
- ρ_0 = initial density (kg/m^3), $\rho_{0(w)}$ = 998.2kg/m^3
- α = volumetric temperature expansion coefficient (m^3/m^3°C), $\alpha_{(water)}$ = 0.0002 m^3/m^3°C
- T_1 = final temperature (°C)
- T_0 = initial temperature (°C), $T_{0(w)}$ = 20°C
- E = bulk modulus fluid elasticity, $E(water)$ = 1/β = 2.27*10^9 N/ m^2 (or Pa)
- p_1 = final pressure (Pa)
- p_0 = initial pressure (Pa), p_0 = 1 atm = 101325 Pa

1.2. Results

Temperature and salinity effect approximately equalize each other in the Study Areas (Table 1.1 and 1.2), which can be explained by the relatively high geothermal gradient (about 55 °C/km) and relatively low salinity of groundwater (maximum 40 g/L). For comparison in Alberta, Canada the salinity of groundwaters is in the 100 g/L order of magnitude, while the average geothermal gradient is 40 °C/km. Consequently, salinity effect dominates and water density is usually significantly higher (1200-1300 kg/m^3) than that of the fresh water (1000 kg/m^3).

In other words, the negative deviation from the fresh water density in the Derecske Study Area (993 kg/m^3) and in the Békés-Battonya Study Area (985 kg/m^3) caused by the relatively low salinity, is practically negligible (Table 1.1 and 1.2). Comparing hydraulic head (h) values calculated from pressure data of the Study Areas with 1000 kg/m^3 and 993 (DSA) or 985 kg/m^3 (BBSA) density values, the changes in h vary between 6 and 2% (decreasing with depth) in the Derecske Study Area, while 32 and 4% (decreasing with depth) in the Békés-Battonya Study Area (Table 1.3). Considering the uncertainties of the pressure data and the height of the

water columns (usually of the order of 100 and 1000 m – increasing with depth), these deviations are negligible. Additionally, hydraulic conditions (see also Chapters 5 and 6) interpreted based on the original and calculated pressure and hydraulic head data are concordant.

1.3. REFERENCES

ADAMS JJ, BACHU S (2002) Equations of state for basin geofluids: algorithm review and intercomparison for brines. Geofluids 2:257-271

BATZLE M, WANG Z (1992) Seismic properties of pore fluids. Geophysics 57:1396-1408

DAVIES PB (1987) Modeling areal, variable-density, ground-water flow using equivalent freshwater head – Analysis of potentially significant errors. Proceedings of the Solving Groundwater Problems with Models Conference and Exposition, NWWA, February 10-12, 1987, Denver Colorado, p. 888-903

DENSITY OF FLUIDS – Changing pressure and temperature. Available via http://www.engineeringtoolbox.com/fluid-density-temperature-pressure-d_309.html. Cited 25 February 2010

FREEZE RA, CHERRY JA (1979) Groundwater. Prentice Hall, Engwood Cliffs, New Jersey, p. 52

MCCUTCHEON SC, MARTIN JL, BARNWELL TO JR (1993) Water Quality – *in* MAIDMENT DR (ed) Handbook of Hydrology. McGraw-Hill, New York NY, pp. 113

	average elevation (m asl)	S_{av} (mg/l)	S_{av} (kg/m3)	T_{av} (°C)	p_{av} (MPa)	Results /ρ (kg/m^3)/ of the equations signed by numbers 1-7 in the text													
						1		2		3		4		5		6		7	
						ρ	$\Delta\rho$	ρ	$\Delta\rho$	ρ	$\Delta\rho$	ρ	$\Delta\rho$	ρ	$\Delta\rho$	ρ	$\Delta\rho$	ρ	$\Delta\rho$
DSA	-400	2139	2.139	36.6	4.05	994.90	-3.30	998.63	0.43	999.80	1.60	999.97	1.74	999.97	1.74	996.63	-1.57	995.09	-3.11
	-900	6958	6.958	66.2	10.18	989.06	-9.14	999.59	1.39	1003.51	5.31	1002.67	4.44	1002.68	4.45	993.47	-4.73	985.04	-13.2
	-1500	19998	19.998	97.2	20.44	983.02	-15.18	1002.19	3.99	1013.55	15.35	1007.20	8.97	1007.25	9.02	991.91	-6.29	976.71	-21.5
	-2000	18100	18.100	121.8	30.50	978.28	-19.92	1001.81	3.61	1012.09	13.89	1011.67	13.44	1011.78	13.55	991.56	-6.64	960.65	-37.6
	-2350	12817	12.817	134.3	36.06	975.89	-22.31	1000.76	2.56	1008.02	9.82	1014.15	15.92	1014.30	16.07	991.60	-6.60	947.29	-50.9
	-2750	13300	13.300	148.7	44.35	973.15	-25.05	1000.86	2.66	1008.39	10.19	1017.86	19.63	1018.08	19.85	992.50	-5.70	939.91	-58.3
	-3200	14731	14.731	175.3	54.84	968.13	-30.07	1001.14	2.94	1009.49	11.29	1022.56	24.33	1022.90	24.67	992.05	-6.15	933.36	-64.8
BBSA	-400	1009	1.009	32.5	4.03	995.71	-2.49	998.40	0.20	998.93	0.73	999.96	1.73	999.96	1.73	997.44	-0.76	995.65	-2.55
	-900	283	0.283	46.7	9.82	992.90	-5.30	998.26	0.06	998.37	0.17	1002.51	4.28	1002.52	4.29	997.17	-1.03	989.73	-8.47
	-1500	494	0.494	101.0	15.76	982.29	-15.91	998.30	0.10	998.53	0.33	1005.13	6.90	1005.16	6.93	989.11	-9.09	957.80	-40.4
	-2000	517	0.517	109.0	21.76	980.74	-17.46	998.30	0.10	998.55	0.35	1007.79	9.56	1007.85	9.62	990.19	-8.01	951.82	-46.4
	-2350	279	0.279	138.4	27.82	975.11	-23.09	998.26	0.06	998.37	0.17	1010.48	12.25	1010.57	12.34	987.16	-11.04	926.96	-71.2
	-2800	381	0.381	149.6	40.56	972.98	-25.22	998.28	0.08	998.45	0.25	1016.16	17.93	1016.34	18.11	990.64	-7.56	916.78	-81.4
	-4000	409	0.409	172.7	69.92	968.62	-29.58	998.28	0.08	998.47	0.27	1029.37	31.14	1029.91	31.68	999.36	1.16	893.98	-104

Table 1.1 Average salinity (S_{av}), temperature (T_{av}), and pressure (p_{av}) data, as well as the corrected density values (ρ) and its deviation from the reference 1000 kg/m^3 value ($\Delta\rho$) regarding (the middle point of) elevation intervals. Calculation equations (#1-7) are presented in sub-chapter 1.1 of this appendix. Abbreviations: DSA – Derecske Study Area, BBSA – Békés-Battonya Study Area

	average elevation (m asl)	Cumulated results /ρ (kg/m^3)/ of the equations signed by numbers 1-7 in the text								average densities for elevation intervals (kg/m^3)			
		1+2+4	1+3+4	1+2+5	1+3+5	4+6	5+6	2+7	3+7				
DSA	-400	997.06	998.23	997.06	998.24	996.82	996.83	997.06	998.23	997.44			
	-900	994.89	998.81	994.90	998.82	989.48	989.49	994.86	998.78	995.00			
	-1500	995.99	1007.34	996.04	1007.39	985.69	985.74	995.90	1007.26	997.67			
	-2000	995.34	1005.61	995.44	1005.72	974.09	974.20	995.17	1005.45	993.88			
	-2350	994.37	1001.63	994.52	1001.78	963.21	963.35	994.16	1001.42	989.30			
	-2750	995.43	1002.97	995.65	1003.19	959.54	959.76	995.15	1002.69	989.30			
	-3200	995.41	1003.76	995.74	1004.09	957.69	958.02	994.99	1003.34	989.13	**993.10**	**kg/m^3**	**DSA average**
BBSA	-400	997.64	998.17	997.64	998.17	997.38	997.38	997.64	998.17	997.77			
	-900	997.23	997.35	997.25	997.36	994.01	994.02	997.22	997.34	996.47			
	-1500	989.29	989.52	989.32	989.55	964.70	964.74	989.21	989.44	983.22			
	-2000	990.40	990.65	990.46	990.71	961.38	961.43	990.29	990.54	983.23			
	-2350	987.41	987.53	987.51	987.62	939.21	939.30	987.22	987.33	975.39			
	-2800	990.99	991.16	991.17	991.34	934.71	934.90	990.71	990.88	976.98			
	-4000	999.84	1000.03	1000.38	1000.56	925.12	925.65	999.44	999.62	981.33	**984.91**	**kg/m^3**	**BBSA average**

Table 1.2 Cumulated results of the single calculations (equations #1-7 are presented in sub-chapter 1.1. of this appendix) in every possible T+S+p combinations, average density values for each elevation interval, and average densities of the two main Study Areas. Abbreviations: DSA – Derecske Study Area, BBSA – Békés-Battonya Study Area

	average elevation (m asl)	Δh (m)	Δh (%)
Derecske Study Area (DSA) (ρ = 993 kg/m^3)	-900	7	6
	-1500	14	3
	-2000	22	2
	-2350	25	2
	-2750	31	2
	-3200	39	2
Békés-Battonya Study Area (BBSA) (ρ = 985 kg/m^3)	-900	15	18
	-1500	24	32
	-2000	33	19
	-2350	42	10
	-2800	62	5
	-4000	106	4

Table 1.3 Average differences in meter and % that caused by the correction in the calculated hydraulic head (h) values, which were calculated by using 1000 kg/m^3 of water density. Abbreviation: Δh = the difference between h values calculated from pressure data by using 1000 kg/m^3 water density or the area specific average density (DSA: 993 kg/m^3, BBSA: 985 kg/m^3)

APPENDIX 2

CORRECTION OF HYDRAULIC HEADS CALCULATED FROM PRESSURE DATA MEASURED IN GAS COLUMN

Since several pressure data were measured during gas inflow, thus presumably in a gas column, calculating hydraulic head (h) by using water density (ρ_w=1000 kg/m^3) or the vertical pressure gradient of water (9.8 MPa/km) from these gaseous pressure data could cause significant deviation compared to the real potential regarding the water leg. These errors may be observed as (apparent) positive anomalies in the fluid potential field, because pressure is higher in a gas column (point #1 in Fig. 2.1) due to the lower vertical pressure gradient of gas than in a water column (point #3 in Fig. 2.1) in the same depth. Consequently, hydraulic head calculated by using water density from a pressure data measured in a gas column is greater than that calculated from a pressure data in a water column in the same depth.

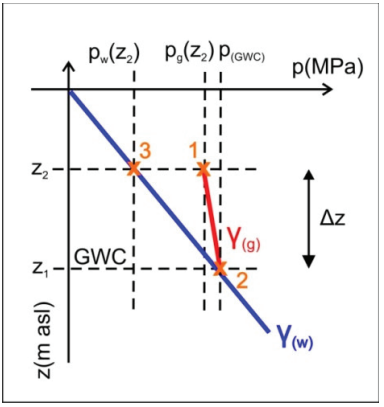

Figure 2.1 Pressure conditions in a gas column and its water leg represented in a pressure-elevation profile. Measuring points: #1 in the gas column /pressure: $p_g(z_2)$/, #2 on the gas-water contact (GWC) /pressure: $p_{(GWC)}$/, #3 in a water column in the depth of #1 /pressure: $p_w(z_2)$/. Δz is the difference of z_2 and z_1, $\gamma_{(g)}$ is the vertical pressure gradient of gas, and $\gamma_{(w)}$ is the vertical pressure gradient of water.

Because one of this Ph.D. research work's objectives was to examine the role of faults and low-permeability formations in the development of fluid potential anomalies, it was necessary to identify among the mapped anomalies the apparent ones caused by the presence of gas accumulations (i.e. hydraulic calculation errors). It is possible through the conversion of pressure measured in the gas column /$p_g(z_2)$/ to the pressure regarding the gas-water contact (GWC) /p_{GWC}/ by using the vertical pressure gradient of the gas /γ_g/ based on the density of the gas /ρ_g/ (in Fig. 2.1, step between #1 and 2). Since pressures regarding the gas and the water leg are equal on the GWC, the pressure that would refer to the water at z_2 elevation /$p_w(z_2)$/ can be calculated from $p_g(z_2)$ by using the vertical pressure gradient of water (in Fig 2.1, step between #2 and 3). Then the corrected hydraulic head could be determined by using $p_w(z_2)$ and water density (based on Eq. 1).

However, some required data (density of the gas, elevation of the GWC /z_1/) were not available, while every hydraulic calculation of this regional study was performed by using the constant (water) density value of 1000 kg/m^3 (for explanation see Chapter 4.3.1 and Appendix 1). Thus an approximate method had to be worked out to determine the difference /Δh_{wg}/ between the water's hydraulic head calculated with water density i) from pressure data measured in the gas column /$h_w(z_2)$/ and ii) from pressure data would be measured in a water column at the same depth /$h_w(z_2)$*/. The following equations were applied based on the principle formula of hydraulic head (h) determination:

$$h = z + \frac{p}{\rho g} \tag{1}$$

where h the hydraulic head [L], z the elevation above datum plane [L], p the gauge pressure (absolute pressure minus atmospheric pressure) [M/LT^2], ρ the density of fluid [M/L^3], g the gravitational acceleration [L/T^2]. Hydraulic head in point #1 in Fig. 2.1 considering unit conversions as well:

$$h_w(z_2) = z_2 + \frac{p_g(z_2) * 10^6}{\rho_w * g} \tag{2}$$

Hydraulic head in point #2 in Fig. 2.1 considering unit conversions as well:

$$h_w(GWC) = z_1 + \frac{p_{(GWC)} * 10^6}{\rho_w * g} = z_1 + \frac{\left[p_g(z_2) + \frac{\gamma_g}{10^3}\Delta z\right] * 10^6}{\rho_w * g} \tag{3}$$

Hydraulic head in point #3 in Fig. 2.1 considering unit conversions as well:

$$h_w(z_2)^* = z_2 + \frac{p_w(z_2) * 10^6}{\rho_w * g} = z_2 + \frac{\left[p_g(z_2) + \frac{\gamma_g}{10^3}\Delta z - \frac{\gamma_w}{10^3}\Delta z\right] * 10^6}{\rho_w * g} \tag{4}$$

Hydraulic head difference between points #1 and #3 based on Eq. (2) and (4):

$$\Delta h_{wg} = h_w(z_2) - h_w(z_2)^* = z_2 + \frac{p_g(z_2) * 10^6}{\rho_w * g} - \left\{ z_2 + \frac{\left[p_g(z_2) + \frac{\gamma_g}{10^3}\Delta z - \frac{\gamma_w}{10^3}\Delta z\right] * 10^6}{\rho_w * g} \right\} \tag{5}$$

Since the vertical pressure gradient of gas (of the order of 10^{-3} MPa/km), and particularly the thousandth part of it is negligible compared to the other parameters, while the constant density value (ρ_w) equals to 1000 kg/m^3, Δh_{wg} can be simplified as:

$$\Delta h_{wg} = \frac{\left(\frac{\gamma_w}{10^3}\Delta z * 10^6\right)}{\rho_w * g} = \frac{\gamma_w \Delta z}{g} \tag{6}$$

where parameters and their units are the followings:

ρ_v	water density	(kg/m^3)
ρ_g	gas density	(kg/m^3)
γ_w	vertical pressure gradient of water (=ρ_w*g/10^3)	(MPa/km)
γ_g	vertical pressure gradient of gas (=ρ_g*g/10^3)	(MPa/km)
z_0	surface elevation	(m asl)
z_1	elevation of the gas-water contact (GWC)	(m asl)
z_2	elevation of the original measuring point (maximum the top of the gas column)	(m asl)
Δz	vertical distance of z_1 and z_2 (=z_1-z_2)	(m)
$p_g(z_2)$	pressure measured at z_2 elevation in the gas column	(MPa)
$p_w(z_2)$	pressure would be measured at z_2 elevation in water column	(MPa)
$p_{(GWC)}$	pressure on the GWC (p_{water}=p_{gas})	(MPa)
$h_w(z_2)$	water's hydraulic head calculated from $p_g(z_2)$	(m asl)
$h_w(z_2)$*	water's hydraulic head calculated from $p_w(z_2)$	(m asl)
$h_w(GWC)$	water's hydraulic head on the GWC (calculated from $p_{(GWC)}$)	(m asl)
Δh_{wg}	difference of $h_w(z_2)$ and $h_w(z_2)$*	(m)
g	gravitational acceleration	(m/s^2)

According to Eq. (6), the error of hydraulic head /Δh_{wg}/ calculated from gaseous pressure data by not using the above described pressure correction in lack of the required data, only depends on and directly proportional to the vertical pressure gradient of water /γ_w/ and the vertical distance of z_1 (elevation of GWC) and z_2 (elevation of the measuring point) /Δz/, while g is constantly 9.8 m/s^2. By determining the maximum values of γ_w and Δz being typical for the Study Areas, also the maximum of Δh_{wg} can be defined. Since the maximum of Δz equals to the height of the gas column, and the maximum known gas column height in both main Study Areas (DSA and BBSA) is about 110 m (KÁROLY KISS, MOL Plc., personal communication, 2010), consequently $\Delta z_{(max)}$ equals to 110 m. If vertical pressure gradient of water is hydrostatic (γ_w=9.8 MPa/km), based on Eq. (6) the maximum error equals to the height of the gas column /$\Delta h_{wg(max)}$ = $\Delta z_{(\max)}$/ (Table 2.1). By raising the vertical pressure gradient of water into super-hydrostatic, also the error increases. The highest vertical pressure gradients of water known from the Study Areas (see also Chapter 5) and the related Δh_{wg} values calculated by changing Δz between 100 and 150 m are presented in Table 2.1.

Consequently, the maximum error ($\Delta h_{wg(max)}$) varies between Δz (maximum 110 m) and 254 m (Table 2.1). In the Derecske Study Area the pressure gradients applied in the calculations were mostly measured in Pre-Pannonian or Pre-Neogene formations and always bellow 2000 m depth where h is usually of the order of 1000 m, and grad$h$ is at least of the order of 100 m (see also Chapter 5). Accordingly, the possible maximum error Δh_{wg} = 254 m is negligible. Thus, development of potential anomalies cannot be explained only by the presence of gas accumulations. However, in shallower depths (mostly in the Great Plain Aquifer) where h is maximum a few 100 m and grad$h$ is of the order of 10 m (see also Chapter 5), the error of 254 m could generate apparent anomalies in the fluid potential field. Thus, it cannot be excluded that the known gas accumulation induces the potential anomaly. On the other hand, in the Békés-Battonya Study Area most of the potential anomalies can be observed in shallower depth than 2000 m and around known hydrocarbon accumulations, thus these anomalies are presumably apparent caused by the presence of gas (i.e. calculation error) (see also Chapter 5), even if the maximum error is lower than in the DSA, i.e. Δh_{wg} = 126 m (Table 2.1).

The same conclusions can be drawn if Δz is raised to an irrelevantly high number (150 m), since $\Delta h_{wg(max)}$ is only 346 m in this case as well (Table 2.1).

In conclusion, also in lack of the required data this approximation can be used for filtering out the apparent potential anomalies induced by the processing of gaseous data in the above described way.

p(z) #	γ_w (MPa/km)	Δz (m)	Δh_{wg} (m)
Example #1	9.8	100	100
Example #2	10.00	100	102
Example #3	11.00	100	112
BB-41	11.21	100	114
D-21	18.21	100	186
D-30-31	18.90	100	193
D-20	21.44	100	219
D-29	22.61	100	231
Example #1	**9.8**	**110**	**110**
Example #2	10.00	110	112
Example #3	11.00	110	123
BB-41	11.21	110	126
D-21	18.21	110	204
D-30-31	18.90	110	212
D-20	21.44	110	241
D-29	**22.61**	**110**	**254**
Example #1	9.8	150	150
Example #2	10.00	150	153
Example #3	11.0	150	168
BB-41	11.21	150	172
D-21	18.21	150	279
D-30-31	18.90	150	289
D-20	21.44	150	328
D-29	22.61	150	346

Table 2.1 Some examples (among them 9.8 MPa/km is the hydrostatic vertical pressure gradient of water) and the highest vertical pressure gradient values of water known from the study areas (see Chapter – hydr. results), as well as the related Δh_{wg} values calculated (Eq. 6) by changing Δz between 100 and 150 m. BB-41 is the p(z) profile #41 in the Békés-Battonya Study Area, D-21 is the p(z) profile #21 in the Derecske Study Area, etc.

In order to confirm the above conclusions the MOL Plc. provided us all of the required data (gas and water densities, elevation of the GWC) in a local study area within the DSA where thus concrete calculations could be performed. In this area contradiction between the approximately hydrostatic pressure data and vertical pressure gradient (see p(z) profiles #17-19 in A-Fig. 5.3.1.42-47) measured in gas columns, as well as the significant positive anomaly (#10) represented by hydraulic heads in the hydraulic cross-sections (see h(s,z) #1 and #7 in A-Fig. 5.3.3.4 and 5.3.3.19) touching the area was conspicuous. Results can be seen in Table 2.2. Since vertical pressure gradient of water was approximately hydrostatic in every cases, Δh_{wg} equals to Δz. Considering the corrected h values (maximum error Δh_{wg} = 113 m), fluid potential field in hydraulic cross-sections h(s,z) #2 and 7 (A-Fig. 5.3.3.4 and 5.3.3.19) was re-contoured, thus the apparent potential anomaly (#10) disappeared, but also the original (erroneous) equipotentials were left in the section in order to demonstrate the difference and the significance of the correction.

parameter	**unit**	Point #1	Point #2	Point #3	Point #4	Point #5	Point #6	Point #7	Point #8
ρ_w	**kg/m^3**	***1001.41***	***1002.68***	***1005.35***	***1002.99***	***1000.87***	***1003.00***	***1003.00***	***1003.00***
ρ_g	**kg/m^3**	***0.83***	***0.85***	***0.83***	***0.81***	***0.84***	***0.83***	***0.83***	***0.83***
γ_w	MPa/km	9.8138	9.8263	9.8524	9.8293	9.8085	9.8294	9.8294	9.8294
γ_g	MPa/km	0.0081	0.0083	0.0081	0.0079	0.0082	0.0081	0.0081	0.0081
z_1	**m asl**	***-1671***	***-1792***	***-1792***	***-1850***	***-1792***	***-2030***	***-2042***	***-1825***
z_2	**m asl**	***-1641***	***-1727***	***-1780***	***-1832***	***-1779***	***-1917***	***-1992***	***-1752***
Δz	m	30	65	12	18	13	113	50	73
$p_g(z_2)$	**MPa**	***17.6***	***18.9***	***18.9***	***19.4***	***18.8***	***21.1***	***21.2***	***18.6***
$p_{(GWC)}$	MPa	17.6	18.9	18.9	19.4	18.8	21.1	21.2	18.6
$p_w(z_2)$	MPa	17.3	18.3	18.8	19.2	18.7	20.0	20.7	17.9
$h_w(z_2)$	m asl	152	196	138	142	138	230	165	140
$h_w(z_2)$*	m asl	123	131	126	124	125	117	115	67
Δh_{wg}	m	29	65	12	18	13	113	50	73
g	**m/s^2**	***9.8***	***9.8***	***9.8***	***9.8***	***9.8***	***9.8***	***9.8***	***9.8***

Table 2.2 Calculation of Δh_{wg} from measured data (signed by numbers in italics) in a gas field in the DSA. Parameters are the same as above. Numbers in bold italics are the measured (or constant) values in points #1-8, while the others were calculated by Equations (2-5).